



UNIVERSITAT DE
BARCELONA

Design, synthesis and biological evaluation of novel molecules with the capacity of inducing the degradation of different proteins by direct signaling to the proteasome

Abdulateef Alqahtani

ADVERTIMENT. La consulta d'aquesta tesi queda condicionada a l'acceptació de les següents condicions d'ús: La difusió d'aquesta tesi per mitjà del servei TDX (www.tdx.cat) i a través del Dipòsit Digital de la UB (diposit.ub.edu) ha estat autoritzada pels titulars dels drets de propietat intel·lectual únicament per a usos privats emmarcats en activitats d'investigació i docència. No s'autoritza la seva reproducció amb finalitats de lucre ni la seva difusió i posada a disposició des d'un lloc aliè al servei TDX ni al Dipòsit Digital de la UB. No s'autoritza la presentació del seu contingut en una finestra o marc aliè a TDX o al Dipòsit Digital de la UB (framing). Aquesta reserva de drets afecta tant al resum de presentació de la tesi com als seus continguts. En la utilització o cita de parts de la tesi és obligat indicar el nom de la persona autora.

ADVERTENCIA. La consulta de esta tesis queda condicionada a la aceptación de las siguientes condiciones de uso: La difusión de esta tesis por medio del servicio TDR (www.tdx.cat) y a través del Repositorio Digital de la UB (diposit.ub.edu) ha sido autorizada por los titulares de los derechos de propiedad intelectual únicamente para usos privados enmarcados en actividades de investigación y docencia. No se autoriza su reproducción con finalidades de lucro ni su difusión y puesta a disposición desde un sitio ajeno al servicio TDR o al Repositorio Digital de la UB. No se autoriza la presentación de su contenido en una ventana o marco ajeno a TDR o al Repositorio Digital de la UB (framing). Esta reserva de derechos afecta tanto al resumen de presentación de la tesis como a sus contenidos. En la utilización o cita de partes de la tesis es obligado indicar el nombre de la persona autora.

WARNING. On having consulted this thesis you're accepting the following use conditions: Spreading this thesis by the TDX (www.tdx.cat) service and by the UB Digital Repository (diposit.ub.edu) has been authorized by the titular of the intellectual property rights only for private uses placed in investigation and teaching activities. Reproduction with lucrative aims is not authorized nor its spreading and availability from a site foreign to the TDX service or to the UB Digital Repository. Introducing its content in a window or frame foreign to the TDX service or to the UB Digital Repository is not authorized (framing). Those rights affect to the presentation summary of the thesis as well as to its contents. In the using or citation of parts of the thesis it's obliged to indicate the name of the author.

UNIVERSITAT DE BARCELONA

FACULTAT DE FARMÀCIA I CIÈNCIES DE L'ALIMENTACIÓ

**Design, synthesis and biological evaluation of novel molecules
with the capacity of inducing the degradation of different
proteins by direct signalling to the proteasome**

Abdulateef Alqahtani
2023

UNIVERSITAT DE BARCELONA

FACULTAT DE FARMÀCIA I CIÈNCIES DE L'ALIMENTACIÓ

Programa de Doctorat en Química Orgànica

**Design, synthesis and biological evaluation of novel molecules
with the capacity of inducing the degradation of different
proteins by direct signalling to the proteasome**

Abdulateef Alqahtani
2023

Memòria presentada Abdulateef Alqahtani per optar al títol de doctor per la universitat de
Barcelona

Director

Prof. Gemma Fabriàs
Research Unit on BioActive Molecules
Dept. of Biological Chemistry
Institute for Advanced Chemistry of Catalonia (IQAC-CSIC)

Tutor

Dr. Rodolfo Lavilla

Departament de Farmacologia, Toxicologia i Química Terapèutica
Laboratory of Medicinal Chemistry. Faculty of Pharmacy
University of Barcelona

ACKNOWLEDGEMENTS

First of all, I would like to thank my thesis director, Dr. Gemma Fabriàs, for giving me the opportunity to carry out the doctoral thesis at RUBAM. Thank you very much for the help and advice you have provided me throughout these years, for kindness and love you have immersed me and my wife with and for the freedom you have always given me to make my own decisions when carrying out this project. To Dr. Josefina Casas and Dr. José Luís Abad, many thanks for acting as “unofficial” co-directors, and for the fundamental role they played in the planning of the experiments and in the discussion of the results of the chemistry and biology parts of this thesis. To you my dear friend Dr. Hector Carneros, thanks to all the hours we have shared between seminars, columns, extractions, for being a reference, for transmitting your scientific rigor, the neat and methodical way of working at the laboratory, and for all the conversations during the “coffee breaks” that I have been missing so much. To all of you my RUBAM family to Dr. Mireia Casasampere and Tania Rodafor for your friendship and for your effort.

I would also like to express my gratitude to Dr. Bernat Crosas (Institute of Molecular Biology of Barcelona, IBMB-CSIC), the mastermind behind this thesis and for his group member Dr. Alice Zuin, Dr. Nuria Gallisà and Alba González-Artero for your effort and for all the good times we have had inside and outside the laboratory. To Dr. Jordi Bujons (IQAC-CSIC) for provided the important data of molecular modelling studies.

I would like to thank my sponsor Albaha University and also CSIC for fund and support. To university of Barcelona, to Barcelona, to Catalonia, and to Spain.

Finally I want to express my deep gratitude to my family, because without your support I would not have gotten here. To my parents, for instilling in me the values of effort and work, for your love and for always giving me your support in the challenges I have encountered throughout my life. To my sisters and brother, for always being there when I needed you.

And to you, Shatha, who has accompanied me practically throughout the entire thesis journey. Thank you for having been part of the happiest memories I have of recent years, for always coming to rescue me in the most difficult moments, for your infinite love and for everything that awaits us to live together when this stage is over.

TO MY

Dear friend... Virtuous teacher... Beloved father

TO HIS

Beautiful mind... Righteous soul... Angelic smile

TO

Antonio Delgado

ABBREVIATIONS

ALP	Autophagy-lysosome pathway
AUTAC	Autophagy targeting chimera
ATTEC	Autophagy-tethering compound
AR	Androgen receptor
BET	Bromodomain and extra-terminal domain
BRD4	Bromodomain-containing protein 4
Boc	<i>tert</i> -Butyloxycarbonyl
Cer	Ceramides
CERT	Ceramide transfer protein
CLIPTAC	In-cell click-formed proteolysis targeting chimeras
CRBN	Cereblon
CRL	Cullin-RING ligases
DIPEA	<i>N,N</i> -Diisopropylethylamine
DMA	<i>N,N</i> -Dimethylacetamide
DMAP	4-Dimethylaminopyridine
DMF	<i>N,N</i> -Dimethylformamide
DMSO	Dimethyl sulfoxide
DSC	<i>N,N'</i> -Disuccinimidyl carbonate
DUBs	Deubiquitinating enzymes
E1	ubiquitin-activating enzyme

E2	ubiquitin-conjugating enzyme
E3	ubiquitin ligase enzyme
ER	Estrogen receptor
EDC	1-Ethyl-3-(3-dimethylaminopropyl)carbodiimide
EtOAc	Ethyl acetate
EtOH	Ethanol
FDA	Food and Drug Administration
HECT	Homology to E6AP C terminus
HIF-1	Hypoxia-inducible factor 1
HOBt	1-Hydroxybenzotriazole
HPLC	High performance liquid chromatography
HRMS	High resolution mass spectrometry
Hz	Hertz
IAP	Inhibitor of apoptosis
ImiD	Immunomodulatory imide drugs
<i>J</i>	Coupling constant
MDM2	Murine double minute 2 homolog
MeOH	Methanol
NMR	Nuclear magnetic resonance
PDB	Protein data bank
PEG	Polyethylene glycol

POI	Protein of interest
PPh3	Triphenylphosphine
ppm	Parts per million
PROTAC	Proteolysis targeting chimera
RBR	RING-between-RING
RING	Really interesting new gene
rt	Room temperature
Rpt	Regulatory particle triple-A ATPase
Rpn	Regulatory particle non-ATPase
TEA	Triethylamine
TES	Triethylsilane
TFA	Trifluoroacetic acid
THF	Tetrahydrofuran
TLC	Thin layer chromatography
TsCl	<i>P</i> -Toluenesulfonyl chloride
Ub	Ubiquitin
UBDs	ubiquitin-binding proteins
UPS	Ubiquitin-proteasome system
VHL	Von Hippel Lindau

ABSTRACT

In 2001, the initial hypothesis of targeted protein degradation (TPD) was born to announce the launching of a new era of therapeutics development not by inhibiting a component of ubiquitin-proteasome system as small molecule inhibitors, but by recruiting the whole system to induce the degradation of specific proteins. TPD techniques can efficiently target long-lived proteins since they are not constrained by protein turnover, thus overcoming some of the drawbacks of UPS inhibitors. The majority of these technologies also share the advantageous pharmacokinetic characteristics of small compounds resembling drugs. Importantly, due to their various modes of action, they may expand the conventional druggable space. Many technologies with the therapeutic potential of targeting protein for degradation have been under massive study and development including PROteolysis TArgeting Chimeras (PROTACs).

PROTAC is a strategy that utilizes the UPS to target a specific protein and induces its degradation by employing hetero-bifunctional molecules consisting of a ligand to bind the protein of interest (POI), another ligand to recruit an E3 Ub ligase and a linker to bind the two ligands. These molecules interact simultaneously and hijack the enzymatic machinery by forming a ternary complex (POI:PROTAC:E3 ligase) that facilitates the transfer of Ub moieties and the formation of polyubiquitin chain(s) on the target protein. The polyubiquitinated protein will be recognized and promoted to degradation by the proteasome.

PROTACs bind specific targets and E3 Ub-ligases, promoting ubiquitination and degradation of targets by the proteasome. Multiple chimeras that degrade proteins relevant in several diseases have been developed, and the number is quickly increasing, indicating their therapeutic projection. Given some limitations of E3-

based PROTACs such as the diversity and complexity of E3 ligases, alternative strategies in target protein degradation are pursued. The main objective of this thesis was to develop a novel type of chimeras with the capacity to induce the degradation of different proteins by direct signaling to the 26S proteasome by interacting with USP14, a 26S-associated deubiquitinating enzyme involved in substrate processing and allosteric regulation of 26S activity. The overall results obtained in the biological studies provide proof of concept for this 26S-directed PROTAC, which should expand the potential of target protein degradation. Although this novel approach lacks the limitations associated to ubiquitination in the classical E3-protacs (i. e. different tissue or cell types' expression patterns of targeted E3, inadequate levels of Ub and/or Ub signaling factors under stressful circumstances), the formation of ineffective ternary complexes threatening the effectiveness of classical E3-based PROTACs is not circumvented by USP14-directed PROTACS. The linker is one of the factors that may lead to weak ternary complexes. Until very recently, linker design and selection was a "trial and error" endeavor. However, future avenues for rational linker design, including advances in computational methods, will accelerate the identification of optimized PROTACs.

TABLE OF CONTENTS

1. GENERAL INTRODUCTION	19
1.1 Overview	20
1.2 The Game of Ubiquitination	21
1.2.1 Ubiquitin, Ubiquitination, and Ubiquitin Chain Structure.....	22
1.2.2 Writing the Ub Code.....	25
1.2.2.1 Assembling Ubiquitin Chain by Ubiquitin Ligase Enzymes (E3s): The Mystery of Specificity	26
I. RING-type E3s: The Masterminds Behind Ubiquitination and the Master Manipulators of E2 Ubiquitin-Conjugating Enzymes	27
1.2.3 Reading and Interpretation of Ub Code.....	28
1.3 The Proteasome: The Machine of Proteolysis	30
1.4 Therapeutical Approaches Targeting UPS.....	35
1.4.1 Small Molecule Inhibitors.....	36
1.4.1.1 Inhibitors of the enzymatic cascade (E1s, E2s, and E3s) of UPS	36
1.4.1.2 Inhibitors of the 26S Proteasome Complex	37
1.4.1.3 Inhibitors of immunoproteasomes complex	41
1.4.2. Targeted Protein Degradation by utilizing UPS	41
1.4.2.1 The Age of Proteolytic Chimeras: Modulating Reactivity and Versatility...43	
I. The Era of Dependency: Ubiquitin-Dependent Proteolytic Chimeras ..44	
II. The Era of Independence: Ubiquitin-Independent Proteolytic Chimeras.....50	
1.5 The Target Proteins for Degradation	51
2. OBJECTIVES	55
3. RESULTS and DISCUSSION.....	61
3.1. DESIGN OF CHIMERAS.	62
3.2. SYNTHESIS OF CHIMERAS.	71
3.3. BIOLOGICAL EVALUATION	93
4. CONCLUSIONS.....	102

5. EXPERIMENTAL SECCION.....	108
6. REFERENCES.....	188

CHAPTER 1

General Introduction

1.1. Overview

Many vital body functions serve to maintain the state of homeostasis or balance, (i.e. temperature regulation or blood pressure). The same principle applies at the level of a single cell. Proteins such as enzymes are the workhorses inside all cells and they are fundamental for normal growth and renewal. Cells maintain a healthy balance of proteins -Proteostasis- and this important regulation is carried out mainly by the ubiquitin-proteasome system (UPS) and the autophagy-lysosome pathway (ALP), both involved in proteolysis. Since they are in charge of degrading unfolded, misfolded, or damaged proteins that severely impair cellular functions and are linked to aging and age-related diseases (neurodegeneration, cancer, immunological and metabolic diseases, etc.), the majority of which are currently incurable, the UPS and ALP are protein quality control systems in cells¹ attractive for therapeutic intervention. In eukaryotes, the two main proteolytic hubs are proteasomes and lysosomes. Moreover, ubiquitination, as a post-translational modification, is a critical enzymatic modification of proteins to control their degradation through UPS and ALP². In recognition of the substantial importance of both degradation systems, two Nobel Prizes have been awarded: in 2004, Aaron Ciechanover, Avram Hershko, and Irwin Rose were jointly awarded the Nobel Prize in Chemistry for the discovery of ubiquitin-mediated protein degradation and in 2016, Yoshinori Ohsumi was acknowledged with Nobel Prize in Medicine and Physiology for groundbreaking studies on autophagy.

1.2. The Game of Ubiquitination

The UPS is responsible to seek and degrade up to 80% of damaged or faulty proteins or those simply becoming surplus to requirements³, thus maintaining the right proteins in the right amount at the right time. The UPS can malfunction in two ways: it can become overzealous -destroying useful proteins- or restrained -building up harmful proteins-, and the imbalance in UPS is thought to contribute to common diseases like Alzheimer, infectious diseases, cancers, and inflammatory diseases like rheumatoid arthritis⁴. There are thousands of different proteins in any cell at any one time and the UPS must operate appropriately to keep them under control. The UPS marks a targeted protein destined for degradation by using a ubiquitous small protein found in all cells aptly named ubiquitin (Ub); in essence, proteins tagged with Ub are given a death sentence. Cells contain large amounts of Ub, but it cannot attach itself to proteins at random, but in a highly regulated and controlled way to avoid unwanted protein degradation. First, Ub must be primed for action by the E1 Ub-activating enzyme in a process that requires energy in the form of ATP (adenosine triphosphate). The activated Ub is then transferred from E1 onto a second enzyme called E2 Ub-conjugating enzyme (E2), and E2 acts as an escort for Ub to its next destination, the E3 ligase enzyme. The E3 enzyme acts as a platform on which the target protein substrate and the active E2 Ub complex can meet and interact. The E3 enzyme is extremely fussy about exactly which E2 enzyme and which protein can interact with. The correct E2 enzyme loaded with activated Ub can move and position itself on the E3; when both protein and Ub are loaded onto the E3 enzyme, they are brought close enough together for Ub to be transferred to the target protein substrate. The process of ubiquitination of the target protein can be repeated several times to create a polyubiquitin chain on the protein. The creation of the polyubiquitin chain is the death knell for the protein; it provides a clear signal to the cell's waste disposal unit -the proteasome- to start working. The

proteasome binds and removes the polyubiquitin chain and unfolds the protein, which is then threaded through the proteasome chamber where it is hydrolyzed into building blocks to be reused for the synthesis of new proteins. Ub is also recycled in this process (Figure 1)⁵.

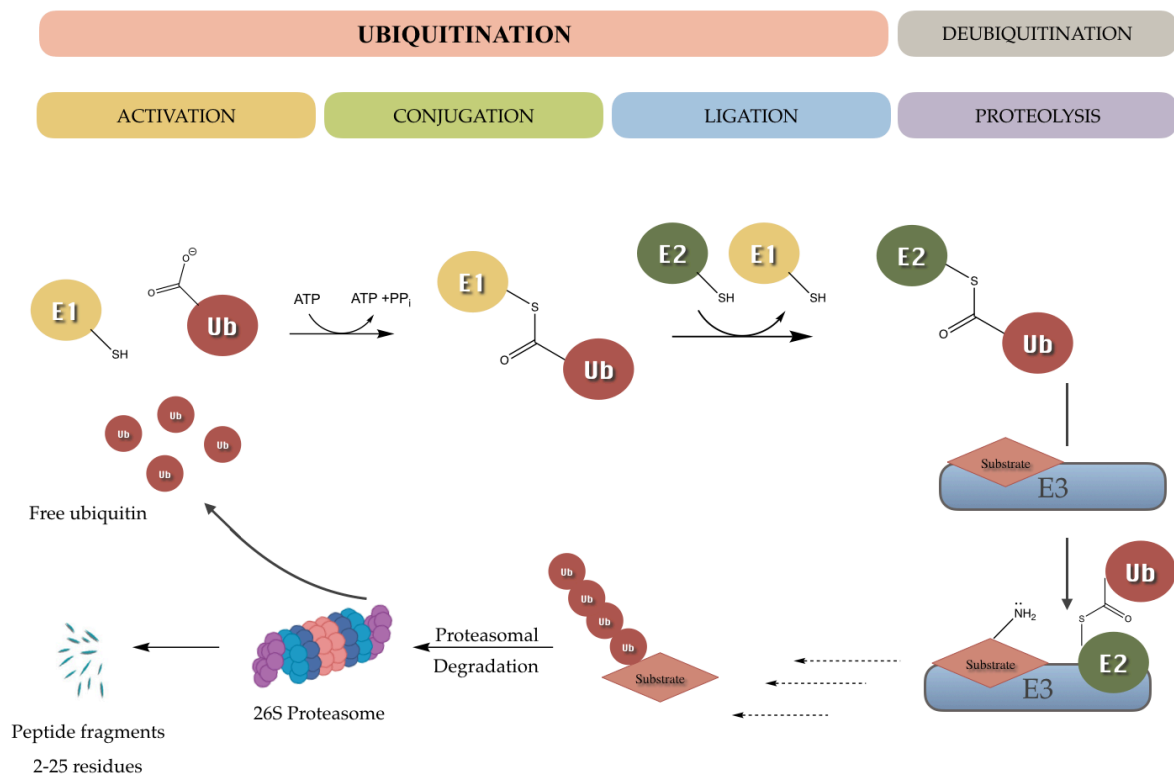


Figure 1. The mechanism of protein degradation through the Ub Proteasome System (UPS).

1.2.1. Ubiquitin, Ubiquitination, and Ubiquitin Chain Structure

Ub is present in all eukaryotic cells. It is a compact 76 amino acid highly stable protein that includes a β -grasp fold, composed of a five-stranded β -sheet that partially wraps around a central α -helix, and a short flexible C-terminal tail that typically ends with at least one glycine residue. The Ub hydrophobic surface contains several regions crucial for interaction with other proteins, such as Ub-binding domains (UBDs), deubiquitinating enzymes (DUBs), E1, E3, and the

proteasome. These regions include the $\beta 1/\beta 2$ loop containing Leu8^{6,7}, and 3 patches: Ile44 (L8, I44, H68 and V70), Ile36 (I36, L71 and L73) and Phe4 (Q2, F4, T14). With respect to the Ub code, the most important feature of the Ub structure is the presence in its surface of seven lysine residues (K6, K11, K27, K29, K33, K48, K63) that, together with the N-terminal methionine (M1), serve as points of ubiquitination. (Figure 2)⁸⁻¹⁰.

Ub is covalently attached to lysine side chains of proteins in a process known as ubiquitination (or ubiquitylation). In this process, the C terminus of Ub (M1) or one of the seven lysine residues are covalently attached to a substrate lysine by an isopeptide linkage, leading to mono-ubiquitination. Multiple lysine residues can form multiple isopeptide linkages with one Ub each leading to multi-monoubiquitination^{11,12}. Furthermore, further modifications of Ub with additional Ub units lead to different polyubiquitinated proteins: with homotypic chains through a particular lysine on Ub or mixed polyubiquitin chains generated by polymerization through different Ub lysines: (Figure 3)^{12,13}. Importantly, these polyubiquitin chains have different cellular roles. Together, they are referred to as the “ubiquitin code”. Thus, K48-linked polyubiquitin chains target the modified proteins to the proteasome for degradation. In contrast, K63-linked polyubiquitin chains regulate proteasome-independent signaling pathways such as DNA repair, inflammatory signaling, and endocytosis. Other types of polyubiquitin chains also exert specific cellular roles. For example, M1-linked chains (also known as linear chains) activate nuclear factor κ B (NF- κ B) signaling, while K11-linked chains regulate proteasomal degradation and intracellular trafficking. Monoubiquitylation serves as diverse signals that trigger cellular processes ranging from epigenetic regulation to proteasomal degradation, which has an enormous impact on cell biology¹⁴.

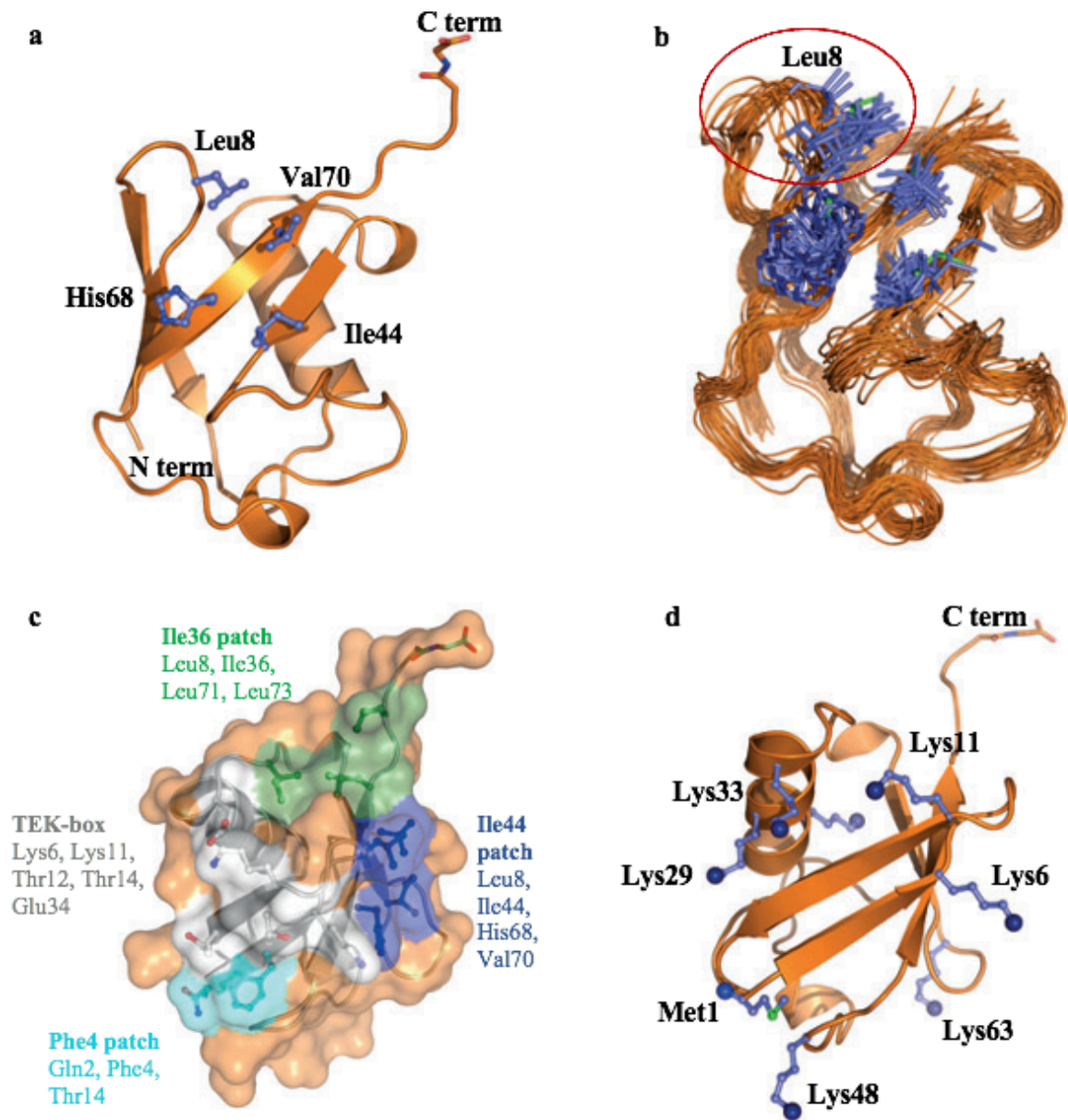


Figure 2. **a:** Structural features of Ub. Protein Data Bank (PDB) codes: 1ubq. **b:** NMR ensemble of Ub (PDB 2k39). **c:** the Ub surface Ile44 (blue), Ile36 (green), Phe4 cyan, and TEK-box (white)^{7,15}.

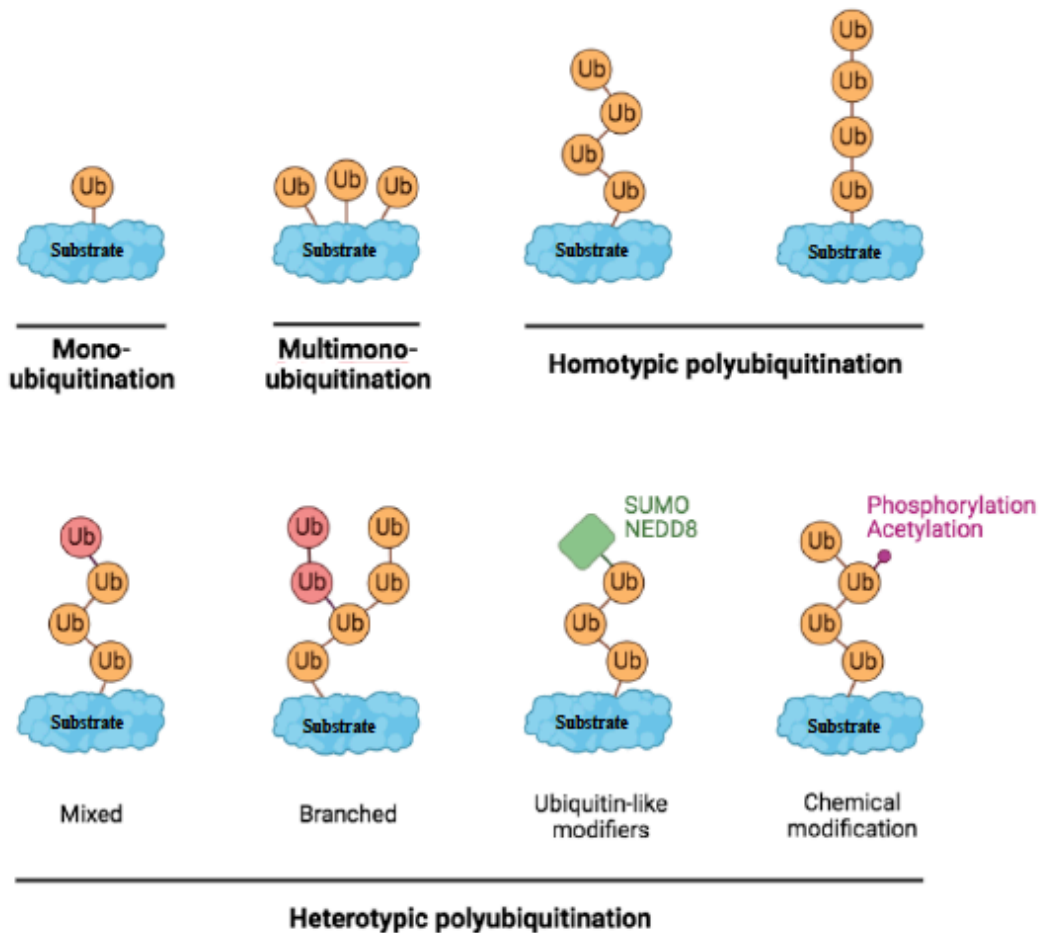


Figure 3. The different topologies of ubiquitylation and Ub chain structure.

1.2.2. Writing the Ub Code

The Ub code is built on the structural diversity of the numerous modifications briefly mentioned above. Writing the Ub code is a process of a three-step enzymatic reactions: (1) Ub activation by the Ub-activating enzyme (E1) in an ATP-dependent manner to form a thioester linkage between the C-terminus of Ub and the active site cysteine of E1; (2) Transfer of the activated Ub to the active site of one of ~40 different Ub carrier proteins (E2; also known as Ub-conjugating enzyme, UBC) via a transthioesterification reaction, and (3) formation of the Ub-protein covalent conjugates mediated by Ub ligase enzymes (E3). E3 interact with both E2~Ub and the substrate to promote the transfer of Ub from E2 to the protein by

forming an isopeptide bond between the Ub C-terminal amino acid (G77) and a lysine residue of the acceptor protein^{16,17}.

1.2.2.1 Assembling Ubiquitin Chain by Ubiquitin Ligase Enzymes (E3s): The Mystery of Specificity

As mentioned above, distinguishing the right substrates from thousands of other proteins, differentiating the right E2s, and bringing them together to increase the rate of Ub transfer is the final step in the ubiquitination cascade, which is carried out by E3 ligases. To seek specificity within a broad array of proteins, a great diversity of E3s (~700) serve dual roles as matchmakers and catalysts to provide a specific Ub signal to a particular target protein. According to their conserved structural domains and their mechanism of Ub transferring, E3 ligases fall into three classes: really interesting new gene (RING), homology to E6AP C terminus (HECT), and RING-between-RING (RBR)^{18,19}. Catalyzing Ub transfer to the acceptor protein by E3s can occur directly from E2 to the substrate lysine via an aminolysis, as is the case in RING-type E3s, or it can take place in a two-step reaction in which Ub is first transferred from E2 to an active site cysteine in E3 via a transthioesterification reaction and then from the E3 to the substrate, as is the case in HECT-type E3s and RBR-type E3s (Figure 4). A series of structural and biochemical studies (mechanism of action of ubiquitination by E3s and their activity regulation) have helped to resolve the mystery behind E3 ligases specificity^{20,21}.

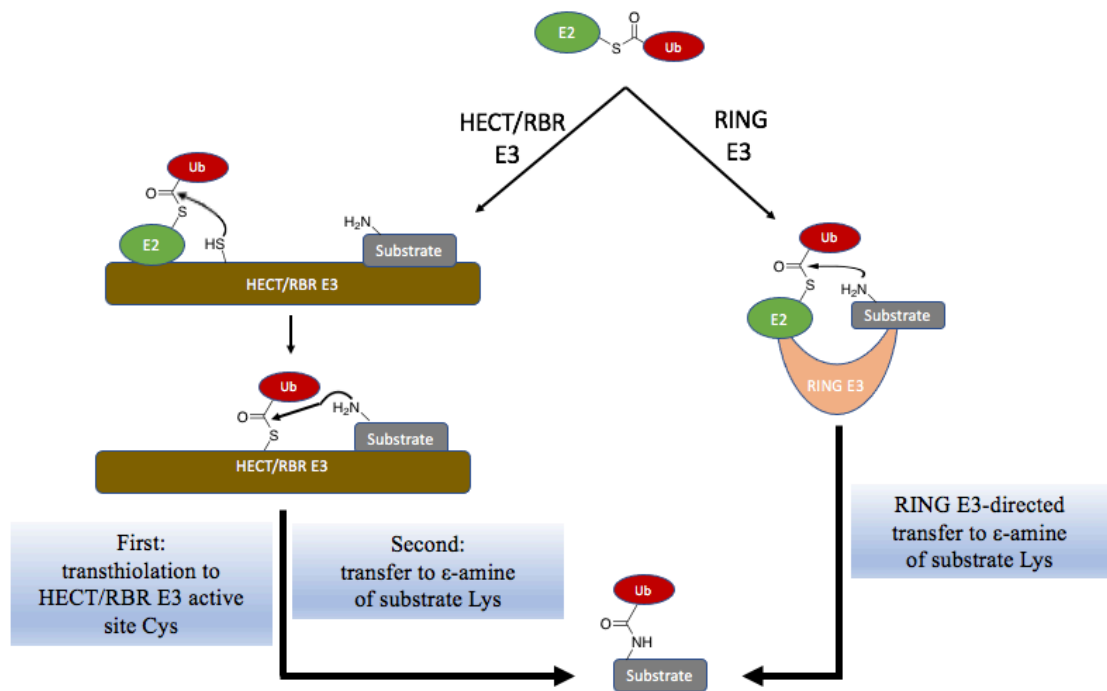


Figure 4: Mechanism of the Ub transfer to a substrate by the three classes of E3s: RING, HECT, and RBR.

I. RING-type E3s: The Masterminds Behind Ubiquitination and the Master Manipulators of E2 Ubiquitin-Conjugating Enzymes

With around 600 members, RING-type E3s and RING like-type E3s, known as U-box proteins, comprise the vast majority (~95%) of E3 ligases. The RING domain is a zinc-finger domain type characterized by two structural zinc ions, two β -strands, one α -helix, and two loops surrounding the zinc ions in cross brace arrangement. The related domain U-box shares the similarity in function and structure of the RING domain; however, it has a hydrophobic core to fulfill the role of metal ions in the RING domain^{22,23}. The morphologies of RING E3 ligases vary; they can be monomeric RING, like c-CBL, monomeric U-box, like E4B, or dimeric, with dimerization either controlled by the RING domain alone or

facilitated by flanking helical regions, such as cIPA (homodimeric RING), CHIP (homodimeric U-box), and BRCA1-BARD1 (heterodimeric RING)²⁴. On the other hand, RING E3 ligases can form multicomponent complexes to assemble the superfamily of RING E3s known as Cullin-RING ligases (CRL). Important members of this family, VHL, CRBN, IAP, and MDM2 have been extensively explored for use in target protein degradation with PROTACS. Cullin-RING ligases contain up to seven multi-subunit families that share the same structural units (scaffold protein, RING-box protein, adaptor protein, and substrate receptor) but with various types of structural units²⁵.

1.2.3. Reading and Interpretation of Ub Code

The final outcomes of the Ub code vary depending on a set of proteins containing single or multiple UBDs, referred to as Ub readers or decoders. The around 300 UBDs classified into nearly 25 subfamilies based on adapted structural folds recognize Ub chain topology and length and enable the execution of specific cellular signaling programmes or proteasomal degradation. Furthermore, intrinsic UBDs frequently dictate how effectively ubiquitinating and DUBs function^{8,26}. The UBDs interact with Ub through the different hydrophobic patches and, more interestingly, with the C-terminal part in a low-affinity way to result in rapid, timely, and reversible cellular responses to a particular stimulus¹¹. Yet, Ub binding's specificity and amplification are necessary for the efficient and prompt delivery of biological information. The UBDs can accomplish preferential recognition of different Ub linkages through a variety of tactics, including the presence of Ub linkage-selective UBDs, differential Ub recognition by UBDs with multiple Ub-binding surfaces, UBD dimerization or through UBD conformational adaptation, as well as the contribution of sequences located outside of UBDs to Ub binding²⁷. The ability of UBDs to sense the length of the Ub chain, cooperative Ub binding by pairing identical or different UBDs, control

of the accessibility of Ub-binding modules (through inter- and intramolecular interactions and steric hindrance), multimerization of Ub-modified proteins and/or Ub receptors, and coupled ubiquitination of UBD-containing proteins are some examples of strategies that can increase the avidity of Ub:UBD interaction (Figure 5)²⁸. As a result of different UBDs' recognition of different surface patches on Ub, linker regions, or the (free) C-terminal tail, various specific cellular events are achieved (Figure 6)¹⁴.

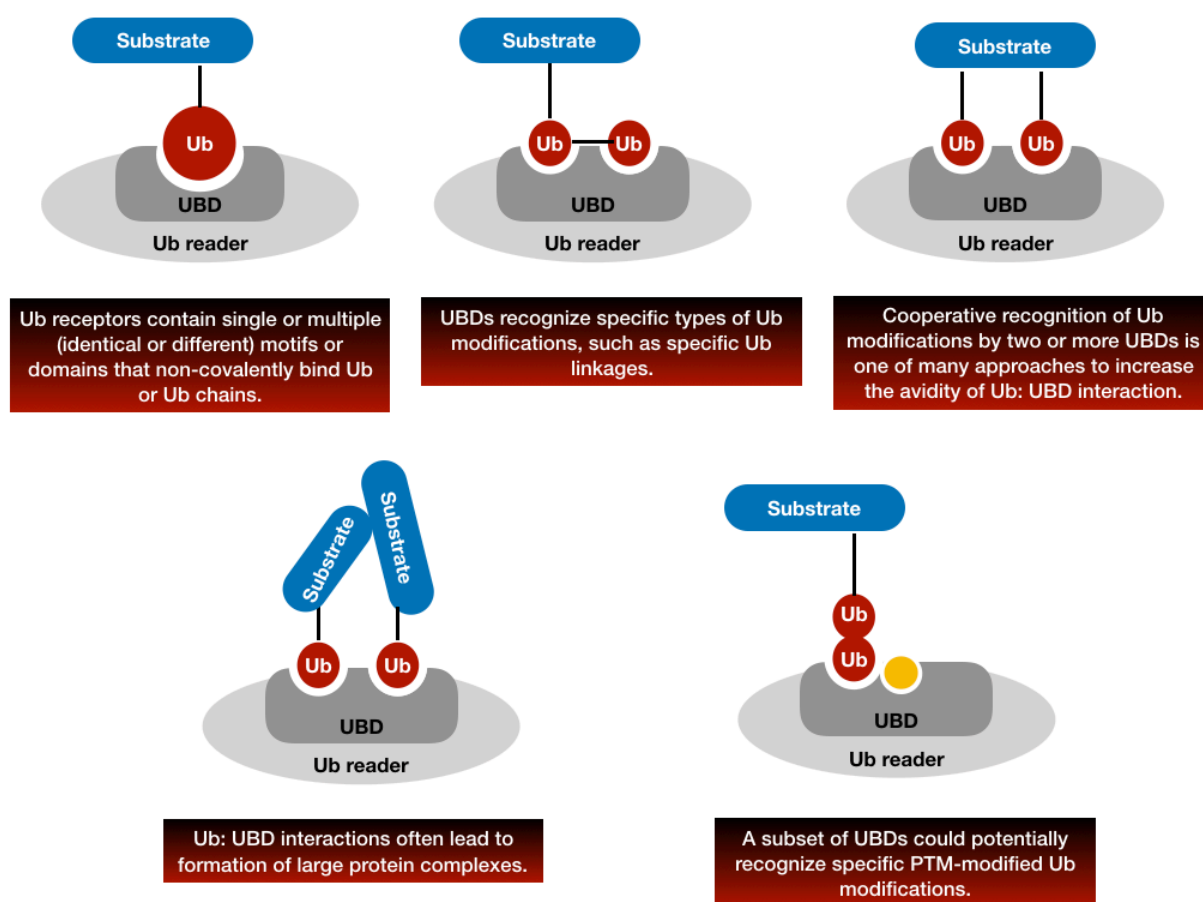


Figure 5: Ub-binding domains come in different shapes and forms to drive different cellular responses.

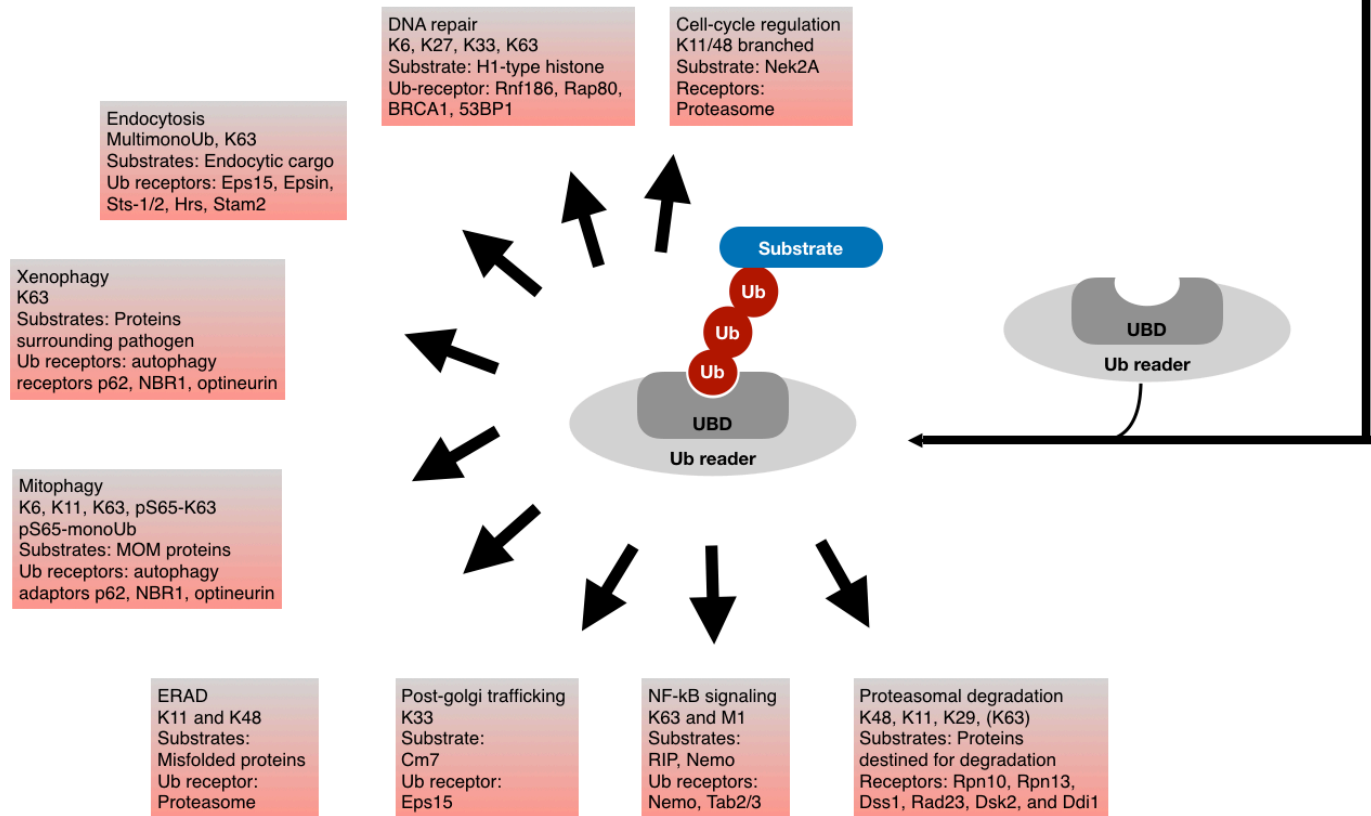


Figure 6: Link of ubiquitination to pathway-specific effectors.

1.3. The Proteasome: The Machine of Proteolysis

Together with autophagy, the proteasome is the cell's main protein degradation machinery. It is an enzyme complex comprised of a core particle (20S, CP), with or without a regulatory particle (19S, RP). Twenty-eight proteins grouped in four heptameric rings make up the assembly of the 20S proteasome²⁹. The rings are made up of either seven alpha- or seven beta-subunits and are stacked one on top of the other. Two beta rings are positioned between two exterior alpha rings to form the α 1-7, β 1-7, β 1-7 and α 1-7 arrangement. The N-terminal portions of the alpha-subunits perform two roles: on the one hand, they create a gate close to

the catalytically active beta-subunits to limit the undesired degradation of proteins, and on the other hand, they make essential contacts with the RP^{30,31}.

The protein hydrolysis within the proteasome is ATP-dependent and is carried out by the N-terminal threonines of three of the seven beta-subunits, which coordinate the nucleophilic attack to the substrate peptide bonds. The three catalytically active beta-subunits follow the same peptide bond hydrolyzing process, but each exhibits varying sequence specificity. As a result, three main proteolytic activities are carried out by proteasomes: caspase-like, trypsin-like, and chymotrypsin-like³². The structural diversity of proteasomes is based on the catalytic beta-subunits composition of the 20S. For instance, the β 1, β 2, and β 5 are the catalytic subunits of constitutive (also referred to as standard 20S) proteasome, which mediate cleavage after acidic (β 1), basic (β 2), or hydrophobic (β 5) amino acids, exhibiting caspase-like, trypsin-like and chymotrypsin-like activities, respectively^{33,34}.

In contrast, type I and type II intermediate proteasomes and immunoproteasomes are different types of the 20S which have different catalytic subunits in place of β 1, β 2, and β 5 of constitutive proteasomes. With a cellular abundance of up to 85%, the constitutive proteasomes dominate the majority of proteasomes³⁵. Because each 20S proteasome has two exterior alpha-subunits that have essential contacts with the regulatory particle, another level of 20S complex diversity can arise from various regulatory particle types. Furthermore, attaching standard 20S to a single 19S regulatory particle result in a 26S proteasome, whereas linking two 19S regulatory particles to both alpha-subunits result in a 30S proteasome³⁵.

The lid and the base are the structurally distinct components of the 19S RP of the 26S proteasome, which has at least 18 protein subunits and is capable of

specifically recognizing ubiquitinated proteins, cleaving the Ub chains, and unfolding and translocating substrates into the 20S core^{29,36}. Two subunits assemble the lid and the base: Rpt (Regulatory particle AAA-ATPase, which breaks down ATP and regulates the proteasome in processing its substrate) and Rpn (Regulatory particle non-ATPase). The lid sub-complex contains nine Rpn subunits (3, 5, 6, 7, 8, 9, 11, 12, and 15) performing as Ub receptors, which hold the ubiquitinated protein in place while Ub hydrolase cleaves Ub from the substrate protein. The most crucial component of the lid is Rpn11, a metalloprotease deubiquitinating enzyme placed atop the Rpt ring's substrate entry port that blocks the substrate entrance at the oligonucleotide- or oligosaccharide-binding (OB) ring³⁷. The base comprises nine subunits, including six Rpt (1-6) proteins belonging to a class of protein unfoldases and 3 Rpn protein (1, 2, and 10). The six Rpt proteins can sense aberrant proteins via N-domains and unfold them via hydrolysis in their ATPase domains. Thus, the Rpt subunits interact with the 20S proteasome and form a heterohexameric ring adjacent to its central pore to perform substrate unfolding, bind to, and facilitate the opening of the 20S proteasome gates (Figure 7)³⁸. The recent models and research indicate that the Rpt subunits differ in their capacity to bind and trigger the entrance to the 20S proteasome gate; the 19S is a dynamic structure and adopts various conformations to enhance substrate binding and ATP hydrolysis, followed by proteolysis by the CP³⁹.

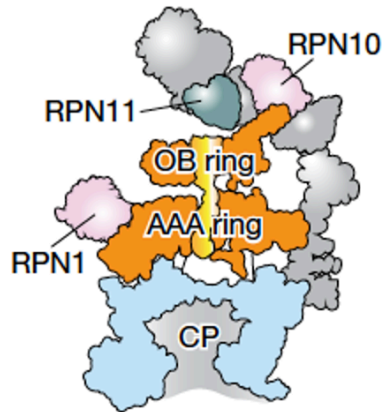


Figure 7: Structure of the 26S proteasome⁴⁰. CP, core particle; RPN, Regulatory particle non-ATPase; AAA ring, Regulatory particle AAA-ATPase; OB-ring, oligosaccharide/oligonucleotide binding ring.

In 26S, the polyubiquitin chain in the protein is not enough for its efficient degradation, and proteasomes need to identify a loosely folded region in the protein. This loosely folded region should be at least 30 residues long, reasonably inflexible, and biased toward its hydrophobic residues. Based on both the Ub chains and the loosely folded parts, the proteasome decides which proteins to destroy and which to spare⁴¹.

Deubiquitination activities, which are catalyzed by DUBs, are noteworthy among the multi-layered processes controlling the proteasome's proteolysis because they not only recycle Ub, but also place the proteasome at a crucial checkpoint for substrate destruction. Among the approximately 100 DUBs, three distinct classes of DUBs, namely USP14, RPN11, and UCH37, are associated with the 19S subunits of the human proteasome. Recent structural and biochemical studies reveal that these enzymes have a dynamic impact on the output of the proteasome. DUBs may therefore fine-tune the degradation in accordance with different cellular circumstances with dynamic proteolysis results⁴².

USP14 is momentarily linked with around 11–40% of isolated proteasomes, indicating the dynamic influence of this DUB over proteolysis. Upon binding to the proteasome, USP14 undergoes a 300–800 fold activation, which is one of its most prominent characteristics^{43,44}. As a result of this isopeptidase activity for the rapid deubiquitination of multiple chains of Ub conjugates at once, USP14 prevents the substrate degradation by reducing its affinity for the proteasome⁴³. The free form of USP14, in contrast, only demonstrates modest deubiquitinating activity. Thus, USP14's interaction with the proteasome is required to de-repress the autoinhibitory state of USP14. In addition to being activated by the proteasome, USP14 can also allosterically regulate the activity of the proteasome^{45,46}.

In an outstanding study using time-resolved cryo-electron microscopy combined with deep learning, Zhang et al⁴⁰ showed the mechanism by which USP14 regulates the proteasome step by step in unprecedented detail. The authors found that USP14 is activated by binding to the entrance ring of the AAA-ATPase by changing its conformation as the proteasome hydrolyses ATP and degrades its ubiquitinated substrate. The authors' data point to two parallel pathways of conformational changes induced by USP14, one that inhibits substrate engagement and another that triggers substrate degradation (Figure. 8). The substrate-engaged states were transiently converted into substrate-inhibited states once the substrate had translocated into the proteasome and been degraded. The overall data suggest a model in which USP14 regulates the proteasome at three checkpoints: Ub recognition, the start of substrate translocation, and recycling of the Ub chain⁴⁰.

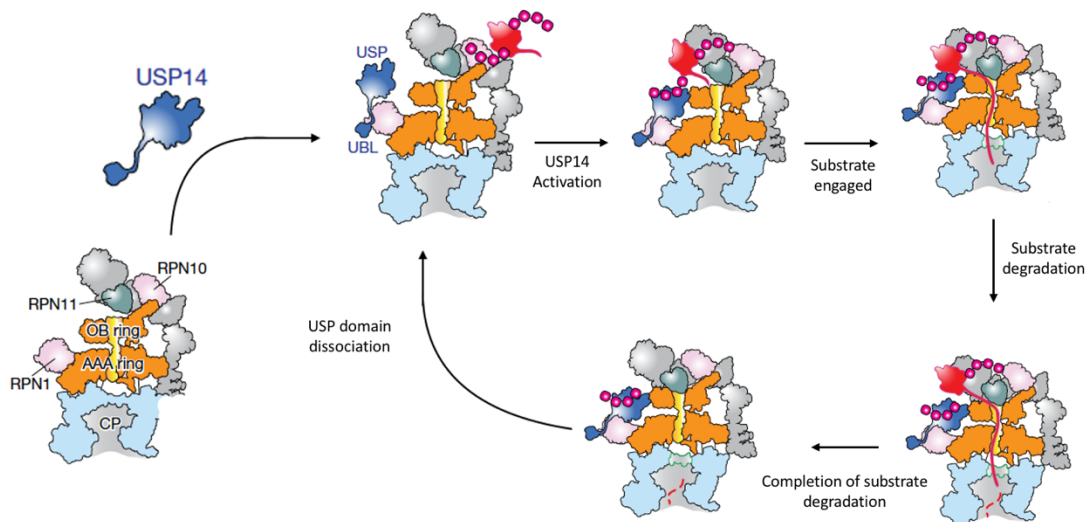


Figure 8: Proposed model of mutual regulation between USP14 and the proteasome based on time-resolved cryo-EM analysis. Credit: Zhang, S. *et al.*, *Nature* 2022, 605, 567–574⁴⁰.

A growing amount of research has conclusively shown that small-molecule-specific inhibition of USP14 increases the degradation of a selection of substrates by increasing proteasomal activity. The mechanism behind the small-molecule USP14 inhibitors' selective inhibition of proteasome-associated USP14, but not the free form, has been revealed in co-crystal structures of USP14⁴⁷.

1.4. Therapeutical Approaches Targeting UPS

In the late 1970s and early 1980s, the discovery of UPS took place. Since then, scientists have been putting tremendous efforts in terms of providing a better understanding of the system and the role of its numerous involved enzymes in different physiological and pathological conditions with the ultimate goal of introducing new therapeutical approaches. For example, during the late 40 years, the Ub system has been targeted at different checkpoints in four different manners; (1) inhibiting ubiquitination cascade enzymes, DUBs, or the proteasomal machinery, (2) blocking the interpretation and translation of Ub

signals, (3) recruiting E3 ligases to form Ub single chains on the desired substrates to induce proteasomal degradation, or (4) inducing the degradation of desired substrates by direct signaling to the proteasome. Collectively, these efforts have resulted in several FDA-approved compounds directed toward UPS.

1.4.1. Small Molecule Inhibitors

1.4.1.1 Inhibitors of the enzymatic cascade (E1s, E2s, and E3s) of UPS

Only UBA1 and NEDD8 E1s have been reported so far and PYR-41 and MLN4924 (Pevonedistat) have been described as E1s inhibitors, respectively. The ability of the PYR-41 inhibitor to irreversibly bind to the active cysteine in UBA1 and abrogate its catalytic activity, which results in cell death via p53-mediated apoptosis, makes it particularly attractive for the treatment of malignancies defined by p53 mutations^{48,49}. The second E1 inhibitor, MLN4924, is an adenosine sulfamate analog that binds covalently to the nucleotide-binding site of NEDD8-activating enzyme (NAE). This leads to a NEDD8-MLN4924 adduct, which further lessens the effectiveness of cullin-RING ligase-mediated protein turnover, resulting in the accumulating of p27, NRF2, CDC25A, HIF1 α , and I κ B and the induction of apoptosis in cancer cells (Table 1)^{50,51}.

Given that Ube2R1 collaborates with the cullin-RING Ub ligase complex enzymes to catalyze substrate ubiquitylation, it is a potential E2 for pharmacological inhibition. A powerful allosteric Ube2R1 inhibitor, CC0651, exhibits extraordinary selectivity to Ube2R1 over other E2s and effectively blocks ubiquitin transfer to the substrate. Covalent inhibitors that target the E2 catalytic cysteine residues have also been reported. Covalent binding of well-known Ubc13 inhibitors, including NSC697923, was shown in co-crystal

structures with Ubc13^{52,53}. More recently, a natural product-derived covalent inhibitor of UbcH5c has been characterized and proposed as a possible treatment for rheumatoid arthritis (Table 1)⁵⁴.

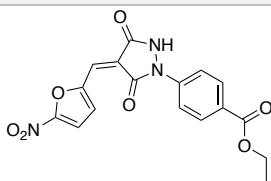
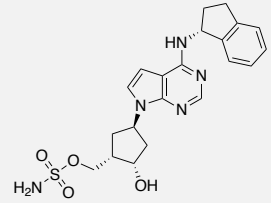
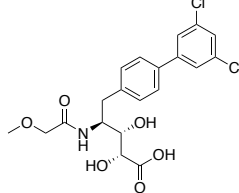
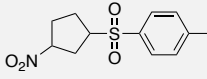
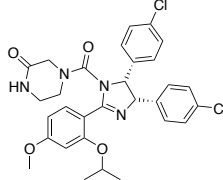
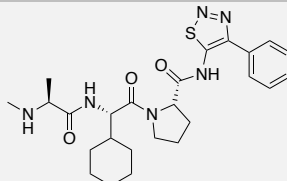
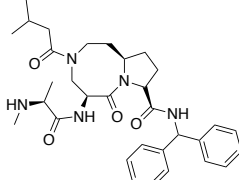
Several compounds have shown their ability to inhibit different E3 enzymes by inhibiting their expression levels, altering their subcellular localization, and preventing their proper assembly and/or interaction with cellular substrates. Nutlin-3a and its derivatives are examples of inhibitors of the E3 ligase MDM2, which negatively regulates p53 and is vital for cell survival. Inhibiting the interaction between MDM2 and p53 has been reported to induce cell death in a p53-dependent manner⁵⁵. Inhibitors of the family of E3 ligases known as inhibitors of apoptosis (IAPs) have also been reported. Both GDC-0152 and SM-406 are orally bioavailable effective inducers of apoptosis in xenograft tumors and produce the complete inhibition of tumor growth. Nevertheless, the clinical trial with both compounds came to an end in phase I in 2009 (Table 1)^{56,57}.

1.4.1.2. Inhibitors of the 26S Proteasome Complex

Inhibiting the 26S proteasome can be achieved by targeting the 20S or the 19S subunits. In the first case, accumulating research efforts resulted in a few approved inhibitors of the 20S core particle. For example, the dipeptide boronate Bortezomib (BTZ, Velcade®) represents the first-in-class proteasome inhibitor by reversibly binding to the $\beta 5$ subunit of the 20S proteasome, leading to inhibition of the chymotrypsin-like proteasomal activity, thus leading to accumulation of polyubiquitinated proteins in cells⁵⁸. Fortunately, the narrow therapeutic window of BTZ, its toxic side effects, and development of resistance during treatment got overcome with a second-in-class proteasome inhibitor, the tetrapeptide epoxyketone Carfilzomib (CFZ, PR-171, Kyprolis®), approved by the FDA in 2012. Ixazomib (the first oral proteasome inhibitor drug), Oprozomib

(a structural homolog of CFZ), and Marizomib are other examples of 20S core particle inhibitors (Table 1)⁵⁹.

While they have different target sites, inhibitors of 19S proteasome regulatory particles, particularly DUBs, are thought to be among the prospective targets for overcoming the acquired drug resistance to proteasome 20S inhibitors. Due to their high effectiveness against cancer cells, the three DUBs of the 19S proteasome, UCHL5 (or UCH37), USP14, and Rpn11, have received extensive attention⁶⁰. For example, IU1 was the first USP14-specific inhibitor, followed by several modifications that resulted in IU1-248, which was ten-fold more potent than the parent IU1. According to its structure, IU1 targets the thiol group of the active site cysteine of USP14⁶¹. Another example of a specific USP14 inhibitor is RA-9, which reacts with the thiol function of the active site cysteine and inhibits proteasome-associated DUB activity⁶². Furthermore, some inhibitors show less specificity by targeting both USP14 and UCHL5, such as b-AP15 and VLX1570, and others show specificity toward Rpn11, such as Quinolin-8 -thiol or 8TQ (Table 1)^{60,63}.

Inhibitors of E1, E2, and E3 enzymes			
Name	Target	Mode of action	Structure
PYR-41	Irreversibly binds to the active cysteine in UBA1.	kills tumor cells by inhibiting cytokine-induced NF- κ B activation and promoting p53 accumulation.	
MLN4924	Covalently binds the nucleotide-binding site of NAE.	Blocks the neddylation of all CRLs, leading to apoptosis in cancer cells.	
CC0651	An allosteric inhibitor of human E2 enzyme hCdc34.	causes large-scale structural rearrangements and affects the discharge of Ub to acceptor lysine residues.	
NSC697923	Competitively binds the Mdm2-P53 interacting site.	Blocks the formation of the E2-Ub thioester conjugate and inhibits NF- κ B signaling.	
Nutlin-3a	Competitively binds the Mdm2-P53 interacting site.	activates the P53 pathway, and thus results in cell cycle arrest, cell death, and growth inhibition.	
GDC-0152	Blocks the formation of the E2-Ub thioester conjugate.	induction of apoptosis in xenograft tumors, and is capable of inhibiting tumor growth.	
SM-406	Blocks the formation of the E2-Ub thioester conjugate.	Induction of apoptosis in xenograft tumors and is capable of inhibition of tumor growth.	

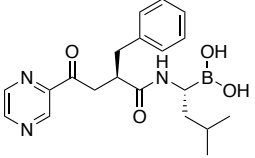
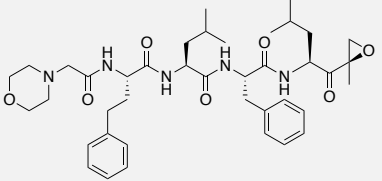
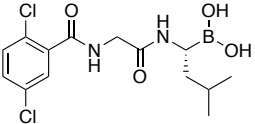
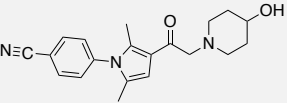
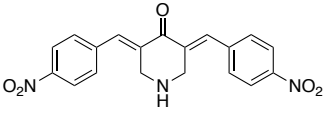
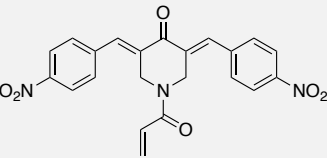
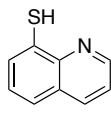
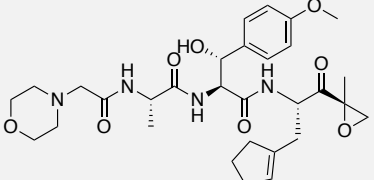
Inhibitors of 26S Proteasome and immunoproteasome complex			
Name	Target	Mode of action	Structure
Bortezomib	20S Proteasome ($\beta 5 > \beta 1$)	Inhibits the chymotrypsin-like activity of the proteasome by reversible binding to the $\beta 5$ subunit and leads to accumulation of polyubiquitinated proteins.	
Carfilzomib	20S Proteasome $\beta 5$	Inhibits chymotrypsin-like activity of proteasome more strongly than BTZ by forming a covalent and an irreversible bond with catalytic subunits, predominantly $\beta 5$.	
Ixazomib	20S Proteasome ($\beta 5 > \beta 1$)	Binds to catalytic β - subunits and inhibits proteasome activity.	
IU1-248	19S RP of Proteasome USP14	Targets the thiol group in the active cysteine site in USP14 protease and significantly decrease cell proliferation, migration, and invasion.	
RA-9	19S RP of Proteasome USP14	Reacts with the sulfurs in the active site cysteine and inhibits proteasome-associated DUBs.	
b-AP15	19S RP of Proteasome both USP14 and UCHL5	Targets both UCHL5 and USP14, disrupts the aggresome formation in cancer cells by activating caspase to further induce apoptosis relating to an upregulation of oxidative stress.	
8TQ	19S RP of Proteasome RPN11	A strong RPN11-specific inhibition of proteasome 19S subunit and is a potent apoptosis inducer in MM cells.	
KZR-616	20S immunoproteasome ($\beta 5i, \beta 1i, \text{ and } \beta 2i$)	The only epoxyketone-based peptidyl immunoproteasome selective inhibitor tested in clinic so far.	

Table 1: Examples of UPS small molecule inhibitors.

1.4.1.3. Inhibitors of immunoproteasomes complex

It has been reported that immunoproteasomes are capable of digesting misfolded proteins that produce aggresome-like protein conjugates with greater efficiency than constitutive proteasomes, making them crucial for eliminating damaged proteins in inflammatory states. According to a number of studies, B-cell malignancies exhibit significantly higher expression levels of immunoproteasome than constitutive proteasomes. This finding highlights the immunoproteasome's significance in regulating protein homeostasis in hematologic diseases and raises the possibility of treating cancer by immunoproteasome activity inhibition^{64,65}. In this regard, ONX-0914, PR-924, and KZR-616 are tripeptide epoxyketone inhibitors that show selectivity toward immunoproteasome $\beta 5i$ over $\beta 5$ in the constitutive proteasome. It is noteworthy that KZR-616 is the only clinically evaluated immunoproteasome-selective inhibitor that has been FDA-approved (Table 1)^{66,67}.

1.4.2. Targeted Protein Degradation by utilizing UPS

In 2001, the initial hypothesis of targeted protein degradation (TPD) was born to announce the launching of a new era of therapeutics development not by inhibiting a component of UPS, but by recruiting the whole system to induce the degradation of specific proteins⁶⁸. TPD techniques can efficiently target long-lived proteins since they are not constrained by protein turnover, thus overcoming some of the drawbacks of UPS inhibitors. The majority of these technologies also share the advantageous pharmacokinetic characteristics of small compounds resembling drugs. Importantly, due to their various modes of action, they may expand the conventional druggable space. Many technologies with the therapeutic potential of targeting protein for degradation have been under massive study and development, including PROteolysis TArgeting Chimeras (PROTACs), LYsosome TArgeting Chimeras (LYTACs), AUtophagy TArgeting

Chimera (AUTAC), ENDosome TArgeting Chimeras (ENDTACs), and Autophagy-Tethering compound (ATTEC) (Figure 9)⁶⁹. Since PROTACs and HyTAGs are of relevance in this thesis, they will be further introduced in the following section.

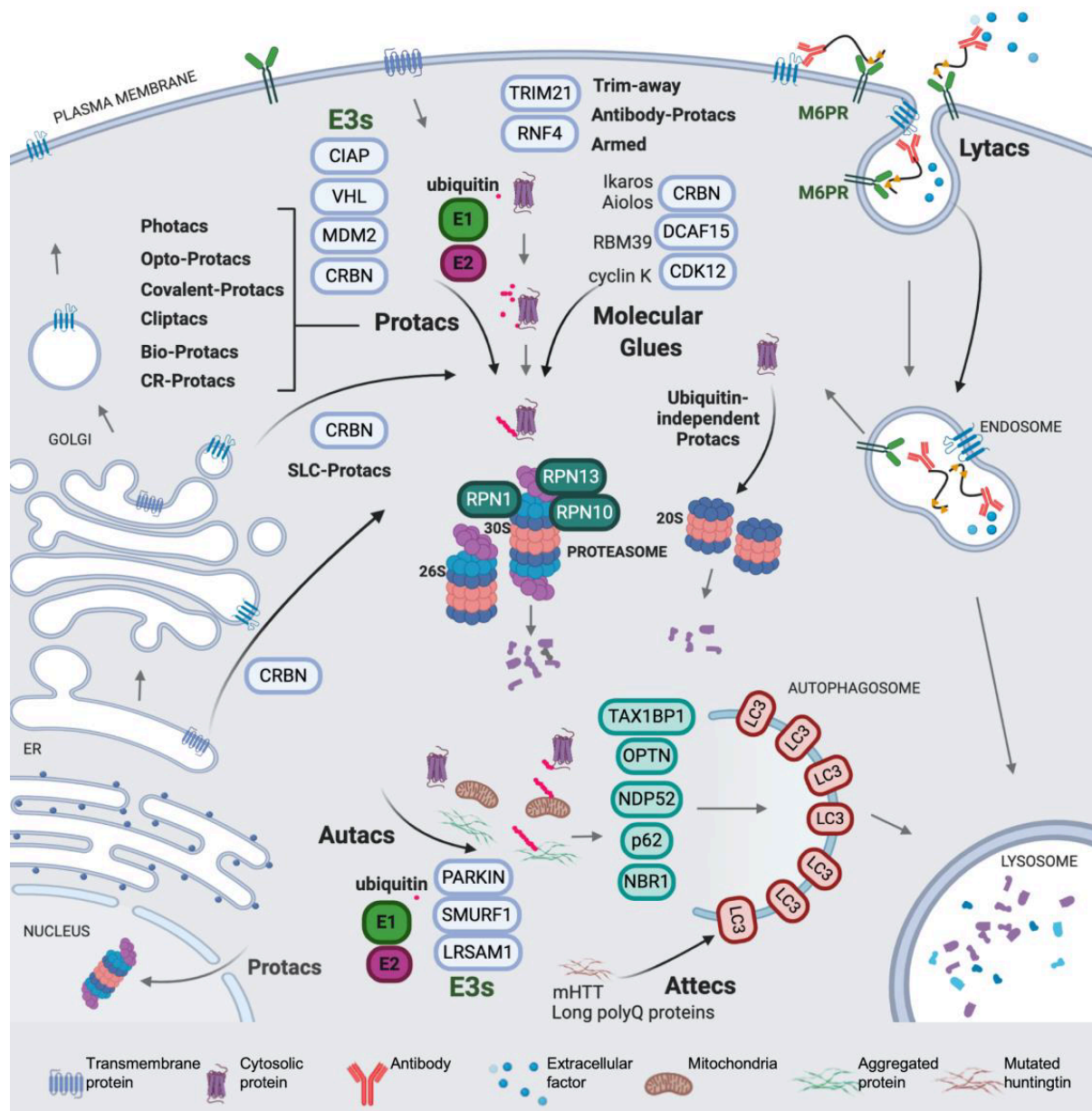


Figure 9: Schematic representation of the main routes of TPD in the cell⁶⁹.

1.4.2.1 The Age of Proteolytic Chimeras: Modulating Reactivity and Versatility

Following the establishment of the proteolytic chimeras' applicability concept by PROTAC technology, tremendous efforts have been put forth to modulate their reactivity by developing strategic chemical modifications. This resulted in the achievement of new and more versatile chimeras. PROTAC is a strategy that utilizes the UPS to target a specific protein and induces its degradation by employing hetero-bifunctional molecules consisting of a ligand to bind the protein of interest (POI), another ligand to recruit an E3 Ub ligase and a linker to bind the two ligands. These molecules interact simultaneously and hijack the enzymatic machinery by forming a ternary complex (POI:PROTAC:E3 ligase) that facilitates the transfer of Ub moieties and the formation of polyubiquitin chain(s) on the target protein. The polyubiquitinated protein will be recognized and promoted to degradation by the proteasome (Figure 10)⁷⁰.

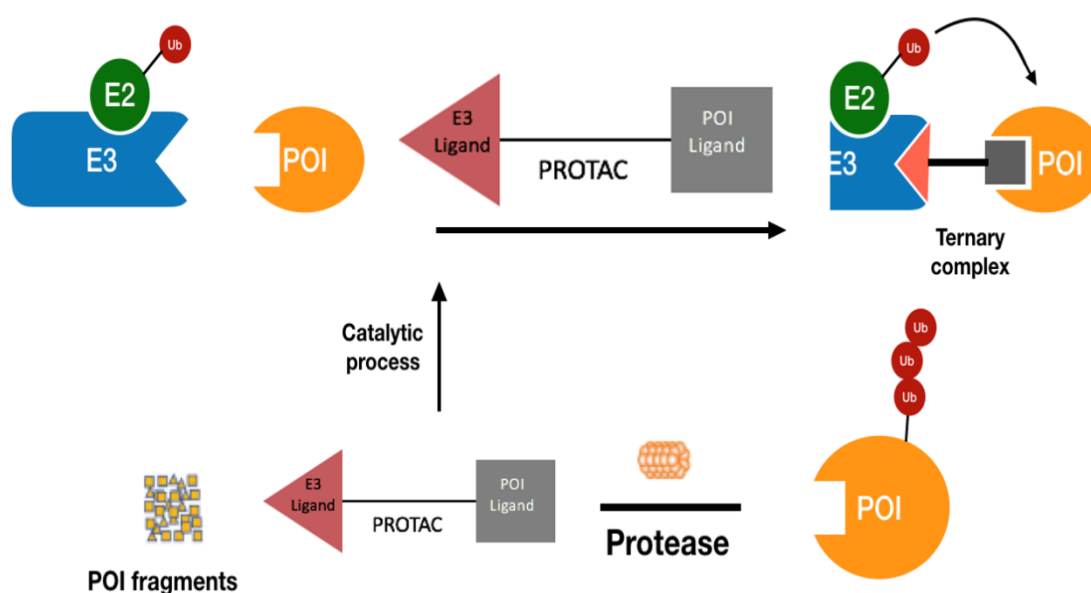


Figure 10: Schematic representation of PROTAC-mediated ubiquitination and proteasomal degradation.

I. The Era of Dependency: Ubiquitin-Dependent Proteolytic Chimeras.

In 2001, a peptide-based PROTAC (PROTAC-1) jointly developed at Craig Crews and Raymond Deshaies laboratories was the starting spark for PROTAC technology⁶⁸. The ternary complex (POI:PROTAC:E3 ligase) of PROTAC-1 contained the covalent inhibitor ovalicin as a ligand for methionine aminopeptidase-2 (MetAP-2), a phosphopeptide derived from I κ B α as a ligand of CRL1^{bTRCP} E3 ligase, and a linker to connect both elements. In *Xenopus* egg cell extracts, PROTAC-1 exhibited the formation of the ternary complex (MeAP-2:PROTAC-1:CRL1^{bTRCP}), and it successfully induced ubiquitination and subsequent 26S proteasome-dependent depletion of MetAP-2⁶⁸. As a result of this achievement, two additional peptide PROTACs were produced from the same phosphopeptide for degradation of the androgen receptor (AR) and the estrogen receptor (ER), two hormone receptors linked to the advancement of breast and prostate cancer, respectively^{68,71}. One significant result was that E3 ligases could readily take neo-substrates by forming the correct protein-protein contacts, which was amply supported in subsequent investigations and is, in fact, the molecular basis for the PROTAC approach's widespread applicability. Furthermore, these molecules gave rise to the initial proof that the PROTAC method does not require covalent interactions with both the POIs and the E3 ligase receptors to cause the proteolysis of a substrate.

Even though peptide-based PROTACs were valuable tools for fundamental research, their low potency (usually in the micromolar range) and metabolic instability in cells due to high protease sensitivity made them unlikely to be used as therapeutic agents⁷². Furthermore, the initial chimeric compounds were large

(they contained phosphopeptides with up to 18 amino acids), hindering their development and pharmacological use. Following the development of this fundamental concept, a considerable amount of effort was put into creating druggable small compounds with enhanced properties based on the structural framework of the E3 ligand-linker-POI ligand. The von Hippel-Lindau (VHL) protein component of the CRL2^{VHL} E3 ligase complex, resulted in 2004 in the first cell permeable PROTAC formulated and used to degrade some clinically significant proteins, such as the AR, the aryl hydrocarbon receptor, the X-protein of the hepatitis B virus, Tau,^{73,74} BRD4 and RIPK2^{69,75}.

The VHL protein has been extensively used in PROTAC technology. In 2012, VHL-1, with high VHL-binding affinity, was developed followed by VHL-2, which was an optimization of VHL-1 by the introduction of an (*S*)-methyl group on the benzylic carbon atom and showed three times better binding affinity to VHL. These two VHL ligands have been widely used in VHL PROTACs ever since. Connection via an amide bond after *tert*-leucine of VHL ligand 1 was present in the majority of VHL PROTACs, whereas the same connection of the (*S*)-methyl group-containing ligand was only present in around one-third of degraders. A phenolic group at the benzene ring was used for linkage less frequently, at roughly 4%. Comparatively, only about 1% of PROTACs had an attachment via a thioether at the left-side amino acid (Figure 11)⁸¹.

Besides VHL, MDM2 (murine double minute 2 homolog), cIAP1 (member of the inhibitor-of-apoptosis protein family), and CRBN (cereblon) are other common CRL complexes effectively used to develop small-molecule PROTACs to date⁷⁶. In 2008, the first small-molecule MDM2-based PROTACs targeting non-steroidal selective AR modulator was reported. Even though it was less effective than its VHL peptide-based equivalents, the MDM2-based chimera promoted AR depletion in prostate tumor cells⁷⁷. Furthermore, since MDM2 binds the *p53*

tumor suppressor protein with high affinity and negatively modulates its transcriptional activity and stability, MDM2-recruiting PROTACs provide synergistic antiproliferative activity via simultaneous degradation of tumorigenic proteins and stabilization of p53⁷⁶. As a result, MDM2-based PROTACS have emerged as promising for cancer treatment. MDM2 recruitment is generally achieved by nutlin-3a (Table 1), a small compound that binds to MDM2 at the p53 interaction interface leading to disrupting MDM2-p53 protein interaction without changing the E3 ligase activity of MDM2.

By controlling the expression of numerous important oncogenes, bromodomain-containing protein 4 (BRD4), a transcriptional and epigenetic regulator belonging to the bromodomain and extra-terminal domain (BET) family, plays a crucial role in the genesis of cancer. Since BRD4 inhibition by small molecules has been demonstrated to induce early cell cycle arrest and death in leukemic cell lines, it has garnered considerable interest in cancer therapy⁷⁸. Targeting BRD4 for degradation instead of inhibition, the MDM2-based PROTAC A1874, consisting of a BRD4 ligand, a polyethylene linker, and idasanutlin (a more potent MDM2-binder than nutlin-3a) showed degradation of BRD4 with nanomolar potency and displayed a remarkable antiproliferative activity against various cancer cell lines⁷⁶.

X-linked IAP (XIAP), cellular IAP 1 and 2 (cIAP1 and cIAP2), livin (ML-IAP), and IAP-like protein 2 (ILP2) are five of the eight inhibitors of apoptosis (IAPs) protein family involved in several signaling pathways that control cell fate. All of them contain a RING-type E3 ligase domain and are utilized in PROTAC technology^{79,80}. The first generation of IAP-based PROTACs, also known as specialized non-genetic IAP-dependent erasers (SNIPERs), was sparked by the finding that methyl bestatin could bind to cIAP1, causing its self-ubiquitination and degradation⁸⁰. The replacement of bestatin with the IAP antagonist LCL161,

which preferentially recruits XIAP rather than cIAP, has helped to overcome the main drawbacks of the first generation of SNIPERs, such as low potency and off-target side effects, and has produced an improved new generation of IAP-based PROTACs with nanomolar potencies⁷⁸.

Taking advantage of the ability of immunomodulatory imide drugs (ImiD) to hijack the CRL4^{CRBN} E3 ligase via cereblon (CRBN), the substrate recognition component of the CRL4^{CRBN} E3 ligase complex, many small-molecule CRBN-based PROTACs have been reported targeting different disease-related proteins⁷⁰. The known ligands for CRBN include thalidomide and other derived immunomodulatory imide drugs (IMiDs), such as pomalidomide, 4-hydroxy thalidomide, alkyl-connected thalidomide derivatives, or lenalidomide (Figure 11)⁸¹.

Although in terms of efficacy, metabolic stability, and physicochemical characteristics, small-molecule PROTACs are better than their peptide-based counterparts, they still have rather large sizes (usually 700–1100 Da) and high polar surface areas, which can hinder their cellular uptake and jeopardize their bioavailability and pharmacokinetic features, particularly with regard to how they are distributed throughout the central nervous system (CNS). In order to get over some of the PROTAC's limitations, a new PROTAC technique called "in-cellulo click-formed proteolysis targeting chimeras" (CLIPTACs) was developed. The two-clickable CLIPTAC precursors are smaller and exhibit superior cell permeability than the corresponding full PROTAC, which is generated inside the cells⁸¹.

Overall, the majority of reported PROTACs recruit the E3 ligases CRBN or VHL^{81,82}.

Although high-affinity ligands for MDM2, VHL, CRBN and cIAP1 have been discovered, the human proteome contains around 600 E3 ligases, but high-affinity ligands have been discovered for only very few of them, which is one of the drawbacks of E3-based PROTACS. Widening the toolbox of hijackable E3 high-affinity ligands capable of inducing the ternary complex formation and persisting long enough for ubiquitination to occur is crucial to overcome the potential disadvantage of the emergence of drug resistance resulting from relying solely on CRBN or VHL for PROTAC development⁸⁵⁸⁶.

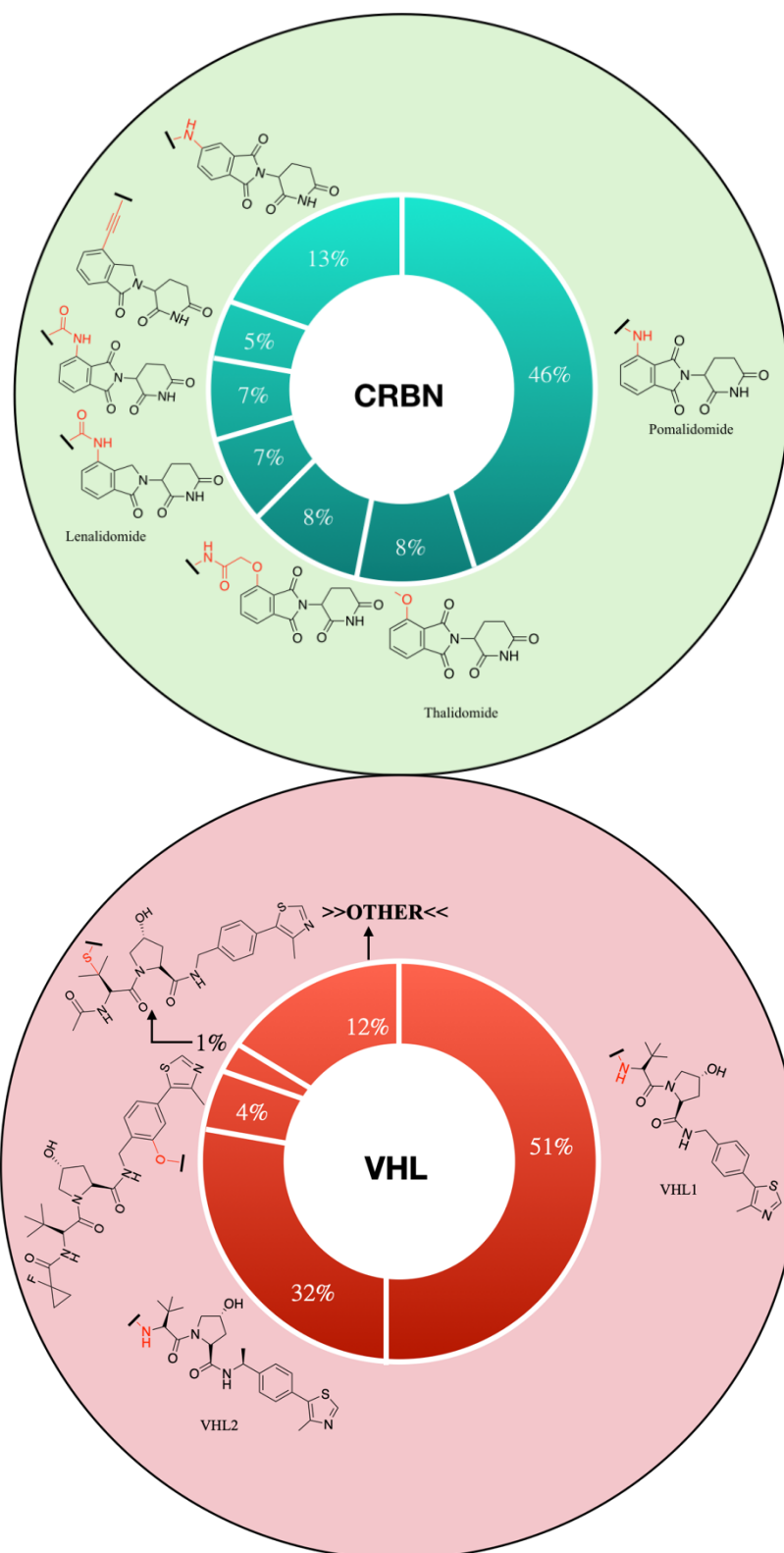


Figure 11: green: Frequency of CRBN ligands used in PROTAC compounds. **red:** Frequency of VHL ligands used in PROTAC compounds.

II. The Era of Independence: Ubiquitin-Independent Proteolytic Chimeras

- **Hydrophobic tags (HyTAGs)**

The most widely employed hydrophobic tags to cause protein degradation when joined to particular ligands are generally adamantyl and Boc₃Arg. Adamantyl-tagged recognition ligands ubiquitinate and eventually degrade their target proteins through the proteasome by destabilizing the target and attracting the molecular chaperone heat shock protein 70 (Hsp70)⁶⁹. In this strategy, promoting the ubiquitination process and proteasomal degradation is achieved by the addition of a hydrophobic tag into a ligand by which the exposure of hydrophobic residues to the solvent may be recognized by molecular chaperones as the signal of a misfolded protein. If the molecular chaperones fail to rescue misfolded protein, the proteasome degradation of the hyTAG modified protein will occur⁸⁷. Examples on this technology include AR degraders by adding an adamantyl tag to an AR agonist, resulting in AR depletion, reduced expression of AR target genes and inhibition of proliferation in androgen-dependent prostate cancer cell lines⁸⁸. These results suggest that selective AR degradation may be an effective therapeutic prostate tumor strategy in the context of AR mutations that confer resistance to second-generation AR antagonists. Another hydrophobic tag used in Ub independent protein degradation is the *tert*-butyl carbamate (Boc₃)-protected arginine unit, which was discovered by serendipity⁸⁹. The covalent inactivators ethacrynic acid and thiobenzofurazan cause the specific degradation of glutathione-S-transferase in mammalian cells when linked to Boc₃Arg⁹⁰. Similarly, the degradation of dihydrofolate reductase is induced when cells are treated with the non-covalent inhibitor trimethoprim linked to Boc₃Arg⁹⁰. In 2020, Merck developed a number of small-molecule binders of the proprotein convertase subtilisin-like/kexin type 9 (PCSK9), a therapeutic target in

hypercholesterolemia, to yield different PCSK9 degraders. Among Merck PCSK9-PROTACs, it should be noted that E3 ligase-based PROTACs did not cause degradation, while the Boc₃Arg tagged ligand was able to cause a notable drop in PCSK9 endogenous levels, even though full target depletion was not achieved⁹¹.

- **26S proteasome-directed degraders**

In a very recent study (2023), a 26S proteasome regulatory subunit Rpn1 macrocyclic binding partner was connected to a BRD4 ligand via a polyethylene glycol linker in another example of a Ub-free strategy for targeted protein degradation⁹². The Rpn1 macrocyclic ligand positions the BRD4 substrate to the Rpn1 region, presenting it directly to 26S without the need for prior ubiquitination, in a Ub-independent mechanism of targeting. The complex structure of the macrocyclic Rpn1 recruiter limits its therapeutic development.

1.5 The Target Proteins for Degradation

Three target proteins for degradation, all of them of therapeutic relevance, have been addressed in this thesis: Inosine-5'-Monophosphate Dehydrogenase 2 (IMPDH2), Receptor Tyrosine Kinases (RTKs), and the Ceramide Transfer Protein (CERT).

I. IMPDH

IMPDH is the rate-limiting enzyme in the *de novo* synthesis of guanine nucleotides. It catalyzes the conversion of inosine 5'-monophosphate (IMP) to xanthosine 5' monophosphate (XMP). Therefore, it plays a vital role in the regulation of cell growth. There are two isoforms of IMPDH in humans: IMPDH1

and IMPDH2, which share 84% amino acid identity. IMPDH1 is the main species in normal cells, while IMPDH2 predominates over IMPDH1 in tumor cells⁹³. Inhibition of IMPDH2 has become an important strategy in treating diseases related to immunosuppression, cancer, and viral and parasitic infections and, more recently, is in clinical trials for COVID-19⁹⁴. There are three types of IMPDH inhibitors: (1) IMP site inhibitors that occupy the binding position of the natural substrate; (2) IMP NAD⁺ site inhibitors that occupy the site of the NAD⁺/NADH cofactor, and (3) allosteric inhibitors that bind to a site remote from the IMP and NAD⁺ binding pockets. . Among the novel IMPDH inhibitors reported in the last decade, VX-497 has been introduced as a new noncompetitive inhibitor and it has shown immunosuppressive activity⁹⁵.

II. RTKs

The bulk of growth factor receptors are made up of cytoplasmic, transmembrane, and extracellular tyrosine kinase (TK) domains. Fiftyeight of the 90 distinct tyrosine kinase genes found in the human genome encode proteins termed receptor tyrosine kinases (RTKs). RTKs are embedded in the plasma membrane of cells and are high-affinity cell surface receptors for a variety of polypeptide growth factors, cytokines, and hormones. The ErbB family of receptors is a group of four closely related RTKs, including the epidermal growth factor receptor (EGFR), HER2 (ErbB-2), HER3 (ErbB-3), and HER4 (ErbB-4). RTKs function in cell signaling by interacting with extracellular molecules⁹⁶. Numerous critical functions, including cell growth and survival, are regulated by RTK activation. The RTK in an irregular state has been identified in a variety of malignancies and has been linked to the onset as well as the progression of several cancers. Consequently, RTKs are becoming appealing therapeutic targets. Inhibiting RTK's catalytic activity with small-molecule inhibitors is one technique to successfully block RTK signaling. Because preclinical studies have revealed that HER-2 and EGFR act cooperatively to transform NIH3T3 cells, it has been

hypothesized that HER-2, the most common heterodimerization partner of EGFR, may play a significant role in the carcinogenic activity of EGFR⁹⁷. Recent research has demonstrated that EGFR-specific inhibitors lessen the proliferation of breast cancer cells that express high levels of HER-2 and the signals it produces. Therefore, inhibiting both EGFR and HER-2 collectively may be more effective than inhibiting each one of them alone. The tyrosine kinases HER-2 and EGFR are selectively inhibited by a synthetic small molecule known as lapatinib^{96,97}. In 2018, targeted RTK degradation by a VHL-recruiting PROTAC utilizing lapatinib as an RTK ligand⁹⁸ was successfully applied and showed several advantages over inhibition, such as more potent inhibition of cell proliferation, and a more durable and sustained downstream signaling response.

III. CERT

The heterogeneous class of biomolecules known as lipids has historically been attributed to play structural and energy-storage functions in the cell. This paradigm, however, has steadily shifted over time, and today lipids are acknowledged as significant effectors in a number of signaling events. Sphingolipids (SLs), a broad category of lipids with sphingosine as their backbone, are crucial elements of cell membranes and significant players in cell signaling, playing a key role in processes like cell proliferation, differentiation, and apoptosis⁹⁹. The precise control of a network of highly compartmentalized yet interconnected enzymatic pathways is essential for maintaining SL homeostasis. The intersection of these interrelated metabolic pathways is where ceramide (Cer), the *N*-acylated form of sphingosine (Sph), stands. Cer plays a crucial role as a ubiquitous modulator of the apoptotic response and a metabolic doorway to a variety of bioactive SLs, in addition to being important skin barrier elements¹⁰⁰. Cer, more specifically, maintains a state of equilibrium and provides a tactical manifold to direct cellular fate. This equilibrium is disturbed in tumor cells by an up-regulation of the Cer metabolism-related enzymes. The intricacy

of this metabolism results from a combination of factors, including the large number of enzymes and SLs involved, as well as the unique subcellular location of the enzymes, which is connected with the strong hydrophobicity of the majority of these lipids. In light of these two factors, transporting SLs between membranes necessitates specialized transport methods. In order for Cer, which is produced by *de novo* synthesis on the cytosolic side of the endoplasmic reticulum (ER), to undergo further transformations, it must be transferred to the trans-Golgi region. The Cer transfer protein (CERT) selectively transports Cer so that it can be transformed by the sphingomyelin synthase 1 into sphingomyelin (SM), while the O-glycosylation follows a vesicular pathway. Thus, by regulating Cer levels, CERT affects the Cer regulated signaling pathways¹⁰¹.

In this regard, in drug-resistant cell lines that overexpress CERT, sensitization to chemotherapeutic drugs like taxanes was reported to be achieved by inhibiting the activity of CERT¹⁰² with HPA-12, a gold standard inhibitor of CERT mediated *de novo* SM production¹⁰². The CERT protein is an intriguing new actor in several other disorders besides cancers. Thus, it has been demonstrated to bind to serum amyloid P-component and to be present in Alzheimer's disease patients' brain amyloid plaques¹⁰³.

CERT fulfils the optimal requirements for the application of the PROTAC technology. First, structural information (PDB) is available, which will ease the design of ligands and linkers, crucial to ensure the success of the PROTAC strategy. Second, well-characterized CERT ligands have been reported for CERT, an issue of paramount importance. Third, CERT is a cytosolic protein, for which the PROTACS technology is better suited¹⁰⁴.

CHAPTER 2

Objectives

The fact that certain proteins are degraded by the proteasome under physiological conditions in the absence of a Ub signal indicates that tagging the protein substrate with Ub is not intrinsically required to induce proteolysis¹⁰⁵. Instead, the key event is the proper localization of the substrate in the proteasome context. This is, making the protein substrate topologically accessible to the ATPase ring in the same way that the polyubiquitin signal does will induce the unfolding and translocation of the substrate to the CP. According to this, a “degradation belt” can be defined, including accessible surfaces of Usp14, Rpn1, Rpt1-6, Rpn10, Rpn2, and Rpn13 and the ATPase ring, which could be potentially used as docking sites for direct protein targeting.

Inspired by the principles of PROTAC technology and the proteasome machinery, the **global objective** of this Ph. D. thesis is to achieve a novel type of chimeras to obtain proof of concept that target protein degradation can be attained by direct signaling to the proteasome using the USP14 regulatory particle as a recruiter (Figure 12).

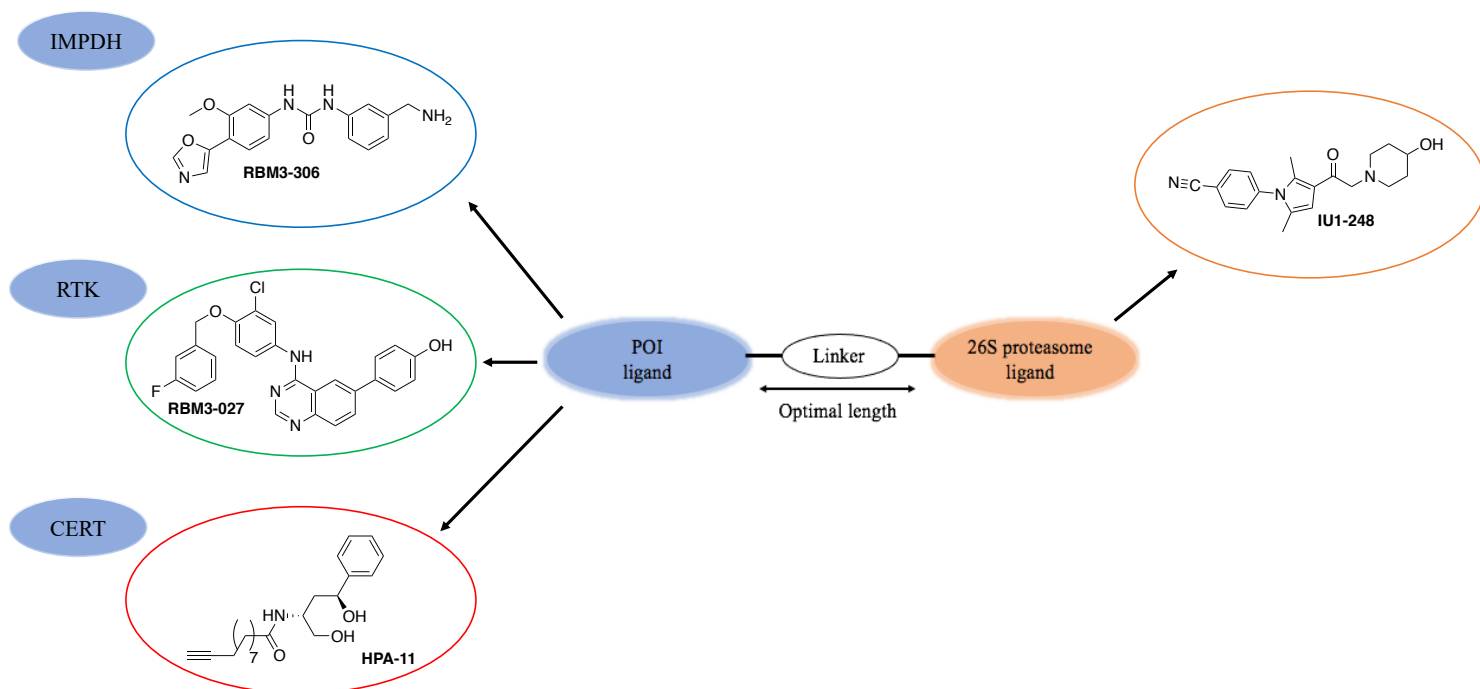


Figure 12: Conceptual approach to the design of bifunctional chimeras targeting a protein of interest (POI) and the 26S proteasome.

To achieve the general goal, the following **specific objectives** were undertaken:

- 1) Synthesis of USP14-based PROTACs for the degradation of IMPDH2, as well as of both classical E3-PROTACs and HyTAGs for comparative purposes.
- 2) Synthesis of USP14-based PROTACs for the degradation of RTKs, as well as of both classical E3-PROTACs and HyTAGs for comparative purposes.
- 3) Synthesis of PROTACs for the degradation of CERT, including both classical E3- and USP14-based degraders for comparative purposes.

These objectives were complemented with molecular modelling studies carried out by Dr. Jordi Bujons (IQAC-CSIC) to determine the best putative point of insertion of linkers to ligands and by biological studies performed by Dr. Mireia Casasampere and Tania Roda, in collaboration with Dr. Bernat Crosas (IBMB-CSIC), to investigate the degradative capacity of the chimeras in different biological contexts.

CHAPTER 3

Results and Discussion

3.1. DESIGN OF CHIMERAS.

Several crucial elements need to be taken into account for a PROTAC to induce degradation successfully. First, several examples evidence the importance of the right POI warhead/recruiter ligand combination. For instance, in a study aimed at degrading BCR-ABL, bifunctional chimeras based on three tyrosine kinase inhibitors (imatininb, bosutinib and dasatinib) and either CRBN or VHL E3 ligase ligands, none of the chimeras containing imatinib and none of the CRBN-based PROTACs induced the degradation of BCR-ABL, despite the CRBN-based PROTAC exhibiting good target engagement. In contrast, VHL-based PROTACs had degradative properties, but only when bosutinib was used as POI warhead (the dasatinib-containing PROTAC was ineffective)⁸³. Second, the site of attachment of linkers to ligands of both POI and recruiter must be such to ensure that the linkers' substitution does not alter the ligand-receptor interactions. Third, the linker length, composition, and rigidity are also crucial¹⁰⁶. The linker serves two important functions: formation of the ternary complex and establishing binding cooperativity¹⁰⁷. Cooperativity in the PROTAC field is defined as the impact of protein association, such as POI:PROTAC, on the PROTAC's affinity to the second protein (recruiter). A too-short linker may sterically hinder the formation of the POI:PROTAC:recruiter ternary complex, while very lengthy linkers may prevent the establishment of the POI-recruiter interactions needed to form an effective POI:PROTAC:recruiter ternary complex (figure 13)¹⁰⁸.

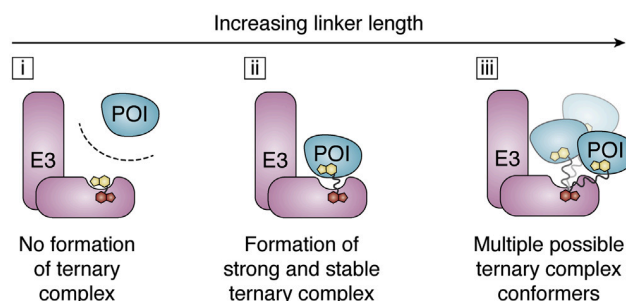


Figure 13: Linkers and ternary complex formation¹⁰⁸.

3.1.1. Building blocks

The building blocks used in this thesis to prepare the candidates for target protein degradation are:

Recruiter ligands

CRBN and VHL have been used as recruiters in the classical E3-based PROTACs using the well reported ligands lenalidomide (thalidomide derivative) and VHL1 (see Figure 11), respectively. In the E3-based PROTACs prepared in this thesis, the linker site of attachment to the recruiter ligands was that extensively reported for other E3-based PROTACs.

As mentioned in the Introduction, in the innovative PROTACs described in this thesis, USP14 is the 19S unit used to recruit our POIs to the proteasome employing compound IU1-248 (and derivatives) as ligands. The site of linker attachment was selected on the basis of molecular modelling studies. The docking analysis of USP14 with IU1 derivatives IU1-248, IU1c and **RBM3-317** performed by Dr. Jordi Bujons (IQAC) provided important data to select the linker attachment point in the USP14 binder. Regarding de IU1-248 efficacy, the CN group on the phenyl ring is bigger than the F- group in IU1c and **RBM3-317**, more fully occupying the inner pocket of USP14 and resulting in stronger Van der Waals interactions. Additionally, the absence of a methylene (CH₂) linker between the ketone and the protonated amine resulted in less stable bound conformation in the case of IU1c and **RBM3-317** (Figure 14). As shown in Figure 15, the most exposed moiety in the USP14 ligands docked into the protein is the hydroxy piperidine unit, which makes it the proper position for linker attachment with expected minimal disruption of binding to USP14.

Linkers

The possibility of polyethylene glycol (PEG) being available with various lengths and functional ends (commercial or synthesized “in house”) for attachment to ligands were the reasons behind utilizing PEG linker in this thesis. Indeed, PEGs are used as linkers in over a 54% of the reported PROTAC molecules, surpassing other bridge structures such as alkyl and alkyne linkers¹⁰⁷.

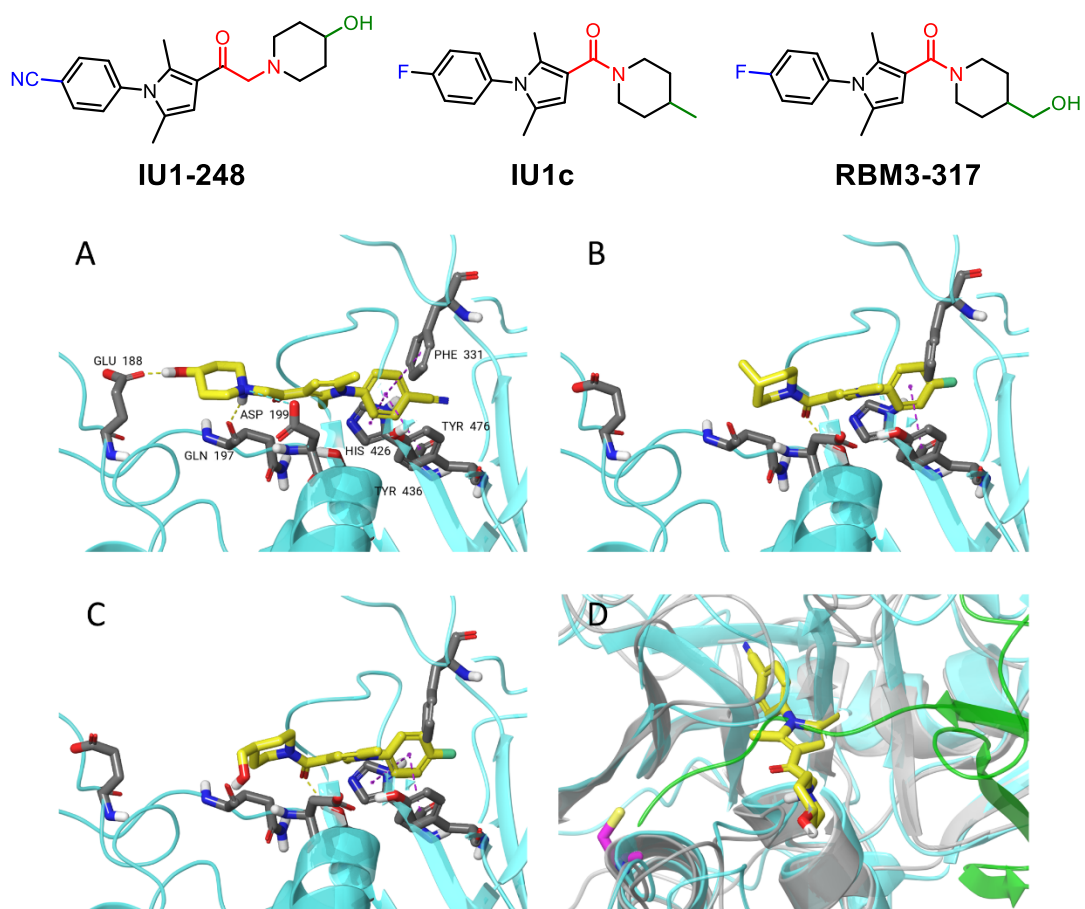


Figure 14: Ligands (A) IU1-248, (B) IU1c and (C) RBM3-317 docked to USP14 using the Induced Fit Docking protocol. (D) Superposition of structure on panel (A) and that of the complex of USP14 with Ub aldehyde (PDB 2AYO).

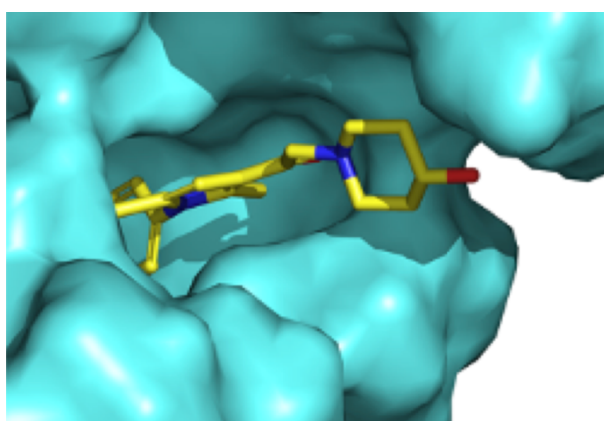


Figure 15: Structures of USP14 with a bound IU1-248 molecule (PDB 6IIN).

POI warheads

IMPDH2. The inhibitor VX-497 was selected as ligand. The redocking visualization done by Dr. Jordi Bujons (IQAC) showed the exposure of the tetrahydrofuran-3-yl formimidate moiety of VX-497 outside the binding pocket, which makes phenylmethanamine the proper position for linker attachment (Figure 16).

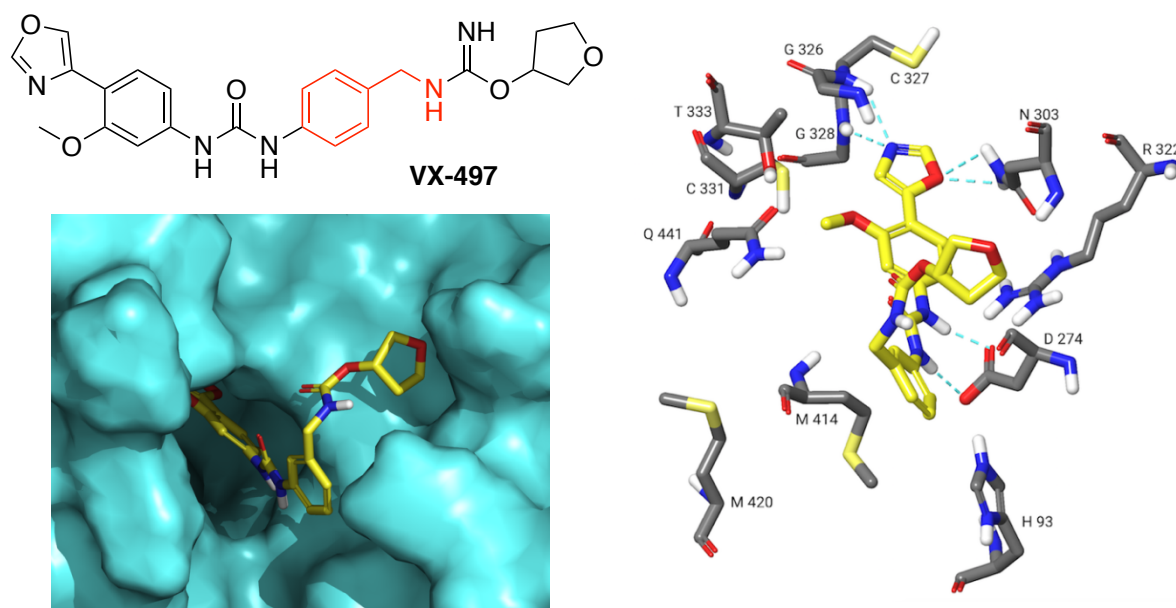


Figure 16: Structure of VX-497 and binding to IMPDH2. The phenylmethanamine portion is in red.

RTKs. The structure of the USP14-based PROTACS described here is inspired in the previously reported classical E3-PROTACS regarding the linker attachment to the lapatinib-like ligand¹⁰⁹.

CERT. Several structures with bound ligands exist in the PDB. A particular family of CERT ligands has been described (HPA family) that sticks the START CERT-domain. HPAs contain a polar head that binds deeply in the binding site cavity, and a flexible alkyl chain (acyl moiety), which is closer to the surface of the protein. Preliminary modeling of one of these ligands derivatized with a PEG chain (HPA-14_PEG₃, Figure 17) suggested that this linker would be exposed to

the bulk solvent and that it would not perturb the structure of the protein nor the binding of the ligand. Therefore, it was considered that this general structure could be a valid starting point for the design of PROTACs able to induce CERT degradation.

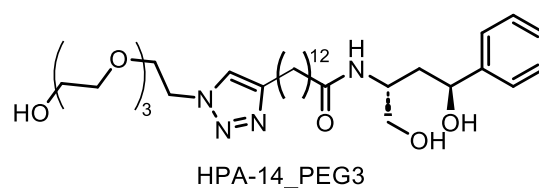
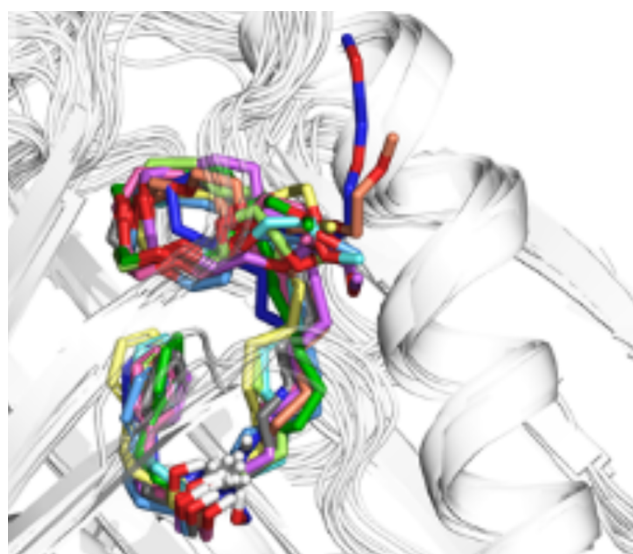
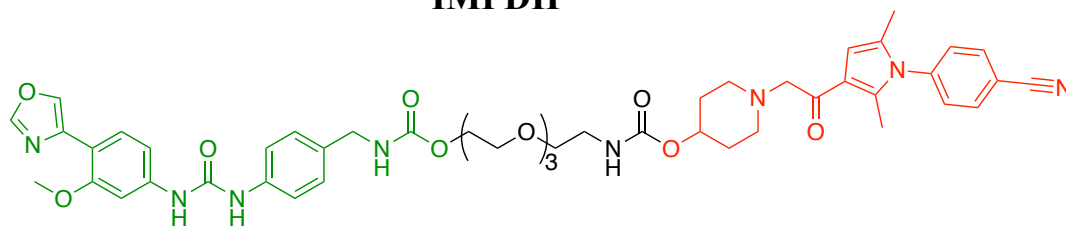


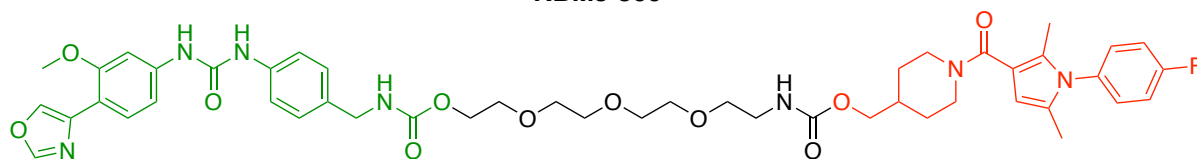
Figure 17: Superposition of 10 snapshots from a 500 ns MD simulation of the HPA-14_PEG₃ ligand bound into the CERT-START domain. (PDB codes 3H3Q, 3H3R, 3H3S and 3H3T)

Taking into account all the above considerations, the following chimeras were proposed and synthesized as candidate degraders of our 3 model POIs (Figure 18).

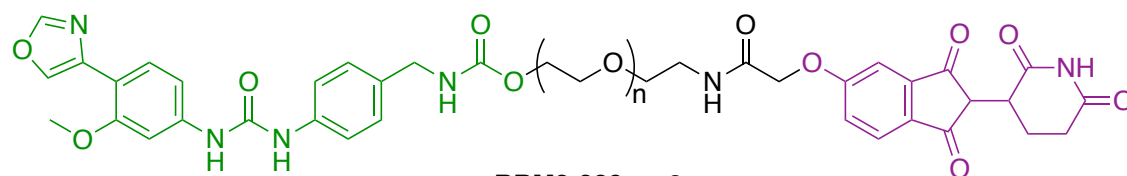
IMPDH



RBM3-300



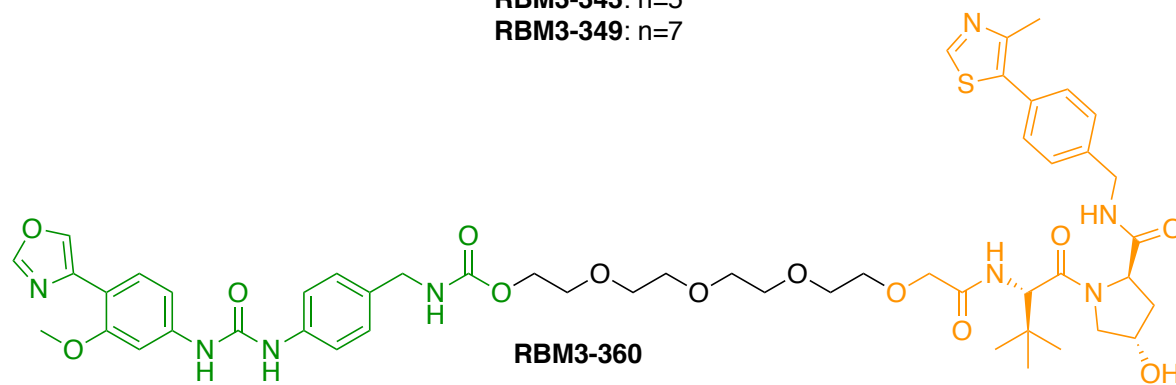
RBM3-354



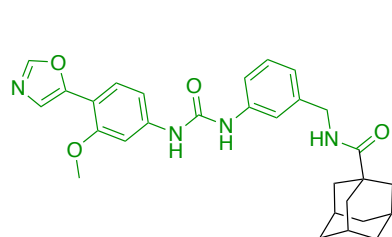
RBM3-320: n=3

RBM3-343: n=5

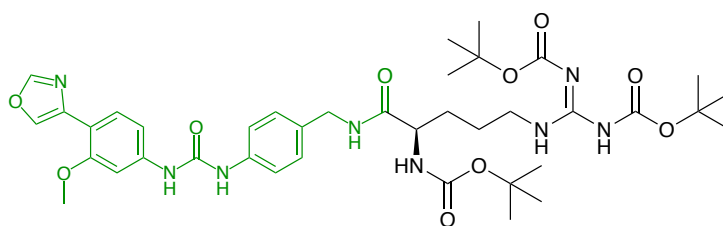
RBM3-349: n=7



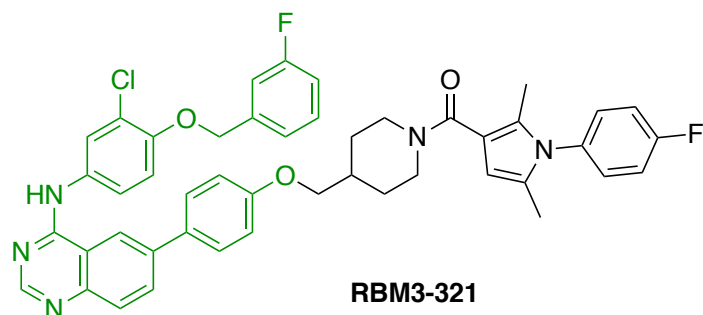
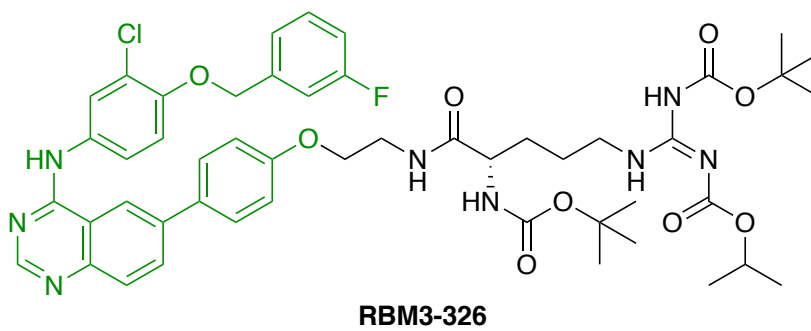
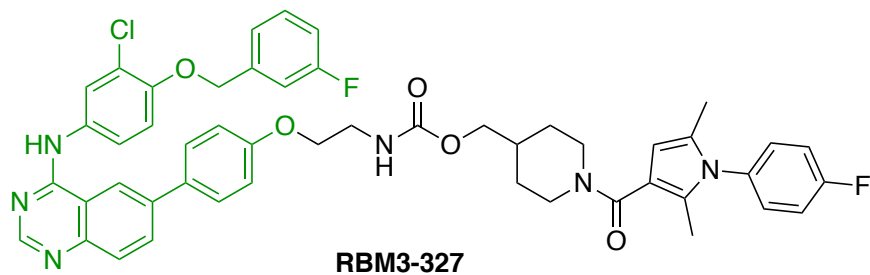
RBM3-360



RBM3-357



RBM3-358



CERT

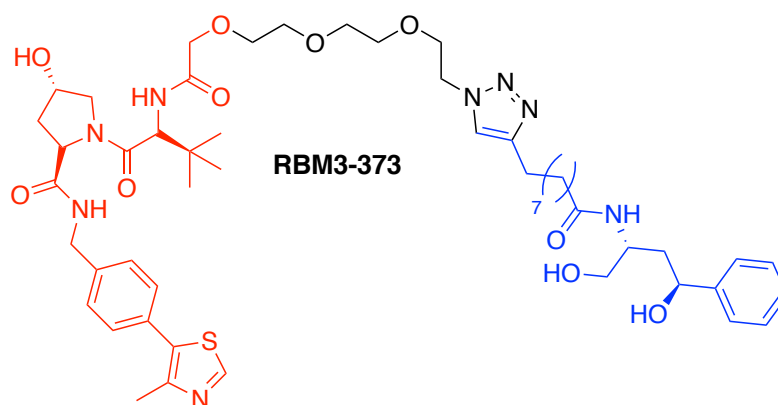
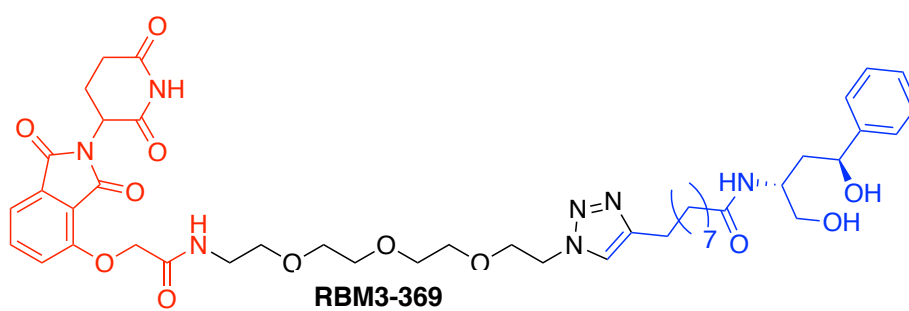
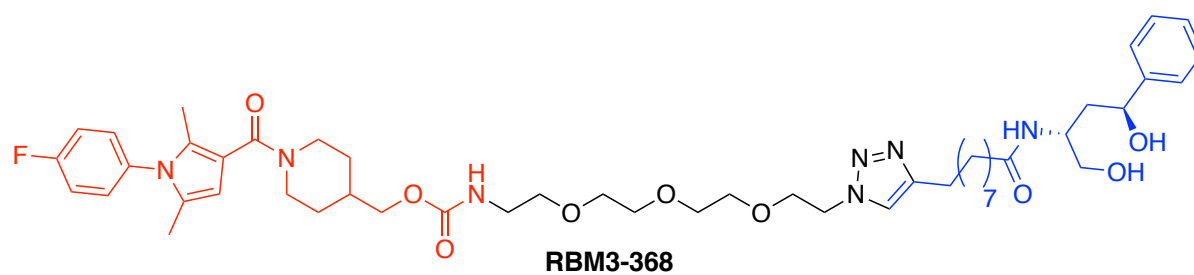


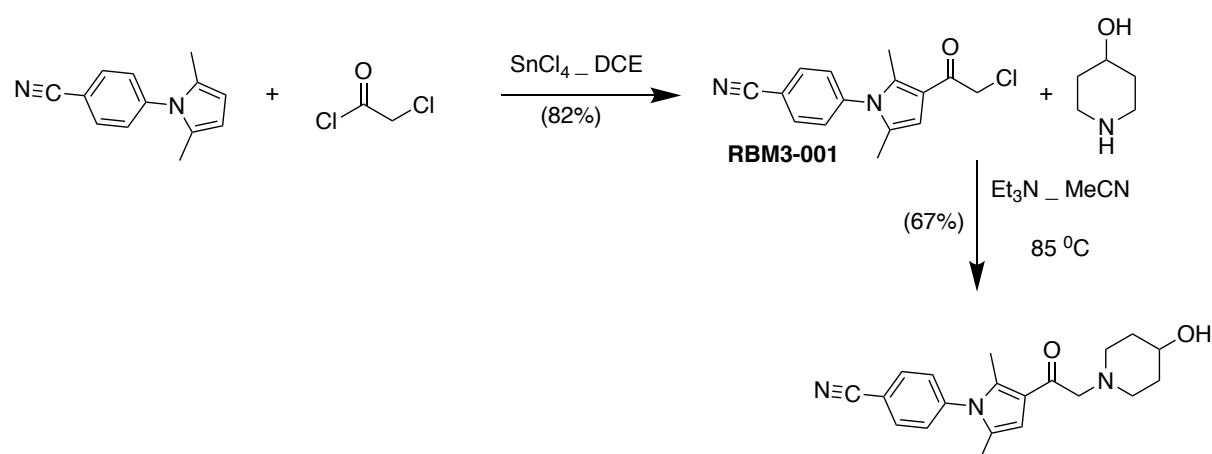
Figure 18: Structures of bifunctional chimeras involved in the IMPDH2, RTK, and CERT case studies.

3.2. SYNTHESIS OF CHIMERAS

3.2.1. USP14 ligands

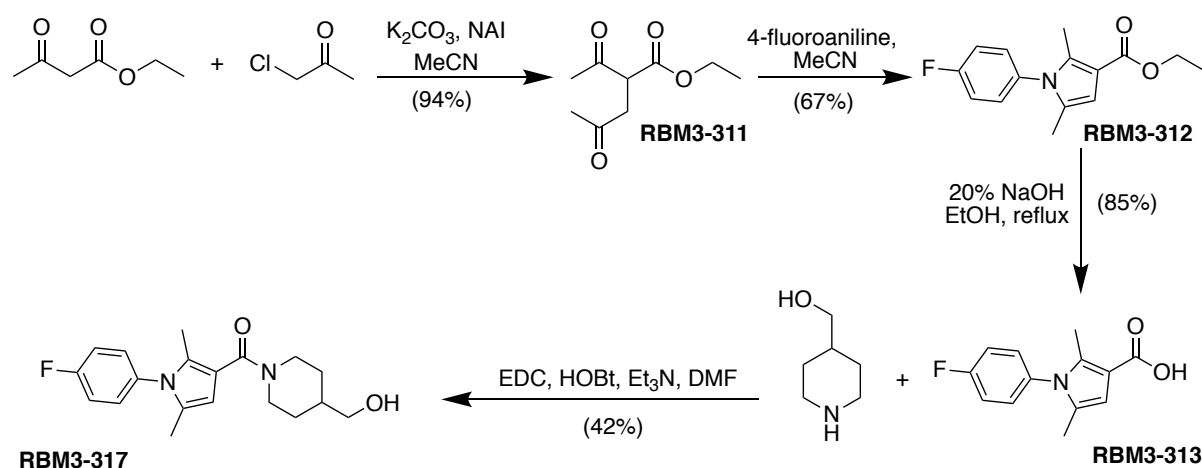
To fulfill the structural differences of **IU1-248** and **RBM3-317**, two synthetic strategies were carried out as follows:

The synthesis of **IU1-248** was accomplished from the commercially available precursor *N*-(4-cyanophenyl)-2,5-dimethylpyrrole in 2 steps: Friedel-Crafts acylation to yield **RBM3-001** followed by alkylation to furnish **IU1-248**. Although **RBM3-001** is commercially available, its extremely high price led us to prepare it in house. Its synthesis was reported in the patent WO2020006269, where **RBM3-001** was obtained with poor yield (33%) using chloroacetyl chloride and SnCl₂ stannous chloride as Lewis acid in 1,2-dichloroethane (DCE). The reaction yield was improved in this thesis to reach 82% by formation of the acylium ion in DCE first and then adding it dropwise to *N*-(4-cyanophenyl)-2,5-dimethylpyrrole in DCE. Next, the acylated pyrrole reacted with 4-hydroxypiperidine to give **IU1-248** in 67% yield (Scheme 1).



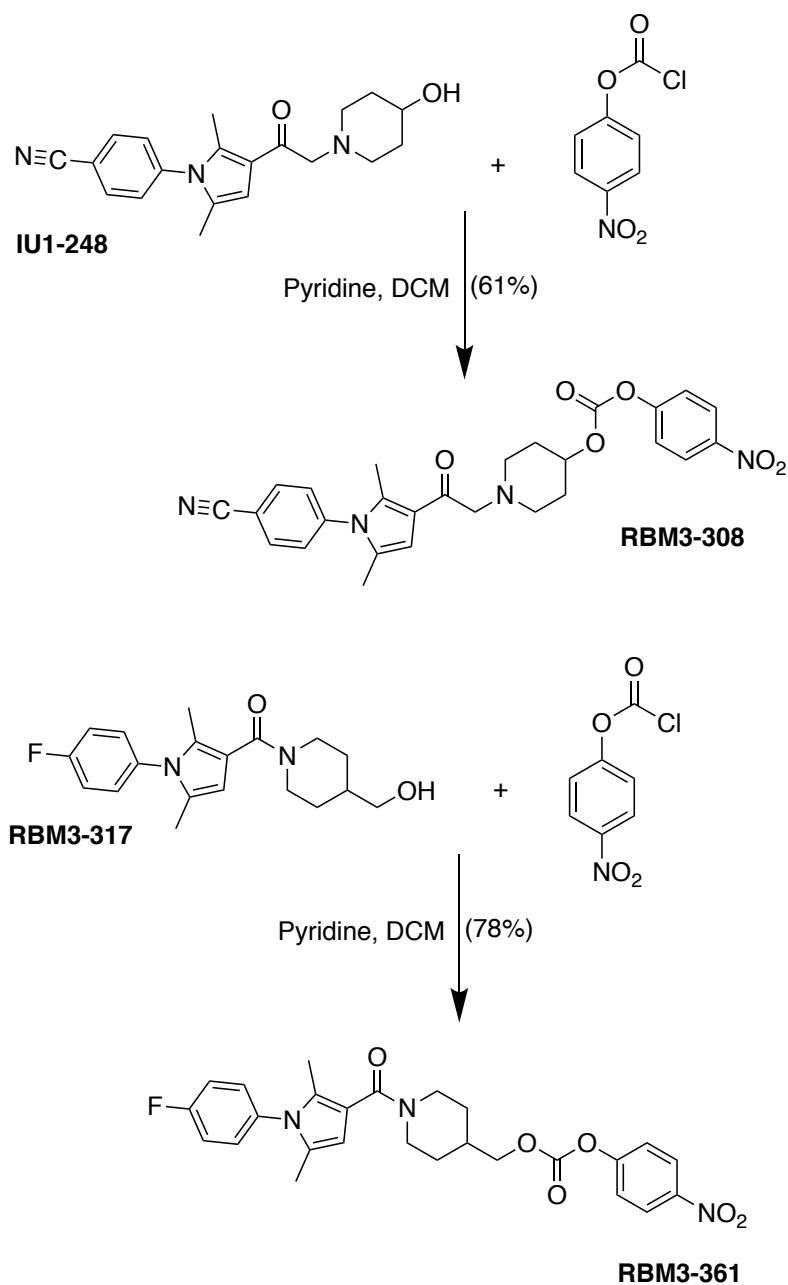
Scheme 1: Synthesis of **IU1-248**.

RBM3-317 was achieved in four steps (Scheme 2). First, **RBM3-311** was prepared by acetoacetic ester synthesis from ethyl acetoacetate and chloroacetone. A strong base deprotonates the dicarbonyl α -carbon, which is more acidic than the α -methyl carbon because the resulting enolate is stabilized by resonance. Further nucleophilic substitution of chlorine of chloroacetone furnishes **RBM3-311**. The pyrrole ring produced by the Paal-Knorr condensation gives **RBM3-312**, which is hydrolyzed (ester function) to **RBM3-313**. A coupling reaction with piperidin-4-ylmethanol (EDC/HOBt) yielded **RBM3-317**.



Scheme 2: Synthesis of **RBM3-317**.

Both hydroxy groups of 4-hydroxypiperidine in IU1-248 and 4-piperidinylmethanol in **RBM3-317** were further reacted with 4-nitrophenyl chloroformate to yield the activated esters **RBM3-308** and **RBM3-361**, respectively, for further reactions with the linkers. The lower reactivity of the secondary over the primary alcohol in IU1-248 and **RBM3-317**, respectively, explains the lower reaction yields in the reaction from IU1-248 (Scheme 3).

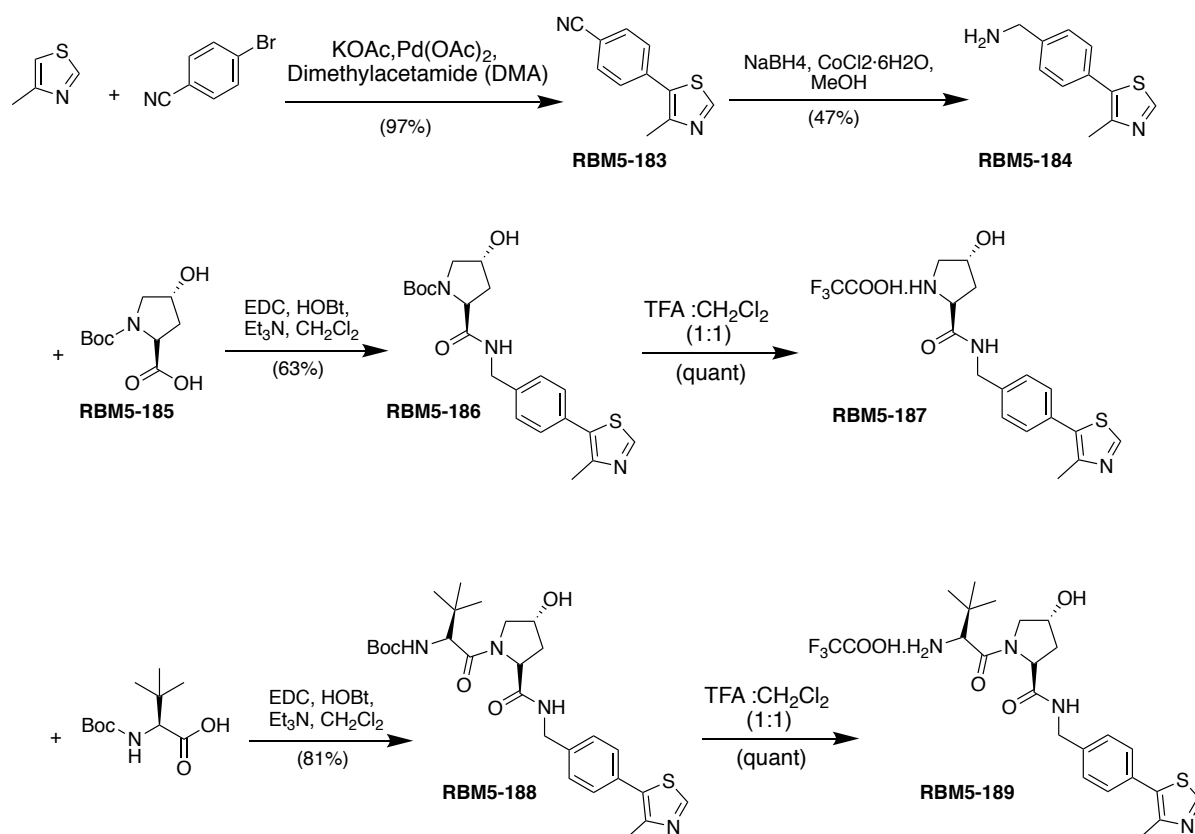


Scheme 3: Synthesis of **RBM3-308** and **RBM3-361**.

3.2.2. E3 recruiter ligands.

A modified version of the six-step process outlined by Galdeano et al¹¹⁰ was adopted to produce the VHL ligand **RBM5-189**. As shown in Scheme 4, a Pd-catalyzed Heck reaction was used to couple 4-methylthiazole and 4-bromobenzonitrile to achieve **RBM5-183** in 82% yield. The close retention factor (R_f) between 4-methylthiazole and **RBM5-183** complicated the isolation of pure **RBM5-183** despite assaying different chromatographic systems and solvents.

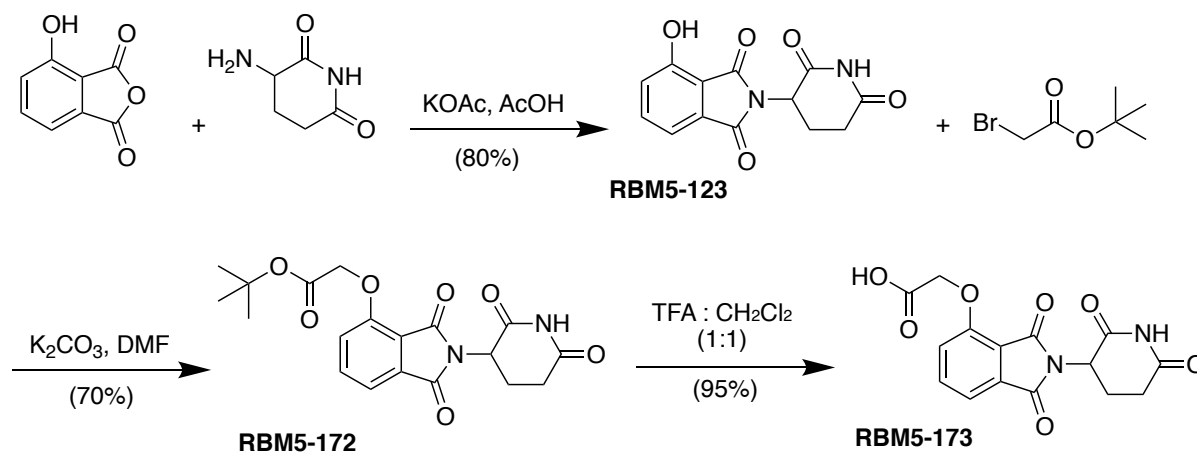
Finally, 4-methylthiazole could be eliminated from the reaction mixture by applying high-pressure vacuum under high temperature (105 °C). Further column chromatography gave pure **RBM5-183** in 97% yield. The nitrile group was then reduced using NaBH₄-CoCl₂ to produce the amine **RBM5-184**. Then, **RBM5-189** was attained by two amide coupling cycles using EDC-HOBt, firstly with Boc-L-hydroxyproline to give **RBM5-186** and then, after acid-mediated *N*-Boc deprotection, with Boc-L-*tert*-butyl-leucine to give **RBM5-188**. Another step of acid-mediated *N*-Boc deprotection furnished **RBM5-189**.



Scheme 4: Synthesis of **RBM5-189**.

The synthesis of the CRBN ligand was carried out as shown in Scheme 5. Reaction of 3-hydroxyphthalic anhydride with 3-aminopiperidine-2,6-dione hydrochloride in the presence of KOAc under reflux produced 4-hydroxythalidomide (**RBM5-123**). In the production of the **RBM5-172** intermediate, the acidity of the imide proton in **RBM5-123** raised the possibility

of obtaining the *N,O*-dialkylated by-product. By reducing the amount of base (1.5 eq.) and alkylating reagent (1 eq.) and conducting the reaction at room temperature, the amount of dialkylated by-product was negligible. Final deprotection of the *tert*-butyl group under acidic conditions gave the carboxylic acid **RBM5-173**.



Scheme 5: Synthesis of **RBM5-173**.

3.2.3. PEG linkers:

The PEG linkers had to be of different chain lengths and contain appropriate functionalities at the terminal ends for orthogonal coupling to POI and recruiter ligands. A summary of the synthetic route to linkers is given in Figure 19.

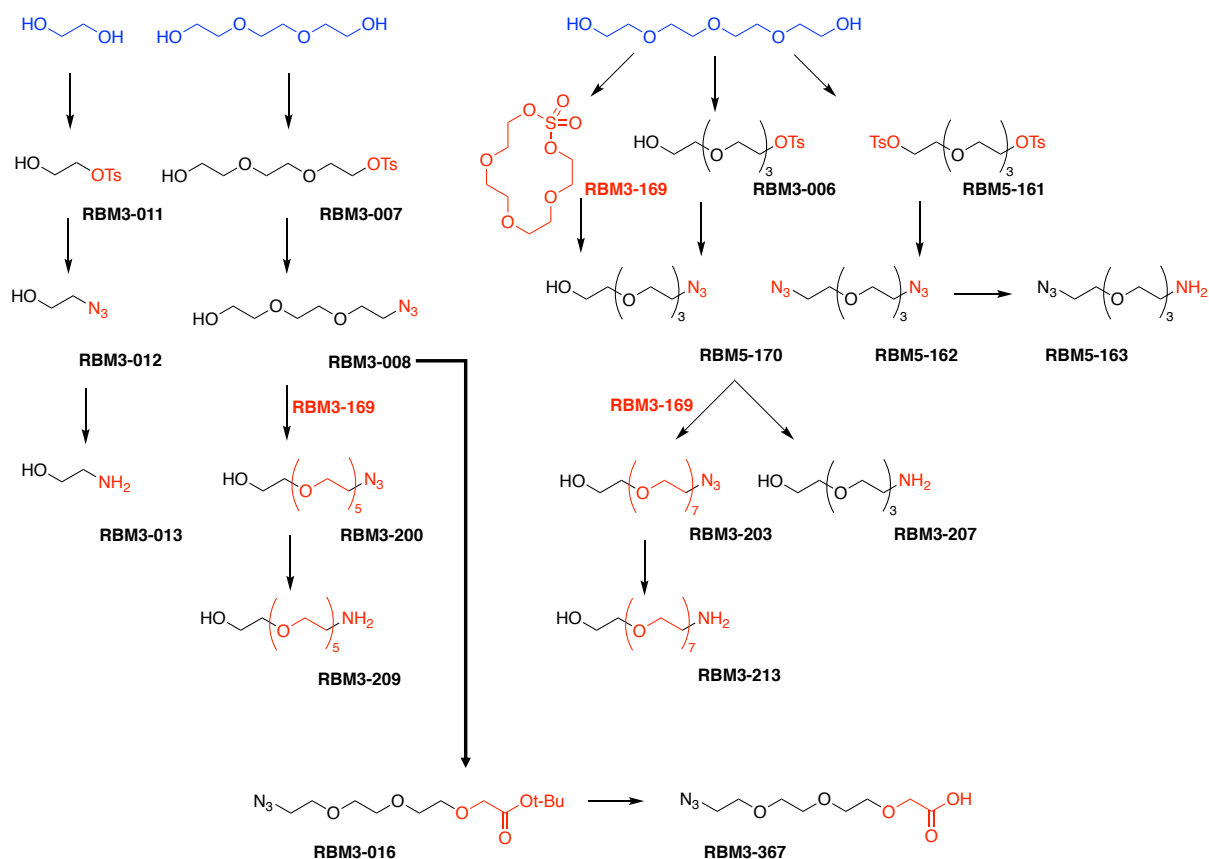
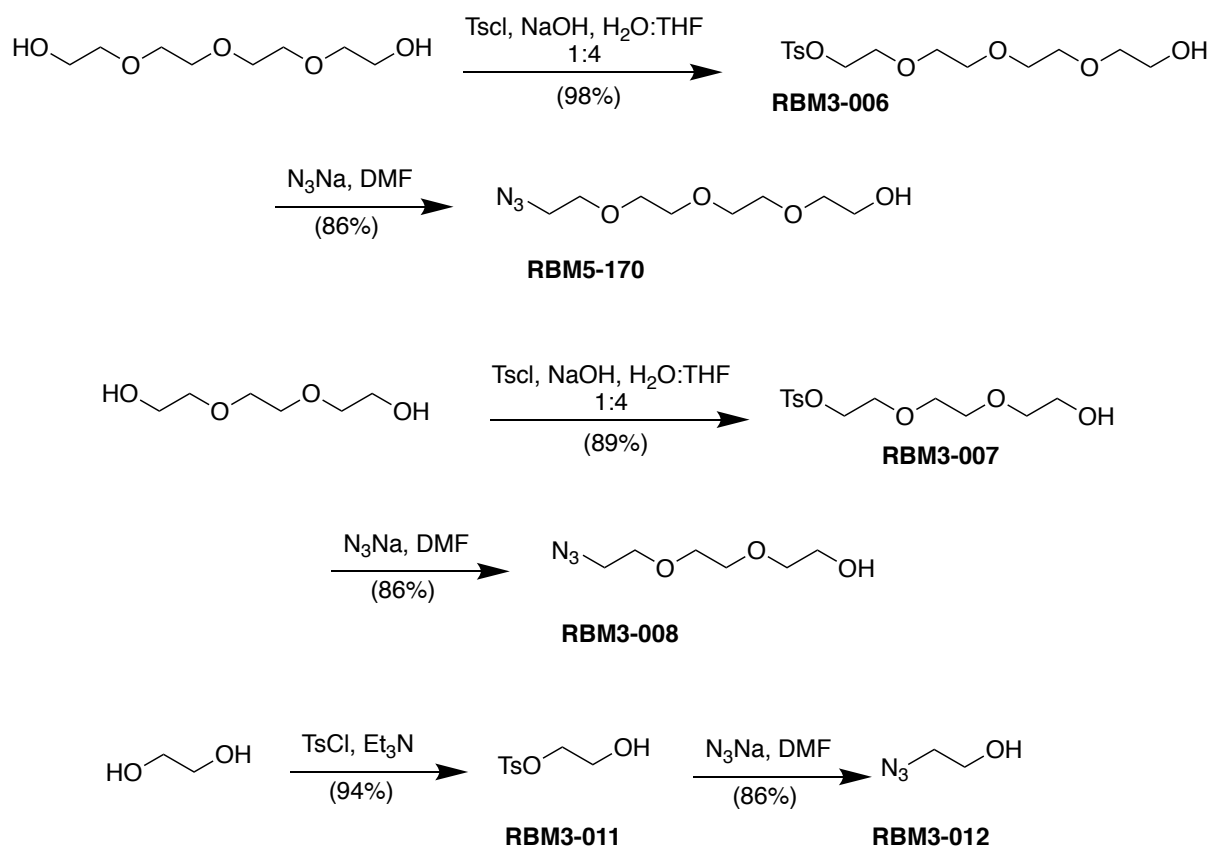


Figure 19. Summary of linkers synthesis.

Tetraethylene glycol was first desymmetrized to obtain the azido alcohol **RBM5-170**, which served as the starting point for the PEG linker synthesis. Two different approaches were successfully examined (Scheme 6). To increase the selectivity of monoalkylation and monoacylation processes of symmetrical alcohols, the use of a substoichiometric amount of mesyl chloride (0.9 equiv.) and an excess of TEA (1.5 equiv.) in the presence of Ag_2O had been previously utilized,¹¹¹ showing that employing Ag_2O significantly increased the yield of tetraethylene glycol monomesylation (from 36% to 69%). However, a substoichiometric quantity of *p*-toluenesulfonyl chloride (0.1 equiv.) to control the monotosylation of tetraethylene glycol was used to provide **RBM3-006** in an excellent yield without the need of Ag_2O . A simple extraction with ethyl acetate of **RBM3-006** from the excess amount of tetraethylene glycol provided pure **RBM3-006** with no need for further purification. Following, the treatment with sodium azide

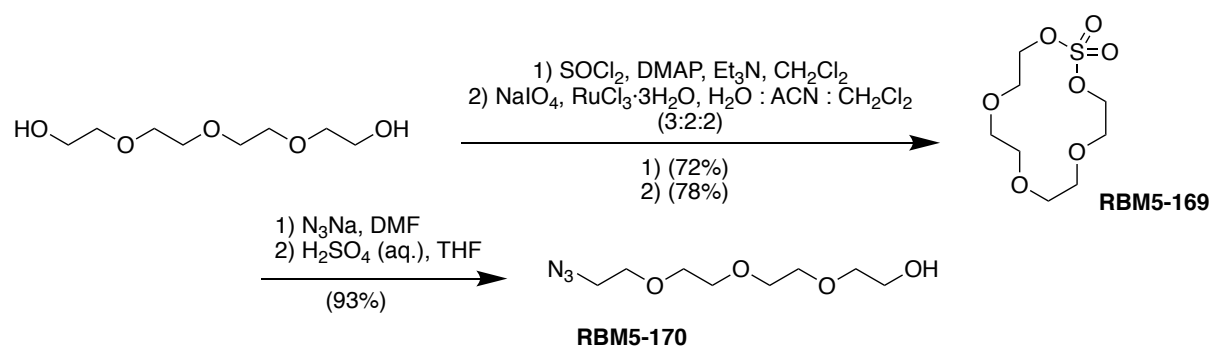
yielded **RBM5-170**. The same methodology was applied to control monotosylation of PEG in triethyleneglycol to yield **RBM3-007**. Reaction of the monotosylate with sodium azide afforded **RBM3-008**. The same tosylation conditions applied to ethyleneglycol led to the ditosylated product, which can be explained by the use of a strong base (NaOH). Fortunately, utilizing a weak nitrogen base (TEA) was the key to control monotosylation of ethylene glycol to lead to **RBM3-011**, which was converted to **RBM3-012** by reaction with sodium azide (Scheme 6).



Scheme 6: Synthesis of **RBM5-170**, **RBM3-008** and **RBM3-012**.

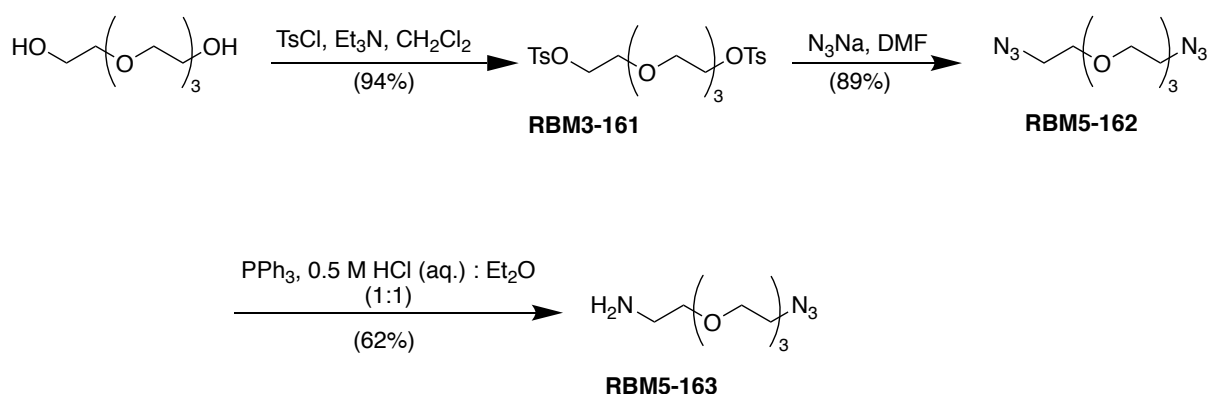
In the second methodology, we adopted Prof. Jiang's group procedure, which undergoes via a crucial macrocyclic sulfate intermediate¹¹². Tetraethylene glycol was macrocyclized with SOCl_2 in the presence of TEA and catalytic DMAP. This method produced a 14-membered macrocyclic sulphite that was oxidized with

ruthenium tetroxide *in situ* to produce the macrocyclic sulphate **RBM5-169** in two steps with a 78% yield. **RBM5-169**'s ring was opened nucleophilically with NaN_3 , and the resultant sulfate salt intermediate was then hydrolyzed under acidic conditions to generate the azido alcohol **RBM5-170** in high yields (Scheme 7).



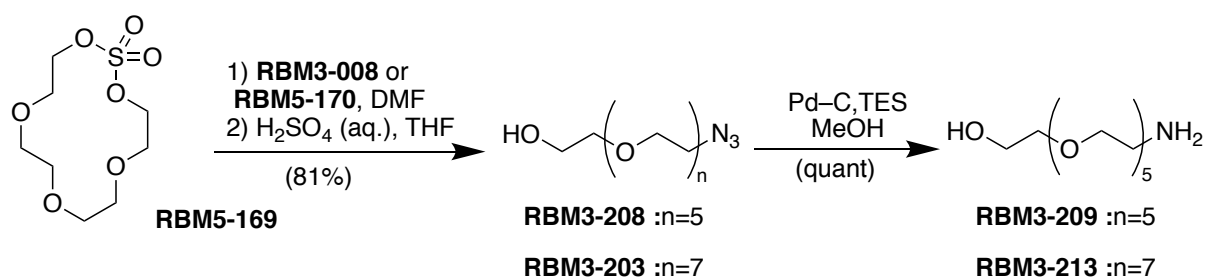
Scheme 7: Synthesis of **RBM5-170** via macrocyclic sulfate intermediate.

In the synthesis of azidoamine linker **RBM5-163**, tetraethylene glycol was reacted with an excess of TsCl (3.0 eq.) to produce the appropriate ditosylated intermediates **RBM3-161**, which were then easily subjected to double nucleophilic substitution with NaN_3 to provide **RBM5-162** in good yields. **RBM5-162** was then submitted to Staudinger reduction with 1.0 eq. of PPh_3 in a biphasic combination of $\text{Et}_2\text{O} : 0.5 \text{ M aq. HCl}$ (1:1) to supply a complex mixture containing the required amino azides together with trace amounts of the over-reduced diamines, triphenylphosphine oxide (TPPO), and unreacted starting material (Scheme 8). Simple acid-base extractions enabled to successfully isolate the pure amino azide **RBM5-163**.

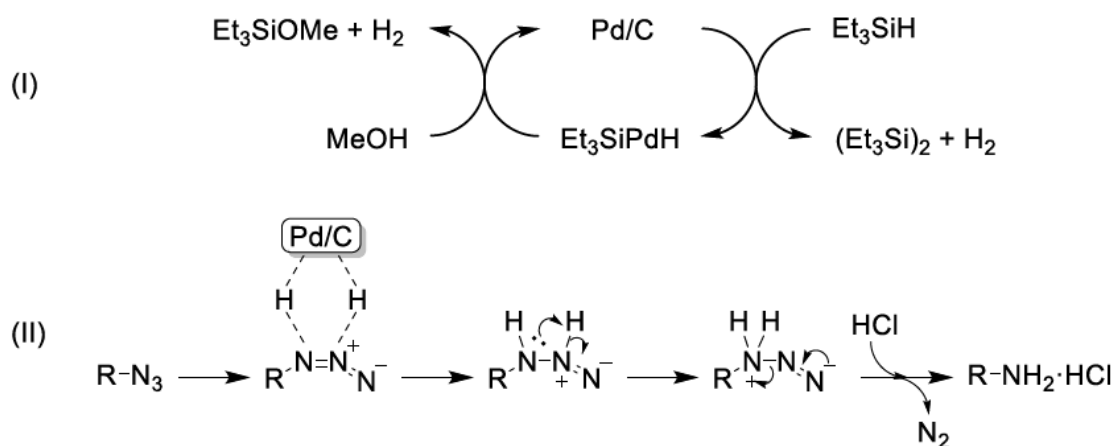


Scheme 8: Synthesis of **RBM5-163**.

Based on our previous experience in controlling monotosylation of PEG of various lengths and taking advantage of macrocyclic sulfate intermediate **RBM5-169**, elongation of PEG linkers was approached by nucleophilic ring opening of **RBM5-169** with azido-PEG-OH linkers. In the case of **RBM3-209**, the nucleophilic ring opening of macrocyclic sulfate intermediate **RBM5-169** with azido alcohol **RBM3-008**, followed by the acidic hydrolysis of the corresponding sulfate salt intermediate, provided the azido alcohol **RBM3-208** in high yields (Scheme 9). The reduction of the azide group of **RBM3-208** to yield **RBM3-209** was carried out by the Pd-C induced catalytic transfer hydrogenation with triethylsilane (TES) (Scheme 9). The same synthetic strategy was applied to yield **RBM3-203** and **RBM3-213** (Scheme 9). Based on a variety of experimental findings, Mirza-Aghayan *et al.*¹¹³ proposed that the Et₃SiPdH complex is formed by the oxidative addition of Et₃SiH to the Pd⁽⁰⁾ species, resulting in the production of molecular hydrogen. The generation of the identifying triethylsilyl ether with the concurrent production of extra molecular hydrogen and the regeneration of the Pd catalyst results from the subsequent displacement of this complex by MeOH. According to Kara *et al.*¹¹⁴, the produced molecular hydrogen is then adsorbable to the catalyst surface and transferred to the azide group. The equivalent amine is produced by proton displacement, followed by nitrogen removal and protonation under the reaction conditions (Scheme 10).

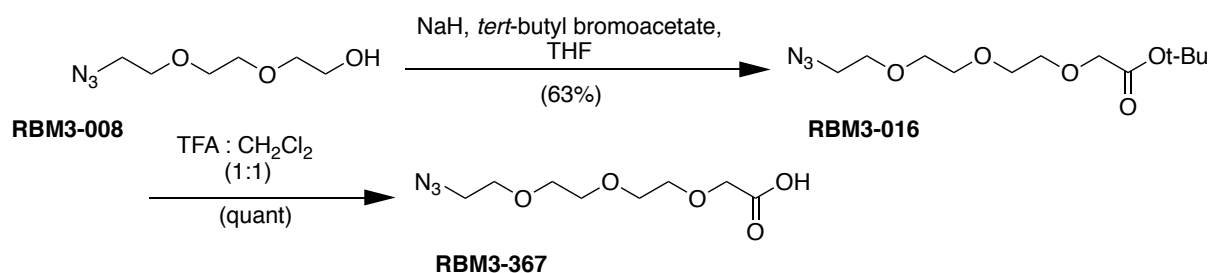


Scheme 9: Synthesis of **RBM3-208**, **RBM3-203**, **RBM3-209**, and **RBM3-213**.



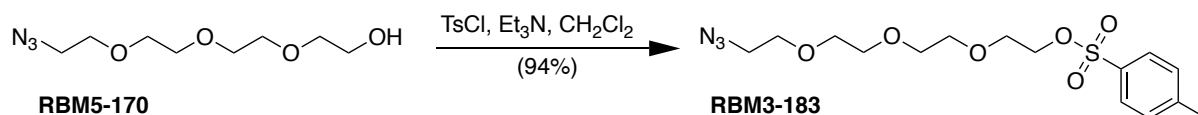
Scheme 10: Proposed mechanism for the reduction of azides by the Pd-C/TES system¹¹⁴.

The PEG linker **RBM3-367** was obtained by *O*-alkylating **RBM3-008** with *tert*-butyl bromoacetate in the presence of NaH to yield **RBM3-316**, followed by cleavage of the resulting *tert*-butyl ester with TFA (Scheme 11).



Scheme 11: Synthesis of **RBM3-367**.

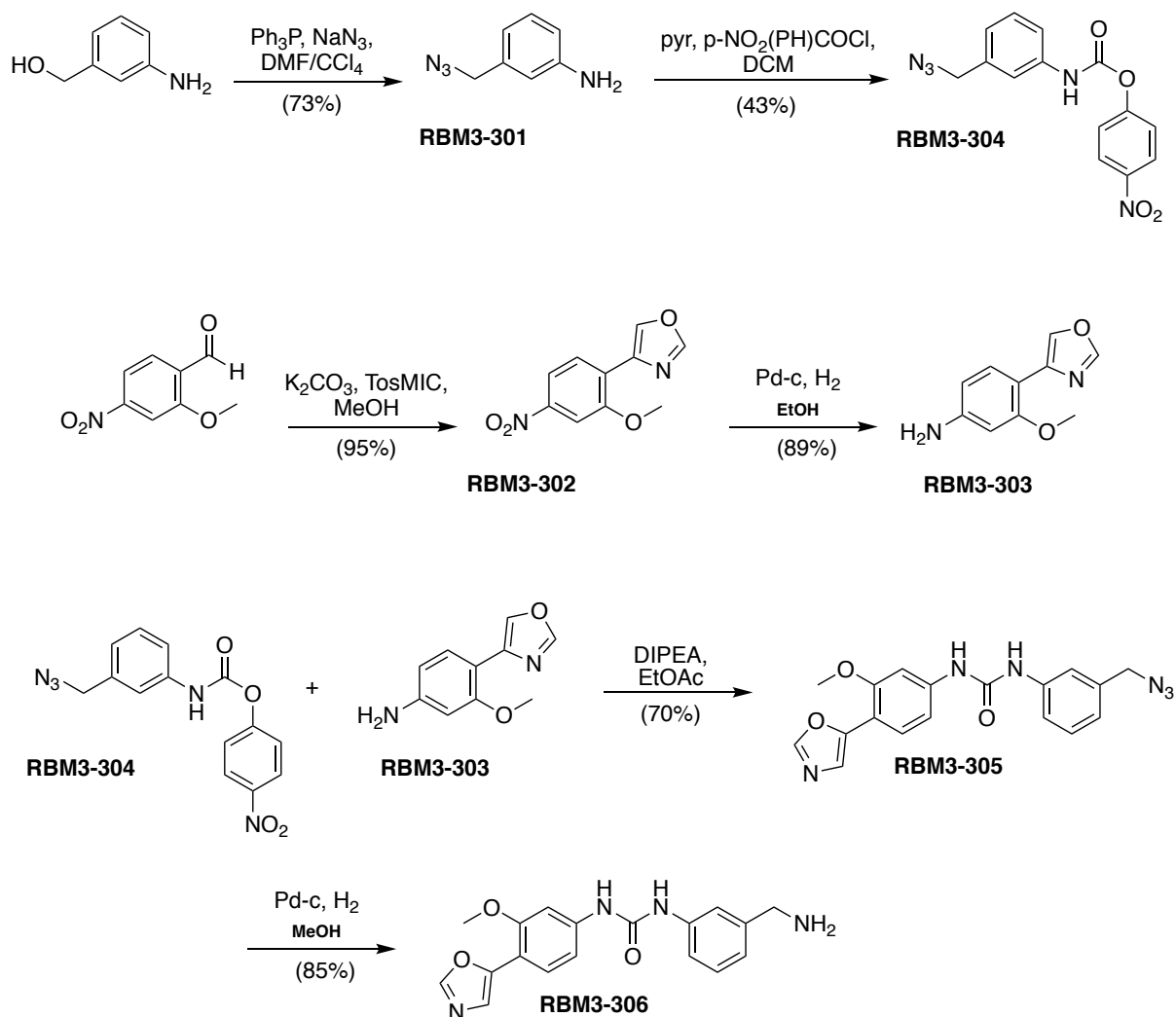
Finally, the tosylation of **RBM5-170** gave **RBM3-183** (Scheme 12).



Scheme 12: Synthesis of **RBM3-183**.

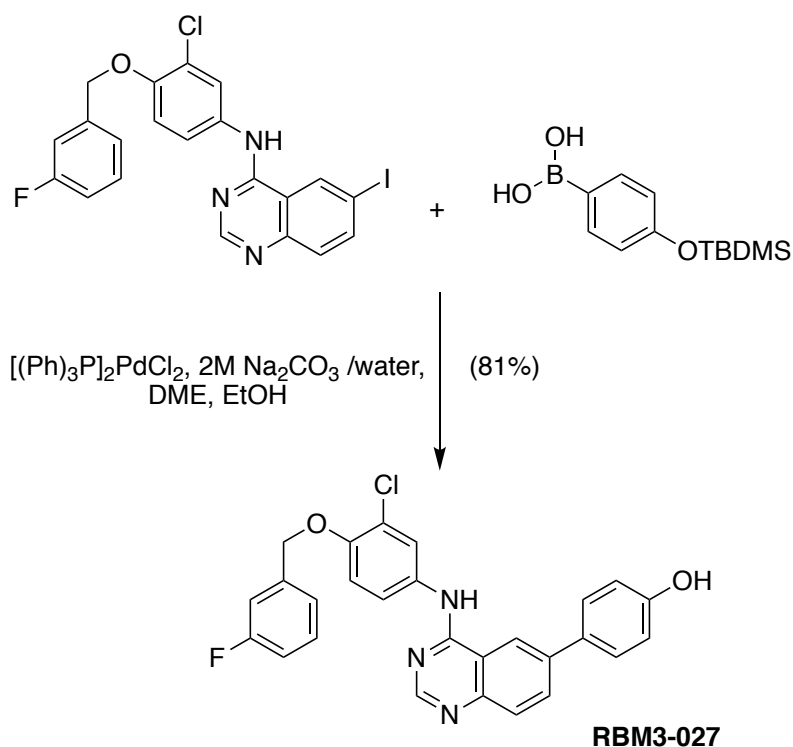
3.2.3. POI recruiters

The truncated analog of VX-497 **RBM3-306** (IMPDH2 ligand) was synthesized starting from the commercially available precursor 3-aminobenzyl alcohol. The azide derivative was produced by activation of the hydroxyl group with triphenylphosphine in CCl₄/DMF and further reaction with sodium azide. **RBM3-301** was then reacted with 4-nitrophenyl chloroformate to yield the carbamate **RBM3-304**. On the other side, Van Leusen reaction of commercially available 2-methoxy-4-nitrobenzaldehyde in the presence of toluenesulfonylmethyl isocyanide (TosMIC) led to oxazole formation in **RBM3-302**. Pd-catalysed hydrogenation of the nitro group yielded **RBM3-303**. The reaction between **RBM3-303** and **RBM3-304** was induced by Hünig's base (DIPEA) in ethyl acetate to achieve **RBM3-305**. Finally, Pd-catalysed hydrogenation of the azido group of **RBM3-305** afforded **RBM3-306** (Scheme 13).



Scheme 13: Synthesis of RBM3-306.

A modified version of the RTK inhibitor lapatinib (**RBM3-027**) was used as RTK ligand. Suzuki reaction between [3-chloro-4-[(3-fluorophenyl)methoxy]phenyl]-6-iodo-quinazolin-4-amine and [4-*tert*-butyl(dimethyl)silyl]oxyphenyl]boronic acid, catalysed by $[(\text{Ph})_3\text{P}]_2\text{PdCl}_2$, provided **RBM3-027** (Scheme 14). The reaction underwent via oxidative addition to the iodoquinazolin moiety after activation by Pd^0 to form the organopalladium intermediate. The boronate complex, which is produced by the reaction of boronic acid with Na_2CO_3 in this case, formed a transient organopalladium species, which produced **RBM3-027** by reductive elimination in good yields.



Scheme 14: Synthesis of **RBM3-027**.

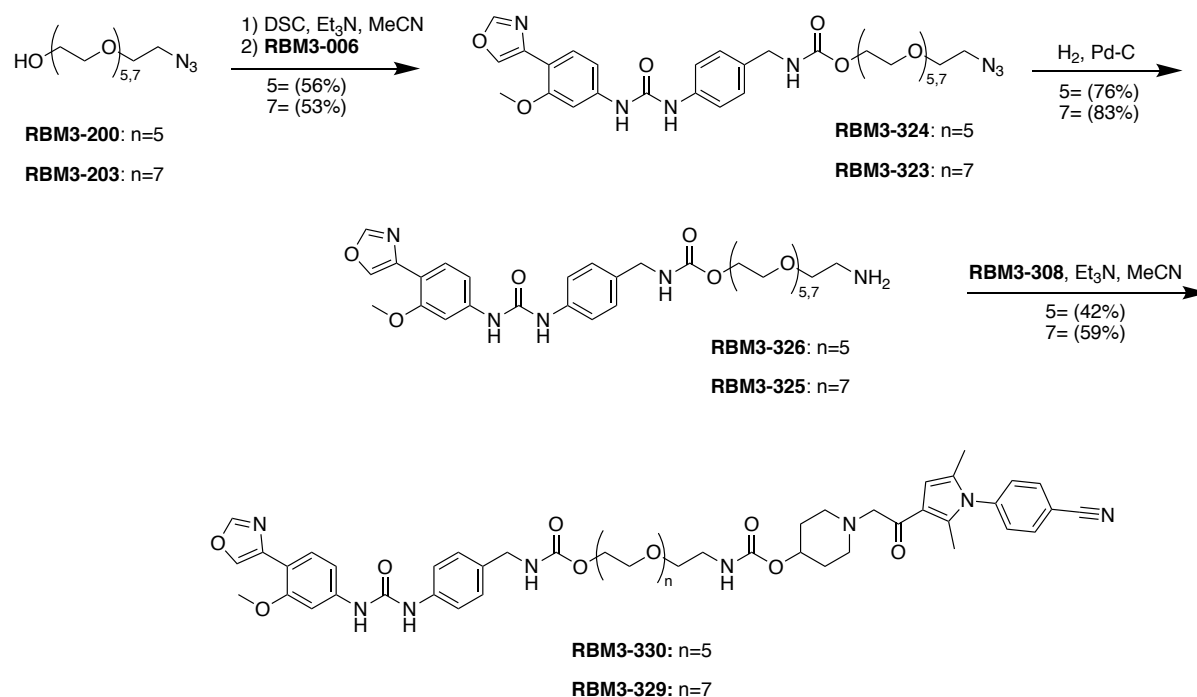
The synthesis of the CERT ligand **RBM3-366** (see Schemes 25, 26 and 27) was carried out by Dr. José Luís Abad.

3.2.4. Synthesis of bifunctional chimeras targeting IMPDH2

Following a convergent synthetic strategy, POI ligands, recruiter ligands and linkers were assembled to afford the final IMPDH2 targeting degraders. In the case of USP14-based PROTACS, carbamate functions were used for linker attachment to both ligands. In the case of E3 ligase-based PROTACS, the carbamate function between linker and recruiter ligand was replaced by an oxyacetamide unit.

Following this general strategy, **RBM3-300** was assembled in three chemical steps (Scheme 15). First, modification of the hydroxyl group of **IU1-248** with CDI followed by reaction with **RBM3-207** to form the first carbamate linkage between **IU1-248** and the linker in a one-pot reaction gave **RBM3-099**. Second,

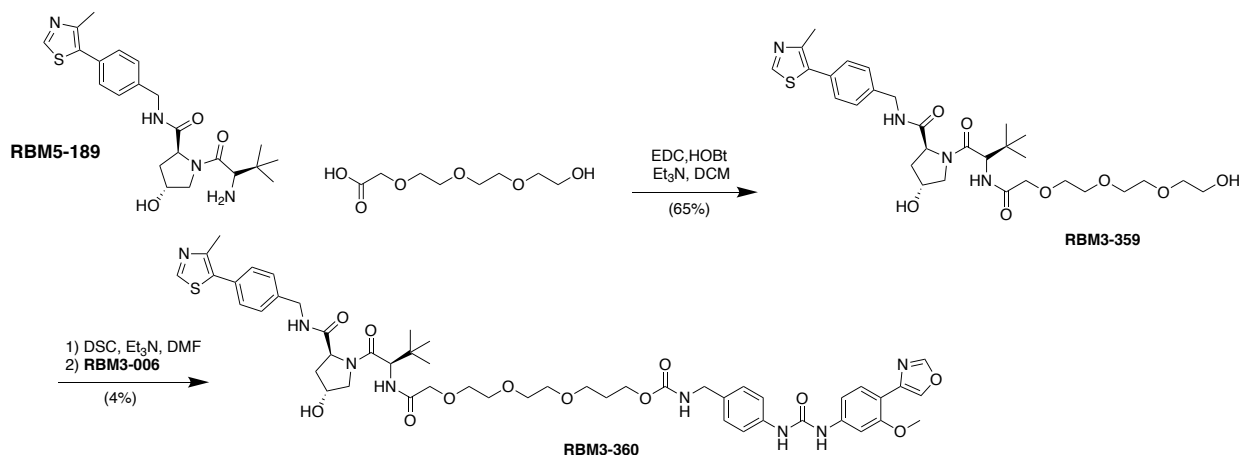
Due to the availability of the linker precursors **RBM3-200** and **RBM3-203**, the synthesis of **RBM3-329** and **RBM3-330** was slightly different from the syntheses above (Scheme 17). Activation of the linkers' hydroxyl moiety with DSC and subsequent reaction with the IMPDH2-ligand (**RBM3-006**) produced the carbamate linkage to yield **RBM3-324** and **RBM3-323** from **RBM3-200** and **RBM3-203**, respectively. Reduction of the azido group of **RBM3-223** and **RBM3-224** to the corresponding amines **RBM3-326** and **RBM3-325**, followed by their reaction with the activated **IU1-248** precursor (**RBM3-308**) generated the second carbamate linkage to produce **RBM3-329** and **RBM3-330**.



Scheme 17: Synthesis of **RBM3-329** and **RBM3-330**.

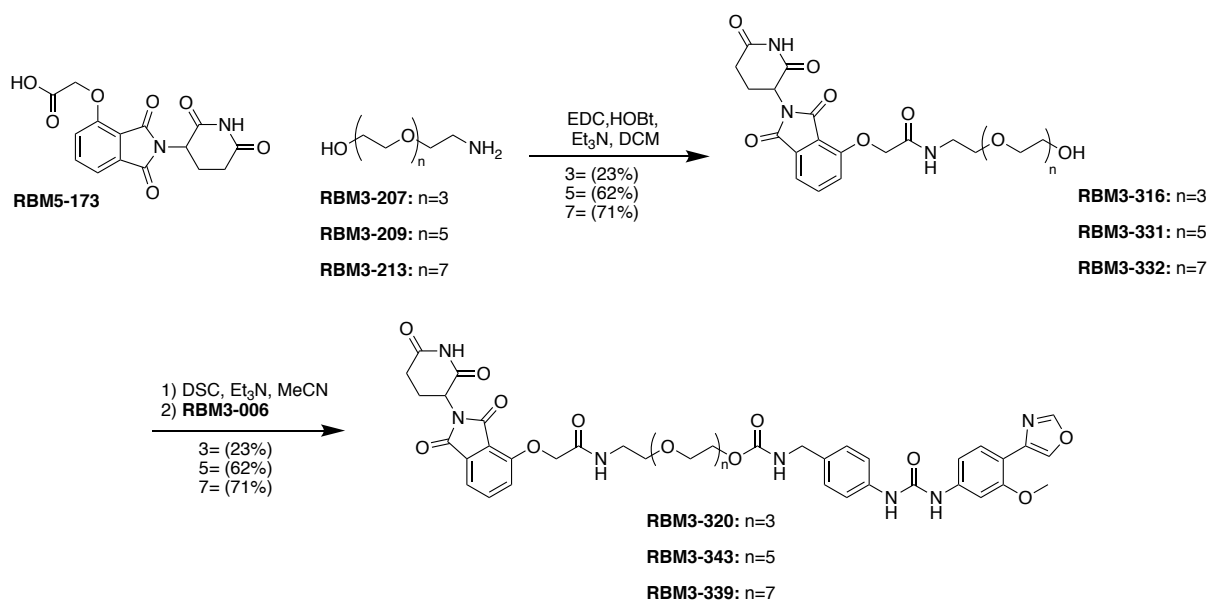
The synthesis of the IMPDH2 directed E3-ligase-based PROTACS was carried out as depicted in Schemes 18 and 19. Standard coupling chemistry of **RBM5-189** to the commercial linker precursor gave **RBM3-359**. Further activation of the hydroxyl moiety with DSC and reaction with **RBM3-306** produced the

carbamate linkage of the conjugate **RBM3-360** (Scheme 18). Despite all the efforts, this reaction proceeded in very low yields and production of unwanted side products due to the activated secondary hydroxy moiety of **RBM5-189** with DSC.



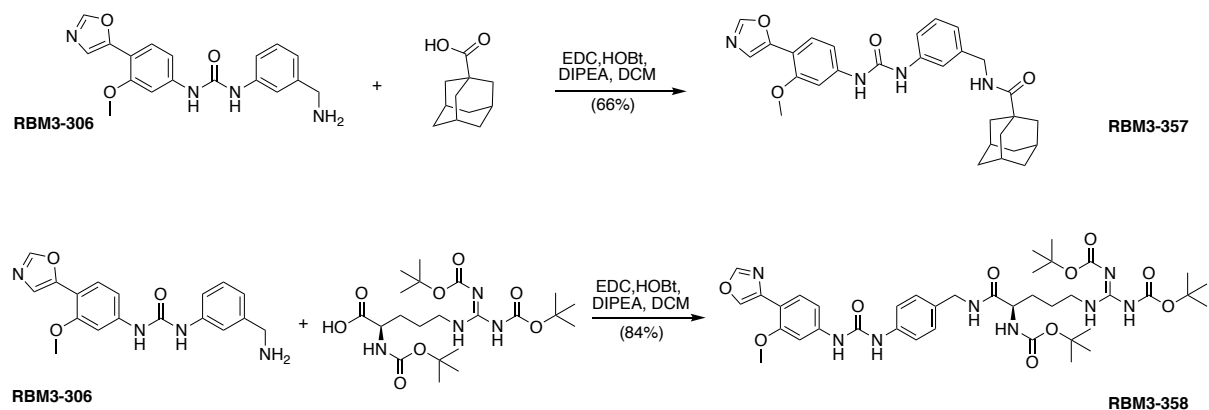
Scheme 18: Synthesis of RBM3-360.

In the synthesis of CRBN-based PROTACS, **RBM3-207**, **RBM3-209**, and **RBM3-213** precursors reacted with the E3 ligand **RBM5-173** under standard amide synthesis conditions with EDC/HOBT to produce the α -acetoxyamides **RBM3-316**, **RBM3-331**, and **RBM3-332**, respectively, which thereafter reacted with DSC and **RBM3-006** in a one-pot reaction to yield the respective final **RBM3-320**, **RBM3-343**, and **RBM3-339** products (Scheme 19).



Scheme 19: Synthesis of RBM3-320, RBM3-339, RBM3-343.

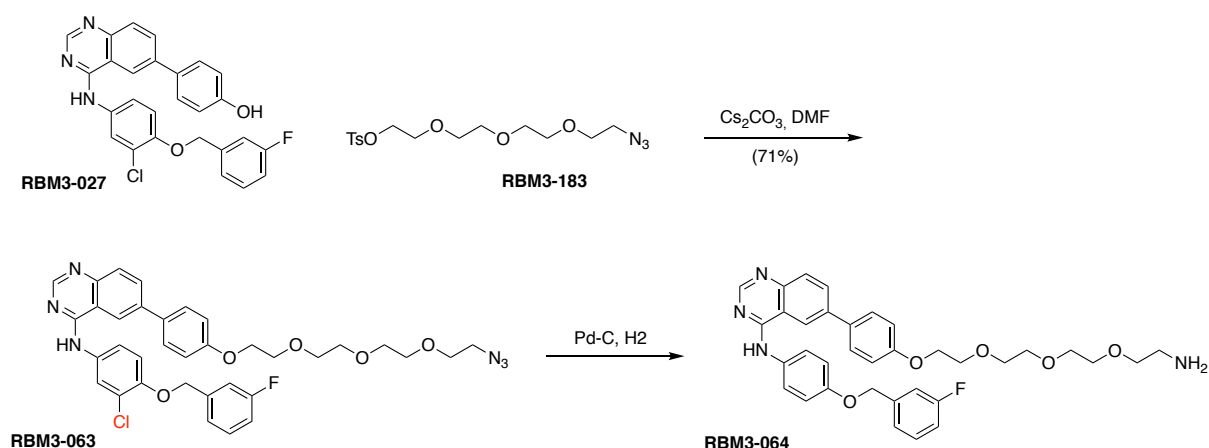
Finally, the direct coupling of **RBM3-006** to the commercially available hydrophobic tags 1-adamantanecarboxylic acid and the *tris*(*tert*-butyl carbamate) protected arginine (Boc₃Arg) yielded **RBM3-357** and **RBM3-358**, respectively (Scheme 20).



Scheme 20: Synthesis of RBM3-357 and RBM3-358.

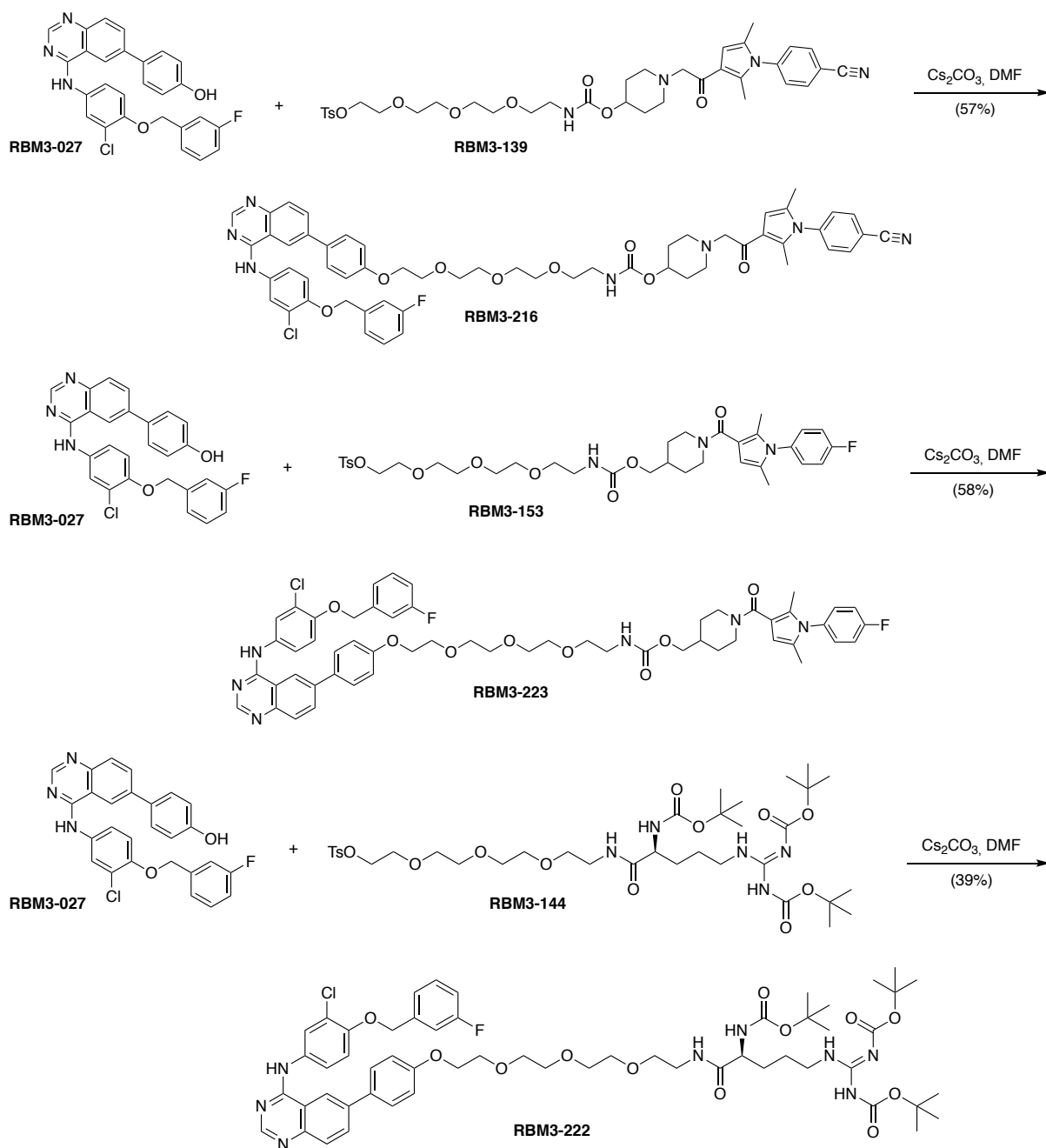
3.2.5. Synthesis of bifunctional chimeras targeting RTK:

The first fragment assembly strategy to achieve hetero-bifunctional molecules for targeted RTK degradation was the *O*-alkylation of **RBM3-027** with **RBM3-183** to yield **RBM3-063**. However, the Pd-catalysed hydrogenation of **RBM3-063** led to dechlorination to the undesired product **RBM3-064** (Scheme 21).



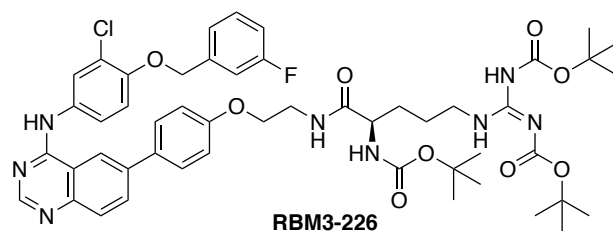
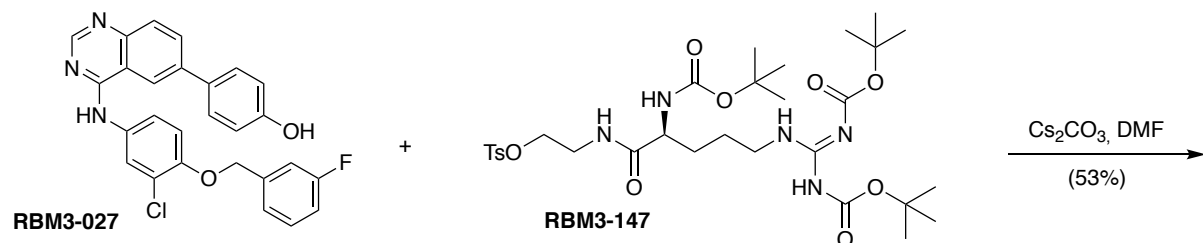
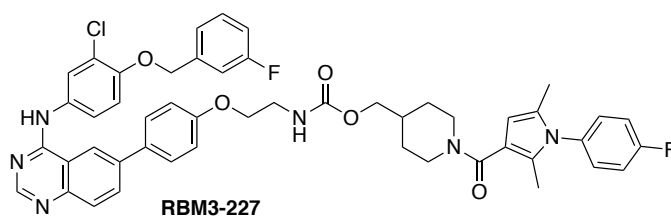
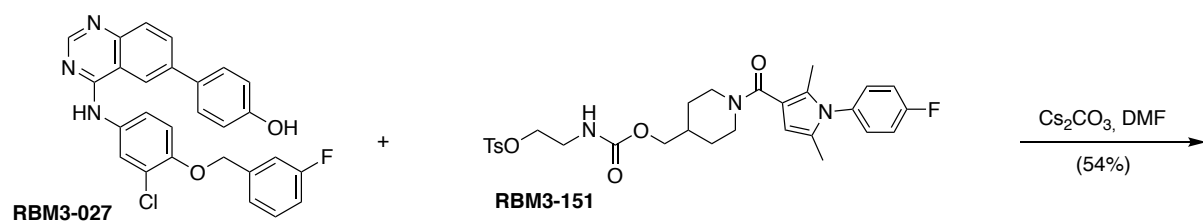
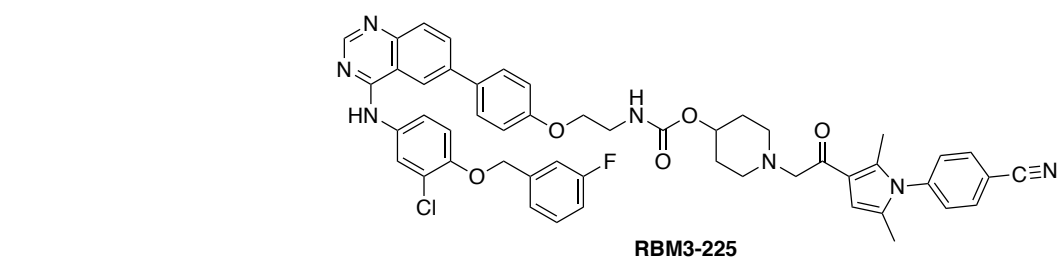
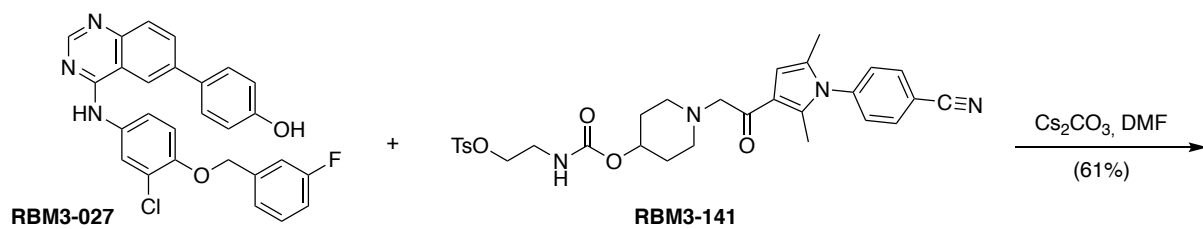
Scheme 21: Hydrogenation of **RBM3-063**.

This result pushed us to modify the fragment assembly strategy. In the new synthetic scheme, classical *O*-alkylation of **RBM3-027** with the tosylate derivatives **RBM3-139**, **RBM3-153** and **RBM3-144** yielded **RBM3-216**, **RBM3-223**, and **RBM3-222**, respectively, all containing three PEG units in the linker. While **RBM3-216** and **RBM3-223** were USP14-based PROTACS, **RBM3-222** was prepared as a HyTag (Scheme 22).



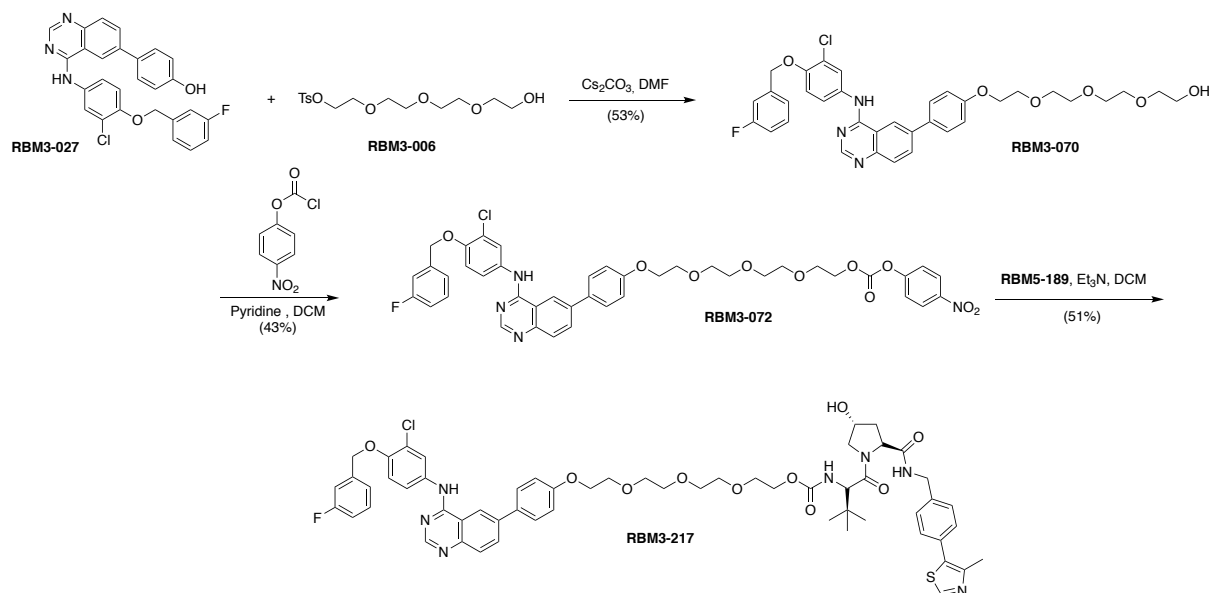
Scheme 22: Synthesis of **RBM3-216**, **RBM3-223** and **RBM3-222**.

Under the same reaction conditions, alkylation of **RBM3-027** with **RBM3-141**, **RBM3-151** and **RBM3-147** provided the USP14-based PROTACS **RBM3-225** and **RBM3-227**, and the HyTag **RBM3-226**, all of them with a shorter PEG linker (Scheme 23).



Scheme 23: Synthesis of **RBM3-225**, **RBM3-227**, and **RBM3-226**.

Finally, a VHL-directed PROTAC (**RBM3-217**) was also synthesized. *O*-alkylation of **RBM3-027** with **RBM3-006** gave **RBM3-070**, which was next activated as the 4-nitrophenol carbonate. Its reaction with **RBM5-189** yielded the chimera **RBM3-217** (Scheme 24).

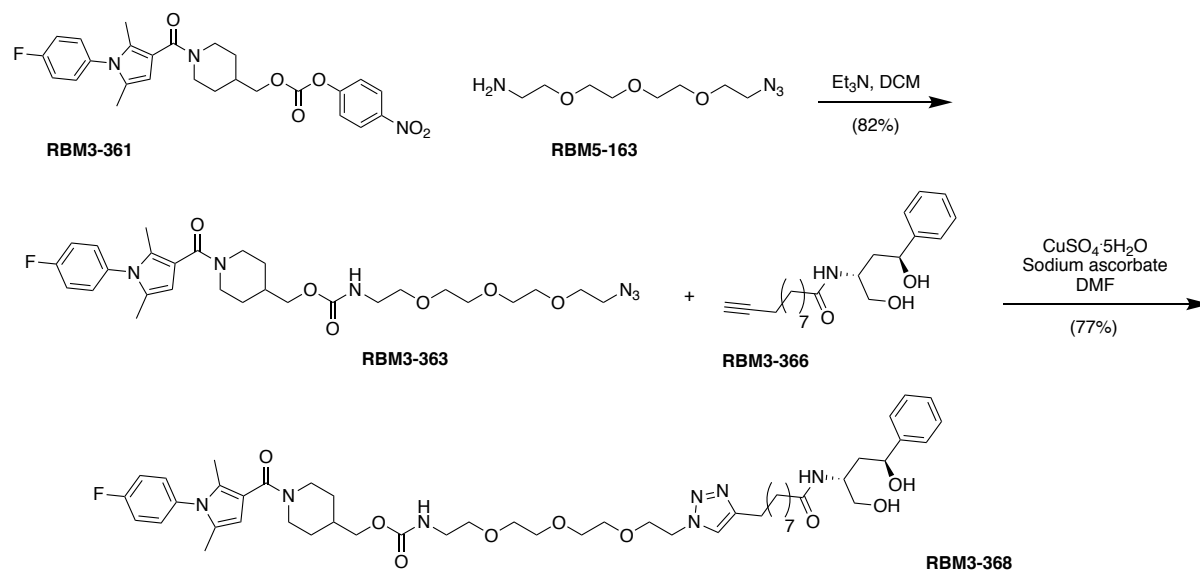


Scheme 24: Synthesis of **RBM3-217**.

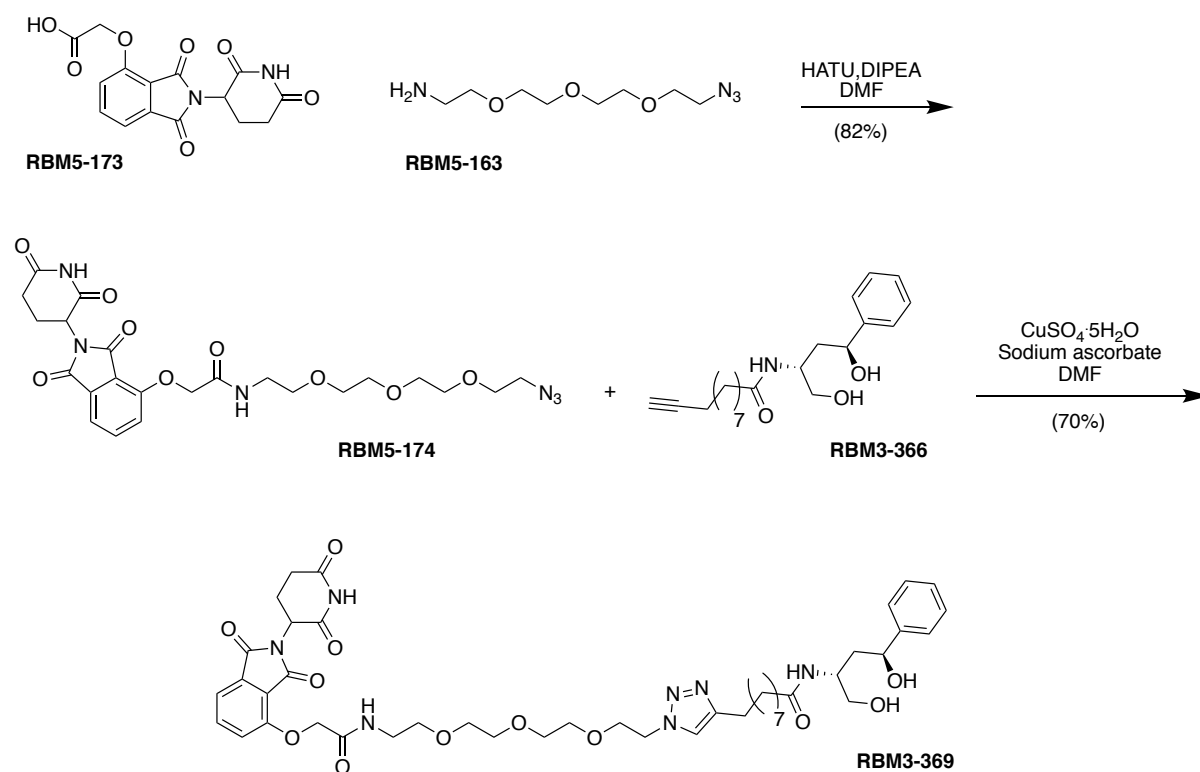
3.2.6. Synthesis of bifunctional chimeras targeting CERT:

The three bifunctional chimeras for CERT degradation used **RBM3-366**, a derivative of the CERT inhibitor HPA12, as CERT ligand. This compound (**RBM3-366**) was synthesized by Dr. José Luís Abad. Carbamate formation between **RBM3-361** and **RBM5-163** provided **RBM3-363**. In the final reactions, **RBM3-366** was condensed with the **RBM3-363** by a Cu-catalyzed alkyne-azide cycloaddition (click chemistry) to provide **RBM3-368** (Scheme 25). **RBM3-369**, a CRBN-based PROTAC that utilized thalidomide as E3 ligand, resulted from amide formation between **RBM5-173** and **RBM5-163** to provided **RBM5-174** which was condensed with the **RBM3-363** to achieve **RBM3-369** by the same click reaction (Scheme 26). Finally, the VHL-based PROTAC was achieved by amide formation between **RBM5-189** and the carboxylic acid linker derivative

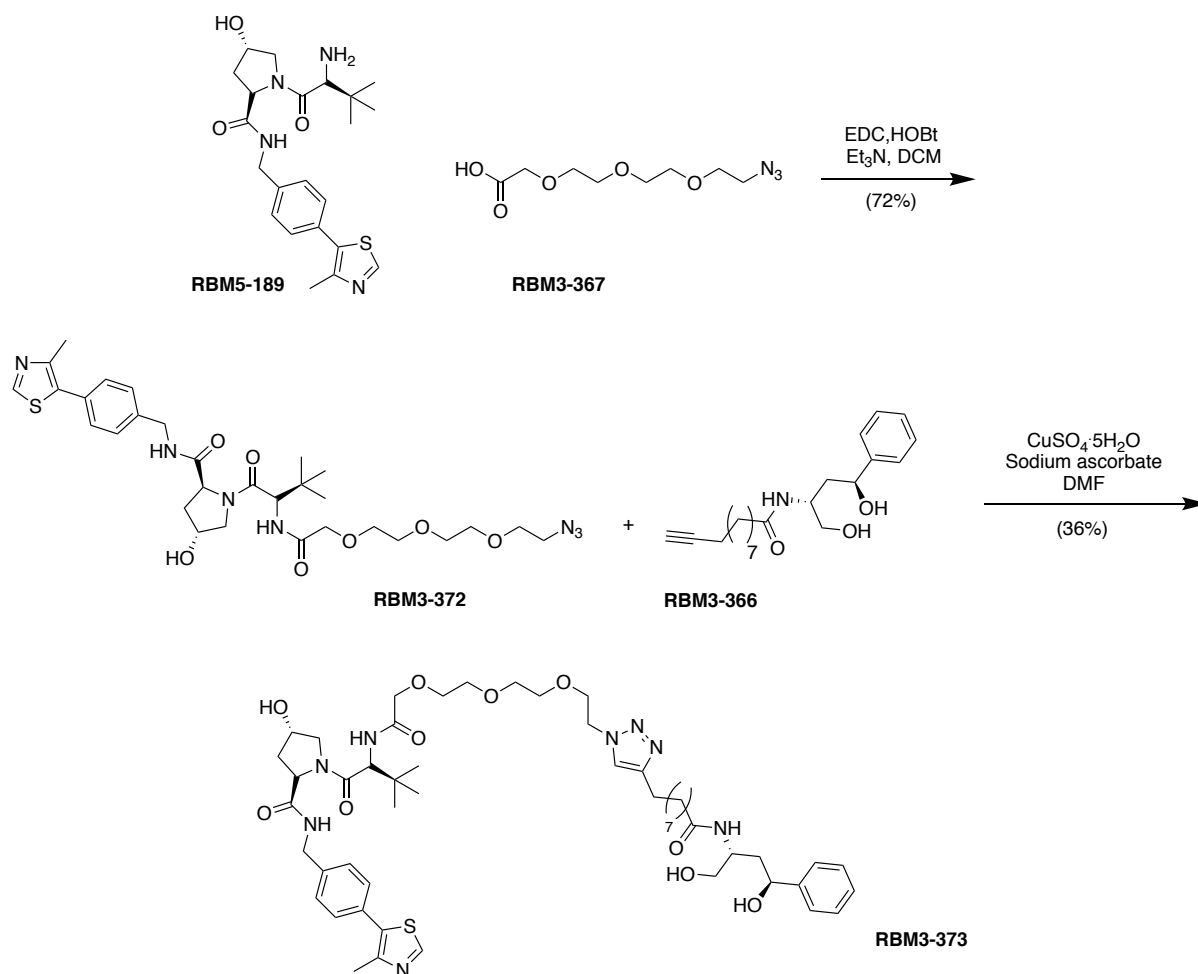
RBM3-367 to provided **RBM3-372**. Following the previous Cu-catalyzed alkyne-azide cycloaddition, reaction between **RBM3-372** and **RBM3-366** provided **RBM3-373** (Scheme 27).



Scheme 25: Synthesis of RBM3-368.



Scheme 26: Synthesis of RBM3-369.



Scheme 27: Synthesis of **RBM3-373**.

3.3. BIOLOGICAL EVALUATION

The biological evaluation of the putative degraders synthesized in this thesis was conducted in our laboratories by Dr. Mireia Casasampere and Tania Roda in collaboration with Dr. Alice Zuin, Dr. Nuria Gallisà and Alba González-Artero from the laboratory of Dr. Bernat Crosas (Institute of Molecular Biology of Barcelona, IBMB-CSIC). A brief account of results is provided next.

In the case of the USP14-based IMPDH2 targeting chimeras featuring IU1-248 as USP14 binder, **RBM3-300**, **RBM3-329** and **RBM3-330** differ in the PEG linker chain length. Among the three compounds, only that with the shorter linker (**RBM3-300**) induced the degradation of IMPDH2 using HeLa cells as models (Figure 20 A-C). These results are in accordance with the reported impact of the linker chain length on the degradative activity of bifunctional chimeras¹¹⁵. An analog of **RBM3-300** with an USP14 binder derived from IU1c (**RBM3-354**) was also prepared. Since IU1c was reported not to inhibit USP14, **RBM3-354** was planned to be used as a negative control of degradation⁴⁰. However, to our surprise, potent IMPDH2 degradation was observed at nM range, with a complete depletion of the target at 0.5 μ M (Figure 20 D), clearly outperforming **RBM3-300**. In agreement with the poor inhibition of USP14 by IU1c⁴³, we confirmed that the IU1c-featuring chimera **RBM3-354** was a weak inhibitor of USP14 *in vitro*. However, quantification of the direct interaction of **RBM3-354** with USP14 by Surface Plasmon Resonance (Dr. Crosas' laboratory) revealed K_D values of 1-6 μ M, 5–10 fold lower than the values corresponding to **RBM3-300**, **RBM3-330** and **RBM3-329**, based on IU1-248 ligand (15-30 μ M). Thus, although IU1c does not inhibit USP14, it is a good USP14 binder so that the IU1c moiety in the context of the chimera appears to offer an optimized profile as a ligand, exhibiting high affinity towards USP14 with low USP14 inhibition. Of note, in agreement with their mechanisms of action, cell treatment with VX-497 did not cause IMPDH2 depletion whereas **RBM3-354** did (Figure 20 D). Importantly, IMPDH2 degradation by **RBM3-300** and **RBM3-354** was attenuated in the presence of the proteasome inhibitors bortezomib and marizomib, but not by the E1-Ub activating enzyme inhibitor MLN7243 (Figure 20 E, F). These results indicated that, in agreement with our new concept of target protein degradation, the USP14-based PROTACS are dependent on proteasome activity, but independent of ubiquitination.

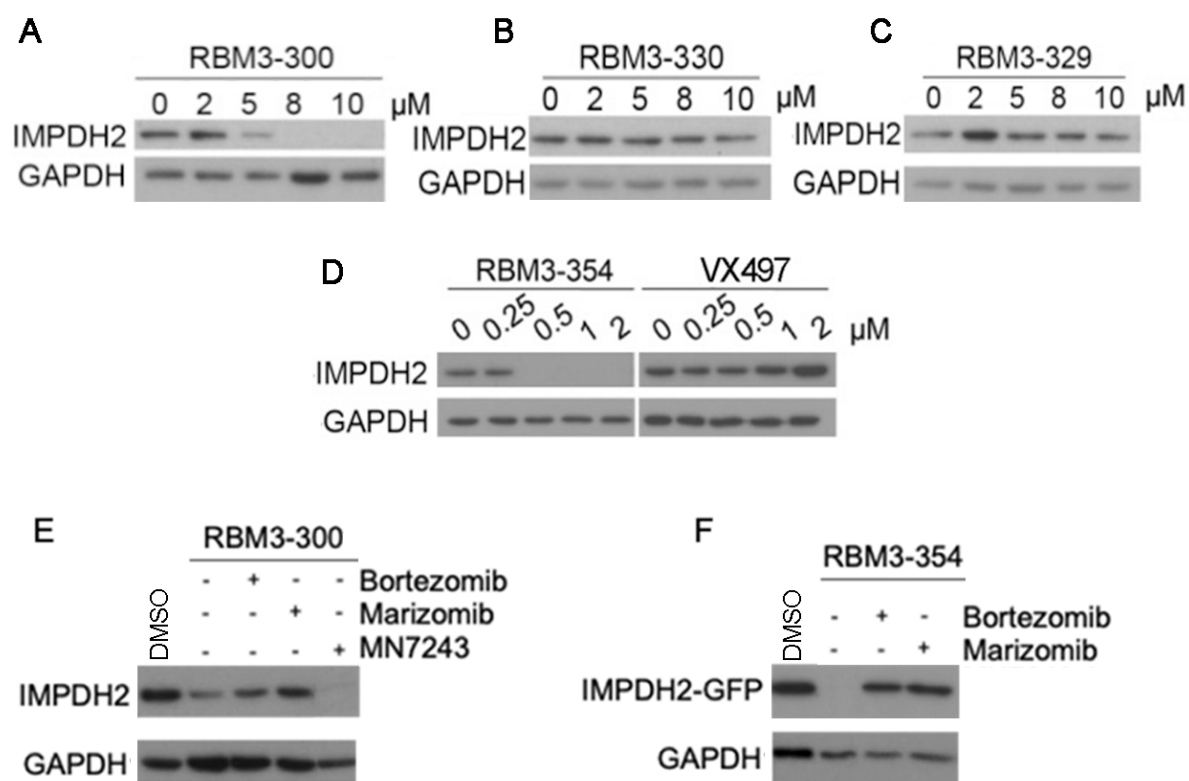


Figure 20: A-D, effect on IMPDH2 levels in HeLa cells treated with the indicated chimeras at the specified concentrations. In A-D, cells were treated with the compounds or DMSO (vehicle control) for 96 h in 5% FBS-containing medium and then cells were lysed and proteins were separated (SDS-PAGE) and immunoblotted with anti-IMPDH2 and anti-GAPDH (loading control). In (D), note that **RBM3-354** but not the IMPDH2 ligand VX-407 promoted IMPDH2 degradation at the sub-micromolar range. E-F, effect of proteasome and E1 Ub-activating enzyme inhibitors on **RBM3-300** and **RBM3-354** activity. HeLa (E) or IMPDH2-GFP overexpressing HeLa cells (F) cells were treated with **RBM3-300** (10 μM) as in A-D, but 16 h before cell collection, proteasome inhibitors (Bortezomib, 20 μM; Marizomib 10 nM) or E1 inhibitor (MN7243, 10 μM) were added.

In order to assess the capacity of chimeras based on E3-ligases at degrading IMPDH2, a set of compounds containing lenalidomide or VHL1-derived moieties for CRBN and VHL recruitment, respectively, instead of the USP14 ligand, were also tested. As shown in Figure 21, treatment of HeLa cells with **RBM3-320**, **RBM3-343**, **RBM3-339** and **RBM3-360** for 24 h at a 2.5-10 μM range failed in the degradation of IMPDH2. Since multiple PROTACS based on CRBN and VHL show rapid proteolytic activity at nanomolar range (Zhou 2017; Lou 2015 Chen, 2022; Zengerle, 2015), we performed treatments in wide concentration and

time ranges, but no degradation of IMPDH2 was observed in any of the conditions tested (data not shown).

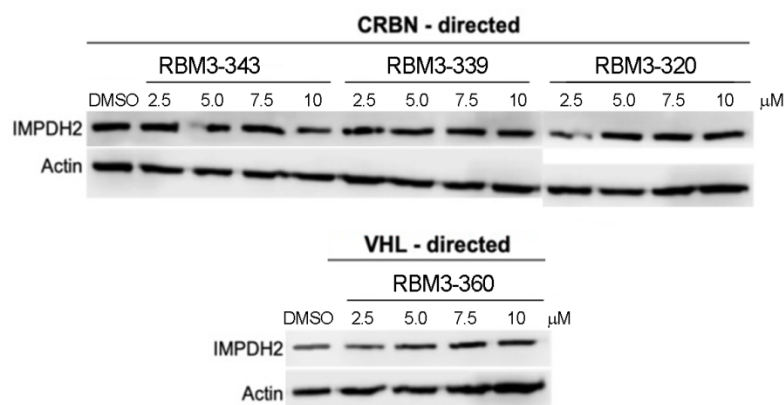


Figure 21: Effect on IMPDH2 levels in HeLa cells treated with the indicated chimeras at the specified concentrations. Cells were treated with the compounds or DMSO (vehicle control) for 24 h in 5% FBS-containing medium and then cells were lysed and proteins were separated (SDS-PAGE) and immunoblotted with anti-IMPDH2 and anti-Actin (loading control).

In a similar experimental setup, chimeras containing hydrophobic tags (**RBM3-357** and **RBM3-358**) exhibited no capacity to induce degradation of IMPDH2 at any of the times and concentrations tested (data not shown).

Having observed good IMPDH2 degradation activity using **RBM3-354**, we asked whether similar results could be obtained for other proteins. CERT, a target in cancer (Swanton, 2007)¹⁰², was first examined. For that purpose, compounds leveraging CERT interaction with HPA-12 antagonist derivatives were designed and synthesized. Treatments of HeLa cells with **RBM3-368** revealed efficient CERT degradation at 24 h (Figure 22-A)¹¹⁶. Furthermore, CERT depletion was abrogated in cells pre-treated with USP14 siRNAs and incubated with **RBM3-368** for 24h (Figure 22-B). Similarly, marizomib rescued CERT degradation induced by **RBM3-368** in MDA-MB-453 breast cancer cells (HER2+/ER-/PR-) (Figure 22-E). These results indicated that CERT degradation by **RBM3-368** involved both the USP14 regulatory particle and the proteasomal activity. Furthermore, CERT degradation was significantly decreased when HPA12 was included in the incubation medium (Figure 22-E). This competition experiment

allowed concluding that CERT depletion involved the engagement of **RBM3-368** with the target protein.

High levels of CERT in breast cancer cells are a well-defined signature of bad prognosis¹¹⁷. Since CERT inactivation has a potential antitumoral effect in cancer, **RBM3-368**-induced degradation was challenged in MDA-MB-231 cells (triple negative phenotype). Twenty-hour treatments with **RBM3-368** showed efficient degradation of CERT (Figure 22-C, left panel), while **RBM3-369** and **RBM3-373**, signaling to CRBN and VHL E3-ligases, respectively, exhibited no capacity to induce CERT degradation in parallel assays (Figure 22-C, middle and right panels) even at different concentrations and treatment times (data not shown). When tested in a time course assay in MDA-MB-231 cells, **RBM3-368** showed a degradation effect in 8-24 h, with a maximum of degradation observed at 16 h (Figure 22-D). Other derivatives of **RBM3-368** differing in the linker length have been synthesized by Dr. Hector Carneros and are currently being tested in breast cancer cell models. As we mentioned in the Introduction, we expect CERT degraders to increase the intracellular levels of ceramides, which triggers signaling pathways leading to programmed cell death, to subsequently sensitize cancer cells to chemotherapeutic drugs. Preliminary experiments with HER2+ BT474 cells showed that the addition of **RBM3-395**, an analog of **RBM3-368** with a shorter linker, to a paclitaxel serial dilution shifted the cell viability curve towards the left, with a 25-fold decrease in the CC₅₀ as compared to paclitaxel alone (Figure 23-A). **RBM3-395** exhibited capacity to degrade CERT (Figure 23-B) with potency similar to **RBM3-368** in this cell line (data not shown). Although a bulk of additional experiments are needed, these preliminary results support that PROTACs against CERT may emerge as sensitizers of cancer cells to chemotherapeutic drugs.

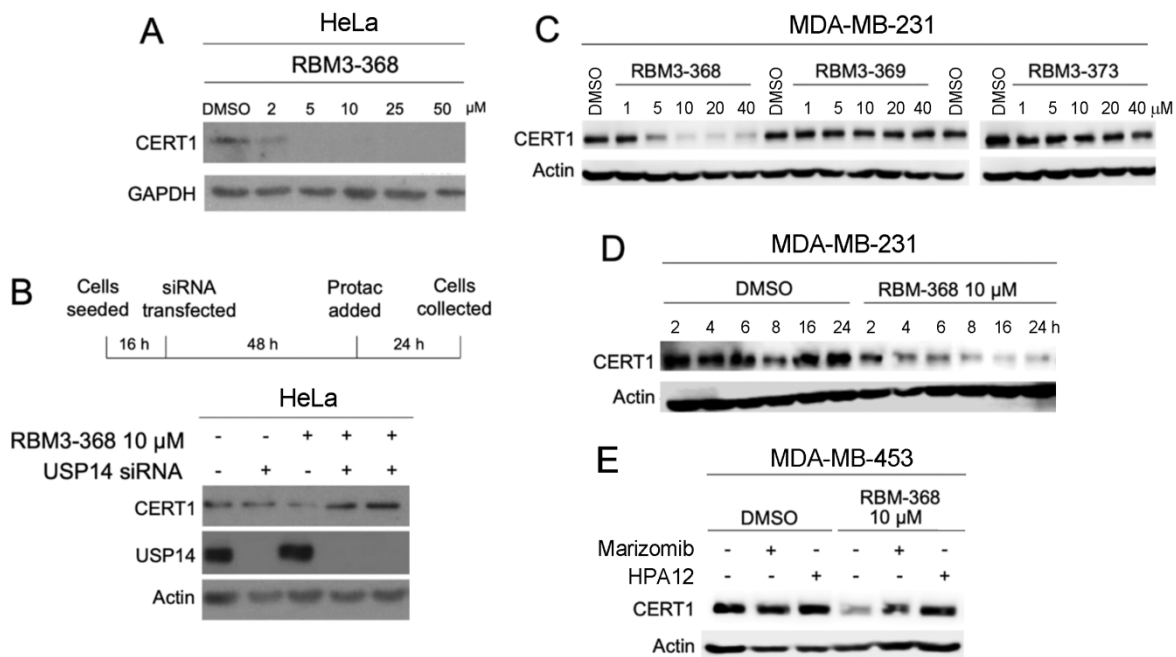


Figure 22: Degradation of CERT by PROTACS in HeLa (A, B) and MDA-MB-231 (C,D) cells. Cells were incubated with the compounds at the indicated concentrations for the specified times (in A, 24 h). B, Effect of USP14 specific siRNAs on stabilizing CERT in the presence of the USP14-based PROTAC **RBM3-368**. The experimental conditions were as indicated. C, Treatment of MDA-MB-231 triple negative breast cancer cells with USP14- (**RBM3-368**) and E3-based protacs (CRBN, **RBM3-369**; VHL, **RBM3-373**). D, Time-course of CERT degradation with **RBM3-368** (10 μ M). E, MDA-MB-453 breast cancer cells (HER2+/ER-/PR-) were treated with HPA-11 (100 μ M) or Marizomib (500 nM) for 3h and then **RBM3-368** (10 μ M) was added (Marizomib, but not HPA-11, was removed before the PROTAC addition). Cells were collected, lysed and processed for immunoblot after 24 h.

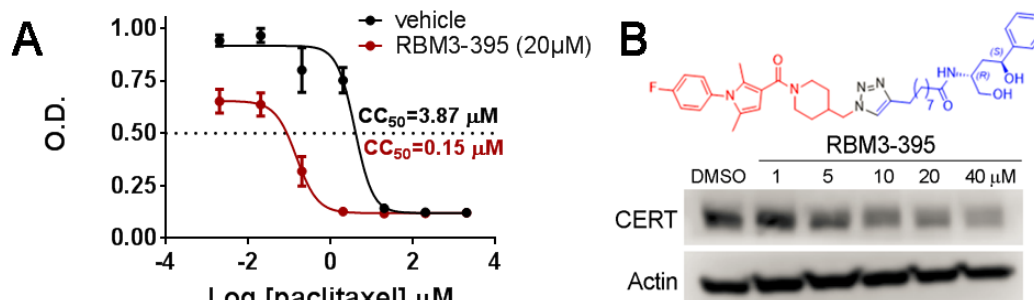


Figure 23: Effect of **RBM3-395** (20 μ M) on the dose response of BT474 breast cancer cells (HER2+/ER+/PR+) to paclitaxel (24 h treatment). Cell viability was determined with the MTT test. The graph corresponds to one experiment with triplicates (mean \pm SD).

Since both IMPDH2 and CERT are cytosolic proteins, we wondered if USP14-based PROTACS could also be useful to degrade cell membrane proteins. Although the paradigm that Lytacs are the appropriate chimeric degraders for transmembrane proteins of the plasma membrane, the Crews' group reported classical, E3-based PROTACS, as inducers of the EGFR, HER2 and c-Met degradation¹⁰⁹ including multiple mutants of EGFR and c-Met. Surprisingly, none of the RTK-targeting chimeras synthesized in this thesis, whether addressed to 26S or E3s, have shown degradation of either EGFR or HER2. Conversely, compound 5 reported by Burslem et al. (commercially available as SJF 1521) behaved as a good EGFR degrader in our hands, thus ruling out the possibility of defective experimental setup. However, while Burslem et al. showed that SJF1521 did not degrade HER2, we also detected HER2 degradation in our experimental conditions (Figure 24). The reasons for this discrepancy are unknown with one possible explanation being the different cell lines used in both studies (OVCAR8 in Crews' work and HeLa in our studies).

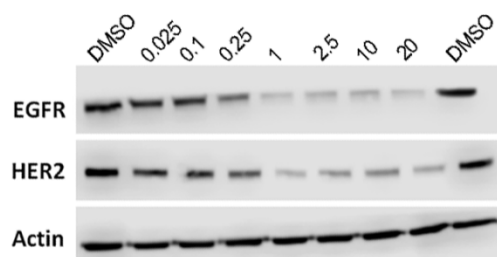


Figure 24: Degradation of EGFR and HER2 by **SJF1521** in HeLa cells. Cells were incubated with the compound at the indicated concentrations for 24 h. Then cells were collected, lysed and processed for immunoblot against EGFR, HER2 and Actin (loading control)

SJF1521 is a VHL-recruiter PROTAC featuring a 12 atoms bridge between ligands. Of note, VHL-based **RBM3-217**, with a 14 atoms bridge, failed to degrade either EGFR or HER2, which adds another instance to the importance of the linker on the degradative capacity of PROTACs. Besides the difference in length, the bridge linkages to the VHL ligand also vary (α -oxyacetamide in

degradation. Although this novel approach lacks the limitations associated to ubiquitination in the classical E3-protacs (i. e. different tissue or cell types' expression patterns of targeted E3, inadequate levels of Ub and/or Ub signaling factors under stressful circumstances), the formation of ineffective ternary complexes threatening the effectiveness of classical E3-based PROTACs is not circumvented by USP14-directed PROTACS. The linker is one of the factors that may lead to weak ternary complexes. Until very recently, linker design and selection was a "trial and error" endeavor. However, future avenues for rational linker design, including advances in computational methods, will accelerate the identification of optimized PROTACs.

CHAPTER 4

Conclusions

- 1) Docking experiments and molecular dynamics of USP14, CERT and IMPDH2 with their respective ligands allowed determining the most suitable placement for the linker moiety in the hetero-bifunctional chimeras prepared in this thesis.
- 2) The synthesized PROTACs were obtained by a convergent, modular approach based on the condensation of suitably modified recruiter ligands and POI warheads with PEG linkers of variable sizes. Linkers were orthogonally functionalized to allow a regiocontrolled condensation with the required ligands. In general, carbamate or amide functional groups were used for condensations of the Usp14 or E3-ligands with IMPDH2 and RTK binders, whereas *O*-alkylation and Cu-catalyzed alkyne-azide cycloaddition (click chemistry) were used to couple the CERT ligands with the linkers.
- 3) Among the three chimeras featuring the USP14 inhibitor IU1-248 (**RBM3-300**, **RBM3-329** and **RBM3-330**), only that with the shorter linker (**RBM3-300**) induced the degradation of IMPDH2. These results are in accordance with the reported impact of the linker chain length on the degradative capacity of bifunctional chimeras.
- 4) The **RBM3-317**-(IU1c analog) featuring chimera **RBM3-354** induced a potent IMPDH2 degradation, clearly outperforming **RBM3-300** (IU1-248 derivative). In agreement with the reported poor inhibition of USP14 by IU1c, **RBM3-354** was a weak USP14 inhibitor *in vitro*. However, it was an excellent UPS14 binder ($K_D=1-6 \mu\text{M}$). Thus, **RBM3-354** exhibits high affinity towards USP14 with low USP14 inhibition, thus emerging as an interesting USP14 recruiter in the context of degradative chimeras.

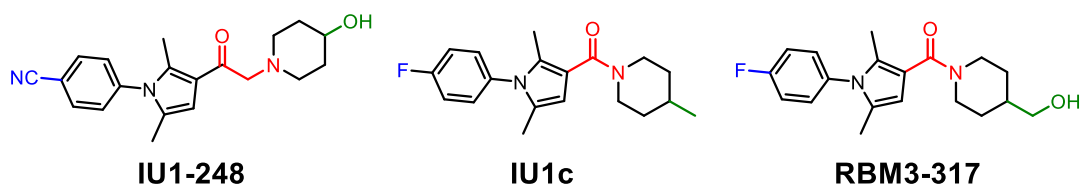


Figure 26: Structures of **IU1-248**, **RBM3-317** and **IU1c**.

- 5) IMPDH2 degradation by **RBM3-300** and **RBM3-354** was attenuated in the presence of the proteasome inhibitors bortezomib and marizomib, but not by the E1-Ub activating enzyme inhibitor MLN7243. Therefore, both USP14-recruited PROTACS are dependent on proteasome activity, but independent of ubiquitination.
- 6) The chimeras based on either E3-ligases (**RBM3-320**, **RBM3-343**, **RBM3-339** and **RBM3-360**) or hydrophobic tags (**RBM3-357** and **RBM3-358**) exhibited no capacity to induce degradation of IMPDH2 at any of the times and concentrations tested.
- 7) The chimera **RBM3-368**, featuring **RBM3-317** as USP14 binder and an analog of the CERT inhibitor HPA12 as warhead induced the degradation of CERT. Such depletion was abrogated by preincubation with marizomib and also by USP14 silencing. Furthermore, **RBM3-368** induced CERT degradation was significantly decreased when HPA12 was included in the incubation medium. These results indicated that CERT degradation by **RBM3-368** involved both the USP14 regulatory particle and the proteasomal activity, as well the engagement with the target protein.
- 8) Preliminary experiments with HER2+ BT474 breast cancer cells showed that **RBM3-395** (an analog of **RBM3-368** with a shorter linker able to induce CERT degradation with a similar potency to **RBM3-368**) sensitized cells to paclitaxel with a 25-fold decrease in the CC₅₀ as compared to paclitaxel alone. These preliminary results support that PROTACS against

CERT may emerge as sensitizers of cancer cells to chemotherapeutic drugs.

- 9) None of the chimeras directed either to USP14 or to E3 were able to degrade the RTKs EGFR and HER2. The most plausible explanation for the lack of activity as RTK degraders of our PROTACS is the formation of weak RTK ligand:linker:recruiter ligand ternary complexes, likely caused by a suboptimal linker. The lack of degradative activity of **RBM3-217** as compared to active **SJF1521** suggests that not only the differences in linker length between both molecules, but also the linkage function to the VHL ligand (α -oxyacetamide in SJF1521 and carbamate in **RBM3-217**. See Figure 27) may play a role in PROTAC induced POI depletion. This hypothesis will be investigated in the near future.
- 10) Overall, we have obtained proof of concept that ubiquitination-independent degradation of cytoplasmatic POIs (i.e. IMPDH2 and CERT) can be achieved by direct recruitment of POIs to the proteasome through the USP14 regulatory particle. Whether this type of novel degraders are able to induce also plasma membrane proteins with cytosolic domains must be further investigated.

CHAPTER 5

Experimental Section

General methods and instruments:

Reactions were performed under Ar atmosphere at rt (25 °C) unless otherwise specified.

Commercially available reagents and solvents were used without any further purification. Anhydrous THF, Et₂O, CH₃CN, DMF and CH₂Cl₂ were obtained by passing through an activated alumina column on a Solvent Purification System and subsequently degassed with inert gas. All reactions were monitored by TLC analysis, using ALUGRAM® SIL G/UV254 (Macherey–Nagel) silica gel pre-coated aluminium sheets (Layer: 0.2 mm, silica gel 60). UV light was used as the visualising agent (at $\lambda = 254$ nm or $\lambda = 365$ nm), and a 5 % (w/v) ethanolic solution of phosphomolybdic acid was used as the developing agent. Flash column chromatography purifications were carried out with the indicated solvent systems using flash-grade silica gel (Chromatogel 60 Å, 35–75 μ m) as the stationary phase. Yields refer to chromatographically and spectroscopically pure compounds, unless otherwise stated.

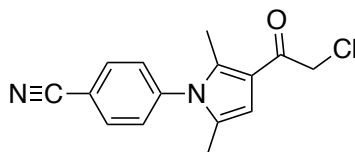
NMR spectra were recorded at room temperature on a Varian Mercury 400 (¹H NMR at 400 MHz and ¹³C NMR at 100.6 MHz) spectrometer using CDCl₃, CD₃OD or DMSO-*d*₆ as solvents. The chemical shifts are reported in parts per million (ppm) relative to the deuterated solvent, and the coupling constants (*J*) are given in Hertz (Hz). The multiplicities in the ¹H NMR spectra have been defined using the following abbreviations: s = singlet, d = doublet, t = triplet, q = quartet, dd = doublet of doublets, ddd = doublet of doublet of doublets, m = multiplet and br = broad signal.

HRMS analyses were performed on an Acquity UPLC system coupled to an LCT Premier orthogonal accelerated time-of-flight mass spectrometer (Waters) through electrospray ionization (ESI). Samples were analysed by FIA (Flow Injection Analysis), using MeCN/water (70:30) as the mobile

phase, and a 10 μL injection volume. m/z ratios are reported in atomic mass units.

I. USP14 ligands

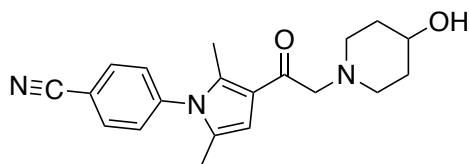
4-(3-(2-chloroacetyl)-2,5-dimethyl-1*H*-pyrrol-1-yl)benzotrile (RBM-001).



In a round-bottom flask equipped with a magnetic stir bar and under an inert atmosphere were placed 4-(2,5-dimethyl-1*H*-pyrrol-1-yl)benzotrile (2.000 g, 10.191 mmol) in 1,2-dichloroethane (10 mL). A mixture of 2-chloroacetyl chloride (0.97 mL, 12.229 mmol) and Sn₄Cl in 1,2-dichloroethane (10 mL) was added dropwise for 1 h. The reaction was maintained at rt and monitored by TLC until complete consumption of the starting material was observed (5 h). The reaction mixture was then quenched by the addition of water, and the aqueous phase was extracted with CH₂Cl₂. The combined organic layers were washed with water, dried with anhydrous MgSO₄, the solvent was evaporated under reduced pressure, and the residues was directly subjected to flash chromatography, using hexane/EtOAc (7.5:2.5) as an eluent to afford **RBM3-001** (2.280 g, 8.360 mmol, 82% yield) as a white solid. Spectral data were in agreement with the reported data (WO2020006269).

¹H NMR (400 MHz, CDCl₃): δ 7.85 (d, *J* = 8.4 Hz, 2H), 7.35 (d, *J* = 8.5 Hz, 2H), 6.36 (d, *J* = 1.2 Hz, 1H), 4.48 (s, 2H), 2.34 (s, 3H), 2.00 (s, 3H). ¹³C NMR (101 MHz, CDCl₃): δ 191.9, 160.6, 141.4, 136.5, 133.6, 129.2, 117.9, 113.2, 107.8, 42.9, 12.9. HRMS calcd. for C₁₅H₁₄ClN₂O ([M+H]⁺): 273.0795, found: 273.0806.

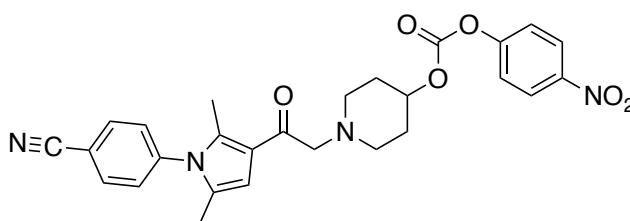
4-(3-(2-(4-hydroxypiperidin-1-yl)acetyl)-2,5-dimethyl-1*H*-pyrrol-1-yl)benzotrile (IU1-248).



4-Hydroxypiperidine (0.638 g, 6.30 mmol) was added to a solution of **RBM3-001** (1.56 g, 5.73 mmol) and TEA (1.59 mL, 11.46 mmol) in 30 mL of acetonitrile. The resulting mixture was heated to 85 °C for 2 h. The reaction mixture was concentrated under reduced pressure, and the residue was redissolved in 30 mL of ethyl acetate, washed with saturated NaHCO₃ aqueous solution, dried with anhydrous Na₂SO₄, and purified by silica gel column chromatography CH₂Cl₂/MeOH (9:1) to obtain IU1-248 (0.93 g, 2.76 mmol, 67% yield). Spectral data were in agreement with those reported in the literature¹¹⁸.

¹H NMR (400 MHz, CDCl₃): δ 7.85 (d, *J* = 8.5 Hz, 2H), 7.35 (d, *J* = 8.4 Hz, 2H), 6.43 (s, 1H), 3.77 (tt, *J* = 8.7, 4.0 Hz, 1H), 3.63 (s, 2H), 2.92 (dt, *J* = 10.9, 4.4 Hz, 2H), 2.45 – 2.34 (m, 2H), 2.34 (s, 3H), 2.01 (s, 3H), 2.00 – 1.91 (m, 2H), 1.78 – 1.67 (m, 2H). ¹³C NMR (101 MHz, CDCl₃): δ 193.9, 160.6, 141.4, 136.5, 133.6, 129.2, 117.9, 113.2, 107.8, 50.9, 33.8, 20.8, 13.2, 12.9. HRMS calcd. for C₂₀H₂₃N₃O₂ ([M+H]⁺): 338.1869, found: 338.1896.

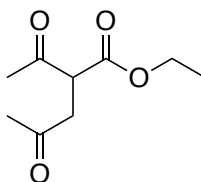
1-(2-(1-(4-cyanophenyl)-2,5-dimethyl-1*H*-pyrrol-3-yl)-2-oxoethyl)piperidin-4-yl(4-nitrophenyl) carbonate (RBM3-308)



To a stirred solution of IU1-248 (182.0 mg, 0.539 mmol) in anhydrous CH₂Cl₂ (9.1 mL), TEA (0.226 mL, 1.618 mmol) and *p*-nitrophenyl chloroformate (272 mg, 1.348 mmol) were sequentially added. After stirring at 25 °C for 30 min, the mixture was quenched with saturated aqueous NH₄Cl (15 mL) and extracted with CH₂Cl₂ (3 x 20 mL). The combined organic layers were dried over MgSO₄, solvent was evaporated and the residue was purified by silica gel column chromatography using 50% to 60% of EtOAc in hexanes to afford the compound **RBM3-308** (177.0 mg, 0.352 mmol, 65%).

¹H NMR (400 MHz, CDCl₃): δ 8.29 (d, *J* = 9.2 Hz, 2H), 7.84 (d, *J* = 8.4 Hz, 2H), 7.37 (dd, *J* = 24.6, 8.8 Hz, 2H), 6.41 (s, 1H), 4.90 – 4.81 (m, 1H), 3.66 (s, 2H), 2.98 – 2.81 (m, 2H), 2.53 (t, *J* = 8.4 Hz, 1H), 2.33 (s, 3H), 2.17 – 2.08 (m, 2H), 2.01 (s, 3H), 2.04 – 1.94 (m, 2H).

Ethyl 2-acetyl-4-oxopentanoate (RBM3-311)

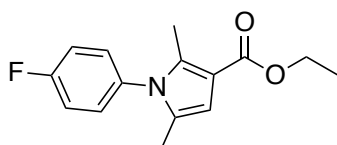


To a round-bottom flask equipped with a condenser was added 2-chloroacetone (460 mg, 5.0 mmol), ethyl acetoacetate (650 mg, 5.0 mmol), and triethylamine (10 mL). The reaction mixture was refluxed and monitored by TLC. After 6 h, the completion of the reaction was achieved. Triethylamine was distilled away by vacuum. The concentrated mixture was added to water, and the aqueous phase was extracted with CH₂Cl₂. The organic layer was washed with brine, dried with anhydrous MgSO₄, and the solvent was evaporated under reduced pressure to yield a crude reaction product. The crude mixture was purified by silica gel column chromatography using ethyl acetate/hexane as eluent in increasing

polarity to yield **RBM3-311** as a colorless liquid (706 mg, 3.791mmol, 76 % yield). Spectral data were in agreement with those reported in the literature¹¹⁹.

¹H NMR (400 MHz, CDCl₃): δ 4.14 (qd, *J* = 7.1, 0.9 Hz, 2 H), 3.96 (dd, *J* = 8.1, 5.8 Hz, 1 H), 3.08 (dd, *J* = 18.5, 8.2 Hz, 1 H), 2.89 (dd, *J* = 18.5, 5.7 Hz, 1 H), 2.30 (s, 3 H), 2.14 (s, 3 H), 1.22 (td, *J* = 7.1, 0.9 Hz, 3 H). ¹³C NMR (101 MHz, CDCl₃): δ 205.58, 202.15, 168.72, 61.66, 53.69, 41.47, 30.01, 29.62, 13.96. HRMS calcd. for C₉H₁₄O₄ ([M+H]⁺): 186.0892, found: 187.0842.

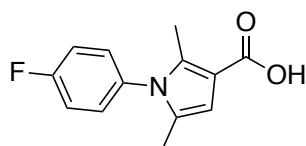
Ethyl 1-(4-fluorophenyl)-2,5-dimethyl-1*H*-pyrrole-3-carboxylate (RBM3-312)



To a stirred solution of **RBM3-11** (8.5 g, 45.584 mmol) in acetonitrile (125 mL), 4-fluoroaniline (6.087 g, 54.778 mmol) was added and the reaction mixture was heated to 90 °C. After 2 h, the mixture was cooled, dissolved in EtOAc (100 mL) and washed with 10% citric acid (3 × 50 mL), water (3 × 50 mL), and brine, and then dried over MgSO₄, filtered and concentrated under reduced pressure. The crude mixture was recrystallised from EtOH/water, dissolved in warm EtOH (10 mL), and cooled in ice until crystallisation was initiated. Then 40% EtOH (40 mL) was added slowly with stirring and cooled in ice for 30 minutes to complete crystallisation and the solution was filtered. The resulting red/brown crystals were finally washed with 20% EtOH and dried under a vacuum to give **RBM3-312** (7.654 g, 29.292 mmol, 64.2% yield). Spectral data were in agreement with those reported in the literature¹²⁰.

^1H NMR (400 MHz, CDCl_3): δ 7.19–7.16 (4H, m), 6.37 (1H, s), 4.28 (2H, q, J 7.1), 2.28 (3H, s), 1.96 (3H, s), 1.34 (3H, d, J 7.1); ^{13}C NMR (101 MHz, CDCl_3): δ 165.6, 162.3 (d, J 248.8), 136.2, 133.7 (d, J 2.9), 129.9 (d, J 8.7), 128.8, 116.4 (d, J 22.8), 111.6, 107.6, 59.3, 14.5, 12.6, 12.3. HRMS calcd. for $\text{C}_{15}\text{H}_{16}\text{FNO}_2$ ($[\text{M}+\text{H}]^+$): 261.1165, found: 262.1115.

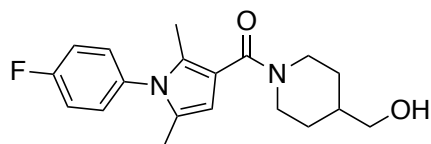
1-(4-Fluorophenyl)-2,5-dimethyl-1*H*-pyrrole-3-carboxylic acid (RBM3-313)



To a round-bottom flask equipped with a condenser was added **RBM3-312** (2.650 g, 10.142 mmol) and 20% aqueous NaOH (40 mL) in EtOH (30 mL). The reaction mixture was refluxed overnight. Then, the reaction mixture was cooled in an ice bath and 15 % HCl was added slowly until a pale precipitate formed. The mixture was stirred for a further 15 min. and then filtered. The pale brown pad was washed with water (2×25 mL). After drying under vacuum, **RBM3-313** was obtained as a pale brown powder (2.012 g, 8.626 mmol, 85% yield). Spectral data were in agreement with those reported in the literature¹²⁰.

^1H NMR (400 MHz, CDCl_3): δ 7.19 (4H, app d, J 6.4), 6.42 (1H, br s), 2.30 (3H, s), 1.97 (3H,s). ^{13}C NMR (101 MHz, CDCl_3): δ 171.09, 162.4 (d, J 249.0), 137.8, 133.6 (d, J 2.7), 129.9 (d, J 8.6), 129.2, 116.5 (d, J 22.8), 110.8, 108.2, 12.6, 12.5.

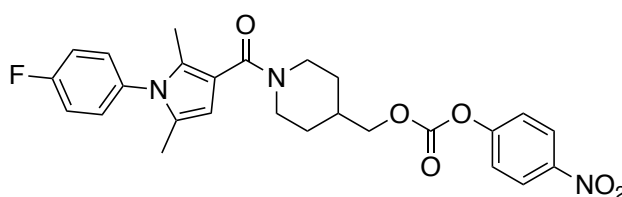
(1-(4-Fluorophenyl)-2,5-dimethyl-1*H*-pyrrol-3-yl)(4-(hydroxymethyl)piperidin-1-yl)methanone (RBM3-317)



EDC·HCl (1.97 g, 10.29 mmol) and HOBT (1.28 g, 8.36 mmol) were sequentially added to a solution of the corresponding carboxylic acid **RBM3-313** (1.5 g, 6.431 mmol) in DMF (30 mL), and the resulting mixture was vigorously stirred at 25 °C under argon atmosphere. After 15 min, the previous mixture was added dropwise to a solution of the 4-(hydroxymethyl)piperidine (0.889 g, 7.72 mmol) and TEA (3.6 mL, 25.72 mmol) in DMF (30 mL), and the reaction was stirred at 25 °C overnight. The mixture was next diluted with CH₂Cl₂ (50 mL) and washed with brine (2 x 25 mL). The organic layer was dried over MgSO₄, filtered, and the volatiles were removed under reduced pressure. Purification of the crude mixture by flash column chromatography CH₂Cl₂/MeOH (9:1) afforded the corresponding amide **RBM3-317** (2.0 g, 6.053 mmol, 94%) as a brown wax.

¹H NMR (400 MHz, CDCl₃): δ 7.23 – 7.14 (m, 4H), 5.97 (s, 1H), 4.49 (br s, 1H), 3.56 (d, *J* = 5.8 Hz, 2H), 2.09 (s, 3H), 1.98 (s, 3H), 1.86 – 1.82 (m, 1H), 1.81–1.79 (m, 2H), 1.75 – 1.71 (m, 3H), 1.33 – 1.18 (m, 2H). ¹³C NMR (101 MHz, CDCl₃): δ 168.0, 163.5, 161.0, 130.7, 130.1, 130.0, 128.3, 116.5, 116.2, 115.1, 106.4, 67.7, 39.3, 29.8, 12.8, 12.1. HRMS calcd. for C₁₉H₂₄FN₂O₂ ([M+H]⁺): 331.1822, found: 331.1849.

(1-(1-(4-Fluorophenyl)-2,5-dimethyl-1H-pyrrole-3-carbonyl)piperidin-4-yl)methyl (4-nitrophenyl) carbonate (RBM3-361)

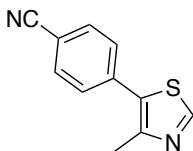


To a stirred solution of **RBM3-317** (0.307 g, 0.929 mmol) in anhydrous CH₂Cl₂ (9.4 mL), pyridine (0.224 mL, 2.788 mmol) and *p*-nitrophenyl chloroformate (0.468 g, 2.323 mmol) were sequentially added. After stirring at 25 °C for 30 min, the mixture was quenched with saturated aqueous NH₄Cl (10 mL) and extracted with CH₂Cl₂ (3 x 10 mL). The combined organic layers were dried over MgSO₄, filtered, and concentrated in vacuo. The residue was purified by flash column chromatography (from 50% to 60% EtOAc in hexanes) to give **RBM3-361** (342 mg, 0.690 mmol, 74% yield).

¹H NMR (400 MHz, CDCl₃): δ 8.34 – 8.25 (m, 2H), 7.44 – 7.35 (m, 2H), 7.22 – 7.13 (m, 4H), 5.97 (s, 1H), 4.54 (br s, 2H), 4.20 (d, *J* = 6.5 Hz, 2H), 2.92 (br s, 2H), 2.13 – 2.03 (m, 1H), 2.09 (s, 3H), 1.98 (s, 3H), 1.89 – 1.83 (m, 2H), 1.36 (qd, *J* = 12.4, 4.3 Hz, 2H). ¹³C NMR (101 MHz, CDCl₃): δ 171.1, 167.9, 163.4, 160.9, 155.5, 152.5, 145.4, 134.1, 130.9, 130.0, 129.9, 128.2, 125.3, 121.8, 116.4, 116.1, 114.8, 106.3, 73.1, 60.4, 35.9, 21.0, 14.2, 12.6, 12.0. HRMS calcd for C₂₆H₂₇FN₃O₆ ([M+H]⁺): 496.1884, found: 496.1814.

II. E3 ligands

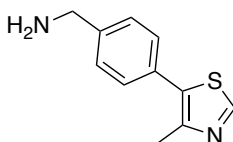
4-(4-Methylthiazol-5-yl) benzonitrile (RBM5-183)



KOAc (1.62 g, 16.479 mmol) and Pd(OAc)₂ (19 mg, 0.085 mmol) were added to a solution of 4-bromobenzonitrile (1.50 g, 8.241 mmol) and 4-methylthiazole (1.634 g, 16.482 mmol) in degassed dimethylacetamide (30 mL). The resulting mixture was heated to 140 °C and stirred overnight under argon. The reaction mixture was subjected to a high-pressure vacuum at 105 °C to eliminate the excess amount of 4-methylthiazole. After cooling to 25 °C, the reaction mixture was diluted with water and extracted with CH₂Cl₂ (3 x 100 mL). The combined organic layers were dried over MgSO₄, evaporated under reduced pressure, and the crude was purified by flash column chromatography on silica gel (from 0 to 24 % EtOAc in CH₂Cl₂) to obtain the corresponding cyano derivate **RBM5-183** (1.6 g, 7.990 mmol, 97 %) as a beige solid. Spectral data were in agreement with those reported in the literature¹¹⁰.

¹H NMR (400 MHz, CDCl₃): δ 8.77 (s, 1H), 7.72 (d, *J* = 8.6 Hz, 2H), 7.56 (d, *J* = 8.5 Hz, 2H), 2.57 (s, 3H). ¹³C NMR (101 MHz, CDCl₃): δ 151.7, 150.1, 136.9, 132.6, 130.2, 129.8, 118.5, 111.6, 16.4. HRMS calcd. for C₁₁H₉N₂S ([M+H]⁺): 201.0481, found: 201.0482.

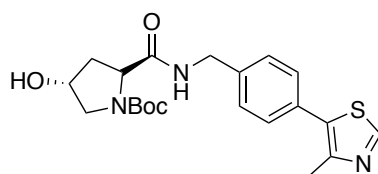
(4-(4-Methylthiazol-5-yl)phenyl)methanamine (RBM5-184)



To an ice-cooled solution of **RBM5-183** (1.3 g, 6.492 mmol) in degassed MeOH (65 mL) containing CoCl₂·6H₂O (2.315 g, 9.731 mmol), NaBH₄ (1.226 g, 32.416 mmol) was added portion-wise. After the addition, the reaction mixture became black, and an apparent bubbling was observed. After stirring for 2 h at 25 °C, the reaction mixture was quenched with water (15 mL) and 30 % (w/w) aq. NH₄OH (15 mL), and the mixture was extracted with CHCl₃ (6 × 30 mL). The combined organic extracts were dried over MgSO₄, filtered, and concentrated to dryness. The resulting crude was purified by flash column chromatography (from 0 to 50 % 0.5 M methanolic NH₄OH in CH₂Cl₂) to yield **RBM5-184** (0.695 g, 3.402 mmol, 52 %) as a yellow oil. Spectral data were in agreement with those reported in the literature¹²¹.

¹H NMR (400 MHz, CD₃OD): δ 8.88 (s, 1H), 7.47 (s, 4H), 3.90 (s, 2H), 2.48 (s, 3H). ¹³C NMR (101 MHz, CD₃OD): δ 152.8, 149.1, 141.2, 133.2, 131.9, 130.5, 129.4, 45.6, 15.9.

***tert*-Butyl(2*S*,4*R*)-4-hydroxy-2-((4-(4-methylthiazol-5 yl) benzyl) carbamoyl) pyrrolidine-1-carboxylate (**RBM5-186**)**

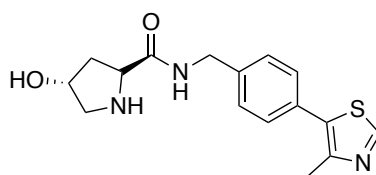


EDC·HCl (526 mg, 2.74 mmol) and HOBT (301 mg, 2.23 mmol) were sequentially added to a solution of 1-(*tert*-butoxycarbonyl)-4-hydroxypyrrolidine-2-carboxylic acid (Boc-*L*-Hyp-OH) (475 mg, 2.06 mmol) in CH₂Cl₂ (15 mL), and the resulting mixture was vigorously stirred at 25 °C under argon atmosphere. After 15 min, the previous mixture was added dropwise to a

solution of **RBM5-184** (350 mg, 1.71 mmol) and TEA (0.96 mL, 6.85 mmol) in CH₂Cl₂ (15 mL), and the reaction was stirred at 25 °C overnight. The mixture was next diluted with CH₂Cl₂ (50 mL) and washed with brine (2 x 25 mL). The organic layer was dried over MgSO₄, filtered, and the volatiles were removed under reduced pressure. Purification of the crude mixture by flash column chromatography (from 0 to 8% MeOH in CH₂Cl₂) afforded **RBM5-186** as a colorless foamy wax (450 mg, 1.078 mmol, 63 %). Spectral data were in agreement with those reported in the literature¹²².

¹H NMR (400 MHz, CD₃OD): δ 8.94 (s, 1H), 8.72 – 8.56 (m, 1H), 7.47 – 7.38 (m, 4H), 4.54 – 4.29 (m, 4H), 3.59 (ddd, *J* = 11.7, 8.5, 4.1 Hz, 1H), 3.54 – 3.46 (m, 1H), 2.47 (s, 3H), 2.31 – 2.20 (m, 1H), 2.03 (ddd, *J* = 13.1, 8.5, 4.5 Hz, 1H), 1.32 (s, 9H). ¹³C NMR (101 MHz, CD₃OD): δ 175.5, 156.5, 156.1, 153.1, 148.7, 148.5, 140.4, 133.5, 131.6, 131.2, 130.5, 130.3, 129.7, 128.9, 81.6, 81.4, 70.7, 70.0, 60.8, 60.6, 56.3, 56.0, 43.9, 43.8, 43.5, 40.8, 39.9, 28.7, 28.5, 15.6. HRMS calcd. for C₂₁H₂₈N₃O₄S ([M+H]⁺): 418.1795, found: 418.1799.

(2*S*,4*R*)-4-Hydroxy-*N*-(4-(4-methylthiazol-5-yl)benzyl)pyrrolidine-2-carboxamide (RBM5-187)

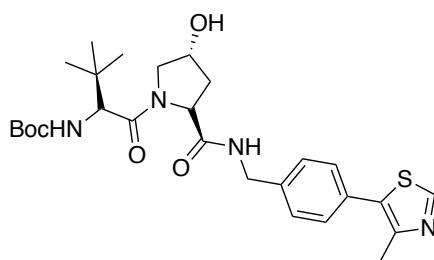


To an ice-cooled solution of **RBM5-186** (400 mg, 0.96 mmol) in CH₂Cl₂ (10 mL) neat TFA (10 mL) was added dropwise. After stirring at 25 °C for 2 h, the reaction mixture was concentrated *in vacuo*. Purification of the crude by flash chromatography on silica gel (from 0 to 20 % MeOH in CH₂Cl₂) afforded **RBM5-**

187 (410 mg, 1.198 mmol, quant.) as a colorless foamy wax. Spectral data were in agreement with those reported in the literature¹²².

¹H NMR (400 MHz, CD₃OD): δ 8.87 (s, 1H), 7.38 (s, 4H), 4.70 – 4.55 (m, 2H), 4.47 (s, 2H), 3.50 (dd, *J* = 12.2, 3.6 Hz, 1H), 3.39 (d, *J* = 12.2 Hz, 1H), 2.53 (dd, *J* = 13.4, 7.4 Hz, 1H), 2.42 (s, 3H), 2.11 (ddd, *J* = 14.1, 10.8, 4.0 Hz, 1H). ¹³C NMR (101 MHz, CD₃OD): δ 169.6, 152.9, 148.8, 139.5, 133.2, 131.7, 130.4, 129.1, 71.2, 60.0, 55.0, 43.9, 39.9, 15.8. HRMS calcd. for C₁₆H₂₀N₃O₂S ([M+H]⁺): 318.1271, found: 318.1273.

***tert*-Butyl ((*S*)-1-((2*S*,4*R*)-4-hydroxy-2-((4-(4-methylthiazol-5-yl)benzyl)carbamoyl) pyrrolidin-1-yl)-3,3-dimethyl-1-oxobutan-2-yl)carbamate (RBM5-188)**

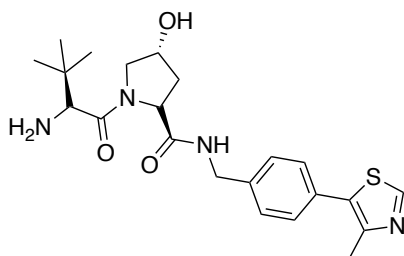


EDC·HCl (256 mg, 1.34 mmol) and HOBt (147 mg, 1.08 mmol) were sequentially added to a solution of (*S*)-2-((*tert*-butoxycarbonyl)amino)-3,3-dimethylbutanoic acid (Boc-*L*-*tert*-Leu-OH) (232 mg, 1.00 mmol) in CH₂Cl₂ (10 mL), and the resulting mixture was vigorously stirred at 25 °C under argon atmosphere. After 15 min, the previous mixture was added dropwise to a solution of **RBM5-187** (360 mg, 0.83 mmol) and TEA (0.58 mL, 4.17 mmol) in CH₂Cl₂ (10 mL), and the reaction was stirred at 25 °C overnight. The mixture was next diluted with CH₂Cl₂ (50 mL) and washed with brine (2 x 25 mL). The organic layer was dried over MgSO₄, filtered, and the volatiles were removed under reduced pressure. Purification of the crude mixture by flash column

chromatography (from 0 to 10% MeOH in CH₂Cl₂) afforded **RBM5-188** as colorless foamy wax (310 mg, 0.584 mmol, 70 %). Spectral data were in agreement with those reported in the literature¹²².

¹H NMR (400 MHz, CD₃OD): δ 8.86 (s, 1H), 7.44 (d, *J* = 8.4 Hz, 2H), 7.39 (d, *J* = 8.4 Hz, 2H), 6.39 (d, *J* = 9.3 Hz, 1H), 4.63 (t, *J* = 8.3 Hz, 1H), 4.52 (d, *J* = 15.5 Hz, 2H), 4.40 – 4.27 (m, 2H), 3.88 (d, *J* = 11.0 Hz, 1H), 3.80 (dd, *J* = 10.8, 3.7 Hz, 1H), 2.45 (s, 3H), 2.22 (dd, *J* = 13.1, 7.8 Hz, 1H), 2.10 (ddd, *J* = 13.0, 8.9, 3.9 Hz, 1H), 1.43 (s, 9H), 1.01 (s, 9H). ¹³C NMR (101 MHz, CD₃OD): δ 174.3, 172.7, 157.7, 152.7, 148.9, 140.1, 133.3, 131.4, 130.3, 128.9, 80.5, 71.0, 60.7, 60.3, 57.9, 49.0, 43.6, 38.8, 36.8, 28.7, 26.9, 15.9. HRMS calcd. for C₂₇H₃₉N₄O₅S ([M+H]⁺): 531.2563, found 532.2570.

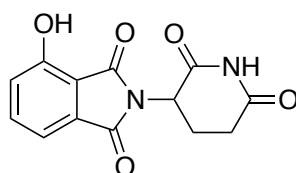
(2*S*,4*R*)-1-((*S*)-2-Amino-3,3-dimethylbutanoyl)-4-hydroxy-*N*-(4-(4-methylthiazol-5-yl)benzyl)pyrrolidine-2-carboxamide (RBM5-189)



To an ice-cooled solution of **RBM5-188** (291 mg, 0.563 mmol) in CH₂Cl₂ (6 mL), neat TFA (6 mL) was added dropwise. After stirring at 25 °C for 2 h, the reaction mixture was concentrated *in vacuo*. Purification of the crude by flash chromatography on silica gel (from 0 to 40 % MeOH in CH₂Cl₂) afforded **RBM5-189** (300 mg, 0.720 mmol, quant.) as yellowish foamy wax. Spectral data were in agreement with those reported in the literature^{110,122}.

^1H NMR (400 MHz, CD_3OD): δ 8.88 (s, 1H), 8.79 (br s, 1H), 7.45 (d, $J = 8.1$ Hz, 2H), 7.39 (d, $J = 8.1$ Hz, 2H), 4.68 (t, $J = 8.5$ Hz, 1H), 4.60 – 4.49 (m, 2H), 4.36 (dd, $J = 15.5, 4.1$ Hz, 1H), 4.07 (s, 1H), 3.85 (d, $J = 11.2$ Hz, 1H), 3.71 (dd, $J = 11.1, 3.4$ Hz, 1H), 2.46 (s, 3H), 2.30 (dd, $J = 13.1, 7.7$ Hz, 1H), 2.09 (ddd, $J = 13.4, 9.7, 4.2$ Hz, 1H), 1.13 (s, 9H). ^{13}C NMR (101 MHz, CD_3OD): δ 174.1, 168.6, 152.9, 148.9, 140.2, 131.4, 130.6, 130.3, 128.9, 71.1, 61.0, 60.3, 58.0, 43.7, 39.0, 35.7, 26.7, 15.8. HRMS calcd. for $\text{C}_{22}\text{H}_{31}\text{N}_4\text{O}_3\text{S}$ ($[\text{M}+\text{H}]^+$): 431.2111, found: 431.2123.

2-(2,6-dioxopiperidin-3-yl)-4-hydroxyisoindoline-1,3-dione (RBM5-123)

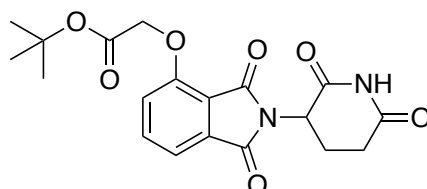


In a round-bottom flask, KOAc was added at 25 °C to a stirred solution of 3-hydroxyphthalic anhydride (2.00 g, 12.19 mmol) and 3-aminopiperidine-2,6-dione hydrochloride (2.01 g, 12.19 mmol) in acetic acid (30 mL). The mixture was stirred under reflux overnight. After cooling to 25 °C, the solvent was removed under reduced pressure, and the resulting residue was taken up in water (15 mL), filtered, and purified by flash column chromatography (from 0 to 5 % MeOH in CH_2Cl_2) to obtain **RBM5-123** (2.67 g, 9.736 mmol, 80 %) as a pale-yellow solid. Spectral data were in agreement with those reported in the literature¹²³.

^1H NMR (400 MHz, $\text{DMSO}-d_6$): δ 11.16 (s, 1H), 11.09 (s, 1H), 7.65 (app t, $J = 8.0$ Hz, 1H), 7.31 (d, $J = 7.2$ Hz, 1H), 7.25 (d, $J = 8.4$ Hz, 1H), 5.07 (dd, $J = 12.9, 5.4$ Hz, 1H), 2.95 – 2.82 (m, 1H), 2.64 – 2.44 (m, 2H), 2.02 (ddd, $J = 10.5, 5.2, 3.0$ Hz, 1H). ^{13}C NMR (101 MHz, $\text{DMSO}-d_6$): δ 172.8, 170.0, 167.0, 165.8,

155.5, 136.4, 133.2, 123.6, 114.4, 114.3, 48.7, 31.0, 22.1. HRMS calcd. for $C_{13}H_9N_2O_5$ ($[M-H]^-$): 273.0517, found: 273.0554.

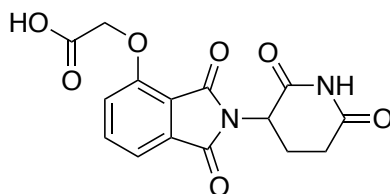
***tert*-Butyl 2-((2-(2,6-dioxopiperidin-3-yl)-1,3-dioxoisindolin-4-yl)oxy)acetate (RBM5-172)**



To a stirred solution of **RBM5-123** (1.50 g, 5.47 mmol) in DMF (50 mL), K_2CO_3 was added portionwise. The mixture was stirred at 25 °C for 30 min. A solution of *tert*-butyl 2-bromoacetate (808 μ L, 5.47 mmol) in DMF (5 mL) was added dropwise to the previous mixture, and the reaction mixture was stirred at 25 °C for 3 h. Water (100 mL) was added, and the mixture was extracted with Et_2O (3 x 50 mL). The combined organic extracts were washed with brine (2 x 50 mL), dried over $MgSO_4$, filtered, and concentrated *in vacuo*. Flash chromatography purification of the crude on silica gel (from 0 to 100 % EtOAc in hexanes) afforded **RBM5-172** (1.49 g, 3.836 mmol, 70 %) as a pale-yellow solid. Spectral data were in agreement with those reported in the literature¹²⁴.

1H NMR (400 MHz, $CDCl_3$): δ 8.33 (s, 1H), 7.65 (dd, $J = 8.4, 7.4$ Hz, 1H), 7.49 (d, $J = 7.2$ Hz, 1H), 7.09 (d, $J = 8.4$ Hz, 1H), 4.97 (dd, $J = 12.0, 5.4$ Hz, 1H), 4.77 (s, 2H), 2.95 – 2.68 (m, 3H), 2.18 – 2.05 (m, 1H), 1.47 (s, 9H). ^{13}C NMR (101 MHz, $CDCl_3$): δ 171.3, 168.2, 167.0, 166.9, 165.6, 155.6, 136.4, 134.0, 119.9, 117.7, 117.0, 83.2, 66.6, 49.3, 31.5, 28.1, 22.7. HRMS calcd. for $C_{19}H_{20}N_2NaO_7$ ($[M+Na]^+$): 411.1163, found: 411.1189.

2-((2-(2,6-Dioxopiperidin-3-yl)-1,3-dioxoisindolin-4-yl)oxy)acetic acid (RBM5-173)

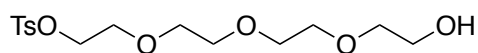


A solution of **RBM5-172** (0.960 g, 2.472 mmol) in TFA (25 mL, 0.1 M) was stirred at 25 °C for 4 h. The reaction mixture was diluted with CH₂Cl₂ (50 mL) and concentrated to dryness to afford the crude **RBM5-173** (780 mg, 2.348 mmol, 95 %), which was sufficiently pure to be carried on to the next step without further purification. Spectral data were in agreement with those reported in the literature¹²⁴.

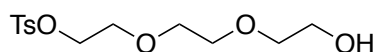
¹H NMR (400 MHz, DMSO-*d*₆): δ 13.21 (s, 1H), 11.11 (s, 1H), 7.79 (dd, *J* = 8.6, 7.3 Hz, 1H), 7.47 (d, *J* = 7.2 Hz, 1H), 7.39 (d, *J* = 8.6 Hz, 1H), 5.10 (dd, *J* = 12.9, 5.4 Hz, 1H), 4.99 (s, 2H), 2.89 (ddd, *J* = 17.2, 13.9, 5.4 Hz, 1H), 2.65 – 2.52 (m, 2H), 2.05 (dddd, *J* = 9.6, 7.9, 5.2, 1.9 Hz, 1H). ¹³C NMR (101 MHz, DMSO-*d*₆): δ 172.8, 169.9, 169.5, 166.8, 165.2, 155.1, 136.8, 133.3, 119.9, 116.3, 115.8, 65.0, 48.8, 31.0, 22.0. HRMS calcd. for C₁₅H₁₃N₂O₇ ([M+H]⁺): 333.0717, found: 333.0740.

III. Linkers

2-(2-(2-(2-Hydroxyethoxy)ethoxy)ethoxy)ethyl 4-methylbenzenesulfonate (RBM3-006) and 2-(2-(2-hydroxyethoxy)ethoxy)ethyl 4-methylbenzenesulfonate (RBM3-007)



RBM3-006



RBM3-007

A solution of corresponding polyethylene glycol (51.486 mmol) in THF (10 mL) was cooled to 0 °C, and then NaOH (16.501 mmol) was added as a solution in H₂O (10 mL). A solution of tosyl chloride (10.307 mmol) in THF (20 mL) was added dropwise to the previous mixture. The reaction was stirred at 0 °C for 2 h and then for 5 h at 25 °C. After this time, the reaction mixture was diluted with EtOAc (200 mL) and H₂O (200 mL). The organic layer was separated, washed with brine (200 mL), dried (MgSO₄), filtered, and concentrated under reduced pressure to afford crude that contained the desired compounds **RBM3-006** (98% yield) or **RBM3-007** (89% yield) as a pale-yellow oils sufficiently pure to be carried on to the next step without further purification. Spectral data were in agreement with those reported in the literature^{123–125}.

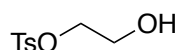
RBM3-006

¹H NMR (400 MHz, CDCl₃): δ 7.76 (d, *J* = 8.1 Hz, 2H), 7.31 (d, *J* = 8.1 Hz, 2H), 4.13 (t, *J* = 4.8 Hz, 2H), 3.55–3.68 (m, 14H), 2.41 (s, 3H). ¹³C NMR (101 MHz, CDCl₃): δ 144.7, 132.7, 129.7, 127.8, 72.3, 70.54, 70.47, 70.3, 70.1, 69.1, 68.5, 61.5, 21.5. HRMS calcd. for C₁₅H₂₅O₇S ([M+H]⁺): 349.1243, found: 349.1283.

RBM3-007

¹H NMR (400 MHz, CDCl₃): δ 7.76 (d, *J* = 8 Hz, 2H), 7.31 (d, *J* = 8 Hz, 2H), 4.16–4.14 (m, 2H), 3.71–3.67 (m, 4H), 3.59 (s, 4H), 3.57–3.54 (m, 2), 2.43 (s, 3H). ¹³C NMR (101 MHz, CDCl₃): δ 145.0, 133.0, 129.9, 128.1, 72.6, 70.9, 70.4, 69.3, 68.8, 61.8, 21.7. HRMS calcd. for C₁₃H₂₁O₆S ([M+H]⁺): 305.0981, found: 305.0931.

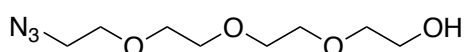
2-Hydroxyethyl 4-methylbenzenesulfonate (RBM3-11)



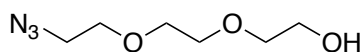
A solution of ethylene glycol (13.023 g, 209.820 mmol) in TEA (8.8 mL, 62.370 mmol) was cooled to 0 °C and tosyl chloride (4.0 g, 20.982 mmol) was added portion-wise. The reaction was stirred at 0 °C for 2 h, the reaction mixture was diluted with CH₂Cl₂, and then the mixture was washed subsequently with saturated brine and 0.5 M HCL three times. The combined organic layers were dried over MgSO₄, filtered, and concentrated *in vacuo* to afford crude **RBM3-011** (4.270 g, 19.749 mmol, 94%) as a pale-yellow oil that was sufficiently pure to be carried on to the next step without further purification. Spectral data were in agreement with those reported in the literature¹²⁶.

¹H NMR (400 MHz, CDCl₃): δ 7.76 (d, *J* = 7.1 Hz, 2H), 7.31 (d, *J* = 7.1 Hz, 2H), 4.14 (q, *J* = 2.3 Hz, 2H), 3.82 (t, *J* = 1.9 Hz, 2H), 2.45 (s, 3H). HRMS calcd. for C₉H₁₃O₄S ([M+H]⁺): 217.0456 found: 217.09567.

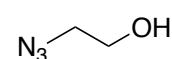
2-(2-(2-(2-azidoethoxy)ethoxy)ethoxy)ethan-1-ol (RBM5-170), 2-(2-(2-azidoethoxy)ethoxy)ethan-1-ol (RBM3-007) and 2-azidoethan-1-ol (RBM3-012)



RBM5-170



RBM3-008



RBM3-012

To a solution of the corresponding tosylate **RBM3-006**, **RBM3-007**, or **RBM3-011** (10.149 mmol) in DMF (7.5 mL), NaN₃ (30.447 mmol) was added portion-

wise. The reaction was stirred for 1 hat 90 °C. After that, the reaction mixture was diluted with a saturated NaCl solution (100 mL) and extracted with CHCl₃ (2 × 200 mL). The combined organic layers were dried over anhydrous MgSO₄, filtered, and concentrated *in vacuo*. Purification of the crude by flash chromatography on silica gel (from 0 to 3 % MeOH in CH₂Cl₂) afforded the desired azido alcohols **RBM5-170** (89% yield), **RBM3-008** (86% yield), **RBM3-012** (86% yield). Spectral data were in agreement with those reported in the literature^{123–126}.

RBM5-170

¹H NMR (400 MHz, CDCl₃): δ 3.72 – 3.68 (m, 2H), 3.67 – 3.64 (m, 10H), 3.60 – 3.57 (m, 2H), 3.37 (t, *J* = 5.1 Hz, 2H), 2.65 – 2.59 (m, 1H). ¹³C NMR (101 MHz, CDCl₃): δ 72.6, 70.8, 70.7, 70.7, 70.4, 70.1, 61.8, 50.7. HRMS calcd. for C₈H₁₈N₃O₄ ([M+H]⁺): 220.1292, found: 220.1302.

RBM3-008

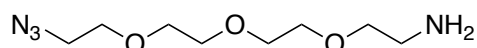
¹H NMR (400 MHz, CDCl₃): δ 3.71-3.68 (m, 2H), 3.68 (s, 6H), 3.64-3.60 (m, 2H), 3.43-3.37 (m, 2H); ¹³C NMR (125 MHz, CDCl₃): δ 72.5, 70.6, 70.4, 70.0, 61.7, 50.6. HRMS calcd. for C₆H₁₅N₃O₃ ([M+H]⁺): 176.0957, found: 176.0960.

RBM3-012

¹H NMR (400 MHz, CDCl₃): δ 3.79 (dd, *J*, 2H), 3.53 - 3.39 (m, 2H), 2.01 (t, *J*, 1H). ¹³C NMR (101 MHz, CDCl₃): δ 61.7, 50.6. HRMS calcd. for C₂H₇N₃O ([M+H]⁺): 88.0433, found: 88.0483.

^1H NMR (400 MHz, CDCl_3): δ 3.70 – 3.65 (m, 12H), 3.39 (t, $J = 5.1$ Hz, 4H). ^{13}C NMR (101 MHz, CDCl_3): δ 70.84, 70.83, 70.2, 50.8. HRMS calcd. for $\text{C}_8\text{H}_{17}\text{N}_6\text{O}_3$ ($[\text{M}+\text{H}]^+$): 245.1357, found: 245.1380.

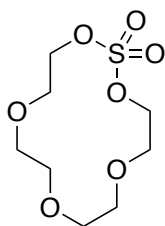
2-(2-(2-(2-Azidoethoxy)ethoxy)ethoxy)ethan-1-amine (RBM5-163)



To an ice-cooled solution of **RBM5-162** (0.400 g, 1.637 mmol) in 0.5 M aq. HCl (10 mL), a solution of triphenylphosphine (0.386 g, 1.474 mmol) in Et_2O (10 mL), was added dropwise. The resulting mixture was stirred overnight at 25 °C. After this time, the reaction mixture was washed with EtOAc (3 x 30 mL) and the aqueous layer was treated at 0°C with 1 M aq. KOH until pH~12 and extracted with CH_2Cl_2 (3 x 30 mL). The combined organic extracts were dried over anhydrous MgSO_4 , filtered, and concentrated to dryness. The acid-base work-up provided the crude **RBM5-163** (0.222 g, 1.017 mmol, 62%) sufficiently pure to be carried on to the next step without further purification. Spectral data were in agreement with those reported in the literature¹²⁴.

^1H NMR (400 MHz, CDCl_3): δ 3.69 – 3.65 (m, 8H), 3.65 – 3.61 (m, 2H), 3.51 (t, $J = 5.2$ Hz, 2H), 3.39 (t, $J = 5.1$ Hz, 2H), 2.86 (t, $J = 5.2$ Hz, 2H), 1.52 (br s, 2H). ^{13}C NMR (101 MHz, CDCl_3): δ 73.4, 70.8, 70.74, 70.71, 70.4, 70.1, 50.8, 41.8. HRMS calcd. for $\text{C}_8\text{H}_{19}\text{N}_4\text{O}_3$ ($[\text{M}+\text{H}]^+$): 219.1452, found: 219.1441.

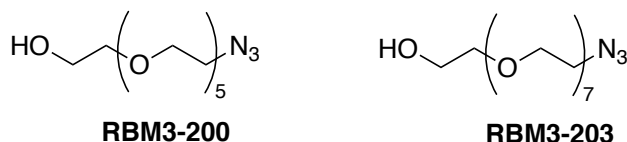
1,3,6,9,12-Pentaoxa-2-thiacyclotetradecane 2,2-dioxide (RBM5-169)



To an ice-cooled solution of tetraethylene glycol (4.00 g, 20.59 mmol) in CH_2Cl_2 (400 mL) containing TEA (13.6 mL, 97.8 mmol) and DMAP (126 mg, 1 mmol) was added drop-wise a solution of SOCl_2 (3 mL, 41.19 mmol) in CH_2Cl_2 (125 mL). The reaction mixture was stirred for 2 h at 25 °C and then poured onto ice/water (200 mL) and extracted with CH_2Cl_2 (3 x 100 mL). The combined organic extracts were washed with water (2 x 100 mL) and concentrated under reduced pressure to provide the macrocyclic sulfite intermediate as a brown oil. An ice-cooled solution of this intermediate (3.3 g, 13.7 mmol) in a mixture of H_2O , CH_2Cl_2 , and CH_3CN (3:2:2 v/v, 560 mL) was sequentially treated with NaIO_4 (3.67 g, 17.17 mmol) and $\text{RuCl}_3 \cdot x\text{H}_2\text{O}$ (29 mg, 137 μmol) and stirred overnight at 25 °C. The reaction mixture was extracted with CH_2Cl_2 (3 x 100 mL), washed with water (2 x 100 mL), filtered through Celite®, and evaporated *in vacuo*. The crude mixture was purified by flash column chromatography (from 0 to 100 % methyl *tert*-butylether in hexanes) to yield the macrocyclic sulfate **RBM5-169** (2.75 g, 10.731 mmol, 78 %) as a white solid. Spectral data were in agreement with those reported in the literature¹¹².

^1H NMR (400 MHz, CDCl_3): δ 4.50 – 4.44 (m, 4H), 3.86 – 3.80 (m, 4H), 3.68 (dd, $J = 4.6, 2.7$ Hz, 4H), 3.66 – 3.63 (m, 4H). ^{13}C NMR (101 MHz, CDCl_3): δ 72.3, 70.9, 70.8, 68.6. HRMS calcd. for $\text{C}_8\text{H}_{16}\text{NaO}_7\text{S}$ ($[\text{M}+\text{Na}]^+$): 279.0509, found: 279.0538.

17-Azido-3,6,9,12,15-pentaoxaheptadecan-1-ol (RBM3-200) and 23-azido-3,6,9,12,15,18,21-heptaotricosan-1-ol (RBM3-203)



Under an argon atmosphere, a solution of the azide derivative (**RBM3-008** or **RBM5-170**) (9.122 mmol) in THF (10 mL) was added to a suspension of NaH (60% in mineral oil, 22.859 mmol) in dry THF (30 mL) at 0 °C. After stirring for 20 min, a solution of **RBM5-169** (XXX mg, 10.947 mmol) in THF (30 mL) was added to the mixture was stirred overnight at 25 °C. Aqueous acidic solution (1 mL) of H₂SO₄ adjusted to pH 2-3 was added to the reaction mixture and stirred under reflux for 1 h. The reaction mixture was quenched with saturated NaHCO₃ solution and extracted with CH₂Cl₂ (3 x 50 mL). The combined organic extracts were dried over anhydrous MgSO₄ filtered and concentrated to dryness. Purification of the crude by flash chromatography on silica gel (from 0 to 10 % MeOH in CH₂Cl₂) yielded **RBM3-200** (81% yield) and **RBM3-203** (90% yield) as a colorless oil. Spectral data were in agreement with those reported in the literature¹²⁷.

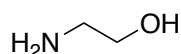
RBM3-200

¹H NMR (400 MHz, CDCl₃): δ 3.39 (t, *J* = 5.2 Hz, 2H), 3.60-3.73 (m, 22H). ¹³C NMR (101 MHz, CDCl₃): δ 72.69, 70.68, 70.63, 70.60, 70.19, 61.8, 61.54, 50.6. HRMS calcd. for C₁₂H₂₅N₃O₆ ([M+H]⁺): 308.1743, found: 308.1703.

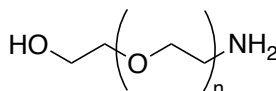
RBM3-203

¹H NMR (400 MHz, CDCl₃): δ 3.38 (t, *J* = 4.8 Hz, 2H), 3.58-3.72 (m, 30H). ¹³C NMR (101 MHz, CDCl₃): δ 72.7, 70.8, 70.8, 70.8, 70.7, 70.7, 70.7, 70.5, 70.2, 61.8, 50.8. HRMS calcd. for C₁₆H₃₄N₃O₈ ([M+H]⁺): 396.2268, found: 396.2218.

2-Aminoethan-1-ol (RBM3-013), 2-(2-(2-(2-aminoethoxy)ethoxy)ethoxy)ethan-1-ol (RBM3-207), 17-amino-3,6,9,12,15-pentaoxaheptadecan-1-ol (RBM3-209) and 23-amino-3,6,9,12,15,18,21-heptaotricosan-1-ol (RBM3-213)



RBM3-013



RBM3-207: n=3

RBM3-209: n=5

RBM3-213: n=7

Under an argon atmosphere, to a solution of the azide (1.4 mmol) and Pd-C (20 % w/w) in degassed MeOH-CHCl₃ (9:1) (20 mL) was added dropwise neat TES (10 equiv), and the resulting suspension was stirred at 25 °C. After stirring for 1 h, the reaction mixture was filtered through a Celite[®] pad, and the solids were rinsed with MeOH (3 x 5 mL). The combined filtrates were concentrated *in vacuo*, and the residue was triturated with hexanes (4 x 2 mL) to give the desired amine hydrochlorides **RBM3-13**, **RBM3-207**, **RBM3-209**, and **RBM3-213** (84%-88% quantitative yield) sufficiently pure to be carried on to the next step without further purification. Spectral data were in agreement with those reported in the literature¹²⁷.

RBM3-013

¹H NMR (400 MHz, CDCl₃): δ 3.25 (t, *J*= 5.2 Hz, 2H), 3.65 (t, *J*= 5.1 Hz, 2H)

RBM3-207

¹H NMR (400 MHz, CDCl₃): 3.79-3.75 (m, 4H), 3.71-3.60 (m, 10H), 3.11 (t, 2H).

¹³C NMR (101 MHz, CDCl₃): δ 72.7, 70.4, 70.4, 70.1, 69.9, 68.7, 61.2, 40.4.

RBM3-209

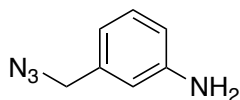
^1H NMR (400 MHz, CDCl_3): δ 3.72-3.58 (m, 22H), 3.37 (t, $J = 5.2$ Hz, 2H). ^{13}C NMR (101 MHz, CDCl_3): δ 72.6, 70.2, 70.0, 69.9, 69.9, 69.8, 69.6, 69.3, 66.9, 60.6, 40.5. HRMS calcd. for $\text{C}_{12}\text{H}_{28}\text{NO}_6$ ($[\text{M}+\text{H}]^+$): 282.1910 found: 282.1910.

RBM3-213

^1H NMR (400 MHz, CDCl_3): δ 3.88 (t, $J = 5.2$ Hz, 2H), 3.79 (br, 2H), 3.76-3.59 (m, 26H), 3.28-3.19 (m, 2H). ^{13}C NMR (101 MHz, CDCl_3): δ 72.5, 70.5, 70.2, 70.0, 70.0, 69.9, 69.8, 69.7, 69.6, 66.8, 60.8, 40.5. HRMS calcd. for $\text{C}_{16}\text{H}_{36}\text{NO}_8$ ($[\text{M}+\text{H}]^+$): 370.2435 found: 370.2432.

IV. POI ligands

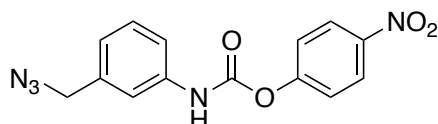
3-(Azidomethyl)aniline (RBM3-301)



A solution of 3-(hydroxymethyl)aniline (1.0 g, 8.12 mmol), triphenylphosphine (2.12g, 8.12 mmol) and NaN_3 (0.63 g, 9.74 mmol) in DMF/ CCl_4 (12 mL/3 mL) was heated at 100 °C overnight. The reaction mixture was poured onto ice/water (100 mL) and extracted with Et_2O . The organic layer was washed with water (3 x 100 mL) and brine (3 x 100 mL), dried over MgSO_4 , filtered and concentrated to dryness. Purification of the crude by flash chromatography on silica gel (20:80 EtOAc /Hexanes) yielded **RBM3-301** (0.883 g, 5.959 mmol, 73%) as a yellow oil. Spectral data were in agreement with those reported in the literature^{128,129}.

^1H NMR (400 MHz, CDCl_3): δ 7.21-7.16 (m, 1 H), 6.75-6.66 (m, 3 H), 4.26 (s, 2 H), 3.91 (br s, 2 H). ^{13}C NMR (101 MHz, CDCl_3): δ 146.31, 136.56, 129.78, 118.60, 115.21, 114.82, 54.77. HRMS calcd. for $\text{C}_7\text{H}_8\text{N}_4$ ($[\text{M}+\text{H}]$): 148.0749 found: 148.0749.

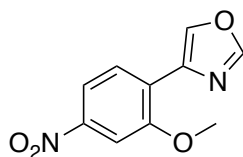
4-Nitrophenyl (3-(azidomethyl)phenyl)carbamate (**RBM3-304**)



To a stirred solution of **RBM3-301** (1.360 g, 9.179 mmol) in anhydrous CH_2Cl_2 (40 mL), pyridine (1.8 mL, 22.947 mmol) and *p*-nitrophenyl chloroformate (2.220 g, 11.014 mmol) was sequentially added. After stirring at 25 °C for 2 h, the mixture was quenched with saturated aqueous NH_4Cl (15 mL) and extracted with CH_2Cl_2 (3 x 20 mL). The combined organic layers were dried over MgSO_4 , filtered, and concentrated *in vacuo*. The crude was purified by flash chromatography (from 0 to 2 % MeOH in CH_2Cl_2) to furnish **RBM3-304** (2.460 g, 7.853 mmol, 86%).

^1H NMR (400 MHz, CDCl_3): δ 8.38 – 8.25 (m, 2H), 7.49 (br s, 1H), 7.44 – 7.32 (m, 4H), 7.16 – 7.08 (m, 1H), 7.05 (br s, 1H), 4.36 (s, 2H). ^{13}C NMR (101 MHz, CDCl_3): δ 155.4, 137.0, 130.0, 125.4, 122.3, 118.6, 54.6. HRMS calcd. for $\text{C}_{14}\text{H}_{11}\text{N}_5\text{O}_4$ ($[\text{M}+\text{H}]^+$): 314.0889, found: 314.0876.

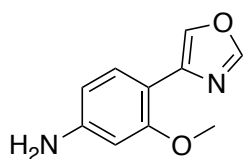
4-(2-methoxy-4-nitrophenyl)oxazole (RBM3-302)



To a round-bottom flask equipped with a condenser was added a solution of 2-methoxy-4-nitrobenzaldehyde (1.04 g, 5.75 mmol) in methanol (10 mL), tosylmethyl isocyanide (1.12 g, 5.75 mmol) and potassium carbonate (2.08 g, 15.06 mmol), and the resulting brown suspension was heated to reflux overnight. The resulting mixture was concentrated under reduced pressure, and then the resulting black solid was partitioned between CH₂Cl₂ (10 mL) and water (10 mL). The organic layer was collected, and the aqueous layer was extracted with CH₂Cl₂. The flash chromatography purification in CH₂Cl₂ yielded the **RBM3-302** (1.2 g, 5.45 mmol, 94.8%). Spectral data were in agreement with those reported in the literature^{128,129}.

¹H NMR (400 MHz, CDCl₃): δ 8.01 (s, 1H), 7.92 (m, 2H), 7.85 (s, 1H), 7.77 (s, 1H), 4.10 (s, 3H). ¹³C NMR (101 MHz, CDCl₃): δ 155.5, 150.8, 147.8, 146.2, 128.3, 126.0, 122.9, 116.3, 106.3, 56.2. HRMS calcd. for C₁₀H₇N₂O₄ ([M+H]⁺): 221.0804, found: 221.0854.

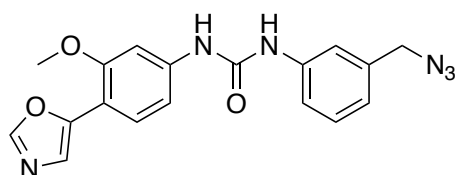
3-methoxy-4-(oxazol-4-yl)aniline (RBM3-303)



Under an inert atmosphere, 5% Pd/C (1.5 g) was added to a solution of **RBM3-303** (1.0 g, 4.542 mmol) in MeOH (35 mL). The flask was repeatedly evacuated and flushed with H₂ gas. The resulting mixture was stirred overnight under H₂. The reaction flask was subsequently purged with Ar gas and the crude reaction mixture was filtered through a short plug of Celite[®]. The reaction flask and Celite[®] pad were rinsed with MeOH. The combined filtrates were concentrated *in vacuo* to provide **RBM3-303** (0.770 g, 4.048 mmol, 89%). Spectral data were in agreement with those reported in the literature^{128,129}.

¹H NMR (400 MHz, CDCl₃): δ 7.88 (s, 1H), 7.60 (d, *J*=8.4 Hz, 1H), 7.41 (s, 1H), 6.42 (dd, *J*=8.4, 2.1 Hz, 1H), 6.36 (d, *J*= 2.1 Hz, 1H), 3.98(s, 3H). ¹³C NMR (101 MHz, CDCl₃): δ 157.5, 149.0, 148.9, 148.4, 126.6, 123.0, 108.2, 107.7, 55.7. HRMS calcd. for C₁₀H₁₀N₂O₂ ([M+H]⁺): 191.0742, found: 191.0752.

1-(3-(Azidomethyl)phenyl)-3-(3-methoxy-4-(oxazol-5-yl)phenyl)urea (**RBM3-305**)

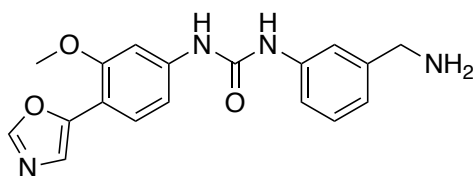


To a solution of **RBM3-303** (1.400 g, 7.361 mmol) and *p*-nitrophenol activated carbamate **RBM3-304** (2.000 g, 6.384 mmol) in EtOAc (92 mL) was added DIPEA (1.4 mL, 8.299 mmol) dropwise. The reaction flask was equipped with a condenser, and the reaction mixture was stirred under reflux overnight. Then, the reaction mixture was cooled to 25 °C, washed with water (3 x 10 mL) and the organic layer was separated, dried with anhydrous Na₂SO₄ and filtered. The solvent was evaporated, and the crude product was purified by flash

chromatography (hexanes:EtOAc 1:1) to give **RBM3-305** (1.64 g, 4.501 mmol, 70% yield).

^1H NMR (400 MHz, CDCl_3): δ 7.99 – 7.79 (m, 3H), 7.53 (d, J = 8.4 Hz, 1H), 7.41 (s, 1H), 7.30 (dd, J = 8.2, 1.8 Hz, 2H), 6.96 (tt, J = 5.5, 2.7 Hz, 1H), 6.71 (dd, J = 8.4, 2.0 Hz, 1H), 4.18 (s, 2H), 3.81 (s, 3H). ^{13}C NMR (101 MHz, CDCl_3): δ 156.4, 153.9, 149.4, 148.3, 139.8, 138.6, 136.7, 129.6, 126.4, 123.9, 120.3, 120.2, 119.9, 112.1, 103.1, 55.5, 54.5. HRMS calcd. for $\text{C}_{18}\text{H}_{17}\text{N}_6\text{O}_3$ ($[\text{M}+\text{H}]^+$): 365.1362, found: 365.1373.

1-(3-(Aminomethyl)phenyl)-3-(3-methoxy-4-(oxazol-5-yl)phenyl)urea (**RBM3-306**)

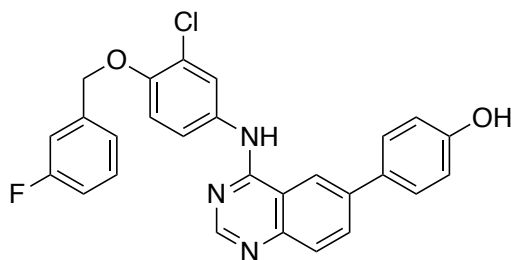


Under an inert atmosphere, Pd/C (10 % w/w – 5 mol%) was added to a solution of **RBM3-305** (1.64 g, 4.501 mmol) in MeOH (82 mL). The flask was repeatedly evacuated and flushed with H_2 gas. The resulting mixture was stirred overnight under H_2 . The reaction flask was subsequently purged with Ar gas and the crude reaction mixture was filtered through a short plug of Celite[®]. The reaction flask and Celite[®] pad were rinsed with MeOH. The combined filtrates were concentrated *in vacuo* to provide **RBM3-306** (1.30 g, 3.842 mmol, 85% yield).

^1H NMR (400 MHz, $\text{DMSO}-d_6$): δ 8.99 (br s, 1H), 8.88 (br s, 1H), 8.35 (s, 1H), 7.60 (d, J = 8.3 Hz, 1H), 7.55 (s, 1H), 7.48 (s, 1H), 7.41 (s, 1H), 7.40 (d, J = 10.0 Hz, 1H), 7.32 (t, J = 7.7 Hz, 1H), 7.06 (d, J = 8.4 Hz, 1H), 6.98 (d, J = 7.4 Hz, 1H), 4.42 (s, 2H), 3.92 (s, 3H). ^{13}C NMR (101 MHz, $\text{DMSO}-d_6$): δ 155.9, 152.4,

150.3 147.3, 141.3, 139.9, 136.3, 129.3, 125.9, 123.4, 122.1, 118.1, 110.4, 110.1, 101.3, 55.5, 53.7. HRMS calcd. for C₁₈H₁₉N₄O₃ ([M+H]⁺): 339.1457, found: 339.1465.

4-(4-((3-Chloro-4-((3-fluorobenzyl)oxy)phenyl)amino)quinazolin-6-yl)phenol (RBM3-027)



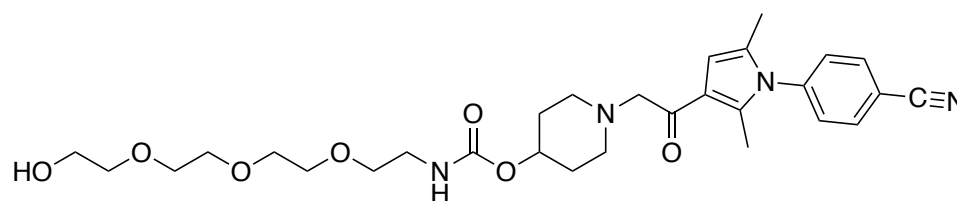
In a round-bottom flask, a 2 M Na₂CO₃ solution in water (13 mL) was added to a suspension of *N*-[3-chloro-4-[(3-fluorophenyl)methoxy]phenyl]-6-iodoquinazolin-4-amine (600 mg, 1.186 mmol) in a mixture of 1,2-dimethoxyethane (24 mL) and ethanol (16 mL). To the previous mixture, [4-*tert*-butyl(dimethyl)silyl]oxyphenyl]boronic acid (209 mg, 0.831 mmol), and [(Ph)₃P]₂PdCl₂ (70 mg, 0.08 mmol) were added. After stirring at 60 °C for 3 h, the reaction mixture was cooled to 25 °C, poured into an aqueous saturated solution of NaHCO₃ (60 mL) and extracted with AcOEt (2x60 mL). The organic extracts were combined, dried (Na₂SO₄), filtered over a Celite[®] pad, and evaporated under vacuum. The crude was purified by flash chromatography (from 0 to 100 % AcOEt in hexanes) to furnish **RBM3-027** (421 mg, 0.890 mmol, 75%). Spectral data were in agreement with those reported in the literature¹⁰⁹.

¹H NMR (400 MHz, DMSO-*d*₆): δ 9.85 (s, 1H), 9.68 (s, 1H), 8.69 (s, 1H), 8.56 (s, 1H), 8.12 (d, *J* = 8.7 Hz, 1H), 8.03 (s, 1H), 7.87 – 7.67 (m, 4H), 7.48 (td, *J* = 8.0, 6.0 Hz, 1H), 7.39 – 7.25 (m, 3H), 7.19 (tt, *J* = 7.8, 1.4 Hz, 1H), 6.93 (d, *J* = 8.6 Hz, 2H), 5.27 (s, 2H). ¹³C NMR (101 MHz, DMSO-*d*₆): δ 163.06, 161.44,

157.66, 157.59, 154.07, 149.69, 148.44, 139.73, 139.69, 138.23, 133.18, 131.45, 130.69, 130.64, 129.86, 128.36, 128.32, 124.20, 123.45, 123.43, 122.38, 121.01, 118.95, 115.88, 115.33, 114.87, 114.73, 114.28, 114.21, 114.07, 69.37. HRMS calcd. for C₂₇H₂₀ClFN₃O₂ ([M+H]⁺): 472.1228. Found 472.1253.

iv. IMPDH PROTACs

1-(2-(1-(4-Cyanophenyl)-2,5-dimethyl-1*H*-pyrrol-3-yl)-2-oxoethyl)piperidin-4-yl (2-(2-(2-(2-hydroxyethoxy)ethoxy)ethoxy)ethyl)carbamate (RBM3-099)

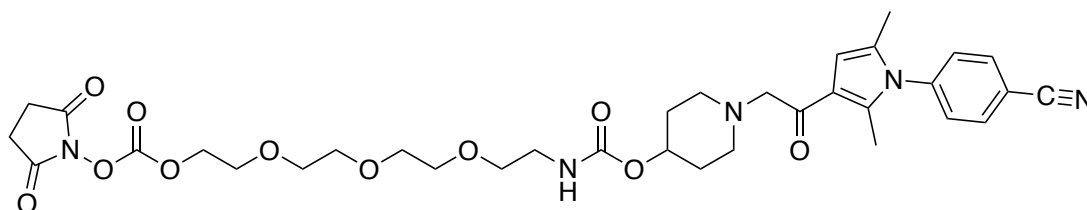


To a solution of *N,N'*-carbonyldiimidazole (0.217 g, 1.337 mmol) in anhydrous DMF (1.5 mL) was added TEA (0.123 mL, 0.884 mmol) at 25 °C. Then a solution of IU1- 248 (0.150 g, 0.445 mmol) in anhydrous DMF (3.0 mL) was added dropwise. The mixture was stirred at 25 °C for 1 h and a solution of the linker **RBM3-207** (0.258 g, 1.334 mmol) in anhydrous DMF (1.5 mL) was added. The resulting mixture was stirred at 50 °C for 24h and concentrated. The residue was diluted with EtOAc (5 mL), and the resulting solution was washed with water (5 mL x 2), dried over Na₂SO₄ and concentrated. Purification of the crude mixture by flash column chromatography (from 0 to 9 % MeOH in CH₂Cl₂) afforded **RBM3-099** (176 mg, 0,316 mmol, 71%yield).

¹H NMR (400 MHz, CDCl₃): δ 7.83 (d, *J* = 8.4 Hz, 2H), 7.33 (d, *J* = 8.5 Hz, 2H), 6.39 (s, 1H), 6.02 (t, *J* = 5.8 Hz, 1H), 4.88 – 4.57 (m, 1H), 3.72 (m, 4H), 3.64 (m, 11H), 3.55 (t, *J* = 4.9 Hz, 2H), 3.36 (q, *J* = 5.3 Hz, 2H), 2.95 – 2.86 (m, 4H), 2.49 – 2.38 (m, 2H), 2.31 (s, 3H), 2.00 – 1.94 (br m, 2H), 1.99 (s, 3H), 1.82 (m, 2H).
¹³C NMR (101 MHz, CDCl₃): δ 192.8, 156.5, 141.4, 136.3, 133.6, 129.2, 128.6,

119.6, 117.9, 113.0, 107.8, 72.8, 70.7, 70.5, 70.4, 70.3 65.2, 61.7, 51.4, 43.0, 40.8, 31.1, 13.1, 12.8. HRMS calcd. for C₂₉H₄₁N₄O₇ ([M+H]⁺): 557.2975, found: 557.2980.

1-(2-(1-(4-Cyanophenyl)-2,5-dimethyl-1*H*-pyrrol-3-yl)-2-oxoethyl)piperidin-4-yl (1-((2,5-dioxopyrrolidin-1-yl)oxy)-1-oxo-2,5,8,11-tetraoxatridecan-13-yl)carbamate (RBM3-316)

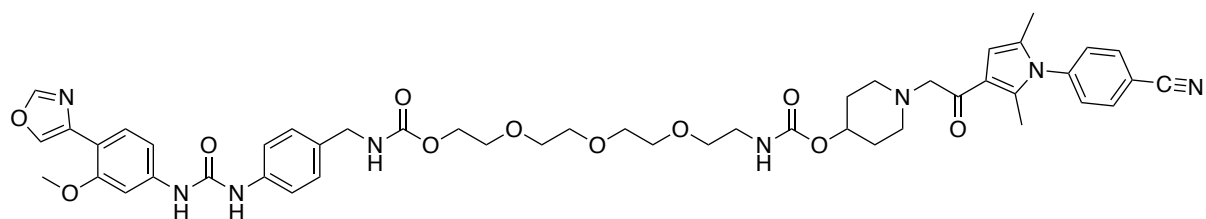


In a round bottom flask, *N,N'*-disuccinimidyl carbonate (0.129 g, 0.503 mmol) was dissolved in MeCN (1.5 mL), then TEA (0.131 mL, 0.944 mmol) was added and finally a solution of the alcohol **RBM3-099** (175 mg, 0.314 mmol) in MeCN (2.0 mL) was added dropwise. The mixture was analyzed by TLC until completion of the reaction. The reaction mixture was concentrated, the residues was diluted with CH₂Cl₂ and a solution of 5% NaHCO₃ was added. The organic phase was washed with the minimal amount of water, dried over Na₂SO₄ and concentrated under reduced pressure to give **RBM3-316** (160 mg, 0.229 mmol, 73 % yield). The next step was performed without further purification.

¹H NMR (400 MHz, CDCl₃): δ 7.83 (d, *J* = 8.5 Hz, 2H), 7.32 (d, *J* = 8.5 Hz, 2H), 6.35 (s, 1H), 5.34 (t, *J* = 6.2 Hz, 1H), 4.80 – 4.70 (m, 1H), 4.49 – 4.44 (m, 1H), 4.30 – 4.26 (m, 1H), 3.82 – 3.75 (m, 2H), 3.74 – 3.70 (m, 3H), 3.70 – 3.62 (m, 9H), 3.58 – 3.50 (m, 2H), 3.39 – 3.33 (m, 2H), 3.02 – 2.91 (m, 2H), 2.84 (s, 2H), 2.62 (s, 2H), 2.60 – 2.53 (m, 2H), 2.28 (s, 3H), 2.09 – 2.01 (m, 3H), 1.98 (s, 3H), 1.95 – 1.84 (m, 2H). ¹³C NMR (101 MHz, CDCl₃): δ 173.6, 168.8, 156.2, 151.7,

141.3, 136.3, 133.6, 129.2, 128.8, 119.3, 117.8, 113.1, 107.6, 71.0, 70.7, 70.7, 70.6, 70.3, 70.1, 68.4, 67.1, 64.4, 54.9, 51.0, 40.8, 30.4, 25.6, 13.0, 12.8. HRMS calcd. For C₃₄H₄₄N₅O₁₁ ([M+H]⁺): 698.3037, found: 698.3075.

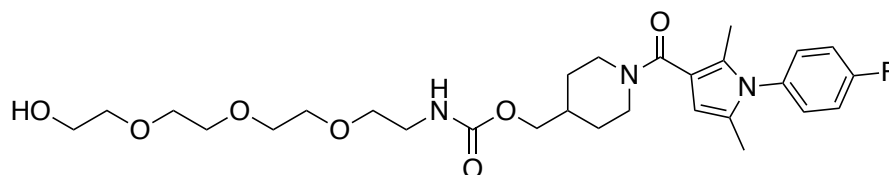
1-((1-(2-(1-(4-Cyanophenyl)-2,5-dimethyl-1*H*-pyrrol-3-yl)-2-oxoethyl)piperidin-4-yl)oxy) -1-oxo-5,8,11-trioxa-2-azatridecyl (4-(3-(3-methoxy-4-(oxazol-4-yl)phenyl)ureido) benzyl)carbamate (RBM3-300)



The carbonate **RBM3-316** (160 mg, 0.229 mmol) was dissolved in MeCN (0.5 ml) and added to a stirred solution of amine **RBM3-306** (77mg, 0.229 mmol) and TEA (64 μ L, 0.458 mmol) in MeCN (1 ml). The resulting mixture was stirred at 25 °C until no mixed carbonate remained by TLC (3 h). The solution was concentrated and purified under reverse phase conditions to give **RBM3-300** (83 mg, 0.090 mmol, 39% yield).

¹H NMR (400 MHz, CD₃OD): δ 8.18 (s, 1H), 7.94 (d, J = 8.4 Hz, 2H), 7.67 (d, J = 8.5 Hz, 1H), 7.51 – 7.40 (m, 5H), 7.34 – 7.23(s, 2H), 7.05 – 6.95 (m, 2H), 6.42 (s, 1H) 4.46 (s, 2H), 4.28 (s, 2H), 4.22 (t, J = 4.6 Hz, 2H), 3.98 (s, 3H), 3.77 – 3.67 (m, 2H), 3.70 – 3.58 (m, 10H), 3.52 (t, J = 5.4 Hz, 2H), 3.42 – 3.33 (m, 2H), 3.31 – 3.22 (m, 2H), 2.31 (s, 3H), 2.22 – 2.13 (m, 2H), 2.01 – 1.95 (m, 2H), 1.97 (s, 3H), 1.36 – 1.27 (m, 2H). ¹³C NMR (101 MHz, CD₃OD): δ 157.8, 151.3, 142.5, 142.0, 141.6, 140.5, 139.0, 134.9, 131.3, 130.5, 130.1, 127.2, 124.0, 122.8, 119.3, 118.8, 114.3, 112.0, 108.2, 103.0, 71.6, 71.5, 71.2, 70.9, 70.5, 65.2, 56.0, 54.8, 45.4, 41.7, 13.1, 12.7. HRMS calcd. for C₄₈H₅₇N₈O₁₁ ([M+H]⁺): 921.4147, found: 921.4194.

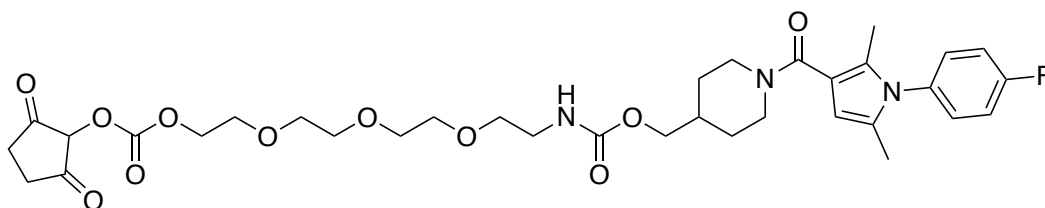
(1-(1-(4-Fluorophenyl)-2,5-dimethyl-1*H*-pyrrole-3-carbonyl)piperidin-4-yl)methyl (2-(2-(2-(2-hydroxyethoxy)ethoxy)ethoxy)ethyl)carbamate (RBM3-352)



To a solution of *N,N'*-carbonyldiimidazole (184 mg, 1.135 mmol) in anhydrous DMF (1.3 mL) were added dropwise TEA (0.105 mL, 0.757 mmol) and a solution of **RBM3-317** (125.0 mg, 0.378 mmol) in anhydrous DMF (2.5 mL). The mixture was stirred at 25 °C for 1h, and a solution of **RBM3-207** (219 mg, 1.135 mmol) in anhydrous DMF (1.3 mL) was added. The resulting mixture was stirred at 50 °C for 24 h and concentrated. The residue was diluted with EtOAc (5 mL), and the resulting mixture was washed with water (5 mL x 2), dried over Na₂SO₄ and concentrated under reduced pressure. The product was purified by flash column chromatography (from 0 to 10 % MeOH in CH₂Cl₂) to give **RBM3-352** (86 mg, 0.156 mmol, 41% yield).

¹H NMR (400 MHz, CDCl₃): δ 7.21 – 7.14 (m, 4H), 6.02 (m, 1H) 5.95 (s, 1H), 3.96 (d, *J* = 6.5 Hz, 2H), 3.75 – 3.69 (m, 4H), 3.68 – 3.60 (m, 10H), 3.57 – 3.53 (m, 2H), 3.40 – 3.32 (m, 2H), 2.07 (s, 3H), 1.97 (s, 3H), 1.96 – 1.87 (m, 2H), 1.80 – 1.73 (m, 2H), 1.34 – 1.21 (m, 4H). ¹³C NMR (101 MHz, CDCl₃): δ 168.0, 130.8, 130.1, 130.0, 128.2, 116.5, 116.2, 115.1, 106.4, 77.5, 77.2, 76.8, 72.7, 70.7, 70.5, 70.3, 70.2, 68.7, 61.7, 41.0, 36.5, 12.8, 12.0. HRMS calcd. For C₂₈H₄₁FN₃O₇ ([M+H]⁺): 551,3007, found: 551.3314.

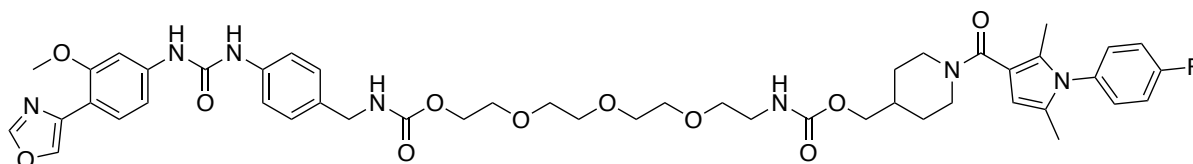
(1-(1-(4-Fluorophenyl)-2,5-dimethyl-1*H*-pyrrole-3-carbonyl)piperidin-4-yl)methyl (1-((2,5-dioxocyclopentyl)oxy)-1-oxo-2,5,8,11-tetraoxatridecan-13-yl)carbamate (RBM3-353)



In a round bottom flask, *N,N'*-disuccinimidyl carbonate (0.052 g, 0.204 mmol) was dissolved in MeCN (0.4 mL), then TEA (0.200 mL, 1.438 mmol) was added and a solution of the alcohol **RBM3-352** (70 mg, 0.127 mmol) in MeCN (1.0 mL) was added dropwise. The mixture was analyzed by TLC until completion of the reaction. The reaction mixture was concentrated, diluted with CH₂Cl₂ and a solution of 5% NaHCO₃ was added. The organic phase was washed with the minimal amount of water, dried over Na₂SO₄, filtered and concentrated under reduced pressure to give **RBM3-353** (67 mg, 0.097 mmol, 76% yield). The next step was performed without further purification.

¹H NMR (400 MHz, CDCl₃): δ 7.20 – 7.12 (m, 4H), 6.00 (m, 1H) 5.94 (s, 1H), 4.49 – 4.43 (m, 2H), 3.95 (d, *J* = 6.5 Hz, 2H), 3.80 – 3.77 (m, 1H), 3.74 – 3.59 (m, 13H), 3.57 – 3.52 (m, 2H), 3.40 – 3.32 (m, 2H), 2.83 (br s, 4H), 2.06 (s, 3H), 1.93 – 1.87 (br s, 1H), 1.78 – 1.75 (m, 2H), 1.32 – 1.21 (m, 4H). ¹³C NMR (101 MHz, CDCl₃): δ 168.0, 130.1, 130.0, 128.2, 116.5, 116.2, 115.1, 106.4, 77.5, 77.2, 76.8, 70.7, 70.6, 70.3, 61.7, 25.6, 12.8, 12.1. HRMS calcd. For C₃₃H₄₄FN₄O₁₁ ([M+H]⁺): 691,2991, found: 691.3012.

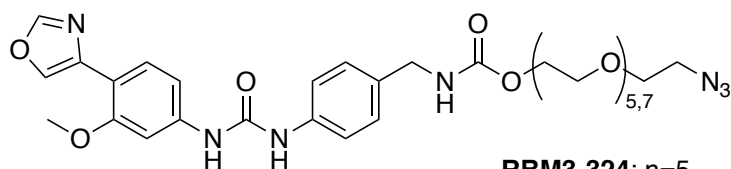
(1-(1-(4-Fluorophenyl)-2,5-dimethyl-1*H*-pyrrole-3-carbonyl)piperidin-4-yl)methyl (1-(4-(3-(3-methoxy-4-(oxazol-4-yl)phenyl)ureido)phenyl)-3-oxo-4,7,10,13-tetraoxa-2-azapentadecan-15-yl)carbamate (RBM3-354)



The carbonate **RBM3-353** (67.0 mg, 0.097 mmol) was dissolved in MeCN (0.485 mL) and added to a stirred solution of **RBM3-306** (43.0 mg, 0.127 mmol) and TEA (0.040 mL, 0.291 mmol) in MeCN (0.5 ml). The resulting mixture was stirred at 25 °C until no mixed carbonate remained by TLC (3 h) and the solution was concentrated. The residue was purified by flash column chromatography (from 0 to 10 % MeOH in CH₂Cl₂) to give **RBM3-354** (40 mg, 0.044 mmol, 45% yield).

¹H NMR (400 MHz, CD₃OD): δ 8.17 (s, 1H), 7.66 (d, *J* = 8.5 Hz, 1H), 7.51 (d, *J* = 2.1 Hz, 1H), 7.42 (s, 1H), 7.40 – 7.37 (m, 1H), 7.36 – 7.34 (m, 1H), 7.29 – 7.22 (m, 5H), 6.99 – 6.95 (m, 2H), 5.95 (s, 1H), 4.28 (s, 2H), 4.22 – 4.18 (m, 2H), 3.98 (s, 3H), 3.91 (d, *J* = 6.2 Hz, 2H), 3.71 – 6.68 (m, 2H), 3.66 – 3.55 (m, 9H), 3.52 – 3.47 (m, 2H), 3.28 – 3.23 (m, 2H), 2.00 (s, 3H), 1.96 (s, 3H), 1.93 – 1.87 (br s, 1H), 1.81 – 1.70 (m, 2H), 1.33 – 1.18 (m, 3H). ¹³C NMR (101 MHz, CD₃OD): δ 170.2, 157.8, 151.3, 142.5, 140.5, 135.4, 132.0, 131.5, 131.4, 130.1, 129.9, 127.3, 124.0, 122.9, 119.2, 117.4, 117.2, 115.6, 112.1, 111.9, 107.1, 103.0, 71.6, 71.5, 71.2, 70.9, 70.6, 69.7, 65.2, 56.0, 49.6, 49.4, 49.2, 49.0, 48.8, 48.6, 48.4, 45.5, 37.4, 12.6, 12.0. HRMS calcd. for C₄₇H₅₇FN₇O₁₁ ([M+H]⁺): 914.4100, found: 914.4141.

17-Azido-3,6,9,12,15-pentaoxaheptadecyl (4-(3-(3-methoxy-4-(oxazol-4-yl)phenyl)ureido) benzyl)carbamate (RBM3-324) and 23-azido-3,6,9,12,15,18,21-heptaoxatricosyl (4-(3-(3-methoxy-4-(oxazol-4-yl)phenyl)ureido) benzyl)carbamate (RBM3-323)



RBM3-324: n=5

RBM3-323: n=7

To a round-bottom flask, a solution of *N,N'*-disuccinimidyl carbonate (2 eq, 1.627 mmol) in MeCN (1 mL) was placed, then TEA (3 eq, 2.440 mmol) was added and a solution of the azido alcohol **RBM3-200** or **RBM3-203** (1 eq, 0.813 mmol) in MeCN (2 mL) was added dropwise at 25 °C. The reaction was monitored by TLC until completion. The reaction crude was concentrated, redissolved in MeCN (1.5 mL), and added to a stirred solution of the corresponding amine **RBM3-006** (210 mg, 620 μmol) and TEA (0.087 mL, 0.628 mmol) in MeCN (1.5 mL). The solution was concentrated and the crude was then purified by flash column chromatography (from 0 to 20 % MeOH in CH₂Cl₂) to give **RBM3-324** (56% yield, in 2 steps) or **RBM3-323** (53% yield, in 2 steps).

RBM3-324

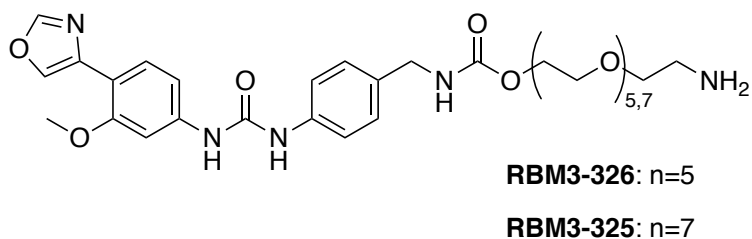
¹H NMR (400 MHz, CD₃OD): δ 8.16 (s, 1H), 7.65 (d, *J* = 8.5 Hz, 1H), 7.50 (br s, 1H), 7.41 (s, 1H), 7.39 – 7.21 (m, 3H), 7.00 – 6.93 (m, 2H), 4.27 (s, 2H), 4.22 – 4.15 (m, 2H), 3.97 (s, 3H), 3.72 – 3.51 (m, 21H), 3.39 – 3.30 (m, 2H). ¹³C NMR (101 MHz, CD₃OD): δ 159.0, 157.8, 155.0, 154.8, 151.24, 151.22, 149.7, 142.5, 141.5, 140.5, 140.1, 139.8, 130.0, 129.8, 127.2, 124.8, 123.95, 123.92, 122.9, 121.0, 119.1, 119.1, 117.5, 112.05, 112.03, 111.9, 102.9, 73.6, 71.57, 71.55, 71.52, 71.50, 71.47, 71.1, 71.08, 70.5, 70.0, 65.2, 56.0, 55.99, 51.7, 51.7, 45.4. HRMS calcd. for C₃₁H₄₂N₇O₁₀ ([M+H]⁺): 672.2993, found: 672.2977.

RBM3-323

¹H NMR (400 MHz, CD₃OD): δ 8.16 (s, 1H), 7.64 (dd, *J* = 8.5, 3.0 Hz, 1H), 7.50 (d, *J* = 2.2 Hz, 1H), 7.40 (br s, 1H), 7.39 – 7.20 (m, 3H), 7.00 – 6.90 (m, 2H),

4.26 (br s, 2H), 4.18 (t, $J = 4.7$ Hz, 2H), 3.96 (s, 3H), 3.71 – 3.56 (m, 29H), 3.38 – 3.31 (m, 2H). ^{13}C NMR (101 MHz, CD_3OD): δ 159.0, 157.7, 154.9, 154.8, 151.2, 149.7, 142.5, 142.5, 141.49, 140.46, 140.1, 139.8, 130.0, 129.8, 127.2, 124.8, 123.9, 122.8, 121.0, 119.1, 119.1, 117.5, 112.0, 112.0, 111.9, 111.8, 108.3, 102.9, 73.6, 71.6, 71.6, 71.5, 71.4, 71.3, 71.10, 71.06, 70.5, 70.0, 65.2, 62.2, 56.0, 55.98, 51.7, 51.69, 45.4. HRMS calcd. for $\text{C}_{35}\text{H}_{50}\text{N}_7\text{O}_{12}$ ($[\text{M}+\text{H}]^+$): 760.3517, found: 760.3569.

17-Amino-3,6,9,12,15-pentaoxaheptadecyl (4-(3-(3-methoxy-4-(oxazol-4-yl)phenyl)ureido) benzyl)carbamate (RBM3-326) and 23-amino-3,6,9,12,15,18,21-heptaoxatricosyl (4-(3-(3-methoxy-4-(oxazol-4-yl)phenyl)ureido)benzyl)carbamate (RBM3-325)



A solution of the selected azide **RBM3-324** or **RBM3-323** (0.412 mmol) and Pd/C (10 % w/w – 5 mol%) in degassed MeOH (4.1 mL) was stirred at 25 °C under an H_2 -filled balloon (previously purged with Ar). After stirring overnight, the reaction mixture was filtered through a Celite[®] pad, and the particles were rinsed with MeOH (3 x 5 mL). The combined filtrates were concentrated in vacuo to give the desired amine compounds **RBM3-326** (76% yield) and **RBM3-325** (83% yield), which were used without further purification.

RBM3-324

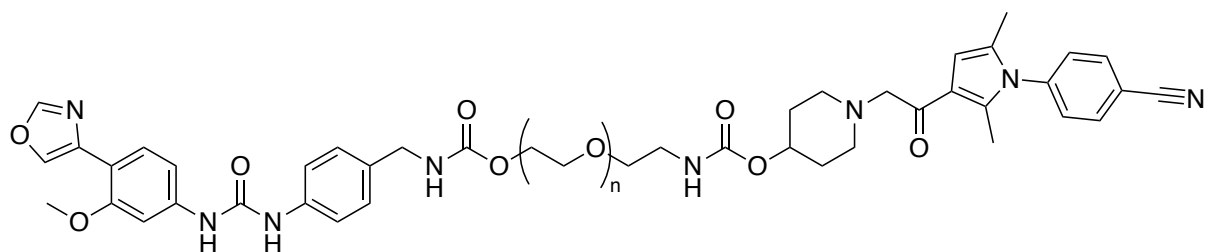
^1H NMR (400 MHz, CD_3OD): δ 8.17 (s, 1H), 7.66 (dd, $J = 8.4, 1.3$ Hz, 1H), 7.51 (d, $J = 2.0$ Hz, 1H), 7.42 (s, 1H), 7.40 – 7.21 (m, 3H), 7.02 – 6.93 (m, 2H), 4.27

(s, 2H), 4.23 – 4.18 (m, 2H), 3.98 (s, 3H), 3.72 – 3.48 (m, 24H), 2.91 – 2.81 (m, 2H). ¹³C NMR (101 MHz, CD₃OD): δ 157.8, 151.3, 149.8, 142.5, 141.5, 140.6, 130.0, 127.2, 124.8, 124.0, 122.9, 121.0, 119.2, 119.1, 117.6, 112.1, 111.9, 102.9, 72.0, 71.52, 71.49, 71.44, 71.40, 71.3, 71.0, 70.6, 65.1, 56.0, 45.5, 41.7. HRMS calcd. For C₃₁H₄₃N₅O₁₀ ([M+H]⁺): 646.3088, found: 646.3048.

RBM3-325

¹H NMR (400 MHz, CD₃OD): δ 8.17 (s, 1H), 7.65 (ddd, *J* = 8.5, 3.4, 1.6 Hz, 1H), 7.51 (s, 1H), 7.41 (s, 1H), 7.39 – 7.19 (m, 3H), 7.09 – 6.93 (m, 2H), 4.26 (d, *J* = 5.1 Hz, 1H), 4.23 – 4.13 (m, 2H), 4.00 – 3.93 (m, 3H), 3.70 – 3.51 (m, 31H), 3.08 – 2.91 (m, 2H). ¹³C NMR (101 MHz, CD₃OD): δ 157.8, 151.2, 149.8, 141.4, 130.0, 129.7, 127.2, 123.9, 119.3, 112.0, 103.0, 71.5, 71.4, 71.3, 71.2, 71.1, 70.9, 70.7, 65.0, 62.0, 56.0, 41.0, 26.1. HRMS calcd. for C₃₅H₅₂N₅O₁₂ ([M+H]⁺): 734.3613, found: 734.3590.

1-((1-(2-(1-(4-Cyanophenyl)-2,5-dimethyl-1*H*-pyrrol-3-yl)-2-oxoethyl) piperidin-4-yl)oxy)-1-oxo-5,8,11,14,17-pentaoxa-2-azanonadecan-19-yl (4-(3-(3-methoxy-4-(oxazol-4-yl)phenyl)ureido)benzyl)carbamate (RBM3-330) and 1-((1-(2-(1-(4-cyanophenyl)-2,5-dimethyl-1*H*-pyrrol-3-yl)-2-oxoethyl) piperidin-4-yl)oxy)-1-oxo-5,8,11,14,17,20,23-heptaoxa-2-azapentacosan-25-yl (4-(3-(3-methoxy-4-(oxazol-4-yl)phenyl)ureido)benzyl)carbamate (RBM3-329)



RBM3-330: *n*=5

RBM3-329: *n*=7

A solution of **RBM3-308** (0.219 mmol, 1.1 eq.) in anhydrous CH₂Cl₂ (1 mL) was added dropwise to a stirred solution of the corresponding amine **RBM3-326** (0.197 mmol, 1 eq.) or **RBM3-325** (0.197 mmol, 1 eq) and TEA (1.2 eq, 0.236 mmol) in anhydrous CH₂Cl₂ (1 mL) at 25 °C. After overnight stirring, the reaction mixture was concentrated *in vacuo*, and the resulting crude was purified by flash chromatography (MeOH 0% to 20% in CH₂Cl₂) to furnish the final compounds **RBM3-330** (42% yield) and **RBM3-329** (59% yield).

RBM3-330

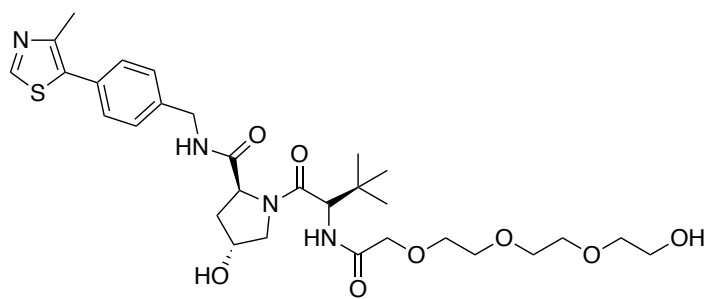
¹H NMR (400 MHz, CD₃OD): δ 8.17 (s, 1H), 7.92 (d, *J* = 8.5 Hz, 1H), 7.65 (d, *J* = 8.5 Hz, 1H), 7.51 (d, *J* = 2.0 Hz, 1H), 7.47 – 7.34 (m, 5H), 7.25 (t, *J* = 7.8 Hz, 1H), 6.97 (dt, *J* = 7.9, 2.3 Hz, 2H), 6.43 (s, 1H), 4.66 – 4.59 (m, 1H), 4.27 (s, 2H), 4.24 – 4.16 (m, 2H), 3.97 (s, 3H), 3.71 – 3.64 (m, 2H), 3.60 (m, 20H), 3.50 (t, *J* = 5.4 Hz, 2H), 3.26 (t, *J* = 5.5 Hz, 2H), 2.85 (br s, 2H), 2.45 (br s, 2H), 2.28 (s, 3H), 1.98 (s, 3H), 1.93 (m, 2H), 1.84 – 1.68 (m, 2H). ¹³C NMR (101 MHz, CD₃OD): δ 194.2, 159.0, 158.4, 157.8, 154.9, 151.3, 149.8, 142.5, 141.5, 140.5, 137.4, 134.8, 130.6, 130.2, 130.0, 127.2, 124.0, 122.9, 120.5, 119.2, 118.9, 114.0, 112.1, 111.9, 108.7, 102.9, 71.56, 71.53, 71.50, 71.2, 71.0, 70.6, 65.2, 56.0, 52.1, 45.4, 41.6, 31.6, 13.2, 12.7. HRMS calcd. for C₅₂H₆₅N₈O₁₃ ([M+H]⁺): 1009.4671, found: 1009.4807.

RBM3-329

¹H NMR (400 MHz, CD₃OD): δ 8.17 (s, 1H), 7.92 (d, *J* = 8.5 Hz, 1H), 7.66 (d, *J* = 8.4 Hz, 2H), 7.52 (d, *J* = 1.9 Hz, 1H), 7.48 – 7.32 (m, 5H), 7.25 (t, *J* = 7.8 Hz, 1H), 7.01 – 6.93 (m, 2H), 6.43 (s, 1H), 4.66 – 4.59 (m, 2H), 4.27 (s, 2H), 4.22 – 4.14 (m, 2H), 3.98 (s, 3H), 3.74 – 3.65 (m, 2H), 3.69 – 3.54 (m, 28H), 3.50 (t, *J* = 5.4 Hz, 2H), 3.26 (t, *J* = 5.5 Hz, 2H), 2.93 – 2.69 (m, 2H), 2.55 – 2.39 (m, 2H), 2.28 (s, 3H), 1.98 (s, 3H), 1.97 – 1.87 (m, 2H), 1.81 – 1.70 (m, 2H). ¹³C NMR

(101 MHz, CD₃OD): δ 159.0, 158.4, 157.8, 154.8, 151.3, 149.8, 142.5, 141.6, 140.6, 137.5, 134.8, 130.6, 130.3, 130.0, 127.2, 123.9, 122.9, 120.4, 119.2, 118.9, 114.0, 112.1, 111.9, 108.9, 102.9, 71.54, 71.51, 71.49, 71.2, 71.0, 70.6, 65.2, 56.0, 52.1, 45.4, 41.6, 31.5, 13.2, 12.7. HRMS calcd. for C₅₆H₇₃N₈O₁₅ ([M+H]⁺): 1097.5195, found: 1097.5193.

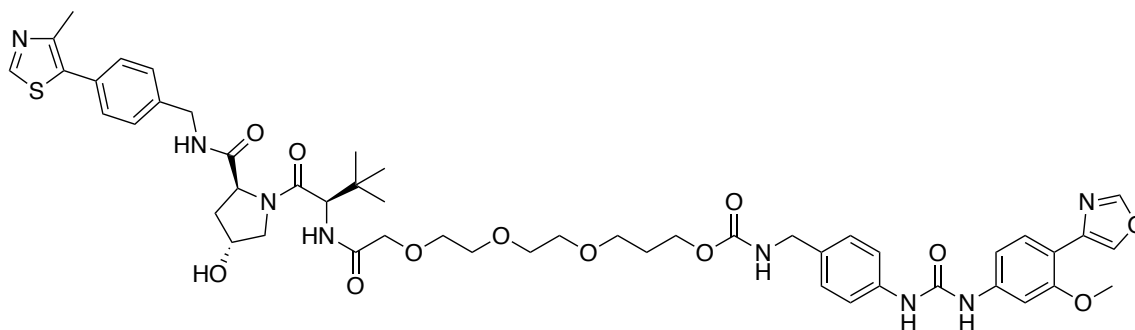
(2*S*,4*R*)-1-((*S*)-2-(*Tert*-butyl)-14-hydroxy-4-oxo-6,9,12-trioxa-3-azatetradecanoyl)-4-hydroxy-*N*-(4-(4-methylthiazol-5-yl)benzyl)pyrrolidine-2-carboxamide (RBM3-359)



EDC.HCl (87 mg, 0.452 mmol) and HOBt.H₂O (61 mg, 0.452 mmol) were sequentially added to an ice-cooled solution of 2-(2-(2-(2-hydroxyethoxy)ethoxy)ethoxy)acetic acid (200 mg, 0.377 mmol) in anhydrous CH₂Cl₂ (2 mL), and the resulting mixture was vigorously stirred at 25 °C under argon atmosphere. After 15 min, the previous mixture was added dropwise to a solution of **RBM5-189** (86 mg, 0.415 mmol) and DIPEA (0.328 ml, 1.885 mmol) in anhydrous CH₂Cl₂ (2 mL) and the reaction was stirred at 25 °C for 2 h. The mixture was next diluted with CH₂Cl₂ (5 mL) and washed with brine. The organic layer was dried over MgSO₄, filtered, and the volatiles were removed under reduced pressure. Purification of the crude mixture by flash column chromatography (MeOH 0% to 20% in CH₂Cl₂) afforded **RBM3-359** (150 mg, 0.246 mmol, 65% yield).

¹H NMR (400 MHz, CD₃OD): δ 8.89 (s, 1H), 7.47 (d, *J* = 8.3 Hz, 2H), 7.41 (d, *J* = 8.3 Hz, 2H), 4.69 (s, 1H), 4.63 – 4.49 (m, 3H), 4.37 (d, *J* = 15.5 Hz, 1H), 4.06 (d, *J* = 3.5 Hz, 2H), 3.88 (d, *J* = 11.3 Hz, 1H), 3.80 (dd, *J* = 11.0, 3.8 Hz, 1H), 3.76 – 3.62 (m, 12H), 3.59 – 3.51 (m, 2H), 2.48 (s, 3H), 2.25 (ddt, *J* = 13.2, 7.6, 1.9 Hz, 1H), 2.09 (ddd, *J* = 13.3, 9.2, 4.4 Hz, 1H), 1.04 (s, 9H). ¹³C NMR (101 MHz, CD₃OD): δ 174.3, 172.0, 171.6, 152.8, 149.0, 140.3, 133.3, 131.4, 130.30, 128.9, 73.53, 72.06, 71.52, 71.38, 71.35, 71.32, 71.00, 62.16, 62.10, 60.8, 58.2, 58.0, 43.6, 39.0, 37.0, 27.0, 15.9. HRMS calcd. for C₃₀H₄₅N₄O₈S ([M+H]⁺): 621.2958, found: 621.2994.

(*R*)-3-((2*S*,4*R*)-4-Hydroxy-2-((4-(4-methylthiazol-5-yl)benzyl)carbamoyl)pyrrolidine-1-carbonyl)-2,2-dimethyl-5-oxo-7,10,13-trioxa-4-azahexadecan-16-yl (4-(3-(3-methoxy-4-(oxazol-4-yl)phenyl)ureido)benzyl)carbamate (RBM3-360)

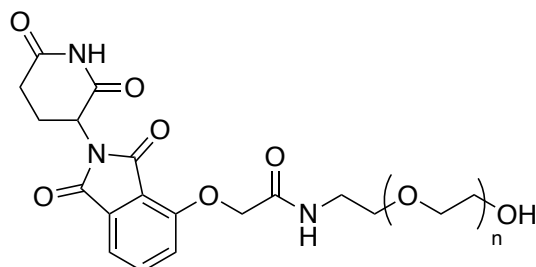


In a round bottom flask, *N,N'*-disuccinimidyl carbonate (0.122 g, 0.476 mmol) was dissolved in DMF (4 mL). Next TEA (0.140 mL, 1.001 mmol) was added and, a solution of the alcohol **RBM3-359** (0.313 g, 0.504 mmol) in DMF (1 mL) was then added dropwise. The mixture was monitored by TLC until completion of the reaction. **RBM3-306** (43.0 mg, 0.127 mmol) was added portionwise followed by TEA (0.210 mL, 1.513 mmol). The resulting mixture was stirred at 25 °C until no mixed carbonate remained by TLC (3 h) and concentrated. The

residue was purified by flash column chromatography (from 0 to 10 % MeOH in CH₂Cl₂) and reverse phase purification to give **RBM3-360** (19 mg, 0.019 mmol, 4 % yield).

¹H NMR (400 MHz, CD₃OD): δ 8.84 (s, 1H), 8.17 (s, 1H), 7.66 (d, *J* = 8.4 Hz, 1H), 7.50 (d, *J* = 2.0 Hz, 1H), 7.47 – 7.29 (m, 8H), 7.24 (t, *J* = 7.8 Hz, 1H), 6.97 (dd, *J* = 8.5, 2.1 Hz, 2H), 4.68 (s, 1H), 4.58 (t, *J* = 8.4 Hz, 1H), 4.49 (s, 1H), 4.41 – 4.29 (m, 2H), 4.26 (s, 2H), 4.17 (dd, *J* = 5.6, 3.8 Hz, 2H), 4.08 – 3.98 (m, 2H), 3.97 (s, 3H), 3.87 (d, *J* = 11.4 Hz, 1H), 3.78 (dd, *J* = 11.0, 3.8 Hz, 1H), 3.69 – 3.59 (m, 12H), 2.45 (s, 3H), 2.22 (dd, *J* = 13.3, 7.7 Hz, 1H), 2.07 (ddd, *J* = 13.3, 9.2, 4.4 Hz, 1H), 1.03 (s, 9H). ¹³C NMR (101 MHz, CD₃OD): δ 174.4, 157.8, 152.8, 140.5, 140.2, 131.5, 130.4, 130.1, 128.9, 127.3, 124.0, 112.1, 111.9, 103.0, 72.3, 71.6, 71.1, 70.6, 60.8, 58.2, 56.0, 43.7, 37.0, 27, 15.8. HRMS calcd. for C₄₉H₆₁N₈O₁₂S ([M+H]⁺): 985.4130, found: 985.4186.

2-((2-(2,6-dioxopiperidin-3-yl)-1,3-dioxoisindolin-4-yl)oxy)-N-(2-(2-(2-(2-hydroxyethoxy)ethoxy) ethoxy)ethyl)acetamide (RBM3-316), 2-((2-(2,6-dioxopiperidin-3-yl)-1,3-dioxoisindolin-4-yl)oxy)-N-(17-hydroxy-3,6,9,12,15-pentaoxaheptadecyl)acetamide (RBM3-331) and 2-((2-(2,6-dioxopiperidin-3-yl)-1,3-dioxoisindolin-4-yl)oxy)-N-(23-hydroxy-3,6,9,12,15,18,21-heptaotricosyl)acetamide (RBM3-332)



RBM3-316: n=3

RBM3-331: n=5

RBM3-332: n=7

EDC.HCl (0.738 g, 3.852 mmol) and HOBt H₂O (0.423 g, 3.130 mmol) were sequentially added to an ice-cooled solution of **RBM5-173** (0.800 g, 2.408 mmol) in anhydrous CH₂Cl₂ (12 mL), and the resulting mixture was vigorously stirred at 25 °C under argon atmosphere. After 15 min, the previous mixture was added dropwise to a solution of the selected amine **RBM3-207**, **RBM3-209** or **RBM3-203** (3 eq, 2.408 mmol) and TEA (1.7 mL, 12.038 mmol) in anhydrous CH₂Cl₂ (12 mL), and the reaction was stirred at 25 °C for 2h. The mixture was next diluted with CH₂Cl₂ (50 mL) and washed with brine (2 x 25 mL). The organic layer was dried over MgSO₄, filtered, and the volatiles were removed under reduced pressure. Purification of the crude mixture by flash column chromatography (MeOH 0% to 20% in CH₂Cl₂) afforded the corresponding amides **RBM3-316** (23% yield), **RBM3-331** (62% yield) and **RBM3-332** (71% yield).

RBM3-316

¹H NMR (400 MHz, CDCl₃): δ 9.14 (br s, 1H), 7.52 – 7.42 (m, 2H), 7.28 (d, *J* = 7.4 Hz, 1H), 6.95 (d, *J* = 8.4 Hz, 1H), 4.78 – 4.68 (m, 1H), 4.41 (s, 2H), 3.49 – 3.34 (m, 16H), 2.72 – 2.39 (m, 3H), 1.95 – 1.82 (m, 1H). ¹³C NMR (101 MHz, CDCl₃): δ 167.0, 166.8, 166.0, 154.7, 137.1, 133.8, 119.5, 117.4, 72.9, 70.7, 70.5, 70.3, 70.3, 69.7, 68.0, 61.6, 49.4, 39.2, 31.5, 29.8, 22.9. HRMS calcd. for C₂₃H₃₀N₃O₁₀ ([M+H]⁺): 508.1931, found:508.1901.

RBM3-331

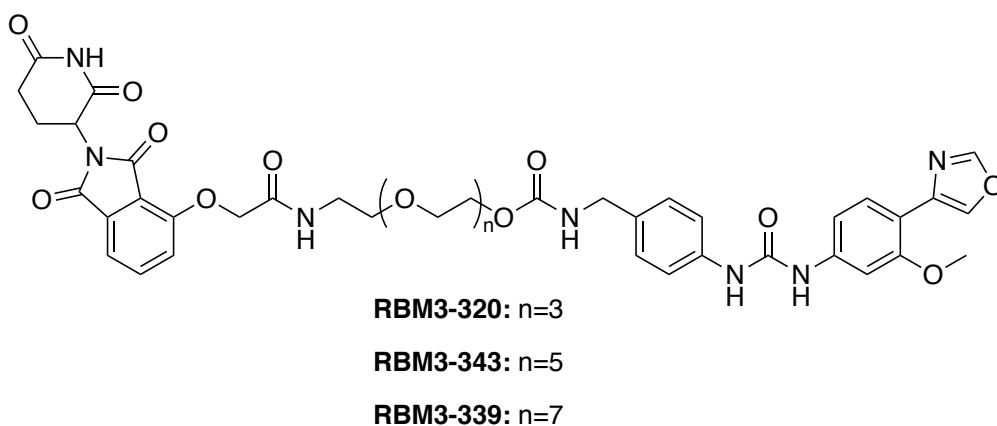
¹H NMR (400 MHz, CDCl₃): δ 7.77 (d, *J* = 5.7 Hz, 1H), 7.72 (dd, *J* = 8.4, 7.3 Hz, 1H), 7.53 (d, *J* = 7.3 Hz, 1H), 7.20 (d, *J* = 8.4 Hz, 1H), 5.03 – 4.90 (m, 1H), 4.66 (s, 2H), 3.70 (dd, *J* = 5.2, 3.5 Hz, 2H), 3.68 – 3.60 (m, 18H), 3.59 – 3.56 (m, 4H), 2.90 – 2.72 (m, 3H), 2.15 – 2.10 (m, 1H). ¹³C NMR (101 MHz, CDCl₃): δ 171.7, 168.6, 167.1, 166.9, 166.0, 154.6, 137.0, 133.8, 119.5, 118.0, 117.3, 77.5, 77.2, 76.8, 72.8, 70.52, 70.50, 70.5, 70.45, 70.40, 70.4, 70.3, 70.1, 69.5, 68.0, 61.6,

50.8, 49.4, 39.2, 31.5, 22.8. HRMS calcd. for C₂₇H₃₈N₃O₁₂ ([M+H]⁺): 597.2534, found: 597.2542.

RBM3-332

¹H NMR (400 MHz, CDCl₃): δ 9.08 (br s, 1H), 7.76 (m, 1H), 7.66 (t, *J* = 5.4 Hz, 1H), 7.55 (d, *J* = 7.3 Hz, 1H), 7.20 (d, *J* = 8.4 Hz, 1H), 5.01 – 4.92 (m, 1H), 4.66 (s, 2H), 3.76 – 3.69 (m, 2H), 3.70 – 3.63 (m, 26H), 3.63 – 3.55 (m, 4H), 2.92 – 2.75 (m, 3H), 2.20 – 2.10 (m, 1H). ¹³C NMR (101 MHz, CDCl₃): δ 171.3, 168.3, 166.9, 166.9, 165.9, 154.6, 137.1, 133.8, 119.4, 118.2, 117.4, 72.7, 70.8, 70.71, 70.67, 70.65, 70.63, 70.61, 70.59, 70.54, 70.48, 70.47, 70.4, 69.6, 68.0, 61.8, 49.5, 39.2, 31.6, 22.8. HRMS calcd. For C₃₁H₄₆N₃O₁₄ ([M+H]⁺): 684.2980, found: 684.3001.

1-((2-(2,6-dioxopiperidin-3-yl)-1,3-dioxoisindolin-4-yl)oxy)-2-oxo-6,9,12-trioxa-3-azatetradecan-14-yl (4-(3-(3-methoxy-4-(oxazol-4-yl)phenyl)ureido)benzyl)carbamate (RBM3-320), 1-((2-(2,6-dioxopiperidin-3-yl)-1,3-dioxoisindolin-4-yl)oxy)-2-oxo-6,9,12,15,18-pentaoxa-3-azaicosan-20-yl (4-(3-(3-methoxy-4-(oxazol-4-yl)phenyl)ureido)benzyl)carbamate (RBM3-343) and 1-((2-(2,6-dioxopiperidin-3-yl)-1,3-dioxoisindolin-4-yl)oxy)-2-oxo-6,9,12,15,18,21,24-heptaoxa-3-azahexacosan-26-yl (4-(3-(3-methoxy-4-(oxazol-4-yl)phenyl)ureido)benzyl)carbamate (RBM3-339)



To a solution of **RBM3-316**, **RBM3-331** or **RBM3-332** (0.300 mmol) and *N,N'*-disuccinimidyl carbonate (0.450 mmol) in 1 mL of MeCN was added TEA (0.125 mL, 0.900 mmol). The resulting solution was stirred at 25 °C for 3 h (complete conversion by TLC). After the reaction was completed, 10 mL of CH₂Cl₂ was added to the reaction mixture. The solution was washed with 5% NaHCO₃ (2 x 5 mL) and then with water. The CH₂Cl₂ organic phase was then dried, filtered, and the solvent removed under reduced pressure. The resulting crude was dissolved in MeCN (0.6 ml) and added to a stirred solution of **RBM3-306** (113 mg, 0.300 mmol) and TEA (0.057 mL, 0.400 mmol) in MeCN (1.35 ml). The resulting mixture was stirred at 25°C until no mixed carbonate remained by TLC (3 h). The reaction mixture was concentrated in vacuo, and the resulting crude was purified by flash chromatography (MeOH 0% to 30% in CH₂Cl₂) to furnish the corresponding compounds **RBM3-320** (14% yield, 2 steps), **RBM3-343** (55% yield, 2 steps) and **RBM3-339** (55% yield, 2 steps).

RBM3-320

¹H NMR (400 MHz, CD₃OD): δ 8.16 (s, 1H), 7.72 (t, *J* = 7.9 Hz, 1H), 7.62 (d, *J* = 8.4 Hz, 1H), 7.55 – 7.43 (m, 2H), 7.39 (d, *J* = 8.1 Hz, 2H), 7.32 (d, *J* = 8.5 Hz, 2H), 7.23 (t, *J* = 7.8 Hz, 1H), 6.99 – 6.90 (m, 2H), 5.09 (dd, *J* = 12.5, 5.4 Hz, 1H), 4.69 (s, 2H), 4.26 (s, 2H), 4.18 (t, *J* = 4.7 Hz, 2H), 3.96 (s, 3H), 3.69 – 3.52 (m,

16H), 3.47 (t, $J = 5.3$ Hz, 2H), 2.15 – 2.06 (m, 1H). ^{13}C NMR (101 MHz, CD_3OD): δ 174.6, 171.4, 168.3, 167.5, 157.7, 156.0, 151.2, 142.5, 138.1, 134.8, 130.0, 127.2, 123.9, 121.3, 119.1, 117.8, 111.9, 102.9, 71.6, 71.5, 71.4, 70.6, 70.3, 69.0, 65.2, 56.0, 50.5, 45.4, 40.2, 32.2, 30.0, 23.6. HRMS calcd. for $\text{C}_{42}\text{H}_{46}\text{N}_7\text{O}_{14}$ ($[\text{M}+\text{H}]^+$): 872.3103, found: 872.3145.

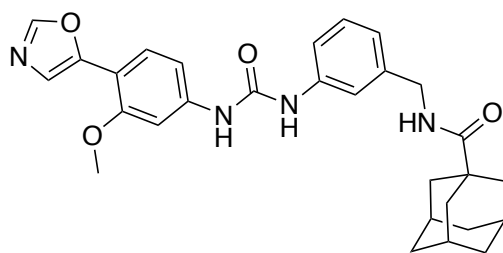
RBM3-343

^1H NMR (400 MHz, CD_3OD): δ 8.17 (s, 1H), 7.80 – 7.70 (m, 1H), 7.64 (d, $J = 8.4$ Hz, 1H), 7.58 – 7.31 (m, 6H), 7.24 (t, $J = 7.8$ Hz, 1H), 7.02 – 6.91 (m, 2H), 5.10 (dd, $J = 12.4, 5.4$ Hz, 1H), 4.71 (s, 2H), 4.27 (s, 2H), 4.19 (t, $J = 4.7$ Hz, 2H), 3.98 (s, 3H), 3.71 – 3.64 (m, 2H), 3.64 – 3.63 (m, 22H), 3.47 (t, $J = 5.3$ Hz, 2H), 2.96 – 2.70 (m, 3H), 2.19 – 2.06 (m, 1H). ^{13}C NMR (101 MHz, CD_3OD): δ 174.3, 171.0, 168.1, 167.3, 157.6, 155.8, 151.0, 142.3, 140.3, 138.0, 134.7, 129.9, 127.1, 123.8, 122.8, 121.2, 119.1, 118.9, 117.8, 111.7, 102.8, 71.41, 71.37, 71.3, 70.4, 70.1, 68.9, 65.1, 64.6, 56.0, 50.4, 45.4, 40.1, 32.1, 23.5. HRMS calcd. For $\text{C}_{46}\text{H}_{54}\text{N}_7\text{O}_{16}$ ($[\text{M}+\text{H}]^+$): 960.3627, found: 960.3645.

RBM3-339

^1H NMR (400 MHz, CD_3OD): δ 8.10 (s, 1H), 7.80 – 7.70 (m, 1H), 7.63 (d, $J = 8.5$ Hz, 1H), 7.53 – 7.47 (m, 2H), 7.40 – 7.32 (m, 4H), 7.23 (t, $J = 7.8$ Hz, 1H), 6.94 (dd, $J = 17.0, 8.0$ Hz, 2H), 5.07 (dd, $J = 12.3, 5.5$ Hz, 1H), 4.69 (s, 2H), 4.27 (s, 2H), 4.22 – 4.16 (m, 2H), 3.97 (s, 3H), 3.71 – 3.65 (m, 2H), 3.69 – 3.52 (m, 28H), 3.52 – 3.45 (m, 2H), 2.90 – 2.69 (m, 3H), 2.18 – 2.07 (m, 1H). ^{13}C NMR (101 MHz, CD_3OD): δ 174.9, 174.6, 171.2, 170.0, 168.3, 167.5, 157.8, 151.3, 142.5, 141.4, 138.1, 130.1, 127.2, 124.0, 123.2, 121.5, 117.8, 112.1, 111.9, 71.6, 71.5, 71.5, 71.4, 70.6, 70.3, 69.1, 65.3, 56.0, 50.6, 45.4, 40.2, 32.2, 26.3, 23.7. HRMS calcd. For $\text{C}_{50}\text{H}_{62}\text{N}_7\text{O}_{18}$ ($[\text{M}+\text{H}]^+$): 1048.4152, found: 1048.4158.

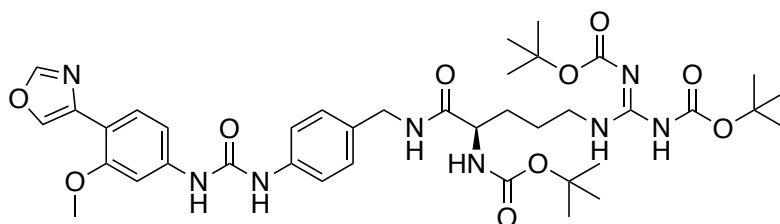
(RBM3-357)



EDC·HCl (136.0 mg, 0.709 mmol) and *N,N*- diisopropylethylamine (0.257 mL, 1.478 mmol) were added to a solution of **RBM3-306** (200.0 mg, 0.591 mmol), 1-adamantanecarboxylic acid (106.5 mg, 0.591 mmol) and HOBt·H₂O (95.8 mg, 0.709 mmol) in DMF (5.9 mL) and stirred for 24h at 25 °C under nitrogen. The solvent was removed *in vacuo* and the residue was purified by reverse-phase chromatography to give **RBM3-357** (195.0 mg, 0.390 mmol, 66% yield) as a white solid.

¹H NMR (400 MHz, DMSO-*d*₆): δ 8.88 (s, 1H), 8.70 (s, 1H), 8.35 (s, 1H), 7.97 (t, *J* = 6.1 Hz, 1H), 7.59 (d, *J* = 8.5 Hz, 1H), 7.49 (d, *J* = 2.0 Hz, 1H), 7.41 (s, 1H), 7.36 – 7.27 (m, 2H), 7.21 (t, *J* = 7.8 Hz, 1H), 7.04 (dd, *J* = 8.5, 2.0 Hz, 1H), 6.83 (d, *J* = 7.5 Hz, 1H), 4.23 (d, *J* = 5.9 Hz, 2H), 3.92 (s, 3H), 2.01 – 1.94 (m, 3H), 1.83 (d, *J* = 2.9 Hz, 6H), 1.68 (dd, *J* = 5.5, 2.9 Hz, 6H). ¹³C NMR (101 MHz, DMSO-*d*₆): δ 177.1, 156.0, 152.3, 150.4, 147.5, 141.2, 140.7, 139.6, 126.1, 123.5, 116.8, 110.4, 101.3, 55.6, 42.0, 40.4, 39.0, 36.4, 27.9. HRMS calcd. for C₂₉H₃₃N₄O₄ ([M+H]⁺): 501.2502, found: 501.2552.

(RBM3-358)

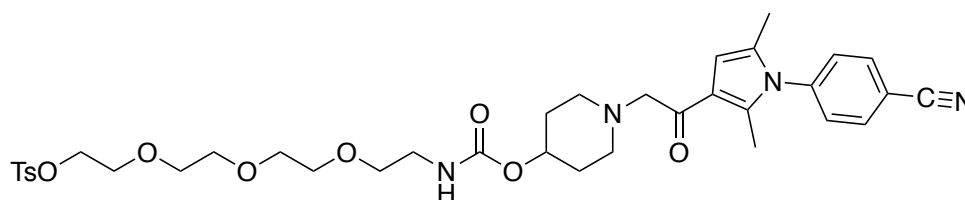


EDC·HCl (48.3 mg, 0.252 mmol) and *N,N*- diisopropylethylamine (0.100 mL, 0.001 mol) were added to a solution of amine **RBM3-306** (0.100 mL, 0.574 mmol), *Tri*-Boc-Arginine (99.6 mg, 0.210 mmol) and HOBt·H₂O (34.0 mg, 0.252 mmol) in CH₂Cl₂ (2.1 mL) and stirred for 24 h at 25 °C under nitrogen. The solvent was removed *in vacuo* and the residue was purified by column chromatography on silica gel (MeOH 0% to 7% in CH₂Cl₂) to give **RBM3-358** (140.3 mg, 0.176 mmol, 84% yield).

¹H NMR (400 MHz, CDCl₃): δ 9.44 (br s, 2H), 8.14 (br s, 1H), 8.00 (br s, 1H), 7.85 (s, 1H), 7.59 (s, 1H), 7.54 (d, *J* = 1.9 Hz, 1H), 7.51 – 7.45 (m, 1H), 7.43 (s, 1H), 7.35 (br s, 1H), 7.18 (t, *J* = 7.9 Hz, 1H), 7.05 (br s, 1H), 6.85 (d, *J* = 7.6 Hz, 1H), 6.76 (d, *J* = 8.5 Hz, 1H), 5.92 (d, *J* = 8.0 Hz, 1H), 4.47– 4.21 (m, 3H), 3.90 (s, 3H), 3.88 – 3.64 (m, 2H), 1.85 – 1.55 (m, 4H), 1.49 (s, 9H), 1.44 (s, 9H), 1.41 (s, 9H). ¹³C NMR (101 MHz, CDCl₃): δ 189.7, 179.1, 173.2, 171.3, 156.5, 155.9, 153.1, 149.1, 148.2, 140.7, 139.2, 138.9, 129.5, 126.3, 124.1, 121.1, 118.4, 117.7, 111.6, 110.8, 102.0, 80.1, 55.6, 53.6, 44.3, 43.3, 29.2, 28.5, 28.3, 28.1, 25.0. HRMS calcd for C₃₉H₅₅N₈O₁₀ ([M+H]⁺): 795.4041, found: 795.4046.

v. RTK PROTACs

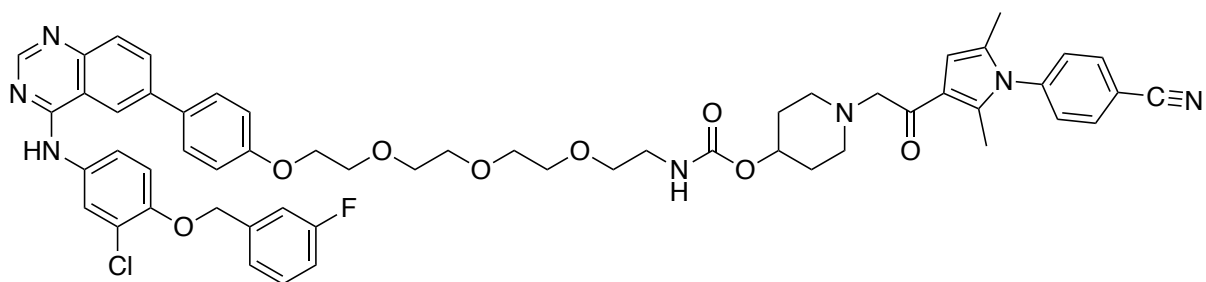
1-((1-(2-(1-(4-cyanophenyl)-2,5-dimethyl-1*H*-pyrrol-3-yl)-2-oxoethyl)piperidin-4-yl)oxy)-1-oxo-5,8,11-trioxa-2-azatridecan-13-yl 4-methylbenzenesulfonate (RBM3-139)



To a stirred solution of **RBM3-099** (60 mg, 0.108 mmol) in anhydrous CH₂Cl₂ (5 mL) and TEA (0.045 mL, 0.323 mmol), a solution of 4-methylbenzenesulfonyl chloride (TsCl) (41 mg, 0.216 mmol) in anhydrous CH₂Cl₂ (2 mL) was added at 0 °C. After the addition was complete, the mixture was allowed to warm to 25 °C and stirred for 3 h. The reaction mixture was then poured into 0.5 M aqueous HCl (15 mL) and extracted with CH₂Cl₂ (3 x 15 mL). The combined organic layers were washed with brine, dried over anhydrous MgSO₄, filtered and evaporated to dryness and the residue was purified by silica gel column chromatography (0% to 7% of MeOH in CH₂Cl₂) to afford **RBM3-139** (70.0 mg, 0.098 mmol, 91%).

¹H NMR (400 MHz, CDCl₃): δ 7.83 (d, *J* = 8.4 Hz, 2H), 7.76 (d, *J* = 8.1 Hz, 2H), 7.33 (d, *J* = 8.5 Hz, 2H), 7.31 (d, *J* = 8.1 Hz, 2H), 6.39 (s, 1H), 6.02 (t, *J* = 5.8 Hz, 1H), 4.88 – 4.57 (m, 1H), 3.72 (m, 4H), 3.64 (m, 11H), 3.55 (t, *J* = 4.9 Hz, 2H), 3.36 (q, *J* = 5.3 Hz, 2H), 2.95 – 2.86 (m, 4H), 2.49 – 2.38 (m, 2H), 2.35 (s, 3H), 2.31 (s, 3H), 2.00 – 1.94 (br m, 2H), 1.99 (s, 3H), 1.82 (m, 2H). ¹³C NMR (101 MHz, CDCl₃): δ 192.8, 156.5, 144.7, 141.4, 136.3, 133.6, 132.7, 129.2, 128.6, 119.6, 117.9, 113.0, 107.8, 72.8, 70.7, 70.5, 70.4, 70.3, 65.2, 61.7, 51.4, 43.0, 40.8, 31.1, 21.5, 13.1, 12.8. HRMS calcd. for C₃₆H₄₇N₄O₉S ([M+H]⁺): 710.3011 found: 710.3012.

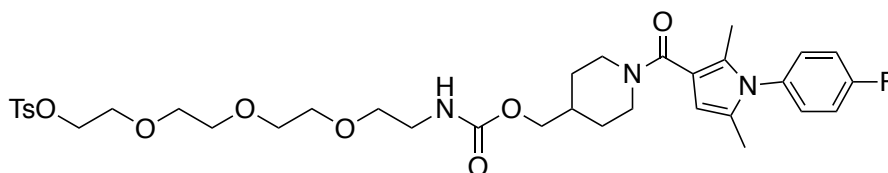
1-(2-(1-(4-cyanophenyl)-2,5-dimethyl-1*H*-pyrrol-3-yl)-2-oxoethyl)piperidin-4-yl (2-(2-(2-(2-(4-(4-((3-chloro-4-((3-fluorobenzyl)oxy)phenyl)amino)quinazolin-6-yl)phenoxy)ethoxy)ethoxy) ethyl) carbamate (**RBM3-216**)



To a mixture of **RBM3-027** (30.0 mg, 0.064 mmol) and **RBM3-139** (30.0 mg, 0.042 mmol) in *N,N*-dimethylformamide (5 mL) was added Cs₂CO₃ (62.1 mg, 0.191 mmol). The reaction mixture was stirred at 50 °C for 6 h. Then it was diluted with AcOEt (30 mL), washed with water (4 x 20 mL), dried (Na₂SO₄) and the solvent was evaporated under vacuum. The crude product was purified by silica gel column chromatography (0% to 100% of EtOAc in hexanes) followed by a second purification by silica gel column chromatography (0% to 20% of MeOH in CH₂Cl₂) and finally by preparative TLC (DCM:MeOH 92:8) to **RBM3-216** (30 mg, 0.030 mmol, 70%).

¹H NMR (400 MHz, DMSO-*d*₆): δ 9.85 (s, 1H), 9.68 (s, 1H), 8.69 (s, 1H), 8.56 (s, 1H), 8.12 (d, *J* = 8.7 Hz, 1H), 8.03 (s, 1H), 7.87 – 7.67 (m, 6H), 7.48 (td, *J* = 8.0, 6.0 Hz, 1H), 7.39 – 7.25 (m, 5H), 7.19 (tt, *J* = 7.8, 1.4 Hz, 1H), 6.93 (d, *J* = 8.6 Hz, 2H), 6.43 (s, 1H), 6.08 (t, *J* = 5.8 Hz, 1H), 5.27 (s, 2H), 4.88 – 4.57 (m, 1H), 3.72 (m, 4H), 3.64 (m, 11H), 3.55 (t, *J* = 4.9 Hz, 2H), 3.36 (q, *J* = 5.3 Hz, 2H), 2.95 – 2.86 (m, 4H), 2.49 – 2.38 (m, 2H), 2.31 (s, 3H), 2.00 – 1.94 (br m, 2H), 1.99 (s, 3H), 1.82 (m, 2H). ¹³C NMR (101 MHz, DMSO-*d*₆): δ 192.8, 163.06, 161.44, 157.66, 157.59, 156.5, 154.07, 149.69, 148.44, 141.4, 139.73, 139.69, 138.23, 133.18, 132.7, 131.45, 130.69, 130.64, 129.86, 129.2, 128.67, 128.36, 128.32, 124.20, 123.45, 123.43, 122.38, 121.01, 119.6, 118.95, 117.9, 115.88, 115.33, 114.87, 114.73, 114.28, 114.21, 114.07, 113.0, 107.8, 72.8, 70.7, 70.5, 70.4, 70.3, 69.37, 65.2, 61.7, 51.4, 43.0, 40.8, 31.1, 13.1, 12.8. HRMS calcd. for C₅₆H₅₈ClFN₇O₈ ([M+H]⁺): 1009.3912 found: 1009.3912.

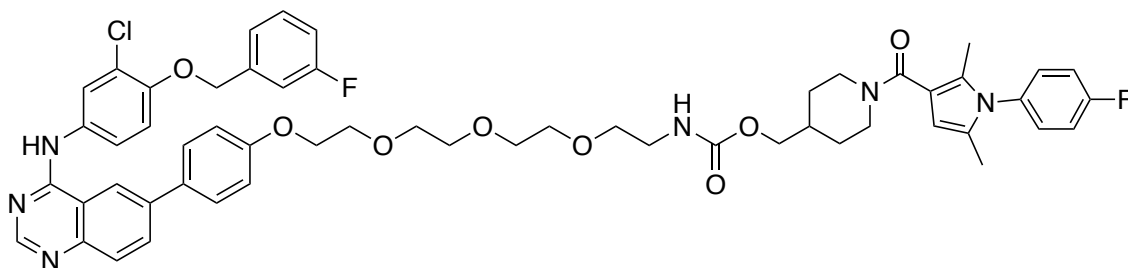
1-(1-(1-(4-fluorophenyl)-2,5-dimethyl-1*H*-pyrrole-3-carbonyl)piperidin-4-yl)-3-oxo-2,7,10,13-tetraoxa-4-azapentadecan-15-yl 4-methylbenzenesulfonate (RBM3-153) **4-**



To a stirred solution of **RBM3-352** (70 mg, 0.127 mmol) in anhydrous CH₂Cl₂ (5 mL) and TEA (0.045 mL, 0.323 mmol), a solution of 4-methylbenzenesulfonyl chloride (TsCl) (39 mg, 0.383 mmol) in anhydrous CH₂Cl₂ (2 mL) was added at 0 °C. After the addition was complete, the mixture was allowed to warm to 25 °C and stirred for 3 h. The reaction mixture was then poured into 0.5 M aqueous HCl (15 mL) and extracted with CH₂Cl₂ (3 x 15 mL). The combined organic layers were washed with brine, dried over anhydrous MgSO₄, filtered and the solvent was evaporated to dryness. The residue was purified by silica gel column chromatography using (0% to 7% of MeOH in CH₂Cl₂) to afford **RBM3-153** (83.0 mg, 0.117 mmol, 92%).

¹H NMR (400 MHz, CDCl₃): δ 7.76 (d, *J* = 8.1 Hz, 2H), 7.31 (d, *J* = 8.1 Hz, 2H), 7.21 – 7.14 (m, 4H), 6.02 (m, 1H), 5.95 (s, 1H), 3.96 (d, *J* = 6.5 Hz, 2H), 3.75 – 3.69 (m, 4H), 3.68 – 3.60 (m, 10H), 3.57 – 3.53 (m, 2H), 3.40 – 3.32 (m, 2H), 2.41 (s, 3H), 2.07 (s, 3H), 1.97 (s, 3H), 1.96 – 1.87 (m, 2H), 1.80 – 1.73 (m, 2H), 1.34 – 1.21 (m, 4H). ¹³C NMR (101 MHz, CDCl₃): δ 168.0, 144.7, 132.7, 130.8, 130.1, 130.0, 128.2, 116.5, 116.2, 115.1, 106.4, 77.5, 77.2, 76.8, 72.7, 70.7, 70.5, 70.3, 70.2, 68.7, 61.7, 41.0, 36.5, 21.5, 12.8, 12.0. HRMS calcd. For C₃₅H₄₇FN₃O₉S ([M+H]⁺): 703.2923. found: 703.2925.

(1-(1-(4-fluorophenyl)-2,5-dimethyl-1H-pyrrole-3-carbonyl)piperidin-4-yl)methyl (2-(2-(2-(2-(4-(4-((3-chloro-4-((3-fluorobenzyl)oxy)phenyl)amino)quinazolin-6-yl)phenoxy)ethoxy)ethoxy)ethoxy) ethyl) carbamate (RBM3-223)

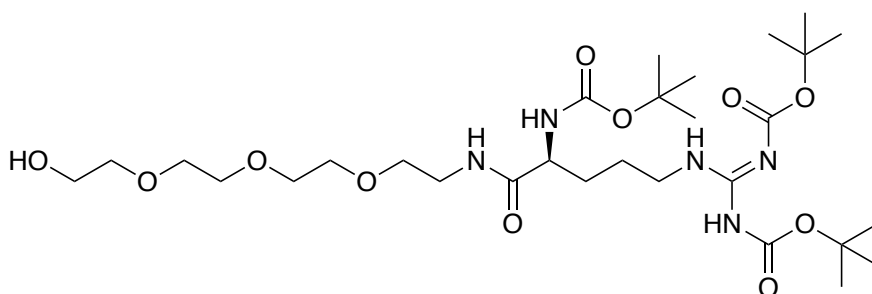


To a mixture of **RBM3-027** (23 mg, 0.048 mmol) and **RBM3-153** (33.0 mg, 0.048 mmol) in *N,N*-dimethylformamide (5 mL) was added Cs_2CO_3 (46 mg, 0.143 mmol). The reaction mixture was stirred at 50 °C for 6 h. Then it was diluted with AcOEt (30 mL), washed with water (4 x 20 mL), dried over Na_2SO_4 and the solvent was evaporated under vacuum. The crude product was purified by silica gel column chromatography (0% to 100% of EtOAc in hexanes) followed by a second purification by silica gel column chromatography (0% to 13% of MeOH in CH_2Cl_2) and then by preparative TLC (CH_2Cl_2 :MeOH 96:4) to give **RBM3-223** (30 mg, 0.030 mmol, 70%).

^1H NMR (400 MHz, $\text{DMSO}-d_6$): δ 9.85 (s, 1H), 9.68 (s, 1H), 8.69 (s, 1H), 8.56 (s, 1H), 8.12 (d, $J = 8.7$ Hz, 1H), 8.03 (s, 1H), 7.87 – 7.67 (m, 4H), 7.48 (td, $J = 8.0, 6.0$ Hz, 1H), 7.39 – 7.25 (m, 3H), 7.21 – 7.117 (m, 4H), 7.15 (tt, $J = 7.8, 1.4$ Hz, 1H), 6.93 (d, $J = 8.6$ Hz, 2H), 6.02 (m, 1H) 5.95 (s, 1H), 5.27 (s, 2H), 3.96 (d, $J = 6.5$ Hz, 2H), 3.75 – 3.69 (m, 4H), 3.68 – 3.60 (m, 10H), 3.57 – 3.53 (m, 2H), 3.40 – 3.32 (m, 2H), 2.07 (s, 3H), 1.97 (s, 3H), 1.96 – 1.87 (m, 2H), 1.80 – 1.73 (m, 2H), 1.34 – 1.21 (m, 4H). ^{13}C NMR (101 MHz, $\text{DMSO}-d_6$): δ 168.0, 163.06, 161.44, 157.66, 157.59, 154.07, 149.69, 148.44, 139.73, 139.69, 138.23,

133.18, 131.45, 130.8, 130.69, 130.64, 130.1, 130.0, 129.86, 128.36, 128.32, 128.2, 124.20, 123.45, 123.43, 122.38, 121.01, 118.95, 116.5, 116.2, 115.88, 115.33, 115.1, 114.87, 114.73, 114.28, 114.21, 114.07, 106.4, 77.5, 77.2, 76.8, 72.7, 70.7, 70.5, 70.3, 70.2, 69.37, 68.7, 61.7, 41.0, 36.5, 12.8, 12.0. HRMS calcd. for C₅₅H₅₈ClF₂N₆O₈ ([M+H]⁺): 1002.3944. Found 1002.3945.

(RBM3-143)

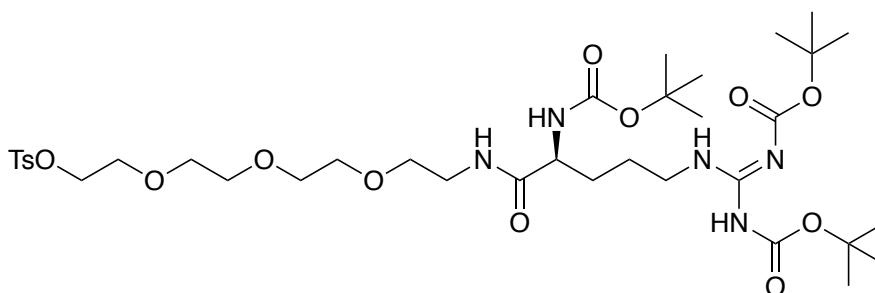


EDC·HCl (127 mg, 0.662 mmol) and HOBt·H₂O (72 mg, 0.538 mmol) were sequentially added to a solution of *tri*-Boc-Arginine (216 mg, 0.455 mmol) in CH₂Cl₂ (10 mL), and the resulting mixture was vigorously stirred at 25 °C under argon atmosphere. After 15 min, the previous mixture was added dropwise to a solution of the amine **RBM3-207** (80 mg, 0.414 mmol) and TEA (0.288 mL, 2.070 mmol) in CH₂Cl₂ (10 mL), and the reaction was stirred at 25 °C overnight. The mixture was next diluted with CH₂Cl₂ (50 mL) and washed with brine (2 x 25 mL). The organic layer was dried over MgSO₄, filtered, and the volatiles were removed under reduced pressure. Purification of the crude mixture by flash column chromatography (from 0 to 6% MeOH in CH₂Cl₂) afforded **RBM3-143** as a colorless oil (250 mg, 0.385 mmol, 93 %).

¹H NMR (400 MHz, CDCl₃): δ 4.47–4.21 (m, 2H), 4.05 (d, *J* = 8.3 Hz, 2H), 3.90 (m, 3H), 3.79–3.75 (m, 4H), 3.71–3.60 (m, 10H), 3.54 (m, 1H), 3.11 (t, 2H), 1.85

– 1.55 (m, 4H) 1.49 (s, 9H), 1.44 (s, 9H), 1.41 (s, 9H). HRMS calcd. for $C_{29}H_{56}N_5O_{11}$ ($[M+H]^+$): 649.3901, found: 649.3902.

(*S,E*)-6,11-bis((*tert*-butoxycarbonyl)amino)-2,2-dimethyl-4,12-dioxo-3,16,19,22-tetraoxa-5,7,13-triazatetracos-5-en-24-yl 4-methylbenzenesulfonate (RBM3-144)

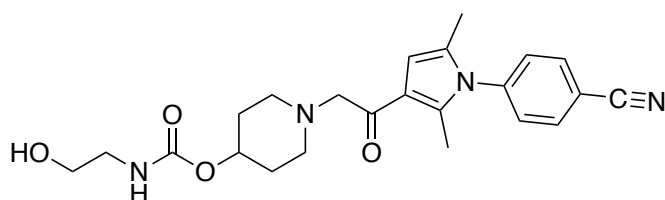


To a stirred solution of **RBM3-143** (180 mg, 0.277 mmol) in anhydrous CH_2Cl_2 (10 mL) and TEA (0.116 mL, 0.831 mmol), a solution of 4-methylbenzenesulfonyl chloride (TsCl) (105 mg, 0.554 mmol) in anhydrous CH_2Cl_2 (3mL) was added at 0 °C. After the addition was complete, the mixture was allowed to warm to 25 °C and stirred for 3 h. The reaction mixture was then poured into 0.5 M aqueous HCl (15 mL) and extracted with CH_2Cl_2 (3 x 15 mL). The combined organic layers were washed with brine, dried over anhydrous $MgSO_4$, filtered and the solvent was evaporated to dryness. The residue was purified by silica gel column chromatography (0% to 4% of MeOH in CH_2Cl_2) to afford **RBM3-143** (73.0 mg, 0.091 mmol, 32%).

1H NMR (400 MHz, $CDCl_3$): δ 7.76 (d, $J = 8.1$ Hz, 2H), 7.31 (d, $J = 8.1$ Hz, 2H), 4.47– 4.21 (m, 2H), 4.05 (d, $J = 8.3$ Hz, 2H), 3.90 (m, 3H), 3.79-3.75 (m, 4H), 3.71-3.60 (m, 10H), 3.54 (m, 1H), 3.11 (t, 2H), 2.41 (s, 3H), 1.85 – 1.55 (m, 4H) 1.49 (s, 9H), 1.44 (s, 9H), 1.41 (s, 9H). HRMS calcd. for $C_{36}H_{61}N_5O_{13}S$ ($[M+H]^+$): 804.3987, found: 804.3937.

114.73, 114.28, 114.21, 114.07, 80.1, 72.7, 70.7, 70.5, 70.3, 70.2, 70.0, 69.37, 55.6, 53.6, 44.3, 43.3, 41.32, 29.2, 28.5, 28.3, 28.1, 25.0. HRMS calcd. for $C_{56}H_{73}ClFN_8O_{12}$ ($[M+H]^+$): 1102.4932. Found 1102.4932.

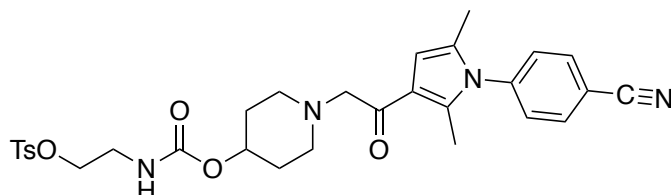
1-(2-(1-(4-cyanophenyl)-2,5-dimethyl-1*H*-pyrrol-3-yl)-2-oxoethyl)piperidin-4-yl (2-hydroxyethyl) carbamate (RBM3-140)



A solution of **RBM3-308** (60.0 mg, 0.119 mmol) in anhydrous CH_2Cl_2 (5 mL) was added dropwise to a stirred solution of **RBM3-013** (10.2 mg, 0.167 mmol) and TEA (36.2 mg, 0.358 mmol) in anhydrous CH_2Cl_2 (1 mL) at 25 °C. After overnight stirring, the reaction mixture was concentrated *in vacuo*, and the resulting crude was purified by flash chromatography (MeOH 0% to 7% in CH_2Cl_2) to furnish **RBM3-140** (41 mg, 0.091 mmol, 81% yield)

1H NMR (400 MHz, $CDCl_3$): δ 7.83 (d, $J = 8.4$ Hz, 2H), 7.33 (d, $J = 8.5$ Hz, 2H), 6.39 (s, 1H), 6.02 (t, $J = 5.8$ Hz, 1H), 4.88 – 4.57 (m, 1H), 3.72 (m, 2H), 3.55 (t, $J = 4.9$ Hz, 2H) 3.40 – 3.32 (m, 2H), 3.31 (q, $J = 5.3$ Hz, 2H), 2.49 – 2.38 (m, 2H), 2.31 (s, 3H), 2.00 – 1.94 (br m, 2H), 1.99 (s, 3H), 1.82 (m, 2H). ^{13}C NMR (101 MHz, $CDCl_3$): δ 192.8, 156.5, 141.2, 141.4, 136.3, 133.6, 132.7, 129.2, 128.6, 119.6, 117.9, 113.0, 107.8, 70.3, 61.7, 51.4, 43.0, 40.8, 31.1, 21.5, 13.1, 12.8. HRMS calcd. for $C_{23}H_{29}N_4O_4$ ($[M+H]^+$): 424.2132, found: 424.2135.

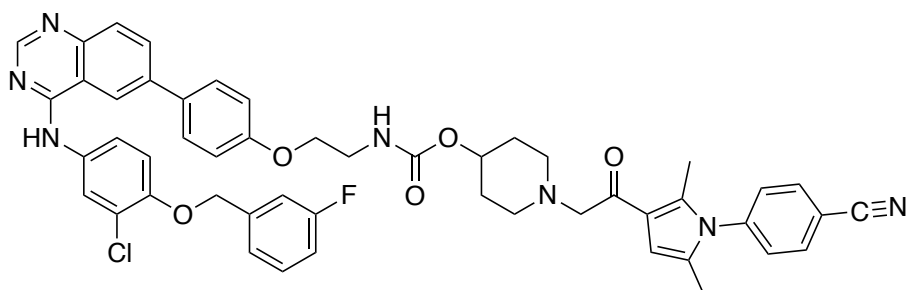
2-((((1-(2-(1-(4-cyanophenyl)-2,5-dimethyl-1*H*-pyrrol-3-yl)-2-oxoethyl)piperidin-4-yl)oxy)carbonyl)amino)ethyl 4-methylbenzenesulfonate (RBM3-141)



To a stirred solution of **RBM3-140** (30 mg, 0.71 mmol) in anhydrous CH₂Cl₂ (5 mL) and TEA (0.049 mL, 0.353 mmol), a solution of 4-methylbenzenesulfonyl chloride (TsCl) (33 mg, 0.177 mmol) in anhydrous CH₂Cl₂ (2 mL) was added at 0 °C. After the addition was complete, the mixture was allowed to warm to 25 °C and stirred for 3 h. The reaction mixture was then poured into 0.5 M aqueous HCl (15 mL) and extracted with CH₂Cl₂ (3 x 15 mL). The combined organic layers were washed with brine, dried over anhydrous MgSO₄, filtered and the solvent was evaporated to dryness. The residue was purified by silica gel column chromatography (0% to 3% of MeOH in CH₂Cl₂) to afford **RBM3-141** (30.0 mg, 0.052 mmol, 73%).

¹H NMR (400 MHz, CDCl₃): δ 7.83 (d, *J* = 8.4 Hz, 2H), 7.76 (d, *J* = 8.1 Hz, 2H), 7.33 (d, *J* = 8.5 Hz, 2H), 7.31 (d, *J* = 8.1 Hz, 2H), 6.39 (s, 1H), 6.02 (t, *J* = 5.8 Hz, 1H), 4.88 – 4.57 (m, 1H), 3.72 (m, 2H), 3.55 (t, *J* = 4.9 Hz, 2H), 3.36 (q, *J* = 5.3 Hz, 2H), 2.49 – 2.38 (m, 2H), 2.35 (s, 3H) 2.31 (s, 3H), 2.00 – 1.94 (br m, 2H), 1.99 (s, 3H), 1.82 (m, 2H). ¹³C NMR (101 MHz, CDCl₃): δ 192.8, 156.5, 144.7, 141.2, 141.4, 136.3, 133.9, 133.7, 132.6, 129.2, 128.6, 119.6, 117.9, 113.0, 107.8, 70.3, 61.7, 51.4, 43.0, 40.8, 31.1, 21.8, 21.5, 13.1, 12.8. HRMS calcd. for C₃₀H₃₄N₄O₆S ([M+H]⁺): 425.2132, found: 425.2135.

1-(2-(1-(4-cyanophenyl)-2,5-dimethyl-1*H*-pyrrol-3-yl)-2-oxoethyl)piperidin-4-yl (2-(4-(4-((3-chloro-4-((3-fluorobenzyl)oxy)phenyl)amino)quinazolin-6-yl)phenoxy)ethyl) carbamate (RBM3-225)

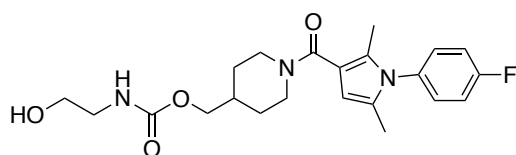


To a mixture of **RBM3-027** (15 mg, 0.032 mmol) and **RBM3-141** (18.0 mg, 0.032 mmol) in *N,N*-dimethylformamide (5 mL) was added Cs₂CO₃ (31.1 mg, 0.095 mmol). The reaction mixture was heated at 50 °C for 6 h. Then it was cooled to 25 °C, diluted with AcOEt (30 mL), washed with water (4x20 mL), dried Na₂SO₄ and the solvent was evaporated under vacuum. The crude product was purified by silica gel column chromatography (0% to 100% of EtOAc in hexanes) followed by a second purification by silica gel column chromatography (0% to 8% of MeOH in CH₂Cl₂) and finally by preparative TLC (CH₂Cl₂:MeOH 96:2) to give **RBM3-225** (17 mg, 0.020 mmol, 62%).

¹H NMR (400 MHz, DMSO-*d*₆): δ 9.85 (s, 1H), 9.68 (s, 1H), 8.69 (s, 1H), 8.56 (s, 1H), 8.12 (d, *J* = 8.7 Hz, 1H), 8.03 (s, 1H), 7.87 – 7.67 (m, 6H), 7.48 (td, *J* = 8.0, 6.0 Hz, 1H), 7.39 – 7.25 (m, 5H), 7.19 (tt, *J* = 7.8, 1.4 Hz, 1H), 6.93 (d, *J* = 8.6 Hz, 2H), 6.43 (s, 1H), 6.08 (t, *J* = 5.8 Hz, 1H), 5.27 (s, 2H), 4.88 – 4.57 (m, 1H), 3.72 (m, 4H), 3.64 (m, 11H), 3.55 (t, *J* = 4.9 Hz, 2H), 3.36 (q, *J* = 5.3 Hz, 2H), 2.95 – 2.86 (m, 4H), 2.49 – 2.38 (m, 2H), 2, 2.31 (s, 3H), 2.00 – 1.94 (br m, 2H), 1.99 (s, 3H), 1.82 (m, 2H). ¹³C NMR (101 MHz, DMSO-*d*₆): δ 192.8, 163.06, 161.44, 157.66, 157.59, 156.5, 154.07, 149.69, 148.44, 141.4, 139.73, 139.69, 138.23, 133.18, 132.7, 131.45, 130.69, 130.64, 129.86, 129.2, 128.67, 128.36,

128.32, 124.20, 123.45, 123.43, 122.38, 121.01, 119.6, 118.95, 117.9, 115.88, 115.33, 114.87, 114.73, 114.28, 114.21, 114.07, 113.0, 107.8, 72.8, 70.7, 70.5, 70.4, 70.3, 69.37, 65.2, 61.7, 51.4, 43.0, 40.8, 31.1, 13.1, 12.8. HRMS calcd. for $C_{50}H_{46}ClFN_7O_5$ ($[M+H]^+$): 878.3223, found: 878.3225.

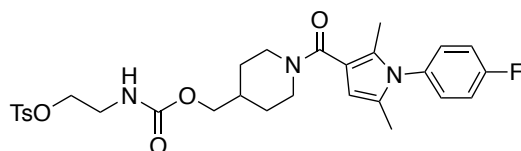
(1-(1-(4-fluorophenyl)-2,5-dimethyl-1H-pyrrole-3-carbonyl)piperidin-4-yl)methyl (2-hydroxyethyl)carbamate (RBM3-150)



A solution of **RBM3-361** (60.0 mg, 0.119 mmol) in anhydrous CH_2Cl_2 (5 mL) was added dropwise to a stirred solution of the amine **RBM3-013** (10.4 mg, 0.170 mmol) and TEA (36.8 mg, 0.363 mmol) in anhydrous CH_2Cl_2 (1 mL) at 25 °C. After overnight stirring, the reaction mixture was concentrated *in vacuo*, and the resulting crude was purified by flash chromatography (MeOH 0% to 5% in CH_2Cl_2) to furnish **RBM3-150** (40 mg, 0.096 mmol, 79.8% yield)

1H NMR (400 MHz, $CDCl_3$): δ 7.21 – 7.14 (m, 4H), 6.02 (m, 1H) 5.95 (s, 1H), 3.96 (d, J = 6.5 Hz, 2H), 3.57 – 3.53 (m, 2H), 3.40 – 3.32 (m, 2H), 2.07 (s, 3H), 1.97 (s, 3H), 1.96 – 1.87 (m, 2H), 1.80 – 1.73 (m, 2H), 1.34 – 1.21 (m, 4H). ^{13}C NMR (101 MHz, $CDCl_3$): δ 168.0, 130.8, 130.1, 130.0, 128.2, 116.5, 116.2, 115.1, 106.4, 77.5, 77.2, 76.8, 72.7, 70.7, 68.7, 61.7, 41.0, 36.5, 12.8, 12.0. HRMS calcd. For $C_{22}H_{29}FN_3O_4$ ($[M+H]^+$): 418.2110. found: 418.2113.

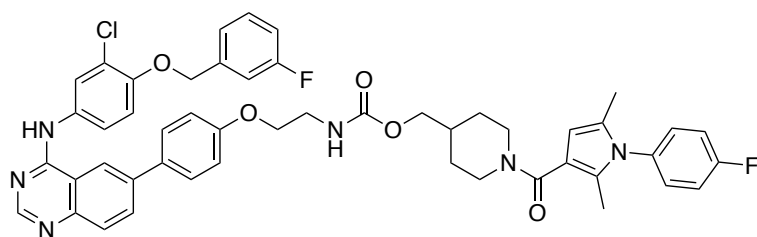
2-(((1-(1-(4-fluorophenyl)-2,5-dimethyl-1H-pyrrole-3-carbonyl)piperidin-4-yl)methoxy)carbonyl)amino)ethyl 4-methylbenzenesulfonate (RBM3-151)



To a stirred solution of **RBM3-150** (70 mg, 0.072 mmol) in anhydrous CH₂Cl₂ (5 mL) and TEA (0.030 mL, 0.216 mmol), a solution of 4-methylbenzenesulfonyl chloride (41.1 mg, 0.216 mmol) in anhydrous CH₂Cl₂ (2 mL) was added at 0 °C. After the addition was complete, the mixture was allowed to warm to 25 °C and was stirred for 3 h. The reaction mixture was then poured into 0.5 M aqueous HCl (15 mL) and extracted with CH₂Cl₂ (3 x 15 mL). The combined organic layers were washed with brine, dried over anhydrous MgSO₄, filtered and the solvent was evaporated to dryness. The residue was purified by silica gel column chromatography (0% to 3% of MeOH in CH₂Cl₂) to afford **RBM3-151** (22.0 mg, 0.038 mmol, 54%).

¹H NMR (400 MHz, CDCl₃): δ 7.76 (d, *J* = 8.1 Hz, 2H), 7.31 (d, *J* = 8.1 Hz, 2H), 7.21 – 7.14 (m, 4H), 6.02 (m, 1H), 5.95 (s, 1H), 3.96 (d, *J* = 6.5 Hz, 2H), 3.57 – 3.53 (m, 2H), 3.40 – 3.32 (m, 2H), 2.41 (s, 3H), 2.07 (s, 3H), 1.97 (s, 3H), 1.96 – 1.87 (m, 2H), 1.80 – 1.73 (m, 2H), 1.34 – 1.21 (m, 4H). ¹³C NMR (101 MHz, CDCl₃): δ 168.0, 144.7, 132.7, 130.8, 130.1, 130.0, 128.2, 116.5, 116.2, 115.1, 106.4, 77.5, 77.2, 76.8, 72.7, 70.7, 68.7, 61.7, 41.0, 36.5, 21.5, 12.8, 12.0. HRMS calcd. For C₂₉H₃₅FN₃O₆S ([M+H]⁺): 572.2223, found: 572.2227.

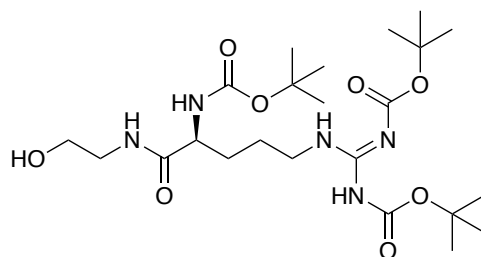
(1-(1-(4-fluorophenyl)-2,5-dimethyl-1H-pyrrole-3-carbonyl)piperidin-4-yl)methyl **(2-(4-(4-((3-chloro-4-((3-fluorobenzyl)oxy)phenyl)amino)quinazolin-6-yl)phenoxy)ethyl) carbamate**
(RBM3-227)



To a mixture of **RBM3-027** (20 mg, 0.042 mmol) and **RBM3-151** (24.0 mg, 0.042 mmol) in *N,N*-dimethylformamide (5 mL) was added Cs_2CO_3 (41 mg, 0.127 mmol). The reaction mixture was heated at 50 °C for 6 h. Then it was allowed to cool, diluted with AcOEt (30 mL), washed with water (4 x 20 mL), dried over Na_2SO_4 and the solvent was evaporated under vacuum. The crude was purified by silica gel column chromatography (0% to 100% of EtOAc in hexanes) followed by a second purification by silica gel column chromatography (0% to 11% of MeOH in CH_2Cl_2) and a final step by preparative TLC (CH_2Cl_2 :MeOH 97:3) to give **RBM3-227** (30 mg, 0.030 mmol, 70%).

^1H NMR (400 MHz, $\text{DMSO-}d_6$): δ 9.85 (s, 1H), 9.68 (s, 1H), 8.69 (s, 1H), 8.56 (s, 1H), 8.12 (d, $J = 8.7$ Hz, 1H), 8.03 (s, 1H), 7.87 – 7.67 (m, 4H), 7.48 (td, $J = 8.0, 6.0$ Hz, 1H), 7.39 – 7.25 (m, 3H), 7.21 – 7.117 (m, 4H), 7.15 (tt, $J = 7.8, 1.4$ Hz, 1H), 6.93 (d, $J = 8.6$ Hz, 2H), 6.02 (m, 1H) 5.95 (s, 1H), 5.27 (s, 2H), 3.96 (d, $J = 6.5$ Hz, 2H), 3.57 – 3.53 (m, 2H), 3.40 – 3.32 (m, 2H), 2.07 (s, 3H), 1.97 (s, 3H), 1.96 – 1.87 (m, 2H), 1.80 – 1.73 (m, 2H), 1.34 – 1.21 (m, 4H). ^{13}C NMR (101 MHz, $\text{DMSO-}d_6$): δ 168.0, 163.06, 161.44, 157.66, 157.59, 154.07, 149.69, 148.44, 139.73, 139.69, 138.23, 133.18, 131.45, 130.8, 130.69, 130.64, 130.1, 130.0, 129.86, 128.36, 128.32, 128.2, 124.20, 123.45, 123.43, 122.38, 121.01, 118.95, 116.5, 116.2, 115.88, 115.33, 115.1, 114.87, 114.73, 114.28, 114.21, 114.07, 106.4, 77.5, 77.2, 76.8, 72.7, 70.7, 68.7, 61.7, 41.0, 36.5, 12.8, 12.0. HRMS calcd. for $\text{C}_{49}\text{H}_{46}\text{ClF}_2\text{N}_6\text{O}_5$ ($[\text{M}+\text{H}]^+$): 871.3111. Found 871.3116.

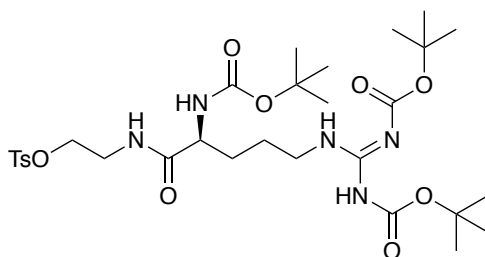
(RBM3-146)



EDC·HCl (60.0 mg, 0.314 mmol) and HOBt·H₂O (34.0 mg, 0.255 mmol) were sequentially added to a solution of *tri*-Boc-Arginine (93.0 mg, 0.196 mmol) in CH₂Cl₂ (10 mL), and the resulting mixture was vigorously stirred at 25 °C under argon atmosphere. After 15 min, the previous mixture was added dropwise to a solution of amine **RBM3-013** (12.0 mg, 0.196 mmol) and TEA (0.288 mL, 2.070 mmol) in CH₂Cl₂ (10 mL), and the reaction mixture was stirred at 25 °C overnight. The mixture was next diluted with CH₂Cl₂ (50 mL) and washed with brine (2 x 25 mL). The organic layer was dried over MgSO₄, filtered, and the volatiles were removed under reduced pressure. Purification of the crude by flash column chromatography (from 0 to 6% MeOH in CH₂Cl₂) afforded **RBM3-146** (77.0 mg, 0.149 mmol, 75 %).

¹H NMR (400 MHz, CDCl₃): δ 4.47–4.21 (m, 2H), 4.05 (d, *J* = 8.3 Hz, 2H), 3.90 (m, 3H), 3.79–3.75 (m, 2H), 3.71–3.60 (m, 2H), 3.54 (m, 1H), 3.11 (t, 2H), 1.85 – 1.55 (m, 4H) 1.49 (s, 9H), 1.44 (s, 9H), 1.41 (s, 9H). HRMS calcd. for C₂₃H₄₄N₅O₈ ([M+H]⁺): 518.3112, found: 518.3162.

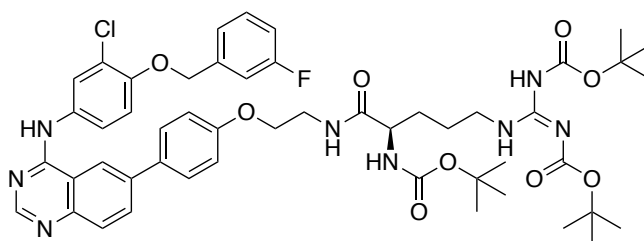
(*S,E*)-6,11-bis((*tert*-butoxycarbonyl)amino)-2,2-dimethyl-4,12-dioxo-3-oxa-5,7,13-triazapentadec-5-en-15-yl 4-methylbenzenesulfonate (RBM3-147)



To a stirred solution of **RBM3-146** (40 mg, 0.077 mmol) in anhydrous CH_2Cl_2 (10 mL) and TEA (0.021 mL, 0.155 mmol), a solution of 4-methylbenzenesulfonyl chloride (29.5 mg, 0.155 mmol) in anhydrous CH_2Cl_2 (3mL) was added at 0 °C. After the addition was complete, the mixture was allowed to warm to 25 °C and stirred for 3 h. The reaction mixture was then poured into 0.5 M aqueous HCl (15 mL) and extracted with CH_2Cl_2 (3 x 15 mL). The combined organic layers were washed with brine, dried over anhydrous MgSO_4 , filtered and the solvent was evaporated to dryness. The crude was purified by silica gel column chromatography (0% to 4% of MeOH in CH_2Cl_2) to afford **RBM3-147** (30.0 mg, 0.045 mmol, 57%).

^1H NMR (400 MHz, CDCl_3): δ 7.76 (d, $J = 8.1\text{Hz}$, 2H), 7.31 (d, $J = 8.1\text{Hz}$, 2H), 4.47– 4.21 (m, 2H), 4.05 (d, $J = 8.3\text{ Hz}$, 2H), 3.90 (m, 3H), 3.79-3.75 (m, 2H), 3.71-3.60 (m, 2H), 3.54 (m, 1H), 3.11 (t, 2H), 2.41 (s, 3H), 1.85 – 1.55 (m, 4H) 1.49 (s, 9H), 1.44 (s, 9H), 1.41 (s, 9H). HRMS calcd. for $\text{C}_{30}\text{H}_{50}\text{N}_5\text{O}_{10}\text{S}$ ($[\text{M}+\text{H}]^+$): 672.3231, found: 672.3235.

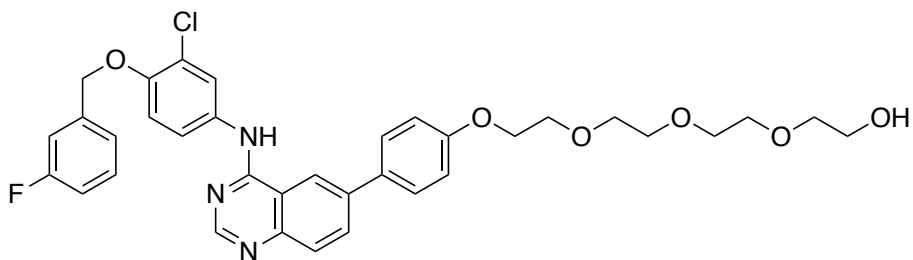
(RBM3-226)



To a mixture of **RBM3-027** (20 mg, 0.042 mmol) and **RBM3-147** (28.5 mg, 0.042 mmol) in *N,N*-dimethylformamide (5 mL) was added Cs₂CO₃ (41.0 mg, 0.127 mmol). The reaction mixture was heated at 50 °C for 6 h, cooled to 25 °C, diluted with AcOEt (30 mL), washed with water (4x20 mL), dried over Na₂SO₄ and the solvent was evaporated under vacuum. The reaction crude was purified by two sequential silica gel column chromatography steps (0% to 100% of EtOAc in hexanes and 0% to 7% of MeOH in CH₂Cl₂) and then by preparative TLC (CH₂Cl₂:MeOH 96:2) to give **RBM3-226** (22 mg, 0.023 mmol, 54%).

¹H NMR (400 MHz, DMSO-*d*₆): δ 9.85 (s, 1H), 9.68 (s, 1H), 8.69 (s, 1H), 8.56 (s, 1H), 8.12 (d, *J* = 8.7 Hz, 1H), 8.03 (s, 1H), 7.87 – 7.67 (m, 4H), 7.48 (td, *J* = 8.0, 6.0 Hz, 1H), 7.39 – 7.25 (m, 3H), 7.19 (tt, *J* = 7.8, 1.4 Hz, 1H), 6.93 (d, *J* = 8.6 Hz, 2H), 5.27 (s, 2H) 4.47– 4.21 (m, 2H), 4.05 (d, *J* = 8.3 Hz, 2H), 3.90 (m, 3H), 3.79-3.75 (m, 2H), 3.71-3.60 (m, 2H), 3.54 (m, 1H), 3.11 (t, 2H), 2.41 (s, 3H), 1.85 – 1.55 (m, 4H) 1.49 (s, 9H), 1.44 (s, 9H), 1.41 (s, 9H). ¹³C NMR (101 MHz, DMSO-*d*₆): δ 171.61, 163.06, 161.44, 157.66, 157.59, 154.07, 149.69, 148.44, 139.73, 139.69, 138.23, 133.18, 131.45, 130.69, 130.64, 129.86, 128.36, 128.32, 124.20, 123.45, 123.43, 122.38, 121.01, 118.95, 115.88, 115.33, 114.87, 114.73, 114.28, 114.21, 114.07, 80.1, 72.7, 70.0, 69.37, 55.6, 53.6, 44.3, 43.3, 41.32, 29.2, 28.5, 28.3, 28.1, 25.0. HRMS calcd. for C₅₀H₆₁ClFN₈O₉ ([M+H]⁺): 971.4156, Found 971.4160.

2-(2-(2-(2-(4-(4-((3-Chloro-4-((3-fluorobenzyl)oxy)phenyl)amino)quinazolin-6-yl)phenoxy)ethoxy)ethoxy)ethoxy)ethan-1-ol (RBM-070)

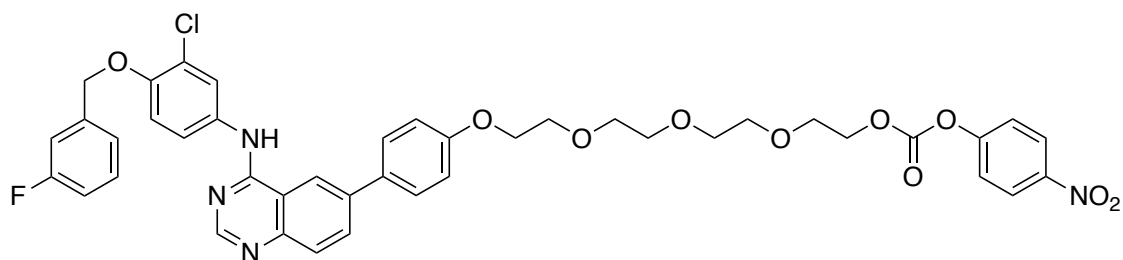


To a mixture of **RBM3-027** (200 mg, 0.424 mmol) and **RBM3-006** (206 mg, 0.042 mmol) in *N,N*-dimethylformamide (20 mL) was added Cs₂CO₃ (414 mg, 1.271 mmol). The reaction mixture was heated at 50 °C for 6 h, it was allowed to cool and then it was diluted with AcOEt (50 mL). The organic solution was washed with water (4 x 40 mL), dried over Na₂SO₄ and the solvent was evaporated under vacuum. The product was purified by silica gel column chromatography (0% to 25% of MeOH in CH₂Cl₂) to give **RBM3-070** (150 mg, 0.0231 mmol, 54%).

¹H NMR (400 MHz, DMSO-*d*₆): δ 9.85 (s, 1H), 9.68 (s, 1H), 8.69 (s, 1H), 8.56 (s, 1H), 8.12 (d, *J* = 8.7 Hz, 1H), 8.03 (s, 1H), 7.87 – 7.67 (m, 4H), 7.48 (td, *J* = 8.0, 6.0 Hz, 1H), 7.39 – 7.25 (m, 3H), 7.19 (tt, *J* = 7.8, 1.4 Hz, 1H), 6.93 (d, *J* = 8.6 Hz, 2H), 5.27 (s, 2H) 4.13 (t, *J* = 4.8 Hz, 2H), 3.55-3.68 (m, 14H), 2.41 (s, 3H). ¹³C NMR (101 MHz, DMSO-*d*₆): δ 163.06, 161.44, 157.66, 157.59, 154.07, 149.69, 148.44, 139.73, 139.69, 138.23, 133.18, 131.45, 130.69, 130.64, 129.86, 128.36, 128.32, 124.20, 123.45, 123.43, 122.38, 121.01, 118.95, 115.88, 115.33, 114.87, 114.73, 114.28, 114.21, 114.07, 72.3, 70.54, 70.47, 70.3, 70.1 69.37, 69.1, 68.5, 61.5, 21.5. HRMS calcd. for C₃₅H₃₆ClFN₃O₆ ([M+H]⁺): 648.2222, Found 648.2256.

2-(2-(2-(2-(4-(4-((3-Chloro-4-((3-fluorobenzyl)oxy)phenyl)amino)quinazolin-6-

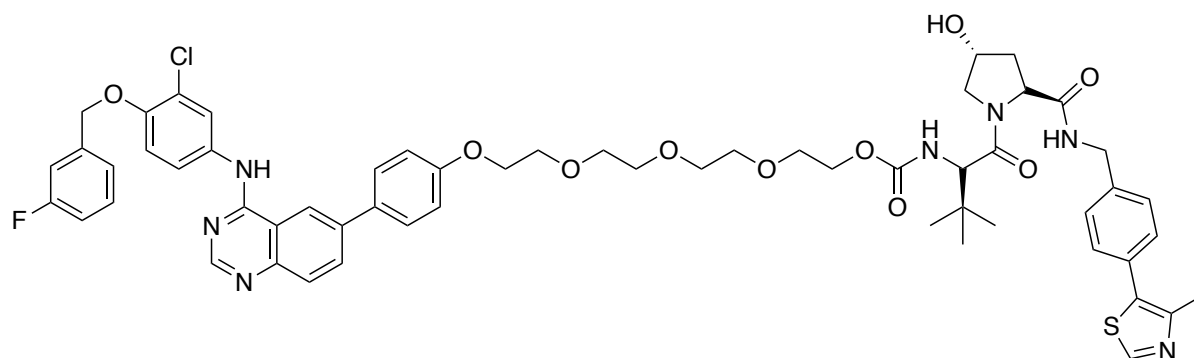
yl)phenoxy)ethoxy)ethoxy)ethyl (4-nitrophenyl) carbonate (RBM3-072)



To a stirred solution of **RBM3-070** (140 mg, 0.216 mmol) in anhydrous CH_2Cl_2 (15 mL), pyridine (0.043 mL, 0.540 mmol) and *p*-nitrophenyl chloroformate (56 mg, 0.281 mmol) were sequentially added. After stirring at 25 °C for 30 min, the mixture was quenched with saturated aqueous NH_4Cl (10 mL) and extracted with CH_2Cl_2 (3 x 10 mL). The combined organic layers were dried over MgSO_4 , filtered, and concentrated in vacuo. The residue was purified by flash column chromatography (0% to 10% of MeOH in CH_2Cl_2) to give **RBM3-072** (76 mg, 0.093 mmol, 43% yield).

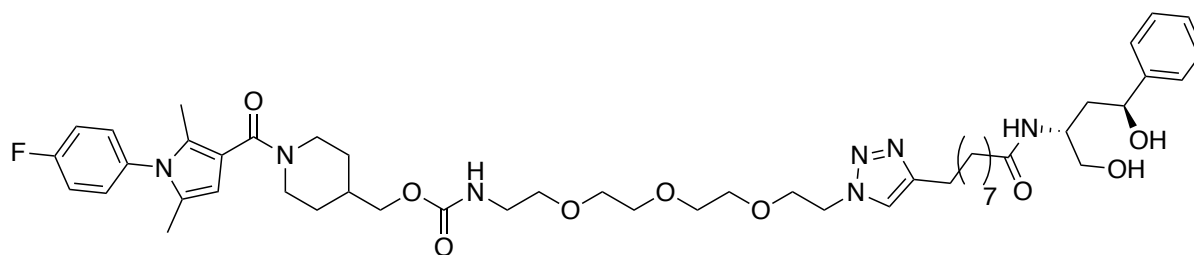
^1H NMR (400 MHz, $\text{DMSO}-d_6$): δ 9.85 (s, 1H), 9.68 (s, 1H), 8.69 (s, 1H), 8.56 (s, 1H), 8.34 – 8.25 (m, 2H), 8.12 (d, $J = 8.7$ Hz, 1H), 8.03 (s, 1H), 7.87 – 7.67 (m, 4H), 7.48 (dd, $J = 8.0, 6.0$ Hz, 3H), 7.39 – 7.25 (m, 3H), 7.19 (tt, $J = 7.8, 1.4$ Hz, 1H), 6.93 (d, $J = 8.6$ Hz, 2H), 5.27 (s, 2H) 4.13 (t, $J = 4.8$ Hz, 2H), 3.55-3.68 (m, 14H), 2.41 (s, 3H). ^{13}C NMR (101 MHz, $\text{DMSO}-d_6$): δ 171.1, 167.9, 163.06, 161.44, 157.66, 157.59, 154.07, 149.69, 148.44, 139.73, 139.69, 138.23, 133.18, 131.45, 130.69, 130.64, 129.86, 128.36, 128.32, 124.20, 123.45, 123.43, 122.38, 121.01, 118.95, 115.88, 115.33, 114.87, 114.73, 114.28, 114.21, 114.07, 72.3, 70.54, 70.47, 70.3, 70.1 69.37, 69.1, 68.5, 61.5, 21.5. HRMS calcd. for $\text{C}_{42}\text{H}_{39}\text{ClFN}_4\text{O}_{10}$ ($[\text{M}+\text{H}]^+$): 813.2313, Found 813.2344.

2-(2-(2-(2-(4-(4-((3-Chloro-4-((3-fluorobenzyl)oxy)phenyl)amino)quinazolin-6-yl)phenoxy)ethoxy)ethoxy)ethoxy)ethyl ((S)-1-((2R,4R)-4-hydroxy-2-((4-(4-methylthiazol-5-yl)benzyl)carbamoyl)pyrrolidin-1-yl)-3,3-dimethyl-1-oxobutan-2-yl)carbamate (RBM3-217)



^1H NMR (400 MHz, $\text{DMSO-}d_6$): δ 9.87 (s, 1H), 8.95 (s, 1H), 8.72 (s, 1H), 8.59 (t, $J = 6.0$ Hz, 1H), 8.55 (s, 1H), 8.13 (dd, $J = 8.7, 1.9$ Hz, 1H), 8.00 (d, $J = 2.5$ Hz, 1H), 7.89 – 7.76 (m, 3H), 7.73 (dd, $J = 9.0, 2.6$ Hz, 1H), 7.54 – 7.23 (m, 8H), 7.22 – 7.12 (m, 1H), 7.09 (d, $J = 8.8$ Hz, 2H), 5.24 (s, 2H), 5.15 (d, $J = 3.5$ Hz, 1H), 4.55 (d, $J = 9.6$ Hz, 1H), 4.48 – 4.18 (m, 5H), 3.95 (s, 2H), 3.80 – 3.69 (m, 2H), 3.69 – 3.51 (m, 8H), 2.41 (s, 3H), 2.08 – 2.00 (m, 1H), 1.93 – 1.82 (m, 1H), 0.92 (s, 9H). ^{13}C NMR (101 MHz, $\text{DMSO-}d_6$): δ 169.12, 168.59, 168.0, 163.01, 161.39, 158.53, 157.60, 154.15, 151.45, 149.70, 148.57, 147.73, 139.68, 139.63, 139.42, 137.72, 133.14, 131.44, 131.42, 131.13, 130.60, 130.55, 129.68, 128.68, 128.32, 128.24, 127.44, 124.19, 123.36, 123.34, 122.36, 121.03, 119.27, 115.28, 114.99, 114.78, 114.64, 114.29, 114.13, 113.98, 70.48, 69.97, 69.90, 69.63, 69.59, 69.38, 68.95, 68.88, 67.26, 58.75, 56.60, 55.69, 41.68, 37.94, 35.73, 26.19, 15.93. HRMS calcd. for $\text{C}_{58}\text{H}_{64}\text{ClFN}_7\text{O}_{10}\text{S}$ ($[\text{M}+\text{H}]^+$): 1104.4030, Found 1104.4035.

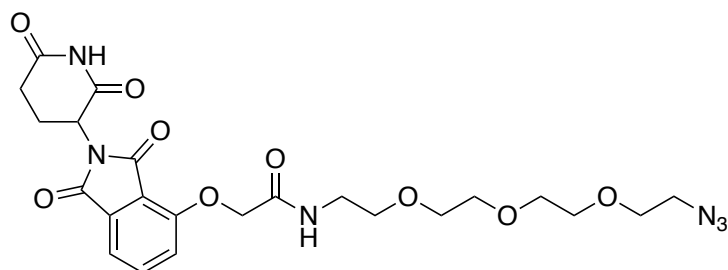
vi. CERT PROTACs



To a solution of **RBM3-363** (25 mg, 0.044 mmol) and **RBM3-366** (15.6 mg, 0.045 mmol) in DMF (2 mL), was added a 1 M aqueous solution of CuSO₄ (131 μL, 0.045 mmol) and a 1 M aqueous solution of sodium ascorbate (65 μL). The resulting mixture was stirred at 25 °C for 10 min and then concentrated *in vacuo* and the residue was purified by flash column chromatography (from 0 to 10% MeOH in CH₂Cl₂) to obtain **RBM3-368** (31 mg, 77%) as a cream-colored wax.

¹H NMR (400 MHz, CDCl₃): δ 7.47 (s, 1H), 7.36 – 7.28 (m, 4H), 7.26 – 7.20 (m, 1H), 7.16 (m, 4H), 6.80 (d, *J* = 6.9 Hz, 1H), 5.93 (s, 1H), 5.42 – 5.33 (m, 1H), 4.82 (dd, *J* = 9.1, 3.4 Hz, 1H), 4.48 (t, *J* = 5.0 Hz, 2H), 4.12 – 4.03 (m, 1H), 3.94 (br d, *J* = 6.1 Hz, 2H), 3.85 (t, *J* = 5.1 Hz, 2H), 3.67 (d, *J* = 4.1 Hz, 2H), 3.61 – 3.56 (m, 9H), 3.54 (t, *J* = 5.1 Hz, 2H), 3.38 – 3.32 (m, 2H), 2.67 (t, *J* = 7.5 Hz, 2H), 2.18 (t, *J* = 7.5 Hz, 2H), 2.09 – 2.06 (m, 1H), 2.05 (s, 3H), 1.96 (s, 3H), 1.95 – 1.88 (m, 2H), 1.80 – 1.71 (m, 2H), 1.69 – 1.57 (m, 4H), 1.36 – 1.19 (m, 11H).
¹³C NMR (101 MHz, CDCl₃): δ 144.8, 134.2, 130.7, 130.1, 130.0, 128.5, 128.4, 127.5, 125.8, 116.5, 116.3, 106.3, 71.8, 70.6, 70.6, 70.4, 70.2, 68.9, 41.3, 40.9, 36.9, 36.4, 29.4, 29.0, 25.7, 12.8, 12.1. HRMS calcd for C₄₉H₇₁FN₇O₉ ([M+H]⁺): 920.5297, found: 920.5330.

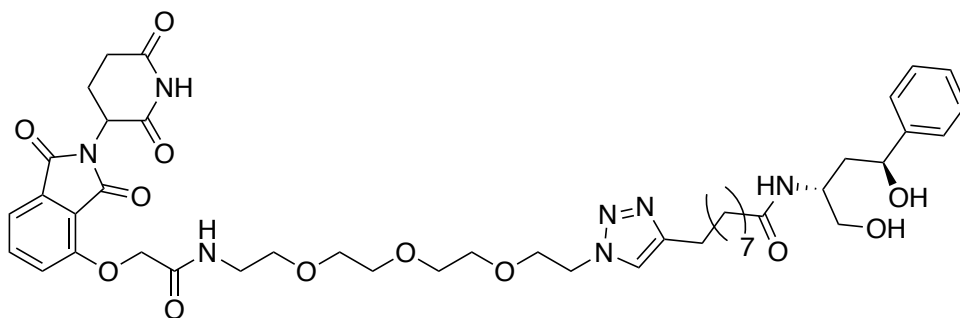
***N*-(2-(2-(2-(2-azidoethoxy)ethoxy)ethoxy)ethyl)-2-((2-(2,6-dioxopiperidin-3-yl)-1,3-dioxoisindolin-4-yl)oxy)acetamide (RBM5-174)**



A solution of **RBM5-163** (0.17 g, 0.66 mmol) in DMF (6 mL) was added to a 0.1 M solution of the carboxylic acid **RBM5-173** (0.20 g, 0.60 mmol) in DMF (6 mL), followed by addition of DIPEA (0.23 g, 1.81 mmol) and HATU (0.23 g, 0.60 mmol), and the resulting mixture was stirred at 25 °C for 19 h. The mixture was next diluted with CH₂Cl₂ (20 mL) and washed with citric acid (2 x 25 ml). The organic layer was dried over MgSO₄, filtered and concentrated. Purification of the crude by flash column chromatography (from 0 to 6% MeOH in CH₂Cl₂) afforded **RBM5-174** (0.26 g, 0.488 mmol, 82% yield).

¹H NMR (400 MHz, CDCl₃): δ 8.69 (br s, 1H), 7.76 – 7.70 (m, 1H), 7.60 (br s, 1H), 7.54 (d, *J* = 7.3 Hz, 1H), 7.18 (d, *J* = 8.4 Hz, 1H), 4.95 (dd, *J* = 12.0, 5.4 Hz, 1H), 4.64 (s, 2H), 3.70 – 3.61 (m, 12H), 3.60 – 3.54 (m, 2H), 3.41 – 3.37 (m, 2H), 2.92 – 2.69 (m, 3H), 2.15 (dt, *J* = 10.4, 4.1 Hz, 1H). ¹³C NMR (101 MHz, CDCl₃): δ 171.1, 168.2, 167.0, 166.8, 165.9, 154.6, 137.1, 133.8, 119.5, 118.2, 117.4, 70.9, 70.6, 70.5, 70.3, 70.0, 69.6, 68.1, 50.8, 49.4, 39.2, 31.5, 22.8. HRMS calcd. for C₂₃H₂₉N₆O₉ ([M+H]⁺): 533.1991, found: 533.2009.

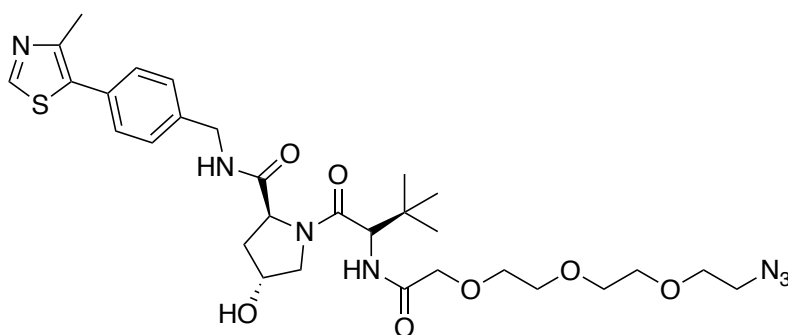
***N*-((2*R*,4*S*)-1,4-dihydroxy-4-phenylbutan-2-yl)-3-(1-(1-((2-(2,6-dioxopiperidin-3-yl)-1,3-dioxoisoindolin-4-yl)oxy)-2-oxo-6,9,12-trioxa-3-azatetradecan-14-yl)-1*H*-1,2,3-triazol-4-yl)propenamide (RBM3-369)**



To a solution of **RBM5-174** (22.3 mg, 0.042 mmol) and **RBM3-366** (15.0 mg, 0.043 mmol) in DMF (2 ml) was added a 1 M aqueous solution of CuSO_4 (131 μL , XXX mmol) and a 1 M aqueous solution of sodium ascorbate (63 μL , 0.063 mmol). The resulting mixture was stirred at 25 °C for 10 min and then concentrated and the residue was purified by flash column chromatography (from 0 to 18% MeOH in CH_2Cl_2) to obtain **RBM3-369** (25 mg, 69%) as a cream-colored wax.

^1H NMR (400 MHz, CD_3OD): δ 7.81 (dd, $J = 8.5, 7.3$ Hz, 1H), 7.54 (d, $J = 7.3$ Hz, 1H), 7.43 (d, $J = 8.4$ Hz, 1H), 7.38 – 7.28 (m, 4H), 7.27 – 7.18 (m, 1H), 5.12 (dd, $J = 12.6, 5.5$ Hz, 1H), 4.76 (s, 2H), 4.69 (t, $J = 6.9$ Hz, 1H), 4.52 (t, $J = 5.0$ Hz, 2H), 3.86 (t, $J = 5.0$ Hz, 2H), 3.84 – 3.78 (m, 1H), 3.68 – 3.55 (m, 11H), 3.49 (t, $J = 5.1$ Hz, 4H), 2.96 – 2.65 (m, 5H), 2.23 – 2.10 (m, 3H), 2.06 – 1.87 (m, 2H), 1.63 (d, $J = 21.9$ Hz, 4H), 1.40 – 1.28 (m, 11H). ^{13}C NMR (101 MHz, CD_3OD): δ 174.5, 171.3, 168.3, 167.5, 156.2, 145.9, 138.2, 134.9, 129.4, 128.4, 127.3, 121.6, 119.1, 117.9, 72.6, 71.5, 71.4, 70.3, 69.2, 68.7, 64.8, 51.6, 50.6, 49.9, 41.4, 40.2, 37.2, 32.2, 30.4, 30.3, 30.2, 30.0, 29.7, 27.0, 26.5, 25.8, 23.6, 23.0. HRMS calcd. For $\text{C}_{44}\text{H}_{60}\text{N}_7\text{O}_{12}$ ($[\text{M}+\text{H}]^+$): 878.4295, found: 878.4267.

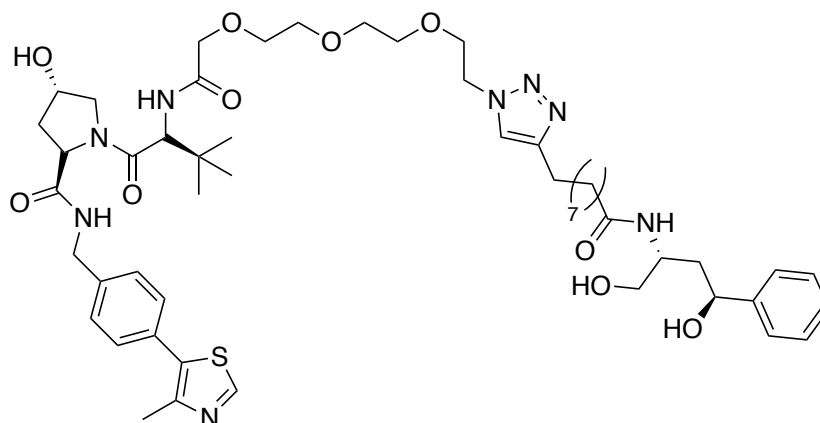
(2*S*,4*R*)-1-((*S*)-14-azido-2-(*tert*-butyl)-4-oxo-6,9,12-trioxa-3-azatetradecanoyl)-4-hydroxy-*N*-(4-(4-methylthiazol-5-yl)benzyl)pyrrolidine-2-carboxamide (RBM3-372)



EDC·HCl (92.0 mg, 0.480 mmol) and HOBt·H₂O (52.7 mg, 0.390 mmol) were sequentially added to an ice-cooled solution of the carboxylic acid **RBM3-367** (77.0 mg, 0.330 mmol) in anhydrous CH₂Cl₂ (5 mL) and the resulting mixture was vigorously stirred at 25 °C under argon atmosphere. After 15 min, the previous mixture was added dropwise to a solution of the amine **RBM5-189** (125.0 mg, 0.300 mmol) and TEA (0.209 mL, 1.500 mmol) in anhydrous CH₂Cl₂ (5 mL), and the reaction was stirred until completion as assessed by TLC analysis. The mixture was next diluted with CH₂Cl₂ (10 mL) and washed with brine. The organic layer was dried over MgSO₄, filtered, and the volatiles were removed under reduced pressure. Purification of the crude mixture by flash column chromatography (from 0 to 8% MeOH in CH₂Cl₂) afforded **RBM3-372** (140 mg, 0,217 mmol, 72% yield).

¹H NMR (400 MHz, CD₃OD): δ 8.67 (t, *J* = 6.0 Hz, 1H), 7.66 (d, *J* = 9.4 Hz, 1H), 7.48 – 7.41 (m, 4H), 4.74 – 4.67 (m, 1H), 4.61 – 4.47 (m, 3H), 4.36 (m, 1H), 4.05 (d, *J* = 2.9 Hz, 2H), 3.88 (d, *J* = 11.0 Hz, 1H), 3.80 (dd, *J* = 11.0, 3.7 Hz, 1H), 3.72 – 3.61 (m, 10H), 3.36 – 3.32 (m, 2H), 2.48 (br s, 3H), 2.23 (ddt, *J* = 13.2, 7.6, 1.9 Hz, 1H), 2.09 (ddd, *J* = 13.3, 9.2, 4.4 Hz, 1H), 1.05 (s, 9H). ¹³C NMR (101 MHz, CD₃OD): δ 208.7, 174.3, 171.7, 140.3, 130.5, 129.0, 72.3, 71.8, 71.6, 71.6, 71.2, 71.1, 60.8, 58.1, 51.8, 49.2, 38.9, 37.1, 26.9. HRMS calcd. for C₃₀H₄₄N₇O₇S ([M+H]⁺): 646.3023, found: 646.3015.

(2*S*,4*S*)-1-((*R*)-2-(*tert*-butyl)-14-(4-(9-(((2*R*,4*S*)-1,4-dihydroxy-4-phenylbutan-2-yl)amino)-9-oxononyl)-1*H*-1,2,3-triazol-1-yl)-4-oxo-6,9,12-trioxa-3-azatetradecanoyl)-4-hydroxy-*N*-(4-(4-methylthiazol-5-yl)benzyl)pyrrolidine-2-carboxamide (RBM3-373)



To a solution of **RBM3-372** (27.1 mg, 0.042 mmol) and **RBM3-366** (15.0 mg, 0.043 mmol) in DMF (2 mL was added a 1 M aqueous solution of CuSO₄ (126 μL, 126 mmol) and a 1 M aqueous solution of sodium ascorbate (63 μL, 0.063 mmol). The resulting mixture was stirred at 25 °C for 10 min and then concentrated and the residue was purified by flash column chromatography (from 0 to 10% MeOH in CH₂Cl₂) to obtain **RBM3-373** (15 mg, 0.015 mmol, 36%) as a cream-colored wax.

¹H NMR (400 MHz, CD₃OD): δ 8.65 (m, 1H), 7.81 (d, *J* = 7.9 Hz, 1H), 7.70 (br s, 1H), 7.52 – 7.38 (m, 4H), 7.39 – 7.29 (m, 5H), 7.28 – 7.21 (m, 1H), 4.75 – 4.67 (m, 2H), 4.62 – 4.49 (m, 5H), 4.35 (d, *J* = 15.6 Hz, 1H), 4.03 (s, 2H), 3.92 – 3.80 (m, 5H), 3.70 (br s, 2H), 3.68 – 3.59 (m, 7H), 3.58 – 3.45 (m, 2H), 2.30 – 1.90 (m, 7H), 1.68 (br s, 2H), 1.62 (br s, 2H), 1.41 – 1.27 (m, 10H), 1.04 (s, 9H). ¹³C NMR (101 MHz, CD₃OD): δ 209.2, 171.6, 146.0, 140.4, 129.4, 129.1, 128.4, 127.3, 72.6, 72.4, 71.7, 71.5, 71.1, 64.8, 60.8, 58.1, 50.0, 49.8, 49.0, 43.7, 41.4,

39.0, 37.2, 30.4, 27.0. HRMS calcd. for $C_{51}H_{75}N_8O_{10}S$ ($[M+H]^+$): 991.5327, found: 991.5312.

Chapter 6

References

- (1) Dikic, I. Proteasomal and Autophagic Degradation Systems. *Annu Rev Biochem* **2017**, *86*, 193–224. <https://doi.org/10.1146/annurev-biochem-061516-044908>.
- (2) MacGurn, J. A.; Hsu, P. C.; Emr, S. D. Ubiquitin and Membrane Protein Turnover: From Cradle to Grave. *Annu Rev Biochem* **2012**, *8*, 231–259. <https://doi.org/10.1146/annurev-biochem-060210-093619>.
- (3) D. H. Lee, A. L. G. Proteasome Inhibitors: Valuable New Tools for Cell Biologists. *Trends Cell Biol* **1998**, *(10)*, 397-403 <https://www.sciencedirect.com/science/article/pii/S0962892498013464>.
- (4) Paul, S. Dysfunction of the Ubiquitin-Proteasome System in Multiple Disease Conditions: Therapeutic Approaches. *BioEssays* **2008**, *30* (11–12), 1172–1184. <https://doi.org/10.1002/bies.20852>.
- (5) Lecker, S. H.; Goldberg, A. L.; Mitch, W. E. Protein Degradation by the Ubiquitin-Proteasome Pathway in Normal and Disease States. *J. Am. Soc. Nephrol* **2006**, *17* (7), 1807–1819. <https://doi.org/10.1681/ASN.2006010083>.
- (6) Weiss, M. S.; Schulz, G. E. Structure of Porin Refined at 1.8 Å Resolution. *J Mol Biol* **1992**, *227* (2), 493–509. [https://doi.org/10.1016/0022-2836\(92\)90903-W](https://doi.org/10.1016/0022-2836(92)90903-W).
- (7) Lange, O. F.; Lakomek, N. A.; Farès, C.; Schröder, G. F.; Walter, K. F. A.; Becker, S.; Meiler, J.; Grubmüller, H.; Griesinger, C.; De Groot, B. L. Recognition Dynamics up to Microseconds Revealed from an RDC-Derived Ubiquitin Ensemble in Solution. *Science* **2008**, *320* (5882), 1471–1475. <https://doi.org/10.1126/science.1157092>.
- (8) Ivan Dikic¹; Soichi Wakatsuki; Kylie J. Walters. Ubiquitin Binding Domains — from Structures to Functions. *Nat Rev Mol Cell Biol* **2020**, *176* (5), 139–148. <https://doi.org/10.1038/nrm2767.Ubiquitin>.
- (9) Shih, S. C.; Sloper-Mould, K. E.; Hicke, L. Monoubiquitin Carries a Novel Internalization Signal That Is Appended to Activated Receptors.

- EMBO Journal* **2000**, *19* (2), 187–198.
<https://doi.org/10.1093/emboj/19.2.187>.
- (10) Sloper-Mould, K. E.; Jemc, J. C.; Pickart, C. M.; Hicke, L. Distinct Functional Surface Regions on Ubiquitin. *J. Biol. Chem.* **2001**, *276* (32), 30483–30489. <https://doi.org/10.1074/jbc.M103248200>.
- (12) Loscalzo, D. E. H. R. C. J.; Boxberger et al., 2008; Loscalzo, D. E. H. R. C. J. Insights into Ubiquitin Transfer Cascades from a Structure of a UbcH5B~Ubiquitin-HECT NEDD4L Complex. *Bone* **2011**, *23* (1), 1–7. <https://doi.org/10.1016/j.molcel.2009.11.010.Insights>.
- (13) Hu, M.; Li, P.; Li, M.; Li, W.; Yao, T.; Wu, J. W.; Gu, W.; Cohen, R. E.; Shi, Y. Crystal Structure of a UBP-Family Deubiquitinating Enzyme in Isolation and in Complex with Ubiquitin Aldehyde. *Cell* **2002**, *111* (7), 1041–1054. [https://doi.org/10.1016/S0092-8674\(02\)01199-6](https://doi.org/10.1016/S0092-8674(02)01199-6).
- (14) Popovic, D.; Vucic, D.; Dikic, I. Ubiquitination in Disease Pathogenesis and Treatment. *Nat Med* **2014**, *20* (11), 1242–1253. <https://doi.org/10.1038/nm.3739>.
- (15) Komander, D.; Rape, M. The Ubiquitin Code. *Annu Rev Biochem* **2012**, *81* (May), 203–229. <https://doi.org/10.1146/annurev-biochem-060310-170328>.
- (16) Martin Scheffner, Ulrike Nuber, Jon M. Huibregtse. Protein Ubiquitination Involving an E1-E2-E3 Enzyme Ubiquitin Thioester Cascade Martin. *Nature* **1995**, *248* (6), 1773–1784.
- (17) Trempe, J.; Sauv e, V.; Grenier, K.; Seirafi, M.; Tang, M. Y.; Nagar, B.; Fon, E. A.; Gehring, K. Structure of Parkin Reveals Mechanisms for Ubiquitin Ligase Activation. *Science* **2013**, *340* (6139), 1451–1455. [0.1126/science.1237908](https://doi.org/10.1126/science.1237908).
- (18) Berndsen, C. E.; Wolberger, C. New Insights into Ubiquitin E3 Ligase Mechanism. *Nat Struct Mol Biol* **2014**, *21* (4), 301–307. <https://doi.org/10.1038/nsmb.2780>.

- (19) Budhidarmo, R.; Nakatani, Y.; Day, C. L. RINGs Hold the Key to Ubiquitin Transfer. *Trends Biochem Sci* **2012**, *37* (2), 58–65. <https://doi.org/10.1016/j.tibs.2011.11.001>.
- (20) Metzger, M. B.; Pruneda, J. N.; Klevit, R. E.; Weissman, A. M. RING-Type E3 Ligases: Master Manipulators of E2 Ubiquitin-Conjugating Enzymes and Ubiquitination. *Biochim Biophys Acta Mol Cell Res* **2014**, *1843* (1), 47–60. <https://doi.org/10.1016/j.bbamcr.2013.05.026>.
- (21) Metzger, M. B.; Hristova, V. A.; Weissman, A. M. HECT and RING Finger Families of E3 Ubiquitin Ligases at a Glance. *J Cell Sci* **2012**, *125* (3), 531–537. <https://doi.org/10.1242/jcs.091777>.
- (22) Zheng, N.; Wang, P.; Jeffrey, P. D.; Pavletich, N. P. Structure of a C-Cbl-UbcH7 Complex: RING Domain Function in Ubiquitin-Protein Ligases. *Cell* **2000**, *102* (4), 533–539. [https://doi.org/10.1016/S0092-8674\(00\)00057-X](https://doi.org/10.1016/S0092-8674(00)00057-X).
- (23) Rashighi, M.; Harris, J. E. Structural Insights into the U-Box, a Domain Associated with Multi-Ubiquitination. *Physiol Behav* **2017**, *176* (3), 139–148. <https://doi.org/10.1053/j.gastro.2016.08.014.CagY>.
- (24) Brzovic, P. S.; Rajagopal, P.; Hoyt, D. W.; King, M.; Klevit, R. E. Letters Structure of a BRCA1 – BARD1 Heterodimeric RING – RING Complex *Nat Struct Biol* **2001**, 833–837. <https://doi.org/10.1038/nsb1001-833>.
- (25) Zimmerman, E. S.; Schulman, B. A.; Zheng, N. Structural Assembly of Cullin-RING Ubiquitin Ligase Complexes. *Curr Opin Struct Biol* **2010**, *20* (6), 714–721. <https://doi.org/10.1016/j.sbi.2010.08.010>.
- (26) Kliza, K.; Husnjak, K. Resolving the Complexity of Ubiquitin Networks. *Front Mol Biosci* **2020**, 7-21. <https://doi.org/10.3389/fmolb.2020.00021>.
- (27) Bienko, M.; Green, C. M.; Crosetto, N.; Rudolf, F.; Zapart, G.; Coull, B.; Kannouche, P.; Wider, G.; Peter, M.; Lehmann, A. R.; Hofmann, K.; Dikic, I. Biochemistry: Ubiquitin-Binding Domains in Y-Family

- Polymerases Regulate Translesion Synthesis. *Science* **2005**, *310* (5755), 1821–1824. <https://doi.org/10.1126/science.1120615>.
- (28) Ye, Y.; Akutsu, M.; Reyes-Turcu, F.; Enchev, R. I.; Wilkinson, K. D.; Komander, D. Polyubiquitin Binding and Cross-Reactivity in the USP Domain Deubiquitinase USP21. *EMBO Rep* **2011**, *12* (4), 350–357. <https://doi.org/10.1038/embor.2011.17>.
- (29) Huang, X.; Luan, B.; Wu, J.; Shi, Y. An Atomic Structure of the Human 26S Proteasome. *Nat Struct Mol Biol* **2016**, *23* (9), 778–785. <https://doi.org/10.1038/nsmb.3273>.
- (30) Groll, M.; Ditzel, L.; Lowe, J.; Stock, D.; Bochtler, M.; Bartunik, H. D.; Huber, R. Structure of 20S Proteasome from Yeast at 2.4 Å Resolution. *Nature* **1997**, *386*, 463–471.
- (31) Livneh, I.; Cohen-Kaplan, V.; Cohen-Rosenzweig, C.; Avni, N.; Ciechanover, A. The Life Cycle of the 26S Proteasome: From Birth, through Regulation and Function, and onto Its Death. *Cell Res* **2016**, *26* (8), 869–885. <https://doi.org/10.1038/cr.2016.86>.
- (32) Muli, C. S.; Tian, W.; Trader, D. J. Small-Molecule Inhibitors of the Proteasome's Regulatory Particle. *ChemBioChem* **2019**, *20* (14), 1739–1753. <https://doi.org/10.1002/cbic.201900017>.
- (33) Heinemeyer, W.; Fischer, M.; Krimmer, T.; Stachon, U.; Wolf, D. H. The Active Sites of the Eukaryotic 20S Proteasome and Their Involvement in Subunit Precursor Processing. *J. Biol Chem* **1997**, *272* (40), 25200–25209. <https://doi.org/10.1074/jbc.272.40.25200>.
- (34) Ciechanover, A.; Schwartz, A. L. The Ubiquitin-Proteasome Pathway: The Complexity and Myriad Functions of Proteins Death. *Proc Natl Acad Sci U S A* **1998**, *95* (6), 2727–2730. <https://doi.org/10.1073/pnas.95.6.2727>.

- (35) Morozov, A. V.; Karpov, V. L. Proteasomes and Several Aspects of Their Heterogeneity Relevant to Cancer. *Front Oncol* **2019**, *9*, 1–21.
<https://doi.org/10.3389/fonc.2019.00761>.
- (36) Chang-Wei Liu Andrew D. Jacobson. Functions of the 19S Complex in Proteasomal Degradation. *Trends Biochem Sci* **2013**, *23* (1), 1–7.
<https://doi.org/10.1016/j.tibs.2012.11.009>.Functions.
- (37) Worden, E. J.; Padovani, C.; Martin, A. Structure of the Rpn11-Rpn8 Dimer Reveals Mechanisms of Substrate Deubiquitination during Proteasomal Degradation. *Nat Struct Mol Biol* **2014**, *21* (3), 220–227.
<https://doi.org/10.1038/nsmb.2771>.
- (38) Nickell, S.; Beck, F.; Scheres, S. H. W.; Korinek, A.; Förster, F.; Lasker, K.; Mihalache, O.; Sun, N.; Nagy, I.; Sali, A.; Plitzko, J. M.; Carazo, J. M.; Mann, M.; Baumeister, W. Insights into the Molecular Architecture of the 26S Proteasome. *Proc Natl Acad Sci U S A* **2009**, *106* (29), 11943–11947. <https://doi.org/10.1073/pnas.0905081106>.
- (39) Tanaka, K. The Proteasome: Overview of Structure and Functions. *Proc Jpn Acad Ser B Phys Biol Sci* **2009**, *85* (1), 12-36.
<https://doi.org/10.2183/pjab/85.12>.
- (40) Zhang, S.; Zou, S.; Yin, D.; Zhao, L.; Finley, D.; Wu, Z.; Mao, Y. *USP14-Regulated Allostery of the Human Proteasome by Time-Resolved Cryo-Nature*; 2022; 605 (7910). DOI: [10.1038/s41586-022-04671-8](https://doi.org/10.1038/s41586-022-04671-8).
- (41) Galen Andrew Collins and Alfred L. Goldberg. The Logic of the 26S Proteasome. *Physiol Behav* **2017**, *176* (5), 139–148.
<https://doi.org/10.1016/j.cell.2017.04.023>.
- (42) Shin, J. Y.; Muniyappan, S.; Tran, N. N.; Park, H.; Lee, S. B.; Lee, B. H. Deubiquitination Reactions on the Proteasome for Proteasome Versatility. *Int J Mol Sci* **2020**, *21* (15), 1–16. <https://doi.org/10.3390/ijms21155312>.

- (43) Lee, B. H.; Lee, M. J.; Park, S.; Oh, D. C.; Elsasser, S.; Chen, P. C.; Gartner, C.; Dimova, N.; Hanna, J.; Gygi, S. P.; Wilson, S. M.; King, R. W.; Finley, D. Enhancement of Proteasome Activity by a Small-Molecule Inhibitor of USP14. *Nature* **2010**, 467 (7312), 179-84. <https://doi.org/10.1038/nature09299>.
- (44) Lee, B. H.; Lu, Y.; Prado, M. A.; Shi, Y.; Tian, G.; Sun, S.; Elsasser, S.; Gygi, S. P.; King, R. W.; Finley, D. USP14 Deubiquitinates Proteasome-Bound Substrates That Are Ubiquitinated at Multiple Sites. *Nature* **2016**, 532 (7599), 398–401. <https://doi.org/10.1038/nature17433>.
- (45) Kim, H. T.; Goldberg, A. L. The Deubiquitinating Enzyme Usp14 Allosterically Inhibits Multiple Proteasomal Activities and Ubiquitin-Independent Proteolysis. *J. Biol. Chem.* **2017**, 292 (23), 9830–9839. <https://doi.org/10.1074/jbc.M116.763128>.
- (46) Chen, S.; Wu, J.; Lu, Y.; Ma, Y. B.; Lee, B. H.; Yu, Z.; Ouyang; Finley, D. J.; Kirschner, M. W.; Mao, Y. Structural Basis for Dynamic Regulation of the Human 26S Proteasome. *Proc Natl Acad Sci U.S.A.* **2016**, 113 (46), 12991–12996. <https://doi.org/10.1073/pnas.1614614113>.
- (47) Finley, D.; Prado, M. A. The Proteasome and Its Network: Engineering for Adaptability. *Cold Spring Harb Perspect Biol* **2020**, 12 (1), 1–25. <https://doi.org/10.1101/cshperspect.a033985>.
- (48) Yang, Y.; Kitagaki, J.; Dai, R. M.; Yien, C. T.; Lorick, K. L.; Ludwig, R. L.; Pierre, S. A.; Jensen, J. P.; Davydov, I. V.; Oberoi, P.; Li, C. C. H.; Kenten, J. H.; Beutler, J. A.; Vousden, K. H.; Weissman, A. M. Inhibitors of Ubiquitin-Activating Enzyme (E1), a New Class of Potential Cancer Therapeutics. *Cancer Res* **2007**, 67 (19), 9472–9481. <https://doi.org/10.1158/0008-5472.CAN-07-0568>.

- (49) Shingo Matsuo, Archana Sharma, Ping Wang, and Weng-Lang Yang, Center. PYR-41, A UBIQUITIN-ACTIVATING ENZYME E1 INHIBITOR, ATTENUATES LUNG INJURY IN SEPSIS. *Shock* **2018**. <https://doi.org/10.1097/SHK.0000000000000931>.PYR-41.
- (50) Soucy, T. A.; Smith, P. G.; Milhollen, M. A.; Berger, A. J.; Gavin, J. M.; Adhikari, S.; Brownell, J. E.; Burke, K. E.; Cardin, D. P.; Critchley, S.; Cullis, C. A.; Doucette, A.; Garnsey, J. J.; Gaulin, J. L.; Gershman, R. E.; Lublinsky, A. R.; McDonald, A.; Mizutani, H.; Narayanan, U.; Olhava, E. J.; Peluso, S.; Rezaei, M.; Sintchak, M. D.; Talreja, T.; Thomas, M. P.; Traore, T.; Vyskocil, S.; Weatherhead, G. S.; Yu, J.; Zhang, J.; Dick, L. R.; Claiborne, C. F.; Rolfe, M.; Bolen, J. B.; Langston, S. P. An Inhibitor of NEDD8-Activating Enzyme as a New Approach to Treat Cancer. *Nature* **2009**, *458* (7239), 732–736. <https://doi.org/10.1038/nature07884>.
- (51) Assumpção, A. L. F. V.; Lu, Z.; Marlowe, K. W.; Shaffer, K. S.; Pan, X. Targeting NEDD8-Activating Enzyme Is a New Approach to Treat Canine Diffuse Large B-Cell Lymphoma. *Vet Comp Oncol* **2018**, *16* (4), 606–615. <https://doi.org/10.1111/vco.12428>.
- (52) Ceccarelli, D. F.; Tang, X.; Pelletier, B.; Orlicky, S.; Xie, W.; Plantevin, V.; Neculai, D.; Chou, Y. C.; Ogunjimi, A.; Al-Hakim, A.; Varelas, X.; Koszela, J.; Wasney, G. A.; Vedadi, M.; Dhe-Paganon, S.; Cox, S.; Xu, S.; Lopez-Girona, A.; Mercurio, F.; Wrana, J.; Durocher, D.; Meloche, S.; Webb, D. R.; Tyers, M.; Sicheri, F. An Allosteric Inhibitor of the Human Cdc34 Ubiquitin-Conjugating Enzyme. *Cell* **2011**, *145* (7), 1075–1087. <https://doi.org/10.1016/j.cell.2011.05.039>.
- (53) Pulvino, M.; Liang, Y.; Oleksyn, D.; DeRan, M.; Van Pelt, E.; Shapiro, J.; Sanz, I.; Chen, L.; Zhao, J. Inhibition of Proliferation and Survival of Diffuse Large B-Cell Lymphoma Cells by a Small-Molecule Inhibitor of the Ubiquitin-Conjugating Enzyme Ubc13-Uev1A. *Blood* **2012**, *120* (8), 1668–1677. <https://doi.org/10.1182/blood-2012-02-406074>.

- (54) Chen, H.; Wu, G.; Gao, S.; Guo, R.; Zhao, Z.; Yuan, H.; Liu, S.; Wu, J.; Lu, X.; Yuan, X.; Yu, Z.; Zu, X.; Xie, N.; Yang, N.; Hu, Z.; Sun, Q.; Zhang, W. Discovery of Potent Small-Molecule Inhibitors of Ubiquitin-Conjugating Enzyme UbcH5c from α -Santonin Derivatives. *J Med Chem* **2017**, *60* (16), 6828–6852. <https://doi.org/10.1021/acs.jmedchem.6b01829>.
- (55) Vassilev, L. T.; Vu, B. T.; Graves, B.; Carvajal, D.; Podlaski, F.; Filipovic, Z.; Kong, N.; Kammlott, U.; Lukacs, C.; Klein, C.; Fotouhi, N.; Liu, E. A. In Vivo Activation of the P53 Pathway by Small-Molecule Antagonists of MDM2. *Science*, **2004**, *303* (5659), 844–848. <https://doi.org/10.1126/science.1092472>.
- (56) Cai, Q.; Sun, H.; Peng, Y.; Lu, J.; Nikolovska-Coleska, Z.; McEachern, D.; Liu, L.; Qiu, S.; Yang, C. Y.; Miller, R.; Yi, H.; Zhang, T.; Sun, D.; Kang, S.; Guo, M.; Leopold, L.; Yang, D.; Wang, S. A Potent and Orally Active Antagonist (SM-406/AT-406) of Multiple Inhibitor of Apoptosis Proteins (IAPs) in Clinical Development for Cancer Treatment. *J Med Chem* **2011**, *54* (8), 2714–2726. <https://doi.org/10.1021/jm101505d>.
- (57) Flygare, J. A.; Beresini, M.; Budha, N.; Chan, H.; Chan, I. T.; Cheeti, S.; Cohen, F.; Deshayes, K.; Doerner, K.; Eckhardt, S. G.; Elliott, L. O.; Feng, B.; Franklin, M. C.; Reisner, S. F.; Gazzard, L.; Halladay, J.; Hymowitz, S. G.; La, H.; Lorusso, P.; Maurer, B.; Murray, L.; Plise, E.; Quan, C.; Stephan, J. P.; Young, S. G.; Tom, J.; Tsui, V.; Um, J.; Varfolomeev, E.; Vucic, D.; Wagner, A. J.; Wallweber, H. J. A.; Wang, L.; Ware, J.; Wen, Z.; Wong, H.; Wong, J. M.; Wong, M.; Wong, S.; Yu, R.; Zobel, K.; Fairbrother, W. J. Discovery of a Potent Small-Molecule Antagonist of Inhibitor of Apoptosis (IAP) Proteins and Clinical Candidate for the Treatment of Cancer (GDC-0152). *J Med Chem* **2012**, *55* (9), 4101–4113. <https://doi.org/10.1021/jm300060k>.

- (58) Zhang, X.; Linder, S.; Bazzaro, M. Drug Development Targeting the Ubiquitin-Proteasome System (UPS) for the Treatment of Human Cancers. *Cancers (Basel)* **2020**, *12* (4).
<https://doi.org/10.3390/cancers12040902>.
- (59) Park, J.; Cho, J.; Song, E. J. Ubiquitin–Proteasome System (UPS) as a Target for Anticancer Treatment. *Arch Pharm Res* **2020**, *43* (11), 1144–1161. <https://doi.org/10.1007/s12272-020-01281-8>.
- (60) Chitta, K.; Paulus, A.; Akhtar, S.; Blake, M. K. K.; Caulfield, T. R.; Novak, A. J.; Ansell, S. M.; Advani, P.; Ailawadhi, S.; Sher, T.; Linder, S.; Chanan-Khan, A. Targeted Inhibition of the Deubiquitinating Enzymes, USP14 and UCHL5, Induces Proteotoxic Stress and Apoptosis in Waldenström Macroglobulinaemia Tumour Cells. *Br J Haematol* **2015**, *169* (3), 377–390. <https://doi.org/10.1111/bjh.13304>.
- (61) Xia, X.; Huang, C.; Liao, Y.; Liu, Y.; He, J.; Guo, Z.; Jiang, L.; Wang, X.; Liu, J.; Huang, H. Inhibition of USP14 Enhances the Sensitivity of Breast Cancer to Enzalutamide. *J. Exp. Clinl Cancer Res* **2019**, *38* (1), 1–17.
<https://doi.org/10.1186/s13046-019-1227-7>.
- (62) Kathleen C, Ravi A, Yoshie I, Joyce M, Lauren Mac, Rachel I Vogel, Robert Z. Orlowski, Michael K. Lee, Richard BS Roden, and M. B. Small-Molecule RA-9 Inhibits Proteasome-Associated DUBs and Ovarian Cancer in Vitro and in Vivo Via Exacerbating Unfolded Protein Responses. *Clin Cancer Res* **2015**, *20*, (12), **3174-3186**.
<https://doi.org/10.1158/1078-0432.CCR-13-2658.Small-Molecule>.
- (63) Jing Li, Tanya Y, Francesco P, Andrew L. Mackinnon, Christian P, Yuyong Ma, Kyle P. Carter, Sharon C, Gavin M, Brock B, Kevin N, Stefan V, Eigo S, Layton H. Smith, Eduard S, Anth, Division. Capzimin Is a Potent and Specific Inhibitor of Proteasome Isopeptidase Rpn11. *Nat Chem Biol* **2017**, *13* (5), **486-493**.
<https://doi.org/10.1053/j.gastro.2016.08.014.CagY>.

- (64) Niewerth, D.; Franke, N. E.; Jansen, G.; Assaraf, Y. G.; van Meerloo, J.; Kirk, C. J.; Degenhardt, J.; Anderl, J.; Schimmer, A. D.; Zweegman, S.; de Haas, V.; Horton, T. M.; Kaspers, G. J. L.; Cloos, J. Higher Ratio Immune versus Constitutive Proteasome Level as Novel Indicator of Sensitivity of Pediatric Acute Leukemia Cells to Proteasome Inhibitors. *Haematologica* **2013**, *98* (12), 1896–1904.
<https://doi.org/10.3324/haematol.2013.092411>.
- (65) Deborah J. Kuhn, Robert Z. Orlowski. The Immunoproteasome as a Target in Hematologic Malignancies. *Semin Hematol* **2013**. 49, (3).
<https://doi.org/10.1053/j.seminhematol.2012.04.003>.
- (66) Muchamuel, T.; Basler, M.; Aujay, M. A.; Suzuki, E.; Kalim, K. W.; Lauer, C.; Sylvain, C.; Ring, E. R.; Shields, J.; Jiang, J.; Shwonek, P.; Parlati, F.; Demo, S. D.; Bennett, M. K.; Kirk, C. J.; Groettrup, M. A Selective Inhibitor of the Immunoproteasome Subunit LMP7 Blocks Cytokine Production and Attenuates Progression of Experimental Arthritis. *Nat Med* **2009**, *15* (7), 781–787.
<https://doi.org/10.1038/nm.1978>.
- (67) Xi, J.; Zhuang, R.; Kong, L.; He, R.; Zhu, H.; Zhang, J. Immunoproteasome-Selective Inhibitors: An Overview of Recent Developments as Potential Drugs for Hematologic Malignancies and Autoimmune Diseases. *Eur J Med Chem* **2019**, *182*, 111646.
<https://doi.org/10.1016/j.ejmech.2019.111646>.
- (68) Sakamoto, K. M.; Kim, K. B.; Kumagai, A.; Mercurio, F.; Crews, C. M.; Deshaies, R. J. Protacs: Chimeric Molecules That Target Proteins to the Skp1-Cullin-F Box Complex for Ubiquitination and Degradation. *Proc Natl Acad Sci U.S.A.* **2001**, *98* (15), 8554–8559.
<https://doi.org/10.1073/pnas.141230798>.

- (69) Coll-Martínez, B.; Delgado, A.; Crosas, B. The Potential of Proteolytic Chimeras as Pharmacological Tools and Therapeutic Agents. *Molecules* **2020**, *25* (24) . <https://doi.org/10.3390/molecules25245956>.
- (70) Qi, S. M.; Dong, J.; Xu, Z. Y.; Cheng, X. D.; Zhang, W. D.; Qin, J. J. PROTAC: An Effective Targeted Protein Degradation Strategy for Cancer Therapy. *Front Pharmacol* **2021**, *12*, 692574. <https://doi.org/10.3389/fphar.2021.692574>.
- (71) Sakamoto, K. M.; Kim, K. B.; Verma, R.; Ransick, A.; Stein, B.; Crews, C. M.; Deshaies, R. J. Development of Protacs to Target Cancer-Promoting Proteins for Ubiquitination and Degradation. *Mol Cell Proteomics* **2003**, *2* (12), 1350–1358. <https://doi.org/10.1074/mcp.T300009-MCP200>.
- (72) Pei, H.; Peng, Y.; Zhao, Q.; Chen, Y. Small Molecule PROTACs: An Emerging Technology for Targeted Therapy in Drug Discovery. *RSC Advances*. 2019, *9* (30), 16967-16976. <https://doi.org/10.1039/c9ra03423d>.
- (73) Schneekloth, J. S.; Fonseca, F. N.; Koldobskiy, M.; Mandal, A.; Deshaies, R.; Sakamoto, K.; Crews, C. M. Chemical Genetic Control of Protein Levels: Selective in Vivo Targeted Degradation. *J Am Chem Soc* **2004**. *126*, (12), 3648-3754. <https://doi.org/10.1021/ja039025z>.
- (74) Bargagna-Mohan, P.; Baek, S. H.; Lee, H.; Kim, K.; Mohan, R. Use of PROTACS as Molecular Probes of Angiogenesis. *Bioorg Med Chem Lett* **2005**, *15* (11), 2724–2727. <https://doi.org/10.1016/j.bmcl.2005.04.008>.
- (75) Bondeson, D. P.; Mares, A.; Smith, I. E. D.; Ko, E.; Campos, S.; Miah, A. H.; Mulholland, K. E.; Routly, N.; Buckley, D. L.; Gustafson, J. L.; Zinn, N.; Grandi, P.; Shimamura, S.; Bergamini, G.; Faeltsh-savitski, M.; Bantscheff, M.; Cox, C.; Gordon, D. A.; Willard, R. R.; Flanagan, J. J.; Casillas, L. N.; Votta, B. J.; Besten, W. Den; Famm, K.; Kruidenier, L.; Carter, P. S.; Harling, J. D.; Churcher, I.; Crews, C. M. Catalytic in Vivo

- Protein Knockdown by Small- Molecule PROTACs. *Nat Chem Biol* **2015**, *11*, 611-617. <https://doi.org/10.1038/nchembio.1858>.
- (76) John Hines, Schan Lartigue, Hanqing Dong, Yimin Qian, and Craig M. Crews. MDM2-Recruiting PROTAC Offers Superior, Synergistic Anti-Proliferative Activity via Simultaneous Degradation of BRD4 and Stabilization of P53. *Cancer Res* **2019**, *79*, (1), 251-262. <https://doi.org/10.1158/0008-5472.CAN-18-2918.MDM2-recruiting>.
- (77) Schneekloth, A. R.; Pucheault, M.; Tae, H. S.; Crews, C. M. Targeted Intracellular Protein Degradation Induced by a Small Molecule: En Route to Chemical Proteomics. *Bioorg Med Chem Lett* **2008**, *18* (22), 5904–5908. <https://doi.org/10.1016/j.bmcl.2008.07.114>.
- (78) Pei, H.; Peng, Y.; Zhao, Q.; Chen, Y. Small Molecule PROTACs: An Emerging Technology for Targeted Therapy in Drug Discovery. *RSC Adv* **2019**, *9* (30), 16967–16976. <https://doi.org/10.1039/c9ra03423d>.
- (79) Kocab, A. J.; Duckett, C. S. Inhibitor of Apoptosis Proteins as Intracellular Signaling Intermediates. *FEBS Journal* **2016**, *283* (2), 221–231. <https://doi.org/10.1111/febs.13554>.
- (80) Naito, M.; Ohoka, N.; Shibata, N. SNIPERs—Hijacking IAP Activity to Induce Protein Degradation. *Drug Discov Today Technol* **2019**, *31*, 35–42. <https://doi.org/10.1016/j.ddtec.2018.12.002>.
- (81) Bricelj, A.; Steinebach, C.; Kuchta, R.; Gütschow, M.; Sosič, I. E3 Ligase Ligands in Successful PROTACs: An Overview of Syntheses and Linker Attachment Points. *Front Chem* **2021**, *9*, 1–46. <https://doi.org/10.3389/fchem.2021.707317>.
- (82) Mullard, A. Targeted Protein Degradation Crowds into the Clinic. *Nat Rev Drug Discov* **2021**, *20* (4), 247–250. <https://doi.org/10.1038/d41573-021-00052-4>.
- (83) Lai, A. C.; Toure, M.; Hellerschmied, D.; Salami, J.; Jaime-Figueroa, S.; Ko, E.; Hines, J.; Crews, C. M. Modular PROTAC Design for the

- Degradation of Oncogenic BCR-ABL. *Angew. Chemie Int Ed Engl* **2016**, 55 (2), 807–810. <https://doi.org/10.1002/anie.201507634>.
- (84) Smith, B. E.; Wang, S. L.; Jaime-Figueroa, S.; Harbin, A.; Wang, J.; Hamman, B. D.; Crews, C. M. Differential PROTAC Substrate Specificity Dictated by Orientation of Recruited E3 Ligase. *Nat Commun* **2019**, 10 (1), 1–13. <https://doi.org/10.1038/s41467-018-08027-7>.
- (85) Kramer, L. T.; Zhang, X. Expanding the Landscape of E3 Ligases for Targeted Protein Degradation. *Curr. Res. Chem. Biol.* **2022**, 2, 100020. <https://doi.org/10.1016/j.crchbi.2022.100020>.
- (86) Zhang, L. ; B. Riley.G, P. Vijay, Y. Shen. Acquired Resistance to BET-PROTACs Targeting Chimeras) Caused by Genomic Alterations in Core Components of E3 Ligase Complexes. *mol. cancer Ther* **2019**, 18 (7), 1302–1311.
- (87) Ciechanover, A.; Kwon, Y. T. Protein Quality Control by Molecular Chaperones in Neurodegeneration. *Front. Neurosci.* **2017**, 11 , 1–18. <https://doi.org/10.3389/fnins.2017.00185>.
- (88) Gustafson, J. L.; Neklesa, T. K.; Cox, C. S.; Roth, A. G.; Buckley, D. L.; Tae, H. S.; Sundberg, T. B.; Stagg, D. B.; Hines, J.; McDonnell, D. P.; Norris, J. D.; Crews, C. M. Angewandte Small-Molecule-Mediated Degradation of the Androgen Receptor through Hydrophobic Tagging. *Angew. Chemie Int Ed Engl* **2015**, 54 (33), 9659–9662. <https://doi.org/10.1002/anie.201503720>.
- (89) Shi, Y.; Long, M. J. C.; Rosenberg, M. M.; Li, S.; Kobjack, A.; Lessans, P.; Coffey, R. T.; Hedstrom, L. Boc3Arg-Linked Ligands Induce Degradation by Localizing Target Proteins to the 20S Proteasome. *ACS Chem Biol* **2016**, 11 (12), 3328–3337. <https://doi.org/10.1021/acscchembio.6b00656>.

- (90) Marcus J. C. Long¹, Deviprasad R. Gollapalli², and L. H. Inhibitor Mediated Protein Degradation Marcus. *Chem Biol*. **2012**, *23* (1), 1–7. <https://doi.org/10.1016/j.chembiol.2012.04.008>.Inhibitor.
- (91) Whitney, L.; Petrilli, W. L.; Adam, G. C.; Erdmann, R. S.; Tata, J. R.; Xiong, Y.; Imbriglio, J. E.; Petrilli, W. L.; Adam, G. C.; Erdmann, R. S.; Abeywickrema, P.; Agnani, V.; Ai, X.; Ha, S.; Huang, Y.; Hubbard, B.; Johnston, J. M.; Kavana, M.; Lisnock, J. From Screening to Targeted Degradation : Strategies for the Discovery and Optimization of Small Molecule Ligands for PCSK9. *Cell Chem Biol* **2020**, 32–40. <https://doi.org/10.1016/j.chembiol.2019.10.002>.
- (92) Bashore, C.; Prakash, S.; Johnson, M. C.; Conrad, R. J.; Kekessie, I. A.; Scales, S. J.; Ishisoko, N.; Kleinheinz, T.; Liu, P. S.; Popovych, N.; Wecksler, A. T.; Zhou, L.; Tam, C.; Zilberleyb, I.; Srinivasan, R.; Blake, R. A.; Song, A.; Staben, S. T.; Zhang, Y.; Arnott, D.; Fairbrother, W. J.; Foster, S. A.; Wertz, I. E.; Ciferri, C.; Dueber, E. C. Targeted Degradation via Direct 26S Proteasome Recruitment. *Nat Chem Biol* **2023**, *19* (1), 55–63. <https://doi.org/10.1038/s41589-022-01218-w>.
- (93) Sintchak, M. D.; Fleming, M. A.; Futer, O.; Raybuck, S. A.; Chambers, S. P.; Caron, P. R.; Murcko, M. A.; Wilson, K. P. Structure and Mechanism of Inosine Monophosphate Dehydrogenase in Complex with the Immunosuppressant Mycophenolic Acid. *Cell* **1996**, *85* (6), 921–930. [https://doi.org/10.1016/S0092-8674\(00\)81275-1](https://doi.org/10.1016/S0092-8674(00)81275-1).
- (94) Poulakou, G.; Barakat, M.; Israel, R. J.; Bacci, M. R.; Abril, J. F. M. H.; Álvarez, S. N.; Fonseca, F. L. A.; Kainis, I.; Kalomoiri, S.; Leontis, K.; Metallidis, S.; Panagopoulos, P.; Papastamopoulos, V.; Ragoonete, H. G.; Ramacciotti, E.; Rapti, V.; Sakka, V.; Syrigos, K. N.; Tsoukalas, G.; Xynogalas, I. Ribavirin Aerosol in Hospitalized Adults with Respiratory Distress and COVID-19: An Open-Label Trial. *Clin Transl Sci* **2023**, *16* (1), 165–174. <https://doi.org/10.1111/cts.13436>.

- (95) Li, R. J.; Wang, Y. L.; Wang, Q. H.; Wang, J.; Cheng, M. S. In Silico Design of Human IMPDH Inhibitors Using Pharmacophore Mapping and Molecular Docking Approaches. *Comput Math Methods Med* **2015**, 2015. <https://doi.org/10.1155/2015/418767>.
- (96) Takeuchi, K.; Ito, F. Anti-Cancer Drugs Targeting Growth-Factor Signaling Molecules Target Therapy for Cancer: Receptor Tyrosine Kinases and Targeted Cancer Therapeutics. *Biol Pharm Bull* **2011**, 34 (12), 1774–1780.
- (97) Nahta, R.; Esteva, F. J. HER2 Therapy: Molecular Mechanisms of Trastuzumab Resistance. *Breast Cancer Res.* **2006**, 8 (6), 1–8. <https://doi.org/10.1186/bcr1612>.
- (98) Burslem, G. M.; Smith, B. E.; Lai, A. C.; Jaime-Figueroa, S.; McQuaid, D. C.; Bondeson, D. P.; Toure, M.; Dong, H.; Qian, Y.; Wang, J.; Crew, A. P.; Hines, J.; Crews, C. M. The Advantages of Targeted Protein Degradation Over Inhibition: An RTK Case Study. *Cell Chem Biol* **2018**, 25, (1), 67-77. <https://doi.org/10.1016/j.chembiol.2017.09.009>.
- (99) Zeidan, Y. H.; Hannun, Y. A. Translational Aspects of Sphingolipid Metabolism. *Trends Mol Med* **2007**, 13 (8), 327–336. <https://doi.org/10.1016/j.molmed.2007.06.002>.
- (100) Van Blitterswijk, W. J.; Van Der Luit, A. H.; Veldman, R. J.; Verheij, M.; Borst, J. Ceramide: Second Messenger or Modulator of Membrane Structure and Dynamics? *Biochemical Journal* **2003**, 369 (2), 199–211. <https://doi.org/10.1042/BJ20021528>.
- (101) Giordano, G. Ceramide-Transfer Protein-Mediated Ceramide Transfer Is a Structurally Tunable Flow-Inducing Mechanism with Structural Feed-Forward Loops. *R Soc Open Sci* **2018**, 5 (6). <https://doi.org/10.1098/rsos.180494>.
- (102) Swanton, C.; Marani, M.; Pardo, O.; Warne, P. H.; Kelly, G.; Sahai, E.; Elustondo, F.; Chang, J.; Temple, J.; Ahmed, A. A.; Brenton, J. D.;

- Downward, J.; Nicke, B. Regulators of Mitotic Arrest and Ceramide Metabolism Are Determinants of Sensitivity to Paclitaxel and Other Chemotherapeutic Drugs. *Cancer Cell* **2007**, *11* (6), 498–512.
<https://doi.org/10.1016/j.ccr.2007.04.011>.
- (103) Albeituni, S; Stiban, J. Roles of Ceramides and Other Sphingolipids in Immune Cell Function and Inflammation. *In Advances in Experimental Medicine and Biology* **2019**, *5347* (1161), 169–191.
https://doi.org/10.1007/978-3-030-21735-8_15.
- (104) Keen, A. C.; Jörg, M.; Halls, M. L. The Application of Targeted Protein Degradation Technologies to G Protein-Coupled Receptors. *Br J Pharmacol* **2023**, No. September 2022, 1–7. In press.
<https://doi.org/10.1111/bph.16079>.
- (105) J. Eroles; P Coffino. Ubiquitin-Independent Proteasomal Degradation. *Biochim Biophys Acta*. **2014**, *1843* (1). [https://doi.org/10.1016/S1553-7250\(12\)38019-7](https://doi.org/10.1016/S1553-7250(12)38019-7).
- (106) Bemis, T. A.; Clair, J. J. La; Burkart, M. D. Unraveling the Role of Linker Design in Proteolysis Targeting Chimeras. *J Med Chem* **2021**, *64* (12), 8042–8052. <https://doi.org/10.1021/acs.jmedchem.1c00482>.
- (107) Troup, R. I.; Fallan, C.; Baud, M. G. J. Current Strategies for the Design of PROTAC Linkers: A Critical Review. *Explor Target Antitumor Ther* **2020**, *1* (5), 273–312. <https://doi.org/10.37349/etat.2020.00018>.
- (108) Alabi, S. B.; Crews, C. M. Major Advances in Targeted Protein Degradation: PROTACs, LYTACs, and MADTACs. *J. Biol. Chem.* **2021**, *296* 100647 <https://doi.org/10.1016/j.jbc.2021.100647>.
- (109) Burslem, G. M.; Smith, B. E.; Lai, A. C.; Jaime-Figueroa, S.; McQuaid, D. C.; Bondeson, D. P.; Toure, M.; Dong, H.; Qian, Y.; Wang, J.; Crew, A. P.; Hines, J.; Crews, C. M. The Advantages of Targeted Protein Degradation Over Inhibition: An RTK Case Study. *Cell Chem Biol* **2018**, *25* (1), 67-77.e3. <https://doi.org/10.1016/j.chembiol.2017.09.009>.

- (110) Galdeano, C.; Gadd, M. S.; Soares, P.; Scaffidi, S.; Van Molle, I.; Birced, I.; Hewitt, S.; Dias, D. M.; Ciulli, A. Structure-Guided Design and Optimization of Small Molecules Targeting the Protein-Protein Interaction between the von Hippel-Lindau (VHL) E3 Ubiquitin Ligase and the Hypoxia Inducible Factor (HIF) Alpha Subunit with in Vitro Nanomolar Affinities. *J Med Chem* **2014**, *57*, (20), 8657-8663.
<https://doi.org/10.1021/jm5011258>.
- (111) Goswami, L. N.; Houston, Z. H.; Sarma, S. J.; Jalisatgi, S. S.; Hawthorne, M. F. Efficient Synthesis of Diverse Heterobifunctionalized Clickable Oligo(Ethylene Glycol) Linkers: Potential Applications in Bioconjugation and Targeted Drug Delivery. *Org Biomol Chem* **2013**, *11* (7), 1116–1126.
<https://doi.org/10.1039/c2ob26968f>.
- (112) Zhang, H.; Li, X.; Shi, Q.; Li, Y.; Xia, G.; Chen, L.; Yang, Z.; Jiang, Z. X. Highly Efficient Synthesis of Monodisperse Poly(Ethylene Glycols) and Derivatives through Macrocyclization of Oligo(Ethylene Glycols). *Chemie Int Ed Engl*. **2015**, *54* (12), 3763–3767.
<https://doi.org/10.1002/anie.201410309>.
- (113) Mirza-Aghayan, M.; Boukherroub, R.; Bolourtchian, M. A Mild and Efficient Palladium-Triethylsilane System for Reduction of Olefins and Carbon-Carbon Double Bond Isomerization. *Appl Organomet Chem* **2006**, *20* (3), 214–219. <https://doi.org/10.1002/aoc.1036>.
- (114) Kara, B. Y.; Kilbaş, B.; Göksu, H. Selectivity and Activity in Catalytic Hydrogenation of Azido Groups over Pd Nanoparticles on Aluminum Oxy-Hydroxide. *New J Chem* **2016**, *40* (11), 9550–9555.
<https://doi.org/10.1039/c6nj01925k>.
- (115) Bashore, F. M.; Foley, C. A.; Ong, H. W.; Rectenwald, J. M.; Hanley, R. P.; Norris-Drouin, J. L.; Cholensky, S. H.; Mills, C. A.; Pearce, K. H.; Herring, L. E.; Kireev, D.; Frye, S. V.; James, L. I. PROTAC Linkerology Leads to an Optimized Bivalent Chemical Degradator of Polycomb

- Repressive Complex 2 (PRC2) Components. *ACS Chem Biol* **2023**, *18* (3), 494–507. <https://doi.org/10.1021/acscchembio.2c00804>.
- (116) Charruyer, A.; Bell, S. M.; Kawano, M.; Douangpanya, S.; Yen, T. Y.; Macher, B. A.; Kumagai, K.; Hanada, K.; Holleran, W. M.; Uchida, Y. Decreased Ceramide Transport Protein (CERT) Function Alters Sphingomyelin Production Following UVB Irradiation. *J. Biol. Chem* **2008**, *283* (24), 16682–16692. <https://doi.org/10.1074/jbc.M800799200>.
- (117) Lee, A. J. X.; Roylance, R.; Sander, J.; Gorman, P.; Endesfelder, D.; Kschischo, M.; Jones, N. P.; East, P.; Nicke, B.; Spassieva, S.; Obeid, L. M.; Birkbak, N. J.; Szallasi, Z.; McKnight, N. C.; Rowan, A. J.; Speirs, V.; Hanby, A. M.; Downward, J.; Tooze, S. A.; Swanton, C. CERT Depletion Predicts Chemotherapy Benefit and Mediates Cytotoxic and Polyploid-Specific Cancer Cell Death through Autophagy Induction. *J. Patho* **2012**, *226* (3), 482–494. <https://doi.org/10.1002/path.2998>.
- (118) Wang, Y.; Jiang, Y.; Ding, S.; Li, J.; Song, N.; Ren, Y.; Hong, D.; Wu, C.; Li, B.; Wang, F.; He, W.; Wang, J.; Mei, Z. Small Molecule Inhibitors Reveal Allosteric Regulation of USP14 via Steric Blockade. *Cell Res* **2018**, *28*(12), 1186–1194. <https://doi.org/10.1038/s41422-018-0091-x>.
- (119) Peng, Y.; Luo, J.; Feng, Q.; Tang, Q. Understanding the Scope of Feist–Bénary Furan Synthesis: Chemoselectivity and Diastereoselectivity of the Reaction Between α -Halo Ketones and β -Dicarbonyl Compounds. *Eur. J Org Chem* **2016**, *2016* (30), 5169–5179. <https://doi.org/10.1002/ejoc.201600975>.
- (120) Wilmlison, A. E.; Ylioja, P. M.; Robertson, M. N.; Avery, V.; Baell, J. B.; Batchu, H.; Batra, S.; Burrows, J. N.; Bhattacharyya, S.; Calderon, F.; Charman, S. A.; Clark, J.; Crespo, B.; Dean, M.; Debbert, S. L.; Delves, M.; Dennis, A. S. M.; Deroose, F.; Duffy, S.; Fletcher, S.; Giaever, G.; Hallyburton, I.; Gamo, F. J.; Gebbia, M.; Guy, R. K.; Hungerford, Z.; Kirk, K.; Lafuente-Monasterio, M. J.; Lee, A.; Meister, S.; Nislow, C.;

- Overington, J. P.; Papadatos, G.; Patiny, L.; Pham, J.; Ralph, S. A.; Ruecker, A.; Ryan, E.; Southan, C.; Srivastava, K.; Swain, C.; Tarnowski, M. J.; Thomson, P.; Turner, P.; Wallace, I. M.; Wells, T. N. C.; White, K.; White, L.; Willis, P.; Winzeler, E. A.; Wittlin, S.; Todd, M. H.; Antonova-Koch, Y. Open Source Drug Discovery: Highly Potent Antimalarial Compounds Derived from the Tres Cantos Arylpyrroles. *ACS Cent Sci* **2016**, *2* (10), 687–701. <https://doi.org/10.1021/acscentsci.6b00086>.
- (121) Madak, J. T.; Cuthbertson, C. R.; Chen, W.; Showalter, H. D.; Neamati, N. Design, Synthesis, and Characterization of Brequinar Conjugates as Probes to Study DHODH Inhibition. *Chem. Eur. J* **2017**, *23* (56), 13875–13878 <https://doi.org/10.1002/chem.201702999>.
- (122) Van Molle, I.; Thomann, A.; Buckley, D. L.; So, E. C.; Lang, S.; Crews, C. M.; Ciulli, A. Dissecting Fragment-Based Lead Discovery at the von Hippel-Lindau Protein:Hypoxia Inducible Factor 1 α Protein-Protein Interface. *Chem Biol* **2012**, *19* (10), 1300–1312. <https://doi.org/10.1016/j.chembiol.2012.08.015>.
- (123) Caroline M. R.; Jacob I. C.; Smit K, Margaret A. T.; Mohammad A, Yogesh A.S; Muhammad Z; Daryl J.M; Amarnath N; Sandeep R. Chemically Induced Degradation of CDK9 by a Proteolysis Targeting Chimera (PROTAC). *Chem commun* **2018**, *53* (54), 7577–7580. doi: 10.1039/c7cc03879h.
- (124) Goswami, L. N.; Houston, Z. H.; Sarma, S. J.; Jalisatgi, S. S.; Hawthorne, M. F. Efficient Synthesis of Diverse Heterobifunctionalized Clickable Oligo(Ethylene Glycol) Linkers: Potential Applications in Bioconjugation and Targeted Drug Delivery. *Org Biomol Chem* **2013**, *11* (7), 1116–1126. <https://doi.org/10.1039/c2ob26968f>.
- (125) Ma, L.; Tu, C.; Le, P.; Chitoor, S.; Lim, S. J.; Zahid, M. U.; Teng, K. W.; Ge, P.; Selvin, P. R.; Smith, A. M. Multidentate Polymer Coatings for

- Compact and Homogeneous Quantum Dots with Efficient Bioconjugation. *J Am Chem Soc* **2016**, *138* (10), 3382–3394.
<https://doi.org/10.1021/jacs.5b12378>.
- (126) Sun, Y.; Liang, Y.; Hao, N.; Fu, X.; He, B.; Han, S.; Cao, J.; Ma, Q.; Xu, W.; Sun, Y. Novel Polymeric Micelles as Enzyme-Sensitive Nuclear-Targeted Dual-Functional Drug Delivery Vehicles for Enhanced 9-Nitro-20(S)-Camptothecin Delivery and Antitumor Efficacy. *Nanoscale* **2020**, *12* (9), 5380–5396. <https://doi.org/10.1039/c9nr10574c>.
- (127) Zhu, J.; Xiao, Y.; Zhang, H.; Li, Y.; Yuan, Y.; Yang, Z.; Chen, S.; Zheng, X.; Zhou, X.; Jiang, Z. X. Peptidic Monodisperse PEG “Combs” with Fine-Tunable LCST and Multiple Imaging Modalities. *Biomacromolecules* **2019**, *20* (3), 1281–1287.
<https://doi.org/10.1021/acs.biomac.8b01693>.
- (128) Chen, B.; Bednarz, M. S.; Zhang, H.; Zhao, R.; Murali, T. G.; Balasubramanian, B.; Barrish, J. C. A New Efficient Synthesis of 5-Aryloxazoles from Arylidene Diacetates and Application to the Preparation of BMS-337197, a Novel IMPDH Inhibitor. *heterocycles* **2006**, *68* (1), 167–173.
- (129) Cao, J.; Ma, C.; Zang, J.; Gao, S.; Gao, Q.; Kong, X.; Yan, Y.; Liang, X.; Ding, Q.; Zhao, C.; Wang, B.; Xu, W.; Zhang, Y. Novel Leucine Ureido Derivatives as Aminopeptidase N Inhibitors Using Click Chemistry. *Bioorg Med Chem* **2018**, *26* (12), 3145–3157.
<https://doi.org/10.1016/j.bmc.2018.04.041>.